NASw-4435

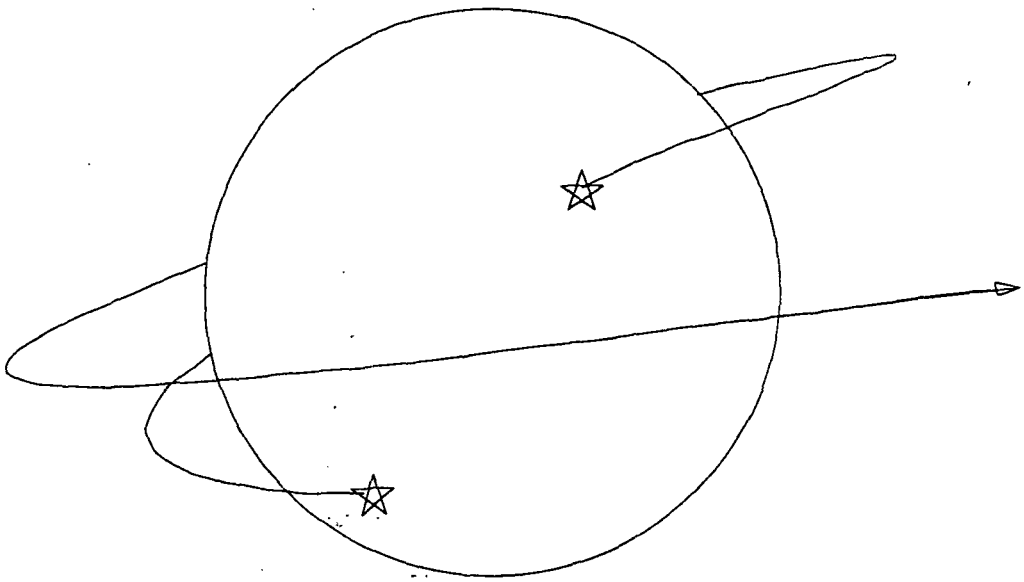

Access to Space

Final Report

Spacecraft Design Team

University of Minnesota

July 1, 1994

TABLE OF CONTENTS

LIST OF FIGURES AND TABLES

Part A: Conceptual Design

Part B: Model Reports

ABBREVIATIONS, ACRONYMS, AND SYMBOLS

AC	Alternating Current
ACC	Advanced Carbon-carbon
ACS	Atmospheric Control System
AFV	Air Face Velocity
AOA	Abort Once Around
APU	Auxiliary Power Unit
ATAS	Abort To Alternate Site
ATC	Air Traffic Control
ATO	Abort To Orbit
BFO	Blood Forming Organ
BITE	Built In Test
C&T	Communication and Tracking
CFD	Computational Fluid Dynamics
CMC	Centralized Maintenance Computers
CO_2	Carbon Dioxide
CP	Cold Plate
CRESST	Crew Entry Support Structure
CRT	Cathode Ray Tubes
DC	Direct Current
DGPS	Differential Global Position System
DOD	Department of Defense
ECLSS	Environmental Control and Life Support System
EFBU	Electric Fan and Backup Fan Unit
EIU	Engine Interface Unit
EPDS	Electrical Power Distribution System
EPRS	Emergency Pressure Relief System
EPS	Electrical Power System
EVA	Extravehicular Activities
FA	Forced Air
FC-40	Fluorinate
FCP	Fuel Cell Powerplants
FM	Frequency Modulation
GEO	Geosynchronous Earth Orbit
GHAME	Generic Hypersonic Aerodynamic Model Example
GN&C	Guidance Navigation & Control
GNSS	Global Navigational Satellite System
GPC	General Purpose Computer
GPS	Global Positioning System
HM	High Modulus
HSLM	High Strength Low Modulus
HTV	Horizontal-to-Vertical Hydraulic Lift
IM	Intermediate Modulus
INU	Inertial Navigation Unit

LCD	Liquid Crystal Display
LEO	Low Earth Orbit
LH_2	Liquid Hydrogen
LiOH	Lithium Hydroxide
LO_2	Liquid Oxygen
LRU	Line Replaceable Unit
MBH	Maintenance Bay/Hanger
MFD	Multifunctional Displays
MTBF	Mean Time Between Failure
NOAA	National Oceanic and Atmospheric Administration
NWA	Northwest Airlines
OMS	Orbital Maneuvering System
PM	Phase Modulated
QFD	Quality Function Deployment
RCC	Reinforced Carbon-carbon
RCS	Reaction Control System
RTAS	Return to Alternate Site
RTG	Radioisotope Thermal Generators
RTLS	Return to Launch Site
SSTO	Single Stage to Orbit
Tacan	Tactical Air Navigation
TDRS	Tracking and Data Relay Satellite
THC	Temperature and Humidity Control
TPS	Thermal Protection System
TVC	Thrust Vector Control
UHF	Ultra High Frequency
UHM	Ultrahigh Modulus
USRA	University Space Research Association
VAC	Voltage Alternating Current
VDC	Voltage Direct Current
WMS	Water Management System
A	cross sectional area
A	surface area
C	constant
F	force
F	view factor
h	angular momentum
hf_g	heat of vaporization
i	inclination angle
I_{sp}	specific impulse
k	thermal conductivity
KE	kinetic energy
L	thickness of material
L_{seam}	total length of seam
m	mass
m^c	pitching moment

q	heat flux
r	radius
R	resistance
r_1	inner radius
r_2	outer radius
r_a	radius of apoapsis
r_p	radius of periapsis
r_r	radius of rotation
SF	safety factor
t	time
t	thickness
T	temperature
T	period
T	throttle factor
u	velocity
v	velocity
V	velocity
Y	side force
W_{seam}	width of seam
β	side slip
ε	specific energy
ε	emissivity
μ	bank angle
μ	gravitational constant
ρ	density
σ	yield strength
σ	Stephan-Boltzmann constant
χ	heading
ω_x	roll rate
ω_y	pitch rate
ω_z	yaw rate
Λ	wing sweep

Part A:

Conceptual Design

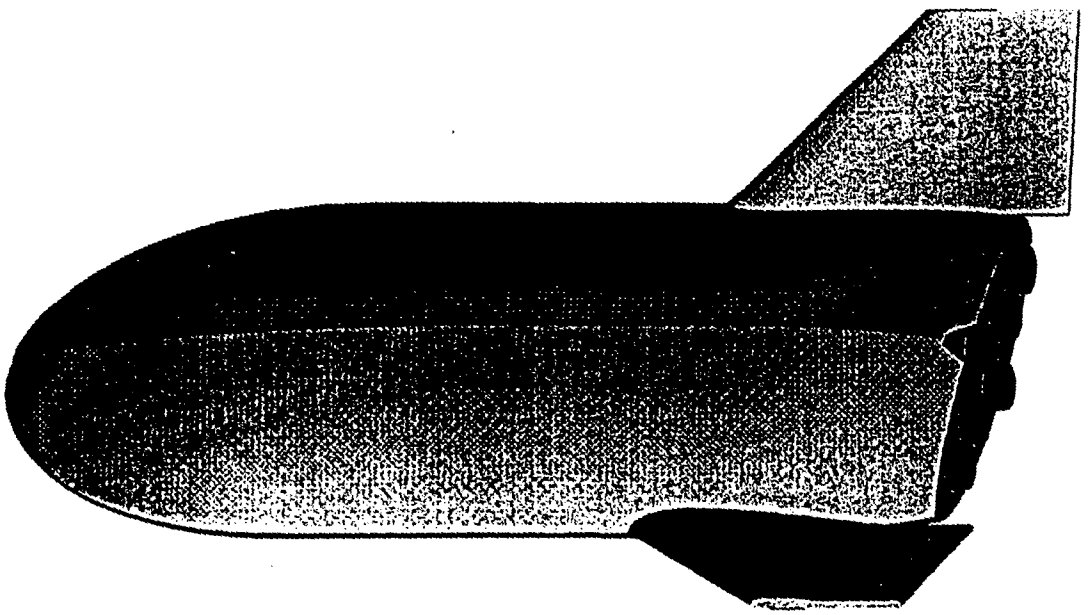

ABSTRACT

The goal of this conceptual design was to devise a reusable, commercially viable, single-stage-to-orbit vehicle. The vehicle has the ability to deliver a 9100 kg (20,000 lb) payload to a low earth orbit of 433 km to 933 km (250 n.mi. - 450 n.mi.). The SSTO vehicle is 51 meters in length and has a gross takeoff mass of 680,400 kg (1,500,000 lb). The vehicle incorporates three RD-701 engines for the main propulsion system and two RL-10 engines for the orbital maneuvering system. The vehicle is designed for a three day stay on orbit with two crew members.

1.0 INTRODUCTION

1.1 Motivation

Space is truly the last great frontier and to date remains an enormous resource virtually undiscovered and untouched. Humankind has just begun its exploration into this unknown wilderness. Man-made satellites have been placed around the earth and people have walked the moon. Both are tremendous accomplishments for this century. In terms of global time though, what has been accomplished is just a scratch on the surface of what will be achieved.

What was previously just a vision into the future is nearing reality. The technology now exists to begin utilization of the vast resources and opportunities that space offers. Currently, designs to place permanently manned space stations in orbit around the earth are being fulfilled. Research is also being done to place a manned station on the moon. With the arrival of permanently manned space locations, a need for a reusable vehicle with the capability of reaching space colonies on a regular basis exits. Such a vehicle would open the door to commercial opportunities, some of which already exist in today's market. Thus, the first commercial venture into space would begin.

The University Space Research Association (USRA), in conjunction with NASA, requested that the University of Minnesota Senior Aerospace Spacecraft Design Team devise a commercial space transportation vehicle that would reach low earth orbit by a single stage. The USRA is an organization that integrates current and future NASA projects into university engineering design curriculums. It brings students and faculty from United States engineering schools together with engineers from NASA and/or industry sponsors. The industrial sponsor for this project is Northwest Airlines (NWA). The Spacecraft Design Team is presented with the opportunity to utilize both resources, NASA and NWA, for the design process. In essence, the motivation for this extensive project is derived from two main sources: the University Space Research Association, in conjunction with NASA, and Northwest Airlines.

Research is currently being performed by various aerospace companies on a single-stage-to-orbit (SSTO) vehicle. Initial designs have been put forth by several commercial companies includes McDonnell/Douglas (the DC-Y), Boeing (with its "mother ship" concept), and Lockheed. Some of these corporations are even to the phase of building and testing scale versions of these designs. Northwest Airlines is exploring the SSTO vehicle as a potential transportation business opportunity.

The main features of the SSTO vehicle are reusability and its single-stage propulsion system. This means that, unlike the Space Shuttle, the all hardware, namely engine components, that launch with the craft return with it. It also incorporates a much simpler design that the Space Shuttle. The perspective taken in this design project is that commercial transportation companies are the customers, and that the designed vehicle must meet commercial application specifications. Northwest Airlines, being the industry sponsor, has provided information to aid in this aspect of the design criteria.

1.2 Design Objectives

For the purpose of uniformity, the Spacecraft Design Team decided that a single, concise mission statement was needed. It was within this statement that the Team's objectives were established. The Team formulated the following:

> "To provide a reliable, timely, reusable, man-rated, and cost-effective single-stage-to-orbit commercial transportation vehicle."

The objectives become very clear and important when compared with existing space transportation and commercial airline transpiration. Reliability and timeliness are best explained with a comparison of the Space Shuttle (existing space transportation) and Northwest Airlines (commercial airline transpiration). The Space Shuttle program, as of March 1992, had completed 45 flights. Of these 45 flights, only nine launched at the scheduled time.[1] At that date, only 20% of the flights had been on time. On the other had, a commercial airline corporation, Northwest, has an on time service of approximately 90%. Timeliness is another main objective. Again, with the Space Shuttle turnaround times are generally measured in months while with airlines, the

turnaround time is in hours. In order to design a spacecraft to be utilized for commercial purposes, turnaround time must be low. High reliability is needed to satisfy customers.

Reusable and cost-effective are two other objectives that coincide. For a commercial company to make a profit, its operational vehicle must be cost-effective. That is, the amount other corporations pay a transportation company for a launch should outweigh the cost of the launch. The best way for a spacecraft to be cost-effective is for it to be fully reusable, like an airplane. With a reusable space vehicle, no expenses are incurred from dropped fuel tanks or one-stage booster rockets like the Space Shuttle's. With a reusable vehicle, a commercial company also experiences ease of operations as compared to a complex vehicle.

The final objectives for this design are that it must be man-rated and be single-stage-to-orbit. Though the definition of man-rated has not been fully defined, it essentially means no "self-destruct" mechanism can exist and full control of the vehicle must be experienced from launch to touchdown while considering all potential failure modes that could affect safe operation. The single-stage requirement simply signifies that vehicle must only incorporate one type of propulsive stage, unlike the Space Shuttle with its multiple stages.

1.3 Executive Summary

The design of an SSTO vehicle has offered many challenges and even more solutions. The current design is a vertical launch/horizontal landing vehicle. The takeoff mass is 680,400 kg (1,500,000 lb) and the empty mass is 58,900 kg (130,000 lb). The vehicle incorporates three RD-701 engines for the main propulsion system, making the vehicle fail-safe 0.9 seconds after launch. The vehicle can carry a payload of 9100 kg (20,000 lb) up to an altitude of 833 km (250 n.mi.). The vehicle is shown in figures 1.1 and 1.2. A complete vehicle specification is included in Appendix A.

Since the number of engines and therefore fuel amount are directly related to empty mass, it is critical to obtain the lowest empty mass possible. The structure of the vehicle is designed using carbon-carbon composites for the frame, carbon epoxy for the skin, and carbon epoxy and kevlar for the fuel tanks. Although the use of these materials is very expensive, it is justified by the savings in mass. The thermal protection system (TPS) is another area where mass conservation is necessary. The TPS is designed utilizing carbon-carbon composites, inconel, and titanium. As with the structure, the mass savings justifies the high cost. A listing of components and their materials is in Appendix A.

Other major design features are: a two person crew, a detailed ground operations plan, the use of Global Positioning Systems and Global Navigation Satellite Systems for navigational purposes, and an extensive communication system. The ground operations design includes details of launch, landing, and maintenance facilities. The communication system features an atmospheric system and an orbital system.

The vehicle specification sheet in Appendix A contains a summary of the important properties of the Team's SSTO vehicle.

1.4 Quality Function Deployment and Design Decisions

Quality Function Deployment (QFD) is a design tool promoted by the American Supplier Institute as a means to "design in" quality and satisfy customer requirements. It

Aggressive Mission Planning Program		
	Several Vehicles	2
	Fast Turnaround	5
Payload		
	Power and Pneumatic Module Support	3
	Changeable Cargo Modules	5
	Standard Commercial Payload Weight	3
	Standard Commercial Payload Size	3
Reliable		
	Mission Abortable	5
	Fail Tolerant Design	4
	Launchable in All Environments	4
Environment		
	Low Air/Noise Pollution	4
	Low Airspace Requirement	3
Mission		
	Automated Launch/Land	3
	3 Day (6 in emergency)	4
	Resupply Missions	3
	Rescue Missions	4
	Low Earth Orbit	3
	Satellite Recovery System	3
	Satellite Delivery	5
	Satellite Repair	3
	Multiple Orbits/Mission	3
	Constant Ground Contact	5
	Microgravity Experiments	3
	Non-damaging Accelerations	4
	Deposit/Recover Fuel in Space	3
Cost Effective		
	Single Stage	4
	No Certification	4
	Reusable	5
	Man-Rated	5
	Long Life/Low Maintenance	5
	Global Launch Facilities	2
	Moderate to Low Risk (Proven Tech.)	4
	Low Initial Cost	3

Table 1.1 Single Stage to Orbit Requirements and Importance (5 is highest and 1 is lowest importance)

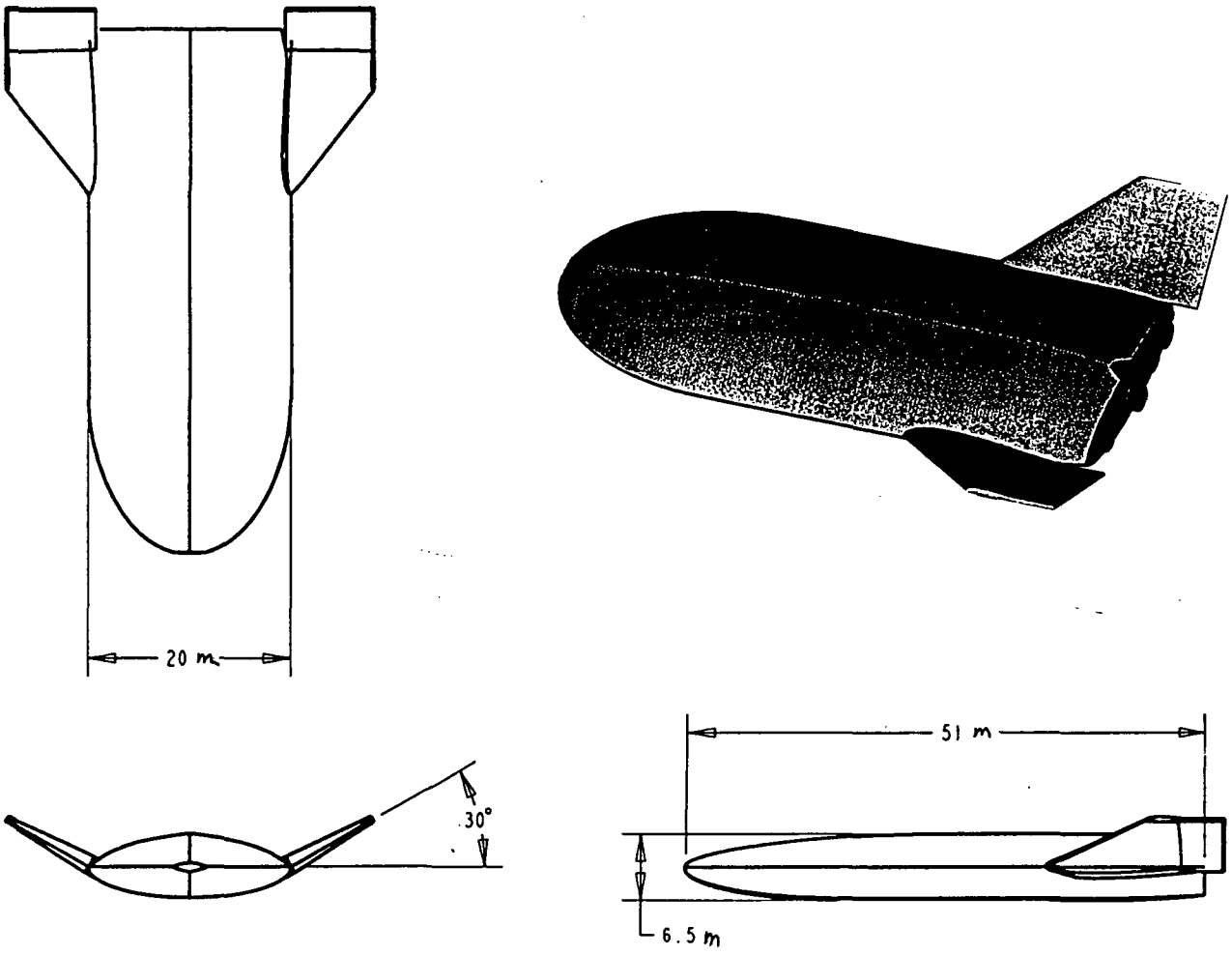

Figure 1.1 Exterior View of SSTO Vehicle

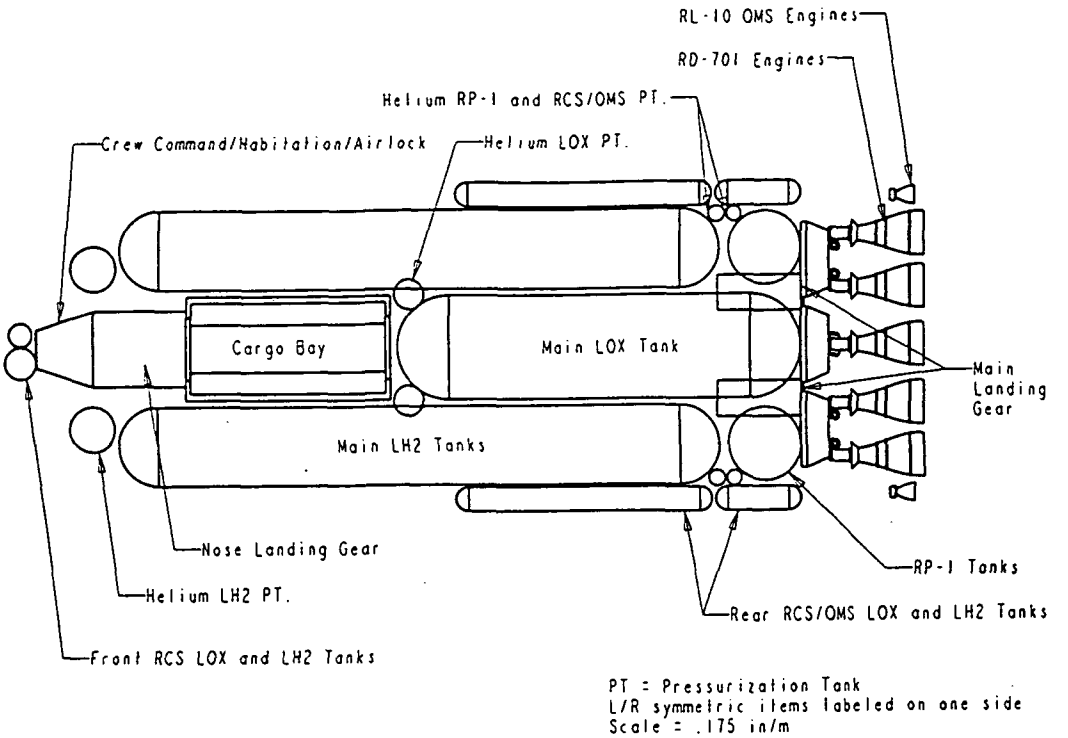

Mass Table

Component	Mass (kg)
Crew Systems / Avionics	7,000
Fuel Tanks	10,200
Fuel Tank Insulation	500
Orbital Maneuvering Fuel	15,000
Payload	9,100
Radiation Shielding	1,000
RD-701 Engines (3)	13,700
RL-10 OMS Engines (2) and RCS Jets (48)	2,000
Thermal Protection System	10,500
Structures: Skin	2,000
Frame	9,000
Landing System	3,500
Propellants: Liquid Oxygen	496,700
Liquid Hydrogen	55,400
RP-1	45,300
Empty Mass with out Orbital Fuel	68,000
Empty Mass with Orbital Fuel	83,000
Takeoff Mass	680,400
Landing Mass (with payload)	68,000
Landing Mass (without payload)	58,900

Figure 1.2 Interior View of SSTO Vehicle

emphasizes customer requirements in the conceptual design of the SSTO vehicle. Its detailed charts served as both a preliminary feature data-base and as a decision-making tool.

The fundamental principal that guided the design process was the interpretation of the customer requirements and their relative importance. After the design requirements had been formally outlined by Northwest Airlines, they were compiled and then
ranked by Northwest to facilitate in the QFD evaluation. Table 1.1 shows the rank of each design criteria.

After the customer requirements had been ranked and compiled on a QFD chart, the design team compiled over 100 "Hows," methods or design features, which would support the realization of those requirements. These ideas constituted the first list of features that would be incorporated into the design. The list was reviewed and added to the requirements to create a full QFD chart. (This chart can be found in Appendix B.) The features that ranked the highest in the QFD evaluation are listed in Table 1.2.

Each of these features or concepts is included in the final conceptual design. The QFD process was helpful in several cases where it was not obvious which feature or concept should be integrated into the design.

The QFD process was used to determine the position of the liquid oxygen and liquid hydrogen tank insulation. The preliminary proposal was to incorporate the insulation on the inside of these tanks. However, after completing a QFD ranking of inside versus outside insulation, it was revealed that the outside insulation met more of the customer requirements. It was easier to manufacture and apply and would be easier to inspect and replace.

Another instance in which the QFD process was used by the design team was in the choice of a launch site. Several potential launch sites were rated against customer requirements to isolate the three most advantageous sites in the world. Please see the Section 2.0 for complete details on this implementation of QFD.

Finally, the decision to implement the horizontal landing configuration was influenced by the customer requirements as rated by QFD. The following discussion outlines the role of QFD and other factors in making this decision.

The horizontal or vertical landing decision was difficult, it was unclear whether the technical considerations justified contradicting the large qualitative customer preference for horizontal land presented by QFD. The advantages and disadvantages for each configuration were intensely debated. These considerations are listed in Table 1.4.

The vertical land configuration was attractive for the reasons listed in Table 1.4. The low airspace and lack of wing aerodynamic heating were the primary advantages of this configuration. However, the fuel requirement for such a vehicle was the major disadvantage.

Safety Factors in Design	Simple Maintenance
No wing configuration	Horizontal Land
Rocket Propulsion	Modular Cargo Bays
Multiple Module Sizes	Carbon Tri-mixture of Fuels
Proven Materials	Full Maintenance and Supply at all Ports
Pre-Packaged Metal Tiles	Cargo Arm
Separate Cryogenic Tanks	Modular Crew/ Avionics Components
Side Loading Canister	Specialized Human Cargo Module
Module Size/Weight Limit	Incorporate New Inspection Techniques
Ports at Various Points on Earth	Standardized Manufacturing
Lightweight Durable Materials	Global Positioning System Capable
Modular Launch and Recovery Systems	Fail-Safe Landing System
Outside Insulation for tanks	

Table 1.2 Top-Rated QFD Hows

Horizontal vs. Vertical Launch and Landing Configurations. The launching and landing configuration decision was the first and most important decision made in the conceptual design. The discussion that led to a vertically-launched craft was much less intricate than the deliberation which concluded that a horizontally-launched craft was the most appropriate. The QFD ranking process was used to identify how each would compliment the customer requirements. The factors that weighedmost heavily in the ranking were mission abort, all-weather launches, low airspace requirements, man-rating, and risk factors. Table 1.3 shows the absolute rankings given each of configurations considered.

Although the QFD process identified the horizontal launch as the most appropriate launch method by a small margin, technical considerations caused the vertical option to be chosen. Vertical launch was selected primarily there was no proven propulsion system that was suitable for a horizontal launch.

Configuration	Rank
Horizontal Launch	87
Vertical Launch	75
Horizontal Land	113
Vertical Land	60
Lifting Body/Vertical Land	88

Table 1.3 Launch and Land Configuration Ranking

A vertical land configuration with a lifting body was a means by which the fuel requirements could be lessened. The shape would also give this design the control benefits of the horizontally landed craft. It was this choice, along with the horizontally landing which, which was most seriously considered by the design team.

A horizontally landed craft has distinct advantages that caused it to be selected as the land configuration for the SSTO vehicle. The most important consideration, which became even more apparent as the design evolved, was that this arrangement would allow for massive fuel savings over the life of the craft, and allow it to remain a large, but manageable vehicle. Another important factor was this configuration's capability to abort. A horizontally landing craft, with its ability to glide to abort landing sites allows many more abort options. The structural considerations were not unmanageable because the spacecraft would land without fuel. Finally, the wing heating considerations could be overcome by using advanced yet proven heat shielding materials.

After considering the QFD analysis and the technical considerations above the team decided to adopt a horizontally landing vehicle. This choice has proven to be are more advantageous than the vertical land option. The fuel savings, abort possibility, and size reduction gained by the vertical launch and horizontal land make this the optimal configuration.

Horizontal Land

Advantages	Disadvantages
Cross Range Benefits	*Large Airspace Requirement*
Controllability in Low Orbit	*Structural Loading on Land*
Less Fuel/Weight	*Wing Heating*
Orbital Plane Changes	*Multiple Control Surfaces*
Manually Landable	
Better Abort Scenarios	
Faster Turnaround Time	

Vertical Land

Advantages	Disadvantages
Low Airspace Requirements	*Fewer Abort Possibilities*
No Heating of Wings	*More Fuel/Weight*
Structural Advantages	*Slower Turnaround Time*
Lower Maintenance	

Table 1.4 Horizontal and Vertical Land Comparison

1.5 Cost Evaluation Summary

In order to prove that the designed SSTO vehicle is commercially viable and cost-effective, a cost analysis was performed. Table 1.5 indicates that the construction cost of one spacecraft totals just over 400 million dollars. This number is entirely an estimate since some component costs could not be obtained and certain aspects of the design haven't been finalized. As detailed in Section 5.0, the estimated launch cost is $9,196,000 including fuel and labor (the main contribution of which is fuel). One earth-based spaceport facility will cost $192,640,000 for construction. In the event of an abort which results in a safe landing, it is estimated that the commercial transportation company will only lose $9,160,900, most of this amount coming from lost fuel. In comparison, the Space Shuttle averages $370 million per flight.[2]

Component	Estimated Cost ($)
Crew and Internal Systems	120,000,000
Total Engine Cost	25,080,000
Radiation Shielding	33,000
Structures:	
Frame and Skin	175,000,000
Landing Gear	300,000
Fuel Tanks	31,200,000
Thermal Protection System	50,000,000
Total:	401,613,000

Table 1.5 Vehicle Construction Cost

Fuel costs will most likely decrease as the design progresses. Weight-saving techniques will probably lower the number of engines, thus lowering the amount of fuel needed. Also, fuel costs are based on current numbers used for the Space Shuttle. Since the designed SSTO vehicle requires much more liquid fuel than the Space Shuttle, buying in bulk supplies will reduce the total fuel cost. Bulk estimates will be supplied in the future research.

2.0 MISSION ANALYSIS

2.1 Introduction

The first step in designing the SSTO vehicle is defining the vehicle requirements. These requirements are necessary to create a safe and commercially viable vehicle. The vehicle requirements can be divided into mission requirements, design guidelines, and safety requirements. Mission requirements define what types of missions the vehicle needs to fulfill. Design guidelines specify the features the vehicle must have to complete these missions. Safety requirements detail the required features for a safe vehicle. Finally, abort scenarios need to be defined for fail-safe operation of the craft.

2.2 Mission Requirements

The primary mission requirements for the SSTO vehicle are as follows:

Commercial Missions
- Low-cost launch of commercial satellites and payloads
- Satellite retrieval and repair

Space Station Requirements
- Crew rotation
- Resupply and service missions

Other Missions
- Department of Defense
- Scientific support.

Commercial Requirements. The focus of the SSTO design is to meet the commercial needs of companies like Northwest Airlines. Northwest specified that the SSTO vehicle was to provide commercially viable and affordable access to space. The primary mission Northwest requires is the low-cost launching of commercial satellites and scientific payloads into low earth orbit (LEO). The launch system must be considered very safe and reliable, thereby reducing insurance costs to an acceptable level.

Along with the launching of payloads, Northwest has expressed the desire to retrieve and repair satellites already in orbit. This is a potentially very lucrative market that has yet to be exploited to its full potential. Therefore, this capability is included in the design of the SSTO vehicle.

The class of payloads that the SSTO vehicle will carry is currently carried by Atlas, Delta, and Ariane launch vehicles. These vehicles cost approximately 70 to 100 million dollars to build and launch. The SSTO vehicle, by being a single stage reusable vehicle, will dramatically reduce the cost of launching payloads. It is this reduction in cost that will make the SSTO vehicle a viable commercial proposition.

Space Station Requirements. Space stations are another potential market niche for the SSTO vehicle. Crew rotation, station resupply and service, are services that the SSTO vehicle could provide. The requirements needed to perform these services have been included in all design criteria. Modifications of the SSTO vehicle required for this mission have not yet been determined. Hence, additional costs incurred by including these missions into the requirements are not yet known.

Other Missions. Other mission include both Department of Defense (DOD) missions and scientific support missions. DOD missions are for the most part very similar to most commercial missions. Currently, these missions are performed by the Atlas and Delta launch vehicles. The vehicles launch the same size and mass of payloads that the SSTO vehicle will launch. Therefore, the inclusion of DOD missions into the mission requirements causes no significant problems.

2.3 Mission Design Guidelines

Payload Capability. Research into payload mass revealed that 90% of all future payloads delivered to LEO are under 9070 kg (20,000 lbm)[3]. Furthermore, 80% of all future commercial satellites are under this mass as well[4]. While most commercial satellites are not in LEO, the 9070 kg mass refers to their low earth orbit equivalent. That is, the 9070 kg mass refers to the mass of the payload and the booster which delivers it to its final orbit. Because the vast majority of payloads are in the 9070 kg range, this payload capability will provide for the most commercially viable payload size. Any larger capability would be wasted on most missions, and thus this added capability would be uneconomical.

Research into the average payload size reveals that 90% of all future payloads are under 7.3 m (20 ft.) in length[3]. Furthermore, the average payload is approximately 3.66 m in diameter and 5.5 m long (10 ft by 15 ft). This leads to a minimum payload bay that is 5.5 m in diameter and 7.3 m long (15 ft by 20 ft). However,

Payload Capability: Maximum: Average:	 9070 kg (20,000 lbm) 7711 kg (17,000 lbm)
Cargo Bay:	Diameter: 4.57 m (15 ft) Length: 9.09 m (30 ft) Modular Cargo Containers
Orbit	460-830 km (240-450 n.mi.)
Crew	2
Mission Duration: Planned: Maximum:	 2-3 Days 6 Days
Turnaround Time:	3 Days
Launch Sites:	White Sands, NM Kennedy Space Center, FL Australia

Table 2.1 Design Guideline Table

Northwest has requested a larger payload bay that is 3.66 m (10 ft) longer. This will meet all minimum commercial requirements and allow for future growth.

The payload bay will contain modular cargo containers. These containers will be standardized much like the cargo containers on current cargo aircraft. The SSTO vehicle will supply the container and its power supply. The customer will be required to fit the payload to the container.

Currently two kinds containers are planned. The first will be a non-pressurized container used for deploying and retrieving satellites. This container will contain a turn table to spin satellites before deployment, a necessary procedure for geosynchronous-orbiting (GEO) satellites. The second kind of container will be pressurized. This will be used for scientific experiments that require a controlled environment.

The payload bay will also have the facilities for a cargo arm. This arm will be removable; it will only be carried on missions that require use of it. These missions include the retrieval of satellites and the deployment of LEO satellites. Removing the arm will save fuel on missions that do not require use of it.

Crew Capacity. A two person crew was chosen for several reasons. First, it provides a redundancy should one crew member be unable to pilot or control the vehicle. Therefore, both crew members will be fully qualified to pilot and perform all mission requirements. Secondly, the second crew member provides additional manpower which may be needed for a multiple-mission trip. Finally, Northwest requested a two person crew. Their extensive experience with piloting led to the conclusion that a two person crew would be the optimum size for a craft of this complexity.

Mission Duration. Northwest gave the 2-3 day mission duration as an SSTO vehicle requirement. An additional 3 days are used as a safety factor, giving a total capability of 6 days in space.

Turnaround Time. The three day requirement came from an analysis of Northwest's operations. This is considered the most reasonable and economic time limit considering the complexity of the SSTO vehicle and its related systems.

Launch Sites. A QFD chart was used to help rank the locations that were chosen as possible sites for space ports. The orbital mechanical requirements were considered concerning the best latitude for launch, and the results were taken into account. Launch, recovery, and turnaround operations effects were also considered. It was decided to have initially three space ports, two in the U.S. and one elsewhere. Because currently 80% of all commercial satellites are manufactured in the United States[5], it makes sense to have the primary launch facilities in the U.S. Furthermore, the U.S. spaceports are to be located on opposite sides of the country, thereby maximizing their utility.

White Sands, NM, is the initial launch facility. This will be the test facility for the SSTO vehicle and the first operational space port. White Sands was chosen because it currently has many of the facilities needed for the SSTO vehicle. Principal among these is the long runway needed for landing.

Kennedy was chosen for many of the same reasons as White Sands. However, some concern was raised over the use of government facilities for a private industry. Given the current political and economic climate, this should not be a problem. Indeed, current commercial airports are not owned by airlines, rather by the federal and state governments. The building of spaceports would simply be an extension of the current airport system.

The information available on Australia was very limited. Therefore, contact was made with both the Australian embassy and the Australian Consulate General in New York. They provided information concerning the economic incentives that Australia would likely give to Northwest if a company like Northwest were to construct a facility there. The economic climate is very favorable in Australia for this type of a project and is forecasted to continue to be so. This was all factored into the QFD chart that was ultimately used to determine locations for spaceports.

2.4 Safety Requirements

Crew safety is of utmost importance in the design of the SSTO vehicle. The safety requirements for the SSTO vehicle define the limits to which the vehicle can be designed and operated.

Crew Safety. The vehicle must be man-rated. This term has not yet been fully defined. However, it is taken here to mean that the SSTO vehicle must be of an equivalent safety level as a commercial airliner. The craft must have controlled flight from launch to landing. From liftoff, the SSTO vehicle must be fail-safe. It must be able to abort to a safe landing at any point during the mission.

The vehicle must have assured crew return capabilities. In the event of an emergency, the vehicle must be able to return the crew safely to earth or be able to transfer the crew to another craft which can execute a crew return. This mandates a full range of abort scenarios, covering the entire flight as well as redundant systems.

The craft must have engine-out capability. This means that the loss of one engine can not cause a catastrophic failure. In the event of the loss of an engine, at any point during the flight, the vehicle must be able to either abort or complete the mission and land safely.

In the event of an emergency, the craft must be able to extend its mission length up to 3 days after the appointed end of mission. As a result, the SSTO vehicle must contain enough food, water, air, and power to sustain the crew for up to 6 days on every mission.

An on-pad egress system is necessary for the vehicle. This system must provide a quick, safe exit to the crew in the case of an on-pad emergency.

The crew must have adequate protection from radiation. The vehicle needs to have sufficient radiation shielding to protect the crew for up to 6 days of normal levels of cosmic radiation. In addition, the vehicle must be able to shield the crew in the event of a solar flare. Since solar flares are brief and infrequent, the solar flare shielding does not need to cover the entire vehicle, but it must be sufficient to protect the crew for short periods of time.

The crew has to be able to pilot the vehicle in the event that the automatic control systems fail. The vehicle needs to provide the pilots with an electronic display system adequate to safely pilot the vehicle to a landing site.

The vehicle must have redundant systems. No single point failure can cause the loss of the SSTO vehicle or the crew.

G-forces can not pose a threat to the crew or the payload. The maximum allowable acceleration of the SSTO vehicle is 3 g's. This will protect the crew, craft, and payload from excessive g-forces.

Fuel Safety. In handling RP-1, current jet fuel safety requirements for commercial aircraft apply. Both liquid hydrogen and liquid oxygen have been used as propulsion fuels for many decades, and general safety standards have been established. Neither liquid hydrogen or liquid oxygen provide an environmental risk if spilled or dumped. In addition, airliners regularly dump JP1, which is the same fuel as RP-1, with minimal environmental damage.

A fuel dumping system is necessary for the RP-1, liquid hydrogen, and liquid oxygen. This is necessary to empty the tanks quickly in the event that the craft is required to land before it has burned all of its fuel. If ejection is not done, the SSTO vehicle will have too much mass, and landing will create damaging stresses on the structure of the vehicle.

2.5 Abort Scenarios

There are four abort scenarios planned for the SSTO vehicle. These are Return to Launch Site (RTLS), Abort Once Around (AOA), Abort to Orbit (ATO), and Abort to Alternate Site (ATAS).

Return to Launch Site. For the Return to Launch Site abort, or RTLS, the SSTO vehicle would return to the spaceport from which it was launched and land. This would be done without violating dynamic pressure and heating load restrictions in the event of a system failure that would make the SSTO vehicle unable to obtain its orbit. This abort could be initiated from 0.9 s after launch with a single engine out failure. At approximately ten seconds, the vehicle would begin a pitch over maneuver. The SSTO vehicle would continue climbing, burning, and/or dumping enough propellant to allow for a safe landing weight after turning around. After the SSTO vehicle turns around, a nominal landing would follow.

Abort Once Around. The Abort Once Around (AOA) scenario would occur when the craft has left the window from which an RTLS abort would occur. The SSTO vehicle would fly once around the planet before returning to land at the launch site. The minimum altitude necessary for the SSTO vehicle to carry out this abort is 120 km (65 n.mi). This abort may be used when multiple engines fail before an Abort to Orbit can be performed.

Abort to Orbit. Abort to Orbit (ATO) would be used after the vehicle obtains a critical altitude in which it would be impossible to maneuver the vehicle due to aerodynamic forces. This may occur, for instance, if a main engine fails during the latter part of the ascent. A low earth orbit (LEO) would then be achieved. The lowest altitude that the craft can safely orbit is 185 km (100 n.mi.). At this orbit the vehicle can remain stable for up to 50 hrs, awaiting a reentry window or rescue. Depending on the severity of the problem during launch, the SSTO vehicle could achieve a higher abort orbit. It would then be possible to carry out some or all of the mission from this lower than planned orbit.

Abort to Alternate Site. The final abort is the Abort to Alternate Site. This would occur in the cases that either the vehicle cannot return to the original launch site, if the launch site becomes unavailable, or if the vehicle cannot achieve enough momentum to make it once around the earth. The vehicle could land at any runway of adequate length or at one of the primary landing sites (spaceports).

A propulsive analysis has determined that the vehicle can abort after 0.9 seconds. During an abort after two seconds, the vehicle would decelerate, drop approximately one meter, and after eleven seconds, would start to accelerate again. These figures can be readily compared with those of the Space Shuttle, which is fail-safe at 40 seconds and fail-operational at 166 seconds. Therefore, the SSTO vehicle provides a substantial improvement in abort capabilities.

Cost Evaluation. The cost analysis for an abort can be broken up into the following categories: fuel and man-hours. Table 2.2 displays the abort cost estimates. The approximate cost of the man hours lost in a mission abort is arrived at by using the following:

- 3 days
  - 3 shifts/day
  - 25 people per shift
  - 8 hours per shift
  - averaging $40 per hour

Fuel:	
RP-1	$7,725
LO_2	$57,565
LH_2	$261,029
Manpower:	$72,000
Total:	$398,320

Table 2.2 Abort Cost Table

2.6 Conclusion

The mission requirements for the SSTO vehicle provide for a commercially viable vehicle which is able to effectively compete in the space launch industry. The safety requirements ensure the safety of the crew, craft, and payload. The abort scenarios detail the various options the vehicle has to safely land in any emergency.

3.0 SYSTEMS LAYOUT

3.1 Introduction

To design a successful SSTO vehicle it is first necessary to determine the design requirements. Then an initial configuration must be chosen based on the decided design criteria. In doing so the configuration is compared to alternate designs to determine the most efficient means of design and revised accordingly. Once the basic requirements are met the conceptual design is finalized and the design is analyzed and tested to provide proof of concept.

This section covers the basic sizing, placing of components, and the downsizing of the overall SSTO dimensions. The course of action was to first come up with a basic design idea and then optimize the size and weight of the SSTO. Through an iterative process of weight reduction and component placement it was possible to continuously down-size the overall vehicle design, conserving weight and cost, until an optimized design for the SSTO was achieved.

With these requirements in mind, a basic design was drawn up, based partially on a vehicle concept created by Lockheed.[6] The design consisted of a vertical take-off horizontal land lifting body design. The optimization process consisted of choosing the placement and size of the internal components such that the external shell surface area could be reduced to lower the drag and weight of the SSTO. Some of the basic ideas involved with this process is given below:

- Keep components close to center of mass and landing gear locations to reduce stress on structure. Since there would be a shorter moment arm from each component on the structure this would result in lower bending moments.

- Optimize shape of components. By choosing an optimal shape, the surface area for a given volume can be reduced, saving weight.

- Reduce the external shell of the SSTO to reduce the drag on the vehicle and lower the weight.

- Maintain a shell design that incorporates a lifting body configuration.

These basic design requirements defined the course of action to optimize the SSTO design by lowering weight, reducing drag, and reducing cost.

3.2 Layout Design Requirements

Size Optimization of Individual Components. The length of the craft is an important consideration. The shorter the vehicle is, the easier it will be to control. Also by reducing the size, the drag on the vehicle and weight of the vehicle will be reduced.

Fuel tanks make up the major portion of the internal volume of the vehicle. By optimizing the shape of the tanks a large amount of weight can be saved. Knowing that a sphere has greatest volume compared to surface area it was chosen as the base design for the fuel tanks. Because of the elongated and non spherical shape of the vehicle the tanks were elongated into cylinders with spherical end caps. The spherical end caps were chosen for two reasons:

- To reduce surface area.
- To distribute the pressure on the tank evenly for reduced stress.

To optimize the cylindrical sections of the tank, the radius of the tanks, rather then the length, was increased as much as possible to maintain the needed volume. This helped in reducing the length of the SSTO, and also reduced the surface area of the tanks.

An airlock connects the habitation module, the payload bay, and the exterior. The airlock is designed in the form of an inverted "T" connecting the crew module to the payload bay and provides access to space. This configuration saves space that would otherwise be wasted. The extra space in the airlock module will contain avionics and life support supplies.

The vertical stabilizers are sized for optimal stability and control. The airfoil has a symmetric cross-section. Due to the hypersonic flight profile, the stabilizers are smooth from root to tip and angled back to avoid the re-entry burn that would disable them.

Placement Optimization of Individual Components. Volume restrictions due to the shape of the SSTO dictate that the fuel tanks be placed in the aft part of the craft. This being the case, the command and habitation modules and payload bay are in the forward section of the vehicle.

The main engines are on the aft of the ship in a configuration that optimizes space. To reduce bending moments the engines need to be as close to the center of the back of the vehicle as possible. The configuration consists of three main RD-701 engines and two smaller RL-10 engines across the rear of the SSTO. The RL-10 Orbital Maneuvering System (OMS) and Reaction Control System (RCS) engines are placed towards the outside edges of the rear for better control. By placing them as far from the center of mass as possible, the moment arms for the maneuvering engines are increased, providing greater sensitivity and better maneuverability. The RCS engines on the nose of the ship are similar to the configuration used on the Space Shuttle. That is, four sets of three nozzles are placed so that they are mutually orthogonal.

The initial design had the fuel tanks in a row with a reduced radius as they moved away from the center axis. The liquid oxygen tank was surrounded by two liquid hydrogen tanks and two kerosene tanks on the end. (See Fig. 3.1.) To reduce the surface area of the tanks, and hence the weight, the kerosene tanks were changed to spheres in the second design. (See Fig. 3.2.) With the need for more fuel, the tanks were upsized and the kerosene tanks turned into cylinders to meet the volume restrictions within the SSTO. (See Fig. 3.3.)

The landing gear were placed under the liquid hydrogen tanks and in front of the crew modules in a tricycle formation. This gives a 14 m base to the rear landing gear for stability in landing. The gear is modeled after the Space Shuttle's landing gear.

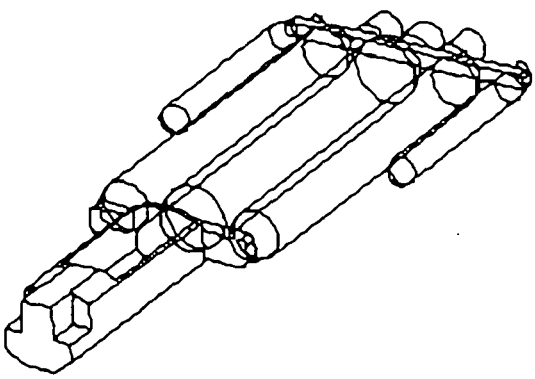

Figure 3.1 Initial Internal Design

The vertical control surfaces are sized to optimize stability and control. They are 40 degrees from vertical so they can assist in the control of the SSTO vehicle in more than one axis of motion. The SSTO vehicle will re-enter the atmosphere at high angels of attack to divert the airflow around the upper surface and the stabilizers. This insures that the thermal heating encountered will not melt them.

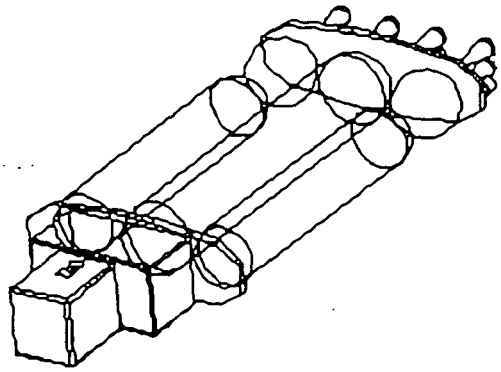

Figure 3.2 Second Internal Design

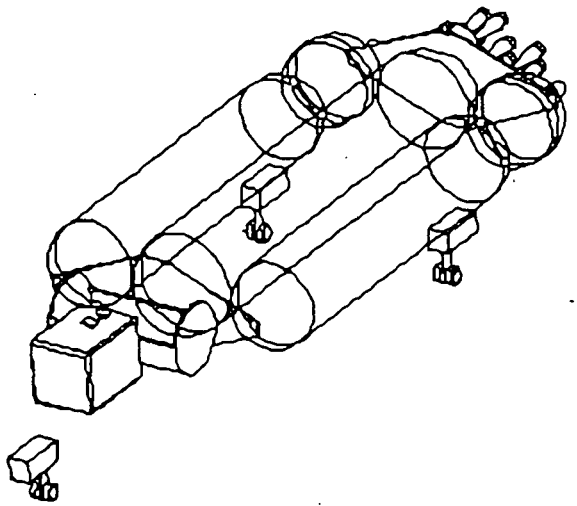

Figure 3.3 Third Internal Design

Down-Sizing the Vehicle. The vehicle has evolved over several designs. Initially, the vehicle was very angular. It was equipped with rockets and ram jets. (See Appendix B, Fig. 1.) In the second stage of evolution, after the launch/landing attitudes were specified, the vehicle was modeled after Lockheed's Skunkworks[7] vehicle. (See Appendix B, Fig. 2.) In the next design, the Skunkworks configurations was modified. A flatter ship was the result. (See Appendix B, Fig. 3.) The fourth design marked a fundamental shift in appearance. The craft was longer and slimmer, but still a little boxy. (See Appendix B, Fig. 4.) The fifth generation of the ship eliminated the boxiness of the previous design. No sharp corners or completely flat surfaces (with the exception of the aft panel) existed. (See Appendix B, Fig. 5.) However, the vehicle was too short.

The sixth design was a lengthened version of the previous design. It had the benefit of being completely smooth on all surfaces and having the necessary internal volume to house the fuel tanks. (See Appendix B, Fig. 6.) However, this design wasted approximately 10 m at the nose of the craft. The final design was the most aerodynamic. The geometry was created utilizing a matrix produced by a lifting body software program called Fusex. The final vehicle is approximately 51 m long, 20 m wide, and 6.5 m tall.

3.3 Detailed Design Elements of Configuration

Elements Based on Lockheed Concept. Lockheed[8] showed they had a viable concept for a vertical-launch/horizontal-landing SSTO vehicle that was designed to meet the launching requirements of commercial applications by reducing launch cost to $1100/kg ($500/lb). The current design contains all the basic elements that Lockheed has outlined for their conceptual design. By publishing their ideas for a conceptual SSTO vehicle, Lockheed has demonstrated that their design is a practical solution for the need of a cheaper low earth orbit transport system. Their design has thus been used as a basis to model the current design after.

The Space Shuttle takes about 3 to 6 months to prepare it for launch again. This enormous turnaround time is part of the reason why a Space Shuttle-type of commercial launch vehicle is not practical at this point in time. A company would lose money while the vehicle is sitting on the ground for maintenance. The fact has driven the need for an improved commercial design.

Lockheed's design will put a 18,181.8 kg (40,000 lb) payload into LEO at 160 km (100 n.mi.). The airframe design is based on NASA's lifting body research and resembles the X-24 lifting body design that flew during the mid 1960's to mid 1970's. Their craft is not designed to achieve orbit in the case of an engine failure. Instead, it is designed to shut down the corresponding engine on the opposite side and continue to burn fuel to lighten the weight until it can land at a safe weight with payload intact. This design has a lift to drag ratio at hypersonic speeds of less than 1, but becomes a good glider at slow speeds, reaching a lift to drag ratio of 5.5-6, allowing it to land around 218 km/hr (135 knots). The vertical fins are shielded by the belly of the SSTO vehicle during hypersonic speeds by maintaining an angle of attack of 45°. This effectively hides the fins from the freestream flow and protects them from heating effects. At subsonic speeds the SSTO vehicle will maintain an angle of attack of a more moderate 10°. This SSTO vehicle concept has been designed for a turnaround time of about 7 days.

Some of the design requirements specified for the SSTO project are fulfilled by Lockheed's SSTO vehicle. Therefore, the current design is modeled after the skunkwork's design. The current design will meet the requirements of a short turnaround time while demonstrating safe abortability in which the cargo is recovered intact.

Fuel Tank Shape Optimization. Optimal fuel tank design requires maintaining the specified volume of the tank while decreasing the surface area of the tank as much as possible. This results in a decreased amount of material used, lower weight and cost, and lowered distribution of weight, which means a smaller structure to support the tanks. The best shape to achieve the smallest surface area for a specified volume is a sphere. The problem arises that if all the fuel tanks were made into spheres, the resulting design would be a grossly misshapen SSTO vehicle instead of the lifting body design that is desired. The compromise is the use of cylindrical tanks with half sphere ends. Obviously, as the length of the cylindrical portion of the tank decreases and the radius increases to maintain volume, the shape will eventually become a sphere. The tank surface area is optimized by minimizing the length of the tank while increasing the radius to maintain volume. This process achieves the goal of reducing the surface area of the tanks.

The largest design restriction is fitting all the internal components to an external shell that has an efficient shape for a lifting body. The tank dimensions are thus dictated by the internal space provided by the aerodynamic shell used. The shape and dimensions of the internal components and the shell are thus directly dependent upon each other. Any modification to the shell or internal space requirements will often drastically change the design of the other.

The internal tank dimensions can only be altered by increasing or decreasing the entire size of the SSTO vehicle. If the tank size increases, the shell size increases, resulting in more weight, cost, and drag. On the other hand, if a small external shell is maintained, either multiple smaller tanks or flattened-out cylindrical tanks will have to be employed. Flattening out the tanks and keeping the number of tanks to a minimum would be the best alternative option assuming the misshapen tanks are still structurally sound. This method will result in a smaller total surface area for the tanks rather then a large number of smaller tanks. Both methods will increase surface area resulting in higher weight and cost for the tanks, but the SSTO shell is minimized reducing weight and drag even more.

The remaining problem is to correspondingly optimize the external shell size along with tank dimensions so that a solution can be found that minimizes both as a working unit. The shell has been designed to hold the internal components without much emphasis put on a completely optimal lifting body design. The fuel tanks have been optimized to dimensions that could reasonably fit within a lifting body shell design while maintaining volume and location close to the center of mass. Once a more exact model of the aeroshell is obtained, an iterative method of optimization will begin to come up with a design to satisfy

requirements for tank dimensions and a low drag lifting body design.

Placement and Weight Distribution. The next concern with fuel tank placement and components in general is their placement from the center of mass and center of thrust. Through the centers of mass and thrust is the imaginary line through which the resultant mass and thrust vectors act respectively. Structurally, the distance from the resultant center of mass/center of thrust of the SSTO vehicle to each component's individual center of mass should be minimized. The moment arm induced on the structure is then reduced. The smaller the moment arm the less stress placed on the structure. The resulting structure becomes lighter, which reduces weight and cost. Ideally it is desired to have no moment arm between the components and the resultant centers of mass and thrust and to have the center of thrust act through the center of mass. The lifting body design has the less than optimal feature of having to spread out the components horizontally in such a way that they fit within the corresponding shell design. Since the components are spread out, a larger structure is required, which will increase weight and cost as the components become more and more spaced out. Thus the design also compromises between component placement within the shell and structure size.

Ideally, the center of thrust should act through the center of mass for control purposes. This is achieved by distributing the weight of the fuel and components equally on either side of the central x-axis and z-axis of the SSTO vehicle. (The axes are displayed in Fig. 3.1.) The current SSTO vehicle design is symmetric about the x-axis but is not about the x-y plane. Since all the weight of the thermal heat shielding is below the center line of the SSTO vehicle, the center of mass location is slightly below the center of thrust location of the SSTO vehicle. When the SSTO vehicle is fully fueled, the center of mass is for all practical purposes at the center of thrust since the centrally located fuel comprises about ninety percent of the total weight of the SSTO vehicle. When the SSTO vehicle is empty, the center of mass[9] location moves about 0.62 meters down from the center plane (center of thrust) or in the negative z direction in our designated coordinate system (This is shown in Table 3.1 Center of Mass Locations). The slight offset of the center of mass location should not pose a major problem to control when gliding during landing.

The even smaller moment arm observed during takeoff should be easily corrected by the gimbaling of the engine nozzles and is probably negligible compared to the atmospheric disturbances encountered during launch.

The other concern with placement of components is that of the maneuvering engines. To make the maneuvering engines more effective and increase their sensitivity, they need to be placed as far from the center of mass as possible. This increases their moment arm to the center of mass thus increasing the resultant moment they can impose on the SSTO vehicle. The resulting SSTO vehicle response to de

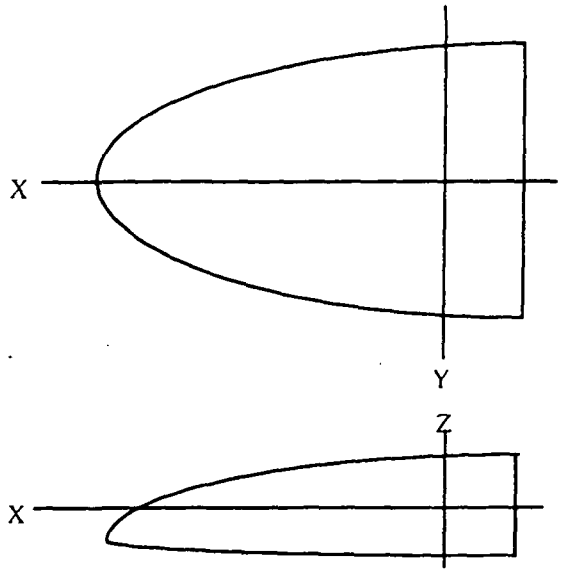

Note: Origin 5m from rear of SSTO shell

Figure 3.4 x-y-z Axes Placement

signated maneuvers should improve and possibly lower the amount of fuel needed to perform a maneuver. This results in the placement of the maneuvering engines as far away from the center of mass as space will allow.

The layout design goal was to come up with a reasonably optimized internal design for the components that optimized the tank surface area and maintained component location close to the center of mass. The accomplished designation of size and positioning of components allowed rough estimates for the center of mass and thrust locations along with moments of inertia about the x-, y-, and z-axes. (These are shown in the Vehicle Specification Sheet in Appendix A.) The goal of providing rough estimates of center of mass locations for the SSTO vehicle in several different payload and fuel scenarios was met. These calculated values for the center of mass are located in Table 3.1. Knowing approximate sizes and shapes of components enabled the calculation of the moments of inertia of the SSTO vehicle. The moments of inertia for the vehicle were calculated for the same fuel and payload scenarios as the centers of mass. The moments of inertia values are located in Table 3.2.

Future considerations require a detailed outer shell design that maps out the exact dimensions for an optimal lifting body at the approximate sizing of the current design. The placement, size, and number of fuel tanks will then be further modified along with the shell to come up with a working optimized model. The criteria are to maintain a light-weight compact structure, a tank shape that lends itself

to easy manufacturing, low mass, and strength, and a lifting body shell design with low surface area to minimize drag.

3.4 Requirement Satisfaction

Initially, a set of requirements was designed for the optimization of the mission. The final design of the SSTO vehicle was dictated by these requirements. Decisions involving the numbers, sizes, and placement of components were guided by these requirements.

The requirement for the SSTO vehicle to have engine-out capabilities dictates the number of engines used for takeoff. The use of three main engines for takeoff allows for engine-out capabilities for the final takeoff mass of the vehicle.

One requirement for the SSTO vehicle involves the ability to launch and recover satellites. This requirement was fulfilled by designing the payload bay to accommodate a satellite of today's dimensions and mass. A payload arm will also be included to aid in the satellite launch and recovery processes.

Quick turnaround and standardization of the SSTO vehicle are two of the most desired options for the final design of the vehicle. By designing the vehicle to make use of standardized cargo containers, the accomplishment of this objective is aided. The same cargo container would be provided for each customer. The container would provide power connections for the customer but keep the interface with the SSTO vehicle the same. This will cut down on the turnaround time of the vehicle by eliminating the need to reconfigure for each payload.

The vehicle is also required to be man-rated. This means the final design must have a safety level comparable to that of a commercial aircraft. To accomplish this, the orbiter is designed with redundancies and the ability to safely abort the mission if needed.

The need to use proven technology in the designing of the spacecraft is also required for the SSTO vehicle design. The equipment and systems used to design the SSTO vehicle are in service today. This eliminates delays in the building of the orbiter due to undeveloped equipment.

3.5 Layout Results

The mass distribution, centers of mass, and moments of inertia[10] are important to the management of the spacecraft. Figure 3.4 shows the placement of the x-, y-, and z-axes used while performing the distribution and calculations.

Mass Distribution. From the a systems layout perspective, the distribution of the mass evenly throughout the spacecraft and as close to the center of mass of the craft is important. The major mass contributing systems were distributed symmetrically with respect to the x-axis of the ship. These systems include the fuel tanks, engines, payload bay, and the crew areas. The masses of the components and a rendering of the final layout can be found in Appendix A.

The fuel tanks are placed symmetrically with respect to the x-axis and centered on the y-axis. The liquid oxygen is contained in one fuel tank and centered in the ship, placed on the x-axis. The liquid hydrogen fuel is divided into two tanks and placed on either side of the oxygen tank. The fronts of the oxygen and two hydrogen tanks are aligned. The kerosene fuel is also divided into two tanks. These tanks are placed on either side of the oxygen tank, lined up at the rear of the tanks.

The payload bay, when full, makes a major contribution to the mass of the SSTO vehicle: 9,072 kg (20,000 lb) when full and estimated at zero mass for no load conditions. The payload bay is located in front of the fuel tanks. The crew areas include the habitation module, the command module, and the airlock. The mass of these systems is located in front of the payload bay.

The final major contribution to the vehicle's mass comes from the main propulsion engines. These engines are distributed across the rear of the SSTO vehicle, behind the fuel tank configuration.

All other systems are distributed throughout the vehicle. These systems include the following: structures, outer shell, radiation shielding for the command module, the thermal protection system, and the OMS/RCS engines.

Centers of Mass. For proper analysis of the actions of the SSTO vehicle during maneuvers, the centers of mass with respect to each axis are determined. The x value of the center of mass is positive towards the nose of the ship. The y value is positive towards the left wing and the z value is positive when traveling up from the origin. The calculated values for the centers of mass are found in Table 3.1. These values are calculated from the coordinate system shown in Figure 3.4. It should be noted that the origin in Figure 3.4 is 5 meters forward from the rear of the SSTO shell. Thus if the center of mass locations are measured from the rear of the SSTO the center of mass locations in the x axis are 5 meters greater than designated in Table 3.1.

Moments of Inertia. The moments of inertia are calculated to help predict the actions of the ship. The moments are calculated about the center of mass locations for each flight scenario. The values are stated in Table 3.2.

3.6 Conclusion

The design requirements, design elements and configurations, requirement satisfaction, and layout results were discussed. Also, during the course of the design

process, several questions were looked at from the systems layout perspective.

In Section 3.2, the size and placement optimization of components are discussed, as well as the down-sizing of the vehicle. This overview gives the requirements for performing these actions. Section 3.3 gives the design elements for the final configuration versus the alternate configurations throughout the design process. This is where the processes laid out in section 3.2 are finalized and compared to prior designs. Section 3.4 details the fulfillment of the requirements set forth at the start of the SSTO vehicle's design. In section 3.5, the results for mass distribution, center of mass, and moments of inertia are presented.

The questions presented throughout the design process can be answered with the best design from a systems layout point of view. The ability to design a lifting-body vehicle with internal fuel tanks is visible in the final design. The vehicle, from a systems layout perspective, took on an internal tank design from the beginning.

Pitch, roll, and yaw motion control surfaces posed a problem in the design. Reconfiguration of the external shell of the SSTO vehicle to provide for control surfaces capable of withstanding reentry heat was a lengthy process. Changes in the desired shape of these surface to eliminate burning up during reentry caused several delays.

The reusability of the designed SSTO vehicle over the time period of years seams feasible from a systems layout view. The layout and design of the orbiter and its systems allow for maintenance and replacement of parts or entire systems on the vehicle. This will allow for the use of the vehicle over years, instead of replacing the entire vehicle when a system fails.

Flight Scenario	x-axis location (m)	y-axis location (m)	z-axis location (m)
With ascension fuel, orbital fuel, and payload	11.42	0.0	-0.10
With orbit fuel and payload and without ascension fuel	14.29	0.0	-0.55
With payload and without ascension or orbital fuel	16.72	0.0	-0.62
Without ascension fuel, orbital fuel, or payload	14.97	0.0	-0.72

Table 3.1 Center of Mass Locations[11]

Flight Scenario	I_{xx} (kgm^2)	I_{yy} (kgm^2)	I_{zz} (kgm^2)
With ascension fuel, orbital fuel, and payload	2.74×10^7	6.28×10^7	6.81×10^7
With orbit fuel and payload and without ascension fuel	3.41×10^6	2.70×10^7	2.95×10^7
With payload and without ascension or orbital fuel	1.81×10^6	2.34×10^7	2.43×10^7
Without ascension fuel, orbital fuel, or payload	1.76×10^6	2.28×10^7	2.37×10^7

Table 3.2 Moment of Inertia Values[12]

4.0 PROPULSION

4.1 Introduction

The requirements of a propulsion system are divided into two categories, performance and non-performance.

For the performance division, two phases must be satisfied: a boost phase and an upper stage phase. The boost phase needs a high thrust-to-weight ratio, high density propellants, a low area ratio, and a high power density. The upper stage phase will need a high specific impulse, deep throttling, and a high area ratio. The non-performance category involves reliability, maintainability, and reusability.

To meet these requirements, 3 RD-701 engines are used for the main propulsion system, along with two RL-10 space engines for orbital maneuvering.

4.2 Engine Requirements

Lifting Capability. The current vehicle mass at liftoff is 680,000 kg (1,500,000 lb) and the thrust of the 3 RD-701 main engines is 971,600 kg (2,142,000 lb). This

gives a thrust to weight ratio of 1.3. By using OPGUID, a computer program from Marshall Flight Center, we determined that the 680,000 kg (1,500,000 lb) liftoff mas would contain sufficient propellant to achieve orbit with an in space mass of 68040 kg (150,000 lb). The in space mass does not include orbital mechanics fuel but OPGUID takes this mass into account. The performance specifications for the main engines are listed in table 4.1.

Engine-Out Capability. *The SSTO vehicle is required to be able to complete its mission even if one of the main engines were to fail after liftoff.*

The solution of this problem was accomplished in 2 ways. First we determined the time it took to have the vehicle mass equal the thrust produced by 2 RD-701s. Using an initial mass of 680,400 kg (1,500,000 lb) and having a propellant flow rate of 2750 kg/s (6505 lb/s) the mass of the vehicle will equal the thrust of 2 engines at a burn time of 115sec.

The second method of analysis is by using Newton's Second Law and comparing the acceleration at the time of an engine loss and finding if the vehicle can build up enough acceleration and positive speed before striking the ground. The result of this method gave a time of 0.9 sec. Graphs 4.1 and 4.2 show graphically the results of these two methods. One thing to note is the fact that the times of fail safe may increase with the addition of a fuel dumping system.

Single Stage Requirement. The SSTO vehicle will be only a single vehicle. The engines used upon lift-off will carry the vehicle to LEO and will accompany the vehicle upon reentry. No part of the vehicle is ejected at any point of the mission excluding the fuel.

It should be noted that the two stages of the main engines refer to dissimilar thrust levels as opposed to different propulsive types. This creates a pseudo-staged vehicle and thusly provides a slightly lighter vehicle weight than other proposed SSTOs.

4.3 Primary Propulsion

Engine Specification. The SSTO vehicle uses 3 NPO Engergomash RD-701 engines for primary propulsion. The RD-701, in the boost mode, uses a tri-propellant mixture of LO_2, LH_2, and RP-1. This gives the high thrust-to-weight ratio that is desired and the high density propellants that are needed for the assent phase of the trajectory. The area ratio in the initial phase is 60, which satisfies the low area ratio needed for the boost phase. In thetrajectory mode, the RD-701 uses a LO_2-LH_2 fuel mixture, which gives the high I_{sp} value required. Also, since the thrust is cut approximately in half from the exclusion of RP-1 in the fuel mixture, the deep throttling requirement is satisfied. Finally, using an extendible nozzle skirt, the area ratio increases from 60 to 170, satisfying the high area ratio need in the second part of ascent, which begins at an altitude of approximately 10 km (6.21 mi.). See Table 4.1 for main engine specifications.

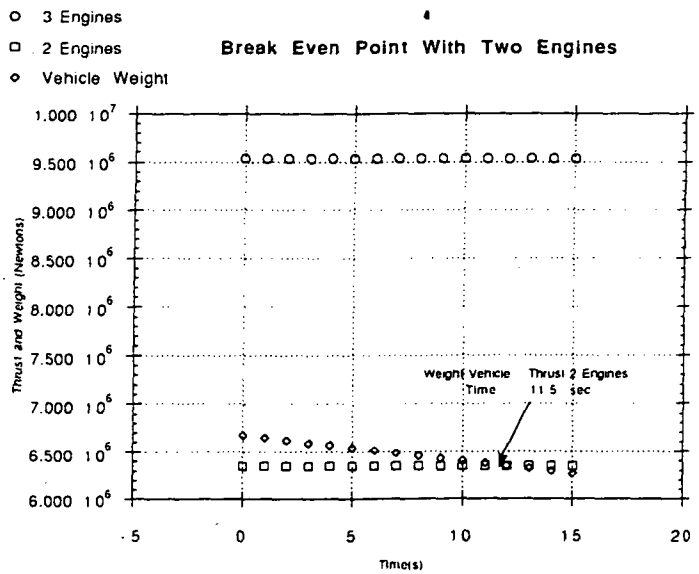

Figure 4.1 Break-Even Point with One Engine Out

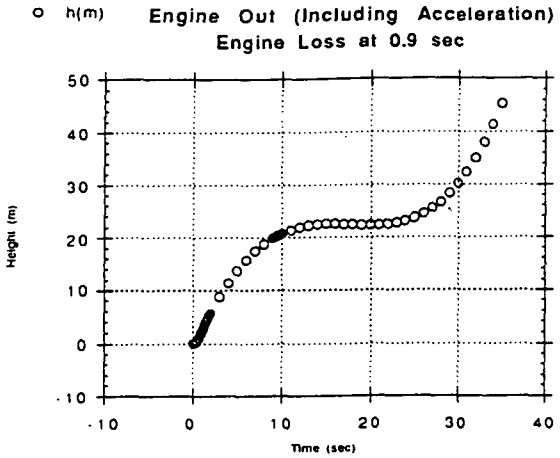

Figure 4.2 Engine-Out Comparisons

Fuel Requirements. Subtracting off the empty mass from the liftoff mass shows that the total mass of the ascension fuel is 680,400 kg (1,500,000 lbm). The mixture ratio for an RD-701 requires that 81.4% of the fuel mass is liquid oxygen, 6% is liquid hydrogen, and 12.6% is RP-1, also fuel for ullage was included. Thus, the necessary fuel masses are as given in Table 4.2.

Exit diameter of chamber	2.265 m
Fuel	RP-1, LH_2
I_{sp}- vacuum	
Stage one {LO_2, LH_2, RP-1}	415 s
Stage two {LO_2, LH_2}	460 s
Length of chamber	5.001 m
Nozzle Area Ratio	60/170
Number	3
Oxidizer	LO_2
Throttle	40-100%
Thrust-vacuum	
Stage one {LO_2, LH_2, RP-1}	$4x10^6$ N
Stage two {LO_2, LH_2}	$1.59x10^6$ N
Weight	43,600 N

Table 4.1 RD-701 Main Engine Specification

Fuel	Mass
RP-1	45,444 kg
LO_2	496,936 kg
LH_2	55,580 kg

Table 4.2 Required Propellant Masses

Volume Requirements. Based on the fuel densities, ullage and necessary masses, the fuel volumes (along with the densities used to calculate them) are as shown in Table 4.3. Each engine requires and internal volume of 7.5 m^3 with dimensions of 1.3 m x 1.3 m x 5 m.

4.4 Secondary Propulsion

Orbital Maneuvering Systems. The OMS consists of two Pratt & Whitney RL-10's. This system provides axial thrust for orbital insertion, orbit circulation, orbit transfer, rendezvous, and various abort scenarios.[14]

Fuel	Density	Volume
RP-1	803 kg/m^3	60 m^3
LO_2	1105.14 kg/m^3	470 m^3
LH_2	68.2 kg/m^3	854 m^3

Table 4.3 Required Propellant Volumes

The RL-10 is a space engine which uses LO_2 and LH_2 and is a turbopump-fed system. This engine uses the same fuels as the RD-701 but has its own fuel tanks. Table 4.4 displays the engine specifications for the RL-10's.

Reaction Controlled Systems.[13] The Reaction Control Systems (RCS) serve as the control surfaces of the SSTO vehicle while in space. There are 3 clusters of RCS units, one in the front and one on each back corner. The rear

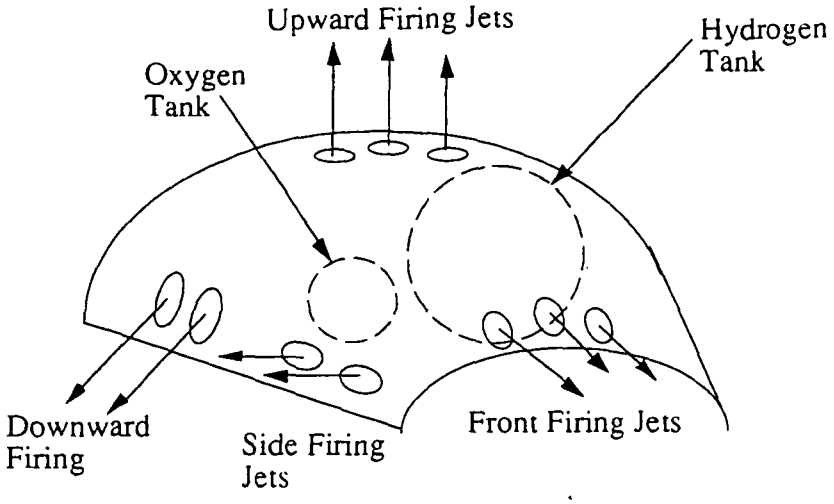

Figure 4.3 Reaction Control System (Forward)

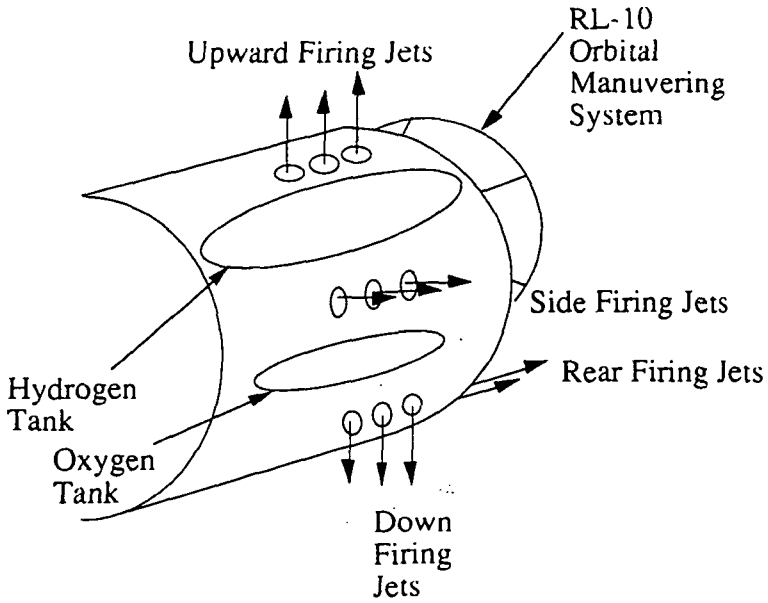

Figure 4.4 RCS Left Rear Pod with OMS Engine

RCS units are also combined with the Orbital Maneuvering System (OMS) so that fuel may be shared. The three clusters allow 6 degrees of freedom while maneuvering in space. Figures 4.3 and 4.4 display the RCS layout. Table 4.5 gives the engine specifications for the RCS.

In emergency situations, the Rear RCS may also be used as the OMS in the deorbit maneuver. The RCS uses gaseous oxygen and hydrogen for propellant. This allows it to tap the OMS tanks in an emergency. The pumping system that would provide for this case would heat the propellants enough to reach a gaseous state.

Exit diameter of chamber	0.8 m
Fuel	LH_2
I_{sp}- vacuum	444 s
Length of chamber	2 m
Nozzle Area Ratio	61
Number	2
Oxidizer	LO_2
Throttle	30-100%
Thrust-vacuum	71,000 N
Weight	1420 N

Table 4.4 RL-10 OMS Engine Specification

Exit diameter of chamber	0.2 m
Fuel	gaseous H_2
I_{sp}- vacuum	400 s
Length of chamber	1 m
Nozzle Area Ratio	61
Number	48
Oxidizer	gaseous O_2
Throttle	10-100%
Thrust-vacuum	$4.5x10^3$ N
Weight	155 N

Table 4.5 RCS Engine Specifications

4.5 Component Safety, Cost, and Lifetime

The RD-701 main engines are the derivative of the RD-170 RP-1/LO_2 engine and the RD-270 engine. Both engines have been proven and are reliable. The RD-701 uses refined technology, making it a low risk product. The expected lifetime of an engine between major overhauls is 5 hours, which with an average use time of 7 minutes would give 42 missions before major repairs would be needed. The turbo-pumps may have to be overhauled every 6-8 missions depending on the amount of wear. The expected cost of one engine is $10 million.

The RCS thruster can sustain 15,000 starts and a cumulative firing duration of 10,000 seconds. Engines can be pulsed in durations of 0.1 seconds and as high as 150 seconds. Since the RCS are relatively simple engines, the reliability of firing is very high. The cost of one engine system is $10,000.

The OMS can have 10 restarts per flight with an expected 1000 starts between overhauls, giving 100 missions. The engine can have up to 10 hours of cumulative firing time. The cost of one engine ranges in the area of $300,000.

The total cost of the engine systems is then approximately $31,080,000.

As was shown in the engine-out consideration, the SSTO vehicle can lose an engine after 2 seconds and still bring the craft back safely. And, since the RCS and OMS fuel systems are linked, if an OMS engine is lost, the RCS system can deorbit the craft. This allows for added safety in space, with the basic philosophy that it is always possible to get back.

Propellant	Cost ($/kg)
LH_2	4.50
LO2	.115
RP-1	0.17

Table 4.6 Fuel Cost

Fuel costs are given in Table 4.6. The estimates for liquid oxygen and liquid hydrogen are relatively high. The are derived from Space Shuttle costs. The Space Shuttle uses much less LH_2 and LO2 than the SSTO vehicle. The cost of these propellants is directly proportional to the amount one purchases. The prices will probably be drastically reduced. Based on the Shuttle fuel estimates the total cost of ascension fuel is $314,983.12.

4.6 Conclusion

As has been shown above, the requirements put forward have been fulfilled. The SSTO vehicle is a single stage to LEO with the lift necessary to launch to LEO.

The propulsion systems satisfy the performance requirements put forward, namely the high thrust to weight ratio. The upper stage has the high specific impulse needed for the mission, along with the high area ratio and deep throttling specified.

In the future our goal is to reduce the liftoff mass of the vehicle without compromising the useful payload. This would increase the safety of the vehicle if an engine was to be lost. A fuel dumping system is being considered to increase the safety factor for a one engine out emergency and also allow for landing of the vehicle after an abort has been decided.

5.0 LAUNCH/RECOVERY/TURNAROUND OPERATIONS

5.1 Introduction

For an effective launch, recovery, and turnaround of an SSTO vehicle, a "spaceport" complex and ground support crew is needed. The facilities required include a mission control center for the safe launch and landing of the SSTO vehicle as well as constant ground communication to the craft. In addition, an efficient Maintenance Bay/Hanger (MBH) building is used for rapid maintenance and payload integration for the SSTO vehicle. A launch pad and landing strip must also be constructed to support these areas.

5.2 Mission Control Operations

Launch and Landing Site. The designed spaceport will have a tower and a small control room for landing and launch control. A small crew of 20 will be necessary for coordinating ground effort during and after landing. The

launch site will require 30 ground crew members for refueling and other launch procedures[15]. The tower will be used to assure a safe landing for the SSTO vehicle and any cargo aircraft that arrives at the spaceport. The tower will have three to four personnel that will be in constant communication with the SSTO vehicle. The main functions of the control room will be to monitor fuel, power, and environmental systems. The control room will be in charge of launch and abort situation decisions. All of these operations will be conducted with a small crew of five per shift.

Dispatch. The communication between craft and ground during the mission will be handled by the commercial airline's dispatch group. The dispatch organization will coordinate contact with air traffic controllers, the spaceport, and the SSTO vehicle. The dispatch group will also have additional hook ups to medical staff, maintenance crew, and the company that owns the payload, in case of an emergency. This staff will consist of five members that will handle all command decisions while the mission is executing.

Security. Security for the spaceport will be similar to the security of an airport. A perimeter will be established around the runways, maintenance bay, and the launch pad. Limited access to each facility will be enforced for all employees and visitors. Tighter security will be enforced around the launch pad due to the hazardous chemicals present. The security will be employed by the commercial airline group and the spaceport owners (if different from the airline).

5.3 Launch

The launch pad is a steel support structure on a concrete pad. In the pad is a six foot flame trench to direct the exhaust flames away from the fuel storage tanks[16]. The area around the launch pad will have a radius of 454 m (1,490 ft)[17]. The launch pad will consist of fuel storage and a crew entry support structure (CRESST), which includes a lightning mast attached to its highest point. A water tower and horizontal-to-vertical hydraulic lift (HTV) are also a part of the launch pad (Figure 1 in Appendix D).

The craft will be rolled horizontally to the launch pad from the maintenance bay by a tow vehicle. The SSTO vehicle will be attached to the HTV truss at hard points near the landing gear, which is retracted, with frangible nuts that explode off at launch. The SSTO vehicle will then be raised to the vertical position in a process that will take about 0.5 hours. Before fueling, a jacking system will be placed at the bottom of the vehicle to help stabilize it. The APU (Auxiliary Power Unit) fuel tanks will then be filled with hydrazine after the main fuel tanks are filled with liquid hydrogen (LH_2) and liquid oxygen (LO_2). The total time of the fueling process should take about 4-6 hours[18]. Pilots will enter the craft through the CRESST. Pre-flight diagnostic tests will be conducted and should take a maximum of one hour.

Launch Pad Support. The estimated number of ground crew personnel that will be needed to ready the SSTO vehicle for launch is 30 workers. Other resources needed include a tow vehicle, an extensive piping system for pumping the fuel, and a water tower for water jets that are under the rockets' engines. The water jets will absorb acoustic energy. The jets will also be used for a massive cooling system if a launch is aborted after firing the rockets.[19]

The fuel storage cells will have to hold enough fuel for multiple flights; therefore, refueling of the storage tanks will not interfere with turnaround time. The LH_2 and LO_2 tanks will have to be kept in cryogenically sealed vacuum tanks. To allow this supercold fluid to flow through the piping system, the pipes will have to be insulated. The RP-1 will be loaded similarly to jet fuel in ordinary fuel tanks. The APU fuel, hydrazine, requires no more storage precautions than regular hazardous materials.[20] RP-1 jet fuel will need to be on hand for refueling of transport aircraft.

The size of the storage vessels is shown in Table 5.1. Spherical tanks will be used because they minimize the surface area that needs to be cooled, thus reducing boiloff. In addition to this, structural integrity is greater for a spherical shape than for others.

Fuel	5 mission storage Mass (kg)	Volume (m^3)	Sphere Radius (m)
LH_2	516,120	6500	11.58
LO_2	7,065,500	7590	12.2
RP-1	1,084,050	1350	6.86
APU	2,391	3	1

Table 5.1 Fuel Storage Containers

Horizontal-to-Vertical Lift. A hydraulic lift system will be used to rotate the SSTO vehicle to its launch position on the launch pad.[21] The truss used to support the SSTO vehicle through this process will double as a support for the SSTO vehicle until launch. The truss will attach to hard points by the landing gears with frangible bolts that explode at takeoff. Research is currently being conducted on the size of the hydraulic system. A support system on the bottom of the vehicle will be installed for stability after lifting the SSTO vehicle to the vertical position (Figure 1 in Appendix D).

Fueling Procedures. The entire fueling process will take about four to six hours. The LH_2 fueling process will require no pumps due to the lighter-than-air characteristics of H_2 gas. Vaporizers convert a small portion of the LH_2 in the tanks to a gas. This gas will exert enough pressure to

force the LH_2 into the transfer lines and then into the tanks. The LO_2 process will require two main pumps of 633.3 L/s (166.7 gal/s) capability. The RP-1 will be pumped using 2 main pumps that have a capability of 166.7 L/s (44.0 gal/s). All of these processes can occur simultaneously. Including the time to prime the tanks before fueling, the total time for this process is 2 hours. Helium tanks which are connected to the main fuel tanks are filled before launch also. These tanks will be filled to 31 MPa (4500 psi) and will pressurize the main fuel tanks to atmospheric pressure to keep the tanks from crumpling. Fueling of the APU will require an isolated launch pad while two crew members in environmental suits pump the fuel into the three APU tanks. Including evacuation of the launch area, the APU fueling process will require 2-3 hours to complete.[22]

Crew Entry. The crew of the SSTO vehicle will enter the CRESST elevator (Figure 1 and Figure 2 in Appendix D) with two ground crew members to assist. They will enter the SSTO vehicle through the airlock on the top of the craft that will be connected to the catwalk. The pilots will strap into their chairs while the ground crew secures the airlock. After the ground crew exits the CRESST, the catwalk that attaches to the SSTO vehicle will rotate clear of the vehicle 30 seconds before launch. This gives the pilots a chance to escape during an abort scenario until time minus 30 seconds.

Airspace Required. The airspace for launch of the SSTO vehicle will be cleared ten minutes before takeoff. This will also include airspace needed for RTLS (Return to Launch Site) and RTAS (Return to Alternate Site) abort scenarios. The position of the airspace required will be dependent on the angle of launch ascent. The downrange airspace will have to be 43.3 km (27 miles) when the vehicle is at 15.24 km (50,000 ft). These numbers were extrapolated from the Space Shuttle.[23] This hold pattern will have to remain until five minutes after launch to ensure no abort scenario situations will be executed.

5.4 Landing

The landing procedures will try to minimize turnaround time. After touchdown, the SSTO vehicle ground crew will approach the vehicle. A fan will be operated to alleviate the area of hazardous hydrazine fumes.[24] After the fumes have dissipated, the crew will exit the vehicle through the top hatch. The landing crew will drive a ladder truck, similar to ones used by commercial aviation, for the pilots to descend from the craft. After about a half an hour, a tow truck will tow the vehicle to the maintenance bay.

Facilities Needed. Two concrete runways are needed for landing the SSTO vehicle successfully. Each runway will be 4572 m (15,000 ft) long with runoff areas on each end 304.8 m (1,000 ft) long and each will be 91.4 m (300 ft) wide. The concrete is 60.96 cm (24 in.) thick. Concrete is used because of its strength and durability. The top surface is grooved for watershed.[25] The runways will be oriented depending on the launch site and the meteorological data of the area. This will insure safe landing conditions in varying weather conditions.

A tow vehicle, a vehicle with a large fan, and a crew transport will be needed at the launch site. The total estimated number of personnel needed for the landing site is 20. A control tower will also be on site to coordinate landing procedures as well as any cargo flights into the spaceport.

Airspace required. The airspace needed to operate the SSTO vehicle landing procedures are as follows. The downrange length is 41.85 km (26 miles) when the SSTO vehicle is at 15.24 km (50,000 ft).[26] The velocity of the SSTO vehicle will be below Mach 1 below a 14.021 km (46,000 ft) altitude This should not cause any problems with sonic booms over populated areas. At this point, the SSTO vehicle is five minutes before touchdown. This is an estimate using the SSTO vehicle's aerodynamic characteristics and space shuttle landing performance data. Therefore, the landing airspace should be cleared around ten minutes before touchdown at the main spaceport.

5.5 Maintenance

Maintenance procedures for the SSTO vehicle will be comparable to commercial airline procedures. The staff for the SSTO vehicle maintenance crew will be about 60 personnel on each of three shifts. The craft will have a quick inspection after each flight. Each inspection will take about 18 hours. (See Table 5.2.) This will be classified as an "A" check. After 10 flights the craft will have a "B" check with an extensive structural and internal system check that will take the craft out of service for 3 days. The number of flights is limited by the life span of the fuel pumps. The fuel pumps need to be overhauled after 7.5 hours of service at maximum operating temperature.[27] Two buildings, the Maintenance Bay/Hanger (MBH) and the Annex, are needed to carryout the maintenance and payload integration of the SSTO vehicle.

Maintenance Bay/Hanger. The MBH (see Table 5.2) will include four main areas. The first area will be the machinery shop and miscellaneous operations. This area will support the MBH work area. A computerized system for the scaffolding will be controlled here. Any other maintenance crew operations will be conducted in this area. This area will contain all spare parts necessary for turnaround. The next bay has two purposes. The main use will be for turnaround when simultaneous missions are conducted with multiple vehicles. This bay will also be used for heavy overhaul of the SSTO vehicle. An overhaul may include such things as replacing an engine, repairing a major systems failure, or fixing structural damage. Bay 3 will be for turnaround only. After landing, the SSTO vehicle will be towed from the runway into this bay. There

Est. Time (hours)	After Touchdown	Before Liftoff	Task
	0:00	18:00	**Touchdown**
0.5	0:30	18:00	APU Vapor Dissipation
1.5	2:00	17:30	Crew Egress/Tow to Building
1	3:00	16:00	Payload Removal
			Thermal Tile Inspection/Replacement
2	5:00	15:00	Repairs from Previous Mission
1	6:00	13:00	Avionics Plug in for Diagnostic
2	8:00	12:00	Control Surface Test
			Structural Inspection
2	10:00	10:00	Environmental Check and Refurbishing
1	11:00	8:00	Payload Installation
1	12:00	7:00	Tow to Launch Pad
			Fasten to HTV Truss
0.5	12:30	6:00	Lift to Vertical Position
2	14:30	5:30	LO_2, LH_2, and RP-1 Fueling
2	16:30	3:30	APU Fueling
0.5	17:00	1:30	Crew Entry
1	18:00	1:00	Pre-Flight
		0:00	**Launch**

Table 5.2 Turnaround Schedule

will be an overhead crane system in both bays. The crane will span the length of the bay and be used for payload installation and removal as well as for assistance in engine or fuel tank replacement. The fourth area is for storage of cargo and will be used as a hangar for the transport aircraft. (Refer to Figure 3 in Appendix D.)

The spaceport will also have an Annex building. This building will house the spaceport's cafeteria, administration offices, and meeting and mission briefing rooms. On-site engineering services will also be in this building (Figures 4 and 5 in Appendix D).

Scaffolding Support. The scaffolding support system will employ simplicity and flexibility in its operation. The scaffolding system consists of two main systems: a payload removal and installation crane and movable catwalks. Both systems will be installed in both bays of the MBH and span the length of the SSTO vehicle. The scaffolding system will be supported by the roof support system.

The payload removal and installation crane serves two purposes. It will remove the payload module at the end of each flight. Before each flight, the crane will lower the new payload into the SSTO vehicle payload bay. The payload will be trucked from the cargo hanger to the MBH Bay 1, next to the SSTO vehicle. The crane will use a cradle to support and raise the payload. Ground crew will then operate inside the payload bay to secure it for launch and subsequent deployment into space. The crane's second purpose will be to lift a rocket engine, or any other large device onto the SSTO vehicle for repair and installation. The crane will have the ability to hook up numerous devices to adjust to its purpose. This will allow crane use in any situation, such as pulling out a rocket engine.

The second part of the scaffolding system will include a catwalk system that will be used to inspect and repair the SSTO vehicle. The setup (Figures 6 and 7 in Appendix D) will consist of two catwalks on each vertical truss. The catwalks would be free to move up and down on these trusses. In addition, the catwalks will be able to retract and extend, so they can follow the shape of the SSTO vehicle structure. There will be two vertical trusses on each side with every truss able to move the length of the SSTO vehicle. After a few maintenance and inspection cycles, a computer program can be installed to move the catwalks automatically to improve efficiency, thus lowering turnaround time.

5.6 Cost and Lifetime Evaluation

The mission cost and initial cost (Tables 5.3 and 5.4) are given as estimates in 1993 dollars. Estimates on labor, scaffolding, and launch pad structures are based on costs of other construction projects recently completed. The lifetime expectations are also estimates with an assumption that upgrading and regular maintenance is included. Cost per

flight does not include any executive costs, maintenance of facilities, and miscellaneous costs that may arise in regular operational procedures.

5.7 Conclusion

The design of the SSTO vehicle ground operations emphasizes fast turnaround and low cost for the user. The spaceport design incorporates all facets of the necessary procedures to maintain a reusable SSTO vehicle. The ability to be flexible with adjustable catwalks and a uniform payload configuration maximizes the spaceport's market.

	Crew	Man-Hours	Cost
Landing			
Labor	20	480	$19,200
Vehicles			$500
MBH			
Labor	60	1440	$57,600
Launch			
Labor	30	720	$28,800
Vehicles			$500
Fuel			
LH_2			$250,110
LO_2			$5,714,810
RP-1			$7,727
APU			$500
Grand Total			$5,973,147

Table 5.3 Cost Per Flight

The horizontal-to-vertical lift system on the launch pad shortens the time needed to move the craft from the MBH to the launch pad area. A small staff will lower labor costs and increase profits. The ability to store large amounts of fuel will lessen the dependency on fuel-producing companies to deliver their product. All of these characteristics will create a viable spaceport system for a SSTO vehicle that will be rapid, efficient, and profitable.

	Cost (in millions of dollars)	Lifetime Expectancy (in years)
Landing		
Runway 1[28]	64.13	20
Runway 2	64.13	20
Support Vehicles	0.13	10
Labor	included above	N/A
Subtotal	128.39	
MBH[29]		
Construction	15.00	40
Annex Construction	1.00	40
Tower Construction	0.50	40
Scaffolding Constr. (Est.)	30.00	25
Subtotal	46.50	
Launch Pad		
Fuel System	0.50	10
Labor	5.00	
Launch Structure	10.00	15
Vertical Lift	2.00	10
Water Tower	0.25	25
Subtotal	17.75	
Grand Total	**192.64**	

Table 5.4 Initial Costs

6.0 STRUCTURES

6.1 Introduction

The primary concern in designing the structure of the SSTO vehicle is to maintain its integrity while keeping the mass low. Completing this design is a challenge due to the diverse loading conditions the vehicle experiences within its flight envelope. A further complexity in the design is introduced by the vertical takeoff/horizontal landing configuration. To solve the design problems, advanced materials such as composites and metal alloys are utilized throughout the structure and an initial concept of the frame geometry has been tested in I-DEAS.[1] The conceptual design consists of the following components:

- Outer Shell
- Structural Frame
  - ~ Crew Module/Cargo bay
  - ~ Engine Attachment
- Takeoff/Landing systems
- Fuel and Cryogenic storage

6.2 Structural Configuration

Outer Shell Design. The outer shell is designed to withstand the intense external loading experienced by the vehicle. The most extreme loading occurs during reentry when thermal loading is of principal concern. Average surface temperatures are between 400° K (260.6° F) and 500°

K (440.6° F); regions such as the nose cone, leading edge, and bottom of the vehicle approach temperatures of 2000° K (3140.6° K). To protect the outer shell from these intense thermal loads, a Thermal Protection System (TPS) is attached to the critical regions, reducing the surface temperature of the outer shell to 403° K (266° F). In addition to thermal loads, the outer shell endures dynamic loading during all phases of the mission.

In designing the initial outer shell, a cylindrical approximation is made and only aerodynamic loading is considered. Using the maximum aerodynamic loading and the stagnation pressure at Mach 2.5, a minimum thickness is computed for the outer shell, the computation includes a safety factor of two. The minimum thickness of the shell was computed using Equation 6.1.

$$\sigma \cdot SF = F / t \qquad (6.1)$$

s is the compressive, lower, yield strength of the material, F is the force per meter, and t is the thickness of the outer shell. The mass of the shell has been computed for three different materials using Equation 6.2.

$$m = \rho \cdot A \cdot t \qquad (6.2)$$

A is the surface area of the vehicle, ρ is the density, and t is found from Equation 6.1. Table 6.1 summarizes the resulting masses and wall thicknesses for different materials.

Material	Thickness (m)	Mass (kg)
Kevlar 49	0.0012	4150
Carbon-Epoxy	0.0003	2000
Aluminum	0.0011	7836

Table 6.1 Structural Material Thicknesses and Masses

The thickness computed does not include the requirements of the TPS. To facilitate the TPS, the outer shell thickness must be increased. This will result in an increased mass, which is not desirable for the SSTO vehicle. To resolve this problem, a semi-monocoque design needs to be employed. A semi-monocoque configuration integrates the outer shell and space frame as one structure. The two then share the loads. This is a more efficient structure which utilizes the increased thickness of the shell and decreases the mass of the space frame.

Carbon epoxy is used for the outer shell for a variety of reasons. Carbon epoxy has an optimum strength-to-weight ratio, which justifies its increased cost. Kevlar 49 and aluminum were not chosen because they are adversely affected at temperatures beyond 450° K (350.6° F); carbon epoxy shows almost no effects up 1273° K (1832° F). Carbon epoxy also demonstrates better fatigue qualities and requires less maintenance over a longer lifetime.

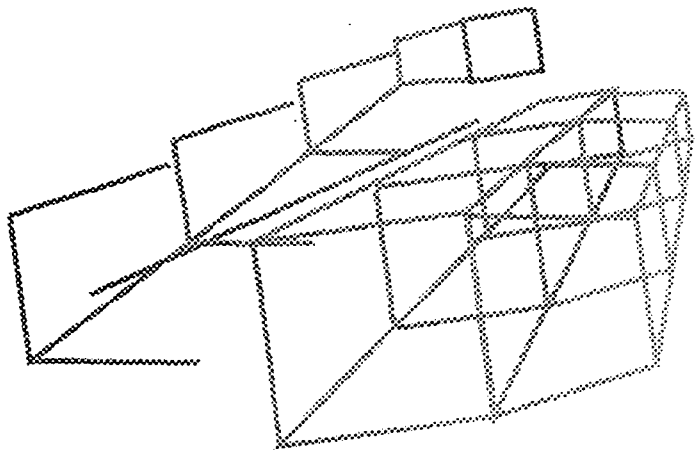

Figure 6.1 Initial Structural Configuration

Structural Frame. The geometry of the structural fram is determined by the position and size of the fuel tanks. Th initial configuration (see Figure 6.1) was designe considering only the fuel tanks. Also, the initial desig used uniform beam cross sections (see Figure 6.2).

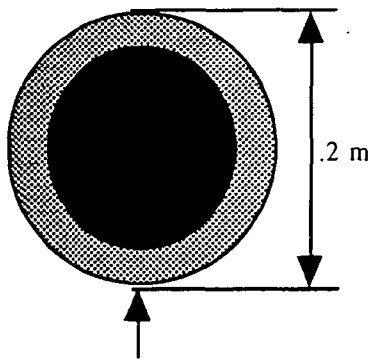

Figure 6.2 Initial Beam Cross Section

The initial design was analyzed and modified to reduce th mass while increasing the load-carrying capability. Thi analysis led to the current design (Figure 6.3), whic includes the following improvements:

- Hexagonal design to improve frame efficiency b reducing the beam lengths
- Angled cross beams to increase
- The use of several different beam cross section to reduce the mass (see Figure 6.4)

All of these improvements were based on the results c several finite element models.

For the preliminary analysis of the frame, severa approximations and estimates for loading conditions wer made. It is assumed that the frame will only be subjected t axial loading. The fuel tanks are not considered to be load bearing components. The mass of the fuel and the fue tanks are assumed to be point forces acting on the frame The dynamic pressure was modeled as point forces applied a the nose of the frame. These assumptions were necessary t

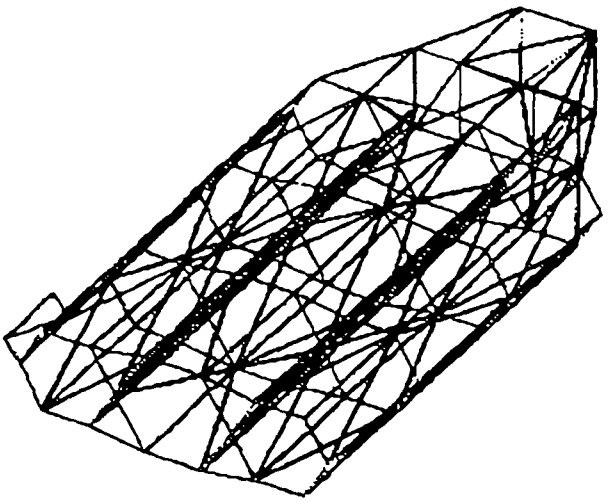

Figure 6.3 Final Space Frame

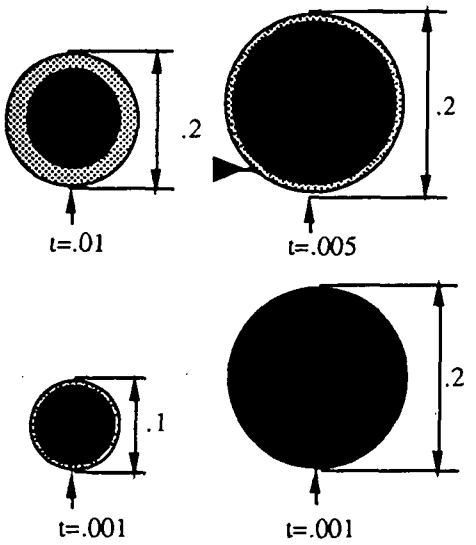

Figure 6.4 Final Beam Cross Sections

allow a preliminary analysis of the frame using the I-DEAS software package. These forces included a 1.4 safety factor as required for a composite frame for manned missions.[33]

The frame has been analyzed at two of the four critical loading conditions. The first loading condition occurs at launch, with an acceleration of 1.8 g's and the maximum mass (fully fueled). The second loading condition occurs when the dynamic pressure is at a maximum and most of the fuel is still being carried. Two critical loading conditions that will be analyzed in the future occur during reentry and landing. The last two loading conditions will effect the design of the frame but should not cause any major changes.

Some optimization was done on the frame by analyzing and optimizing small sections of the initial frame, utilizing the I-DEAS software. Then these optimizations were used to refine the entire frame design. This led to a final design that was dramatically different from the initial sketches and reduced the original mass by about 70%.

Titanium alloys and carbon-carbon composites were initially considered for materials, but the analysis showed that only a carbon-carbon composite or similar material has a high enough strength-to-weight ratio to meet the design requirements. The analysis showed that a carbon-carbon composite can carry the same load while only requiring 25% of the mass of titanium alloys. This caused the frame mass to drop from a value of 22,000 kg (49,500 lb) using titanium alloys to a value of 5,500 kg (12,100 lb) using carbon-carbon composites. These values for the mass of the frame do not include the attachment of the fuel tanks, engine and nozzle assemblies, crew modules, cargo modules, or the structural skin. However, the masses of these items are included in the total mass of the structure, accounting for 3,000 kg (6750 lb) out of the total mass of 24,700 kg (55,600 lb).

Crew Modules. The crew area has three components: the command module, the habitation module, and the airlock. The size of each module is approximately:

- command module
  - Inside dimensions: 1.9 m x 1.9 m x 1.6 m (6 ft x 6 ft x 5 ft)
  - Outside dimensions: 2.2 m x 2.2 m x 1.9 m (7 ft x 7 ft x 6 ft)
- Habitation module
  - Inside dimensions: 3.1 m x 2.5 m x 2.2 m (10 ft x 8 ft x 7 ft)
  - Outside dimensions: 4.7 m x 2.8 m x 1.9 m (15 ft x 9 ft x 10 ft)

The dimensions are given in the order of length, width, and height.

The command module will be located in front of the habitation module. Both modules will be structurally connected to reduce volume and material. The frame will incorporate a simple design, but be strong enough to withstand the pressurization of the modules.

The material used for the frame will be aluminum alloy since the modules require a certain level of conductivity. Also, aluminum alloy has a good strength-to-weight ratio.

The space between the inside and outside of the modules will be filled with insulation, cables, pipes, radiation shielding, and so on. The surface of the modules will be covered by aluminum foil coated with gold to give the necessary thermal protection.

Fuel Tanks. The fuel tanks will be attached to the main frame, at 2 to 3 points along its length, with carbon-

	Titanium Alloy	Carb.-Carb. UHM
Density (kg/m^3)	4650	1800
Ultimate Tensile Strength (MPa)	1385	1865
Material Cost ($/kg)	44	2200
Young's Modulus (GPa)	110	175
Frame Mass (kg)	22,000	5500
Frame Cost (millions of dollars) (Production Cost)	9.80	121

Table 6.2 Structural Material Properties and Costs [31,35,40]

carbon composite beams. Carbon-carbon is used for its high strength-to-weight ratio and good fatigue properties. These tanksare not considered to carry any external axial loads.

Main Engines and Nozzles. The main engines and nozzles will be attached with carbon-carbon, boron alloys, or titanium alloys. Carbon-carbon does have a better strength-to-weight ratio, but it may not be possible to mold it into the necessary configurations. The RD-701 engines have six hard points on each engine that the space frame will attach to. It would be most beneficial from a structural perspective to attach the engines as close to the fuel tanks as possible so as to reduce the frame work, and plumbing connecting the engines and fuel tanks.

Materials. Carbon-carbon composites cost about 50 times more than titanium alloys per unit mass, See Table 6.2. However, since the mass of a frame constructed from carbon-carbon composites is one fourth that of a similar frame with the same loading capabilities that is constructed using titanium alloys, the carbon-carbon frame will cost only thirteen times more. This extra cost is not a factor since the vehicle would be unable to fulfill the design requirements without the mass savings achieved from the composite materials.

Carbon-carbon composites can withstand heating up to 2000° K (3140.6° F)[40] with minimal material property changes. This would allow the vehicle to retain its structural integrity during reentry into the earth's atmosphere even with the loss of some of the thermal protection panels. Carbon-carbon composites also have better fatigue properties than metals, which will result in a longer operational lifetime.[40]

6.3 Takeoff and Landing Gear

Takeoff. To place the vehicle in a vertical position for takeoff, a horizontal-to-vertical (HTV) truss is used. The HTV truss hydraulically lifts the vehicle from its horizontal landing position into a vertical launch position. The vehicle is attached to the HTV truss at four hard points located on its underside. See Fig 6.5. Two of the hard points are located at one fourth of the distance from the front of the structural frame, the remaining two are 3/4 of the distance from the front.

The vehicle is attached to the HTV truss by inserting pins into the holes located at the hard points on the structural frame. After the HTV truss lifts the empty vehicle into the vertical launch position, it is bolted to the HTV truss at additional hard points along the back of the structural frame. At launch, these bolts are exploded to release the vehicle.

The pins must be able to distribute the mass of the empty vehicle across the HTV truss. With the empty mass of the vehicle at 101,754 kg (223,858.8 lb), this creates large stresses at the pins. Ultrahigh-strength steel will be used to fabricate the pins. Steel was selected because it has a low cost. With weight not an issue for ground structures, many of the expensive, low density materials such as composites or titanium were not considered. The HTV truss dimensions are: 8 m (26.25 ft) wide, 5 m (16.4 ft) long, and 60 m (196.86 ft) tall.

Landing Gear. The SSTO vehicle has a maximum landing mass of approximately 83000 kg (183000 lb). The average touchdown speed is approximately 102.89 m/s (337.56 ft/s). The similarity between the Space Shuttle's landing conditions[34,39] and those of the SSTO vehicle make it a good model to begin the design. The Shuttle has a nominal landing speed of approximately 92.6 m/s (303.81 ft/s) and a maximum of 115.75 m/s (379 ft/s), a glide slope of 1.5°, and a maximum mass of 104,326.25 kg (230,000 lb) at touchdown. The Space Shuttle needs a runway length of 4645 m (15,240 ft) to land. These figures are comparable to those expected for the SSTO vehicle.

The layout of the landing gear is a tricycle configuration and each gear retracts in the forward direction. One unit is placed at the nose and the two main gear are slightly aft of the center of mass, which is the same as the center of gravity (CG). See Figure 6.6. One main landing gear unit is centered under each liquid hydrogen tank.

Each landing gear unit is composed of an oleo shock absorber and two wheel-tire assemblies. See Fig. 6.7.

The two main landing gear units have 1.22 m (48 in.) diameter tires, and the nose gear has 1.02 m (40 in) diameter tires. Each wheel-tire assembly has a mass of approximately 78.02 kg (172 lb), roughly 453.59 kg (1000 lb) for all six sets.

Radial tires are used instead of bias tires for a variety of reasons.[46] They result in a mass savings of about 20% over bias. They are more reliable because they reduce the chance of sudden failure. On a radial tire, early signs of failure can usually be detected before the failure of the component. Radial tires also permit higher sink rates and distribute loads more efficiently. Also, radial tires have higher overall cornering coefficients and run cooler.

Each of the main landing gear units is contained in a volume with approximate dimensions of: 4.50 m (177 in) long, 1.90 m (74.80 in) wide, and 1.40 m (55.12 in) high. The height from the axle of the main gear to the bottom of the craft is about 2.75 m (108 in). The nose gear is

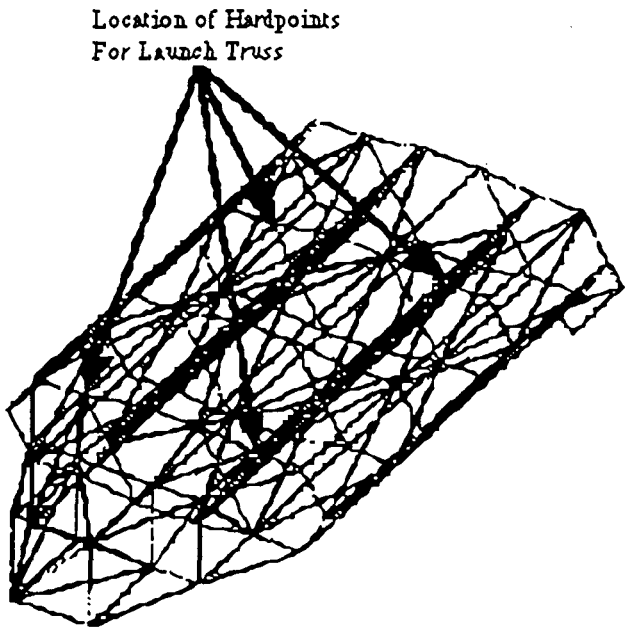

Figure 6.5 Location of Hard Points for HTV Truss

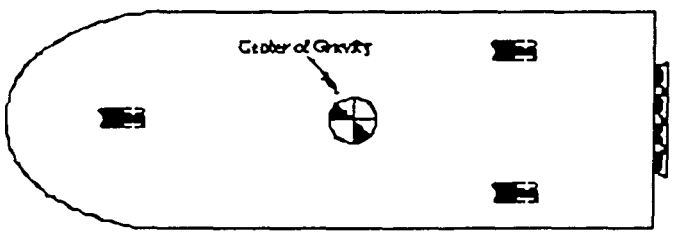

Figure 6.6 Landing Gear Configuration

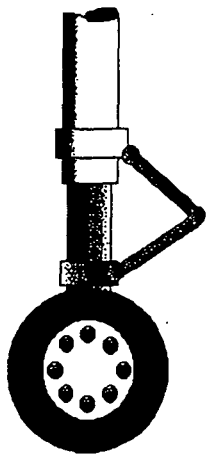

Figure 6.7 Landing Gear Unit

contained in a volume with approximate dimensions of: 3.50 m (137.80 in) long, 1.60 m (63 in) wide, and 1.10 m (43 in) high. The height from the axle of the nose gear to the bottom of the craft is 1.65m (65 in).

It is critical that the landing gear be deployed an instant just before touchdown to maintain a proper lift to drag ratio. A hydraulic system will be used for the landing gear deployment, assuming that lift will not be critically affected. Since hydraulics are used for the control surfaces and hatches, it would be ideal to use the existing system. There will be at least one backup hydraulic and pneumatic system for emergencies. Also, because a mechanical uplock system is used to hold the gear, exploding bolts will be an included safety device.

Typical landing gear configurations account for 4-5% of a vehicle's maximum takeoff mass. In this design, the gear need only support the maximum landing mass. With a landing mass of 83000 kg (183000 lb) a landing gear system of approximately 5000 kg (11,000 lb) can be expected for this vehicle. This mass includes a safety factor for normal landing conditions, however, it does not take into account the extra mass for a partially fueled landing which can occur during abort scenarios. By designing for this possibility the mass of the landing system increases by roughly 5% of the total fuel mass present in an abort landing.

The materials considered for the landing gear are titanium Ti-10-2-3 (Ti-10V-2Fe-3Al), AerMet 100 alloy, and ultrahigh-strength steel. These materials were selected for their high strength, deep hardening, and high toughness characteristics. See Table 6.3.

In selecting the material the deciding factors are price, mass and manufacturing capabilities. The density of AerMet is 7888.77 kg/m^3 (0.285 lb/in^3), titanium's density is 4650.22 kg/m^3 (0.168 lb/in^3) and steel is 7888.77 kg/m^3

	AerMet 100 Alloy	Titanium Ti-10-2-3	Ultrahigh-Strength Steel
Density , kg/m^3 (lb/in^3)	7892 (0.285)	4650.22 (0.168)	7892 (0.285)
Yield Strength, MPa (ksi)	1724 (250)	1270 (184)	1682 (244)
Ultimate Tensile Strength, MPa (ksi)	1965 (285)	1385 (201)	1965 (285)
Young's Modulus, GPa	194	110	Not Available
Fracture Toughness, MPa$\sqrt{m}$ (ksi$\sqrt{in.}$)	126 (115)	62 (56)	88 (80)
% Reduction in Area	65	30	50
% Elongation	15	12	10
Axial Fatigue Resistance 10^6 Cycles to Failure, MPa (ksi)	1379 (200)	960 (139)	1103 (160)
Material Cost, $/kg ($/lb)	26 (11.80)	44-46 (20-30)	26 (11.80)
Manufacturing Difficulty (1-5)	4	5	4

Table 6.3 Landing Gear Material Properties [31,35,44,45]

(0.285 lb/in^3). Although titanium is not as strong as AerMet, it is half as dense, resulting in a component savings of about 30%. For this reason titanium is selected for the vehicle. Titanium is the most expensive material but its characteristics make it cost effective. Titanium has a naturally high resistance to the environment, which results in longer life expectancy and reduced maintenance costs, in addition to its ability to reduce componentmass. Not all components can be made from titanium, this will result in a lower mass savings for the entire landing gear system. Parts that can not be made from titanium will be made from AerMet, which has slightly better properties than ultrahigh-strength steels.

A typical aircraft uses steel pads in the braking system. The SSTO vehicle will use carbon-carbon pads. They have an increased thermal conductivity, lower coefficient of thermal expansion, and reduced mass[37]; this makes them ideal for the application. Compared with steel, there is a mass savings of 35%, the heat capacity is 2.5 times greater, and the service life is doubled when measured as landings per overhaul.[37] The disadvantages of carbon-carbon for the brakes are increased cost. The approximate cost is 150-220 $/kg ($68-100$/lb)[37] as compared to 26 $/kg ($11.80/lb). Another disadvantage of using carbon-carbon is the need for coatings to prevent environmental deterioration. The increased performance of carbon-carbon justifies the extra cost.

An estimate of the required braking energy is calculated from Equation 6.3, yielding a value of 545 MJ (400x10^6 ft*lb).

$$KE = \frac{1}{2} \cdot m \cdot v^2 \qquad (6.3)$$

If the brakes can not supply enough braking energy, a chute, or some other device will need to be employed.

6.4 Fuel Tanks

Materials and Processing. The material chosen for the liquid hydrogen fuel tanks is Kevlar 49 because of its high strength-to-weight ratio and thermal conductivity characteristics. Kevlar 49 has the following properties:

- Ultimate strength - 2750 MPa (400 ksi)
- Thermal Conductivity - 0.53 W/mK
- Density - 1440 kg/m^3 (89.7 lb/ft^3)

The tanks will be made as shown in Figure 6.8 with circular windings restraining the hoop stresses and an Ovaloid end winding restraining the axial forces.[39] The optimum lay-up angle for pressure vessels is 54.5° while the most efficient number of layers is 2. See figure 6.8 for the definition of lay-up angle and layering.

The oxygen tank is constructed out of an aluminum lithium alloy since composites and titanium alloys are not compatible with the liquid oxygen. Adding lithium to aluminum increases the ultimate strength and reduces the mass of aluminum to achieve the following material properties:

- Ultimate strength - 500 MPa (72.7 ksi)
- Density - 2410 kg/m^3 (150 lb/ft^3)

Construction of the oxygen tank will involve manufacturing procedures that are already established, which will keep production costs down.

Thickness of the Tank Walls. Tank pressure is the main driving force in the design of fuel tanks.[39] Tank pressure is made up of two components: operating pressure and maximum hydrostatic pressure due to the depth of the fuel and the acceleration placed on it. These are the two largest loads placed on the tanks and are the main design concern in deciding thickness. There will be a total of five main tanks, two hydrogen, two kerosene (RP-1), and one

Tank	Volume (m^3)	Pressure (MPa)	Material	Tank Mass, kg (lb)	Production Cost (millions of $)
Oxygen	1300	0.3	Aluminum Lithium	5500 (12,400)	0.620
Kerosene (2 tanks)	270	0.2	Kevlar 49	52.8 (119)	3.57
Hydrogen (2 tanks)	1518	0.3	Kevlar 49	395 (889)	26.7
OMS, RCS and helium (includes helium mass)			Aluminum Lithium	2500 (5600)	.28
Total mass & cost (mass includes a growth factor of 1.2)				10,200 (23,000)	31.2

Table 6.4 Fuel Tank Properties

oxygen. The hydrogen tanks will be operating at a total tank pressure of 0.397 MPa (57.7 psi). This results in a tank cylinder wall thickness of 0.303 mm (.0119 in) and a spherical end cap thickness of 0.197 mm (0.00773 in). The kerosene tanks will be operating at a total tank pressure of .438 MPa (63.51 psi). This results in a cylinder wall

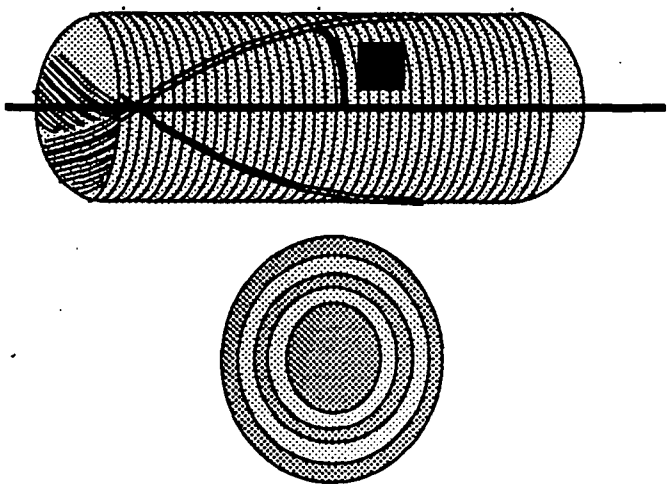

Figure 6.8 Fuel Tank Structural Configuration

thickness of .311 mm (0.0122 in) and a spherical end thickness of 0.202 mm (0.00793 in). The oxygen tank will be operating at a total tank pressure of 1.00 MPa (145 psi), which results in a cylinder wall thickness of 5.56 mm (.218in) and a spherical end thickness of 3.61 mm (.142 in). See Table 6.4 for tank layout.

Tank Masses. The masses of the tanks are given in Table 6.4. The liquid oxygen tank accounts for most of the fuel tanks' mass since it has the highest total pressure, and is made of an aluminum lithium alloy instead of composites.

Thermal considerations. Kevlar fibers thermally degrade in a vacuum at temperatures above 648 K (707° F). Also, aluminum lithium experiences material property changes at 450 K. Therefore, the maximum operating temperature is set at 453 K (356° F).

Material and Production Costs. Material costs for the hydrogen and kerosene tanks will be high, on the order of $2,200/kg ($1000/lb), but should be well offset by the savings in fuel and maintenance costs over the life of the vehicle. The oxygen tank will be relatively inexpensive, about $5/lb, and easy to manufacture. Manufacturing costs for the composite tanks will be on the order of three times higher than the aluminum lithium tank in order to get the proper fiber alignment. At the current tank masses, this would put the cost at 31.2 million dollars. As the composite industry advances, these costs are certain to drop substantially.

Operational Lifetime and Characteristics. At this time, it is not possible to give an expected lifetime for the configuration other than to say that due to the fatigue characteristics of composites, the tanks should have a much longer service time than metallic tanks. In looking at fatigue Aramid composites exhibit, their outstanding performance is on the order of 10^6 cycles to failure. Also, aluminum lithium alloys have better creep and fatigue characteristics than other aluminum alloys. Kevlar fiber, being an organic compound, undergoes photodegradation when exposed to light (both visible and ultraviolet), but this can be minimized by the use of light-absorbing coatings. The creep strain for Kevlar 49 is among one of the highest in the carbon composites arena and is an area of concern in the design.[40] A possible alternative to look at in the future would be unidirectional carbon composites such as Toray T300 or T1000.

Loading Considerations. As structural members, propellant tanks must be designed to withstand a combination of the following probable structural loads:

- Internal pressures and their dynamic effects
- Axial thrust loads and their dynamic effects
- Bending moments due to vehicle transverse accelerations, wind loads, and shifting of the center of gravity
- Aerodynamic forces
- Thrust-vector-control forces
- Loads produced by mounting arrangements
- Loads caused by thermal transients and gradients
- Loads produced during ground handling

In most vehicle systems internal tank pressure loads and axial-thrust loads are the principal forces of concern. Currently, the tanks are not considered for structural support of the airframe although this would be something to examine in the future. The tank design only considers supporting the fuel load at this time and ignores loads due to structural loading.

6.5 Conclusion

For the preliminary design of the structure, the simplest design was employed, a space frame. This was a sufficient model to investigate the preliminary materials and masses to be expected for the SSTO vehicle's structure. Future configurations should attempt to integrate the three main systems (frame, tank, and shell) into one structure. Each component should contribute to the overall structural integrity of the vehicle, thus decreasing the total mass. Another system that could be used to complement this structure would be an integral TPS system.

The following summarizes the masses achieved for the different components:

• Support Structure and attachments	9000 kg
• Outer Shell 1225 kg * 1.5 (SF)=	2000 kg
• Fuel/Cryogenic Tanks	10,200 kg
• Landing gear system	3500 kg
Total	24,700 kg

7.0 THERMAL ANALYSIS

7.1 Introduction

The current conceptual design is a reusable fast turn-around, single-stage-to-orbit vehicle, which attains speeds of Mach 25 on reentry and incorporates cryogenic fuels as major propellants. Since the ship will be in space for a maximum of seven days, it is necessary to insulate the cryogenic fuels from excessive boiloff. Research shows that the duration in space and the surface area of the tanks are directly related to the amount of fuel mass that will boiloff.[53] In order to keep the amount of boiloff low, it is necessary to use insulation materials that have low thermal conductivities and more importantly, low emissivities. Low conductivity impedes the heat transfer through conduction and the low emissivity decreases the transfer through radiation. Density is also a factor because it effects the overall weight of the entire vehicle. Research on materials with both desirable thermal and physical properties facilitates weight reduction efforts that are conducted in the optimization stage. Once the material and configuration are determined, the thickness, heat flux, and later boiloff masses are calculated.

Because of the high reentry speeds, the external shell needs to be thermally protected. Since leading edges and portions of the ship exposed to the direct flow will experience the largest temperature gradients, it is necessary to protect them with a material, namely reinforced carbon-carbon, which can withstand the temperatures experienced in these regions. Other areas on the bottom of the ship see increases in temperature, but since they are not as severe, a lighter less expensive insulation is used as protection in these regions.

Finally, a suitable radiation shield is needed to protect the crew from harmful solar flares. With 8.89 cm (3.5 in.) of aluminum placed as a barrier between the crew and the sun, there is sufficient protection against the strongest recorded flare. The aluminum works to decrease the amount of radiation experienced by the crew to a level of maximum allowable radiation for a thirty day time period.

7.2 Cryogenic Fuel Tanks

Many factors need to be considered when designing a thermal insulation system for longer storage, cryogenic tanks. To begin with, the physics need to be understood in order to answer the questions that arise in design. Next, the physical equations need to be examined to determine which parameters have the largest effect on the overall outcome. Some assumptions are necessary to find an approximate solution to the problem, but later more detailed analysis will need to be made to completely quantify the physical problem. Finally, materials and configuration should be chosen to yield the best possible solution to the simplified physical equations.

Multilayer Insulation Configuration. There are three modes of heat transfer: conduction, convection, and radiation. Conduction is the flow of heat from a region of high kinetic energy to one of lower kinetic energy through particle interaction. Convection is a collection of molecules moving across a surface where a temperature gradient exists between the outside air and the wall. Radiation is emitted energy of an object that is at a finite wall temperature. It does not need air to travel through and works very well in a vacuum. Since the environment in which the fuel tanks are contained will not be controlled, it is assumed to be nearly

devoid of air, therefore making the contribution of natural convection negligible. On the other hand, radiation thrives and conduction adds a slight effect to the overall heat transfer.

In an attempt to quantify the heating rate and eventual mass boiloff of the cryogen, some simplifications are necessary. The first assumption is that conduction on earth is analogous to that on the ship. This, however, does not take into account that the distance between molecules in space is much greater than on earth. More analysis of the effect of particle spacing on conduction will need to be made in the next phase of the design process. The outside temperature of the insulation is another assumption made in the analysis. A program written for determining the cryogenic boiloff rates did not have a way of determining the temperature, but instead calculated the boiloff rates and masses for a specific temperature input. Another assumption is made concerning the interior of the ship surrounding the tanks. In the present case, a cylindrical shape is assumed to simplify view factor calculations, but in the future a rigorous calculation of the view factor involving the actual interior geometry is necessary. The view factor refers to the way one wall "sees" another when the two are involved with heat transfer through radiation. Yet another assumption deals with the sloshing of fuel within the tanks. Sloshing occurs when the vehicle changes attitudes and could cause slight heat production due to circulation within the tank. Instead the fuel is assumed to be everywhere stationary within the tank, causing conductive and radiative heat exchange throughout all surfaces of the tank. The final assumption concerned contact resistances between the different insulation materials. This contact resistance is dependent on the materials that are in contact with each other and the method by which they are fastened together. A series of experiments would have to be carried out to quantify these resistances. Therefore, they are neglected here. However, by neglecting this phenomena, an additional safety factor is created as a bi-product. With contact resistance present, the total resistance would actually be higher than our analysis shows which in turn would result in a lower heat flux.

Once the simplifications are made, the physical equations are studied to better understand the problem and pose a solution. As stated previously, there are two major components of heat transfer to consider: conduction, and radiation. Conduction can be analyzed as a circuit where the thermal conductivities and areas combine according to the specific geometry and create a resistance. The temperature gradient across the insulation provides the voltage drop, and the current is analogous to the heat in or out of the system (in this case heat would be flowing in). Fig. 7.1 represents a schematic of the circuit used to find the heat transfer through the tank which consists of a cylinder for the main body and two hemispherical endcaps. Equations 7.1 and 7.2

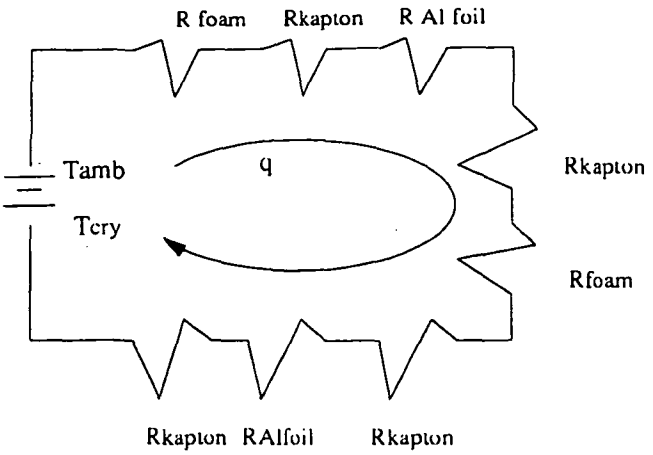

Fig. 7.1 Thermal Circuit

represent the resistances of the geometries present in the tanks. Equation 7.1 represents the resistance for a cylinder

$$R_{t,cond,cylinder} = \frac{\ln\left(\frac{r_2}{r_1}\right)}{2\pi L k} \tag{7.1}$$

$$R_{t,cond,sphere} = \frac{1}{4\pi k}\left(\frac{1}{r_1} - \frac{1}{r_2}\right) \tag{7.2}$$

and Equation 7.2 represents that for a sphere. In the equations, k represents the thermal conductivity through the material, r_1 represents the inner radius of the insulation, and r_2 is the outer radius. In Equation 7.1, L refers to the thickness of the material over which the resistance is being measured. Research shows that layered materials have resistances that add in series, thus contributing to a design with a decreased thickness and an increased impedance to heat flux.[53,56] This fact is true for both the cylindrical and spherical portions of the tank. To obtain the total heat flux, q, through the material over both the spherical and cylindrical portions, their respective heat flux values are added linearly. Equation 7.3 describes this in mathematical terms.

$$q_{cond} = \frac{\left(T_{jac} - T_{cry}\right)}{R_{t,cond,cylinder}} + \frac{\left(T_{jac} - T_{cry}\right)}{R_{t,cond,sphere}} \tag{7.3}$$

A more rigorous approach would have involved the solution to the three dimensional heating equation governed by the partial differential Equation 7.4. The operator

$$\nabla^2 T = q_{source} \tag{7.4}$$

indicates a temperature gradient in three dimensions, expressed in terms of the cylindrical and spherical coordinate systems. This equation would account for the possible sloshing of fuel within the tank. Since this undertaking is outside of the scope of this phase of the design process, it will be looked into in the future. Note that this equation is nonhomogeneous in nature and will require the solution of Bessel functions.

Lexan pins will hold the insulation on the tank. These pins will conduct heat into the tank according to Equation 7.5. *NPINS* is the number of pins used to attach the

$$q_{pin} = \frac{NPINS \cdot A_p k_{pin}\left(T_{jac} - T_{cry}\right)}{t} \qquad (7.5)$$

insulation, A_p is the cross sectional area of the pin, t is the thickness of the insulation tile, T_{jac} is the temperature of the outside of the insulation, and T_{cry} is the temperature of the cryogen.

Because of the vacuum or near vacuum conditions surrounding the tanks, radiation becomes the overriding factor in heat transfer. Like conduction, radiation is governed by geometry, and in addition, exposed surface area. Equation 7.6 is used to calculate the radiative heat transfer,

$$q_{surface} = \sigma F_{j-jac} F_e A\left(T_{amb}^4 - T_{jac}^4\right) \qquad (7.6)$$

$$F_e = \left(\frac{1}{\varepsilon_{jac}} + \frac{A_1}{A_2}\left(\frac{1}{\varepsilon_{amb}} - 1\right)\right)^{-1} \qquad (7.7)$$

where F_e (Eq. 7.7) is the emissivity factor for concentric cylinders. $F_{j\text{-}jac}$ is the view factor governing the way the interior of the ship "sees" the exterior of the tanks. Since an assumption of concentric cylinders is made, this term takes on a value of one. In Equation 7.6, σ refers to the Stephan-Boltzmann constant, A is the surface area of the insulation, T_{amb} is the surrounding ambient temperature, T_{jac} is the temperature on the outside of the insulation, and A_1/A_2 is the ratio of the internal surface area of the ship to the surface area of the insulation system.

Radiative heating is also present in the seams which exist between the attached tiles. Equation 7.8 represents this heat gain. e_1 represents the emissivity of the tank, e_2 is the

$$q_{seam} = \varepsilon_1 \varepsilon_2 F_{seam} L_{seam} W_{seam} \sigma\left(T_{jac}^4 - T_{cry}^4\right) \qquad (7.8)$$

emissivity of the outside layer of insulation, F_{Seam} is the two dimensional view factor of a rectangular tile, L_{seam} is the total length of the seams, W_{Seam} is the width of the seam, and σ is the Stephan-Boltzmann constant. The temperatures are the same as those in Equations 7.5 and 7.6.

Once all of the various heat fluxes have been determined a total heat flux can be found using Equation 7.9. The heat

$$q_{tot} = q_{cond} + q_{seams} + q_{surface} + q_{pins} + q_{structure} \qquad (7.9)$$

loss due structural considerations is estimated to be approximately 20% of q_{tot}. This gives a final heat flux according to Equation 7.10.

$$q_{final} = 1.2 q_{tot} \qquad (7.10)$$

Finally the boiloff mass can be calculated according to Equation 7.11. hf_g refers to the heat of vaporization, and m is the amount of mass that is boiled off.

$$m = \frac{q_{tot}}{h_{fg}} \qquad (7.11)$$

By close examination of the formulas, it becomes apparent that materials with low conductivity and emissivity are needed to reduce the rate of transfer by both radiation and conduction. The actual materials will be discussed in greater detail later. Table 7.1 illustrates the boiloff mass in the hydrogen tanks and the oxygen tank, the maximum allowable boiloff mass, the mass of the insulation, and the thickness. As a design parameter, the maximum amount of

Tank	Mass boiloff (kg)	Max. Boiloff Mass (kg)	Mass of Insulation (kg)	Insulation Thickness (mm)
LH_2	.1024	.73097	79.73	7
LO_2	.0653	3.998	24.94	5.5

Table 7.1 Tank Insulation and Boiloff

allowable boiloff is 1% of the amount of fuel that will be present in space. A safety factor of about 1.2 is used in the hydrogen tank. The oxygen tank never approaches the maximum allowable boiloff, but insulation is used to compensate for any errors associated with the jacket temperature calculation. These situations have not been fully optimized and will need to be scrutinized further in the next phase of the design.

Tank Insulation. One of the first steps in designing adequate cryogenic fuel tanks is to analyze where insulation is necessary. Since the main liquid oxygen and liquid hydrogen tanks for this SSTO will be filled until just prior to liftoff and then subsequently will be completely depleted of fuel during ascent, these tanks will require very little insulation. It was determined that the only necessary protection will be an approximately two millimeter thick

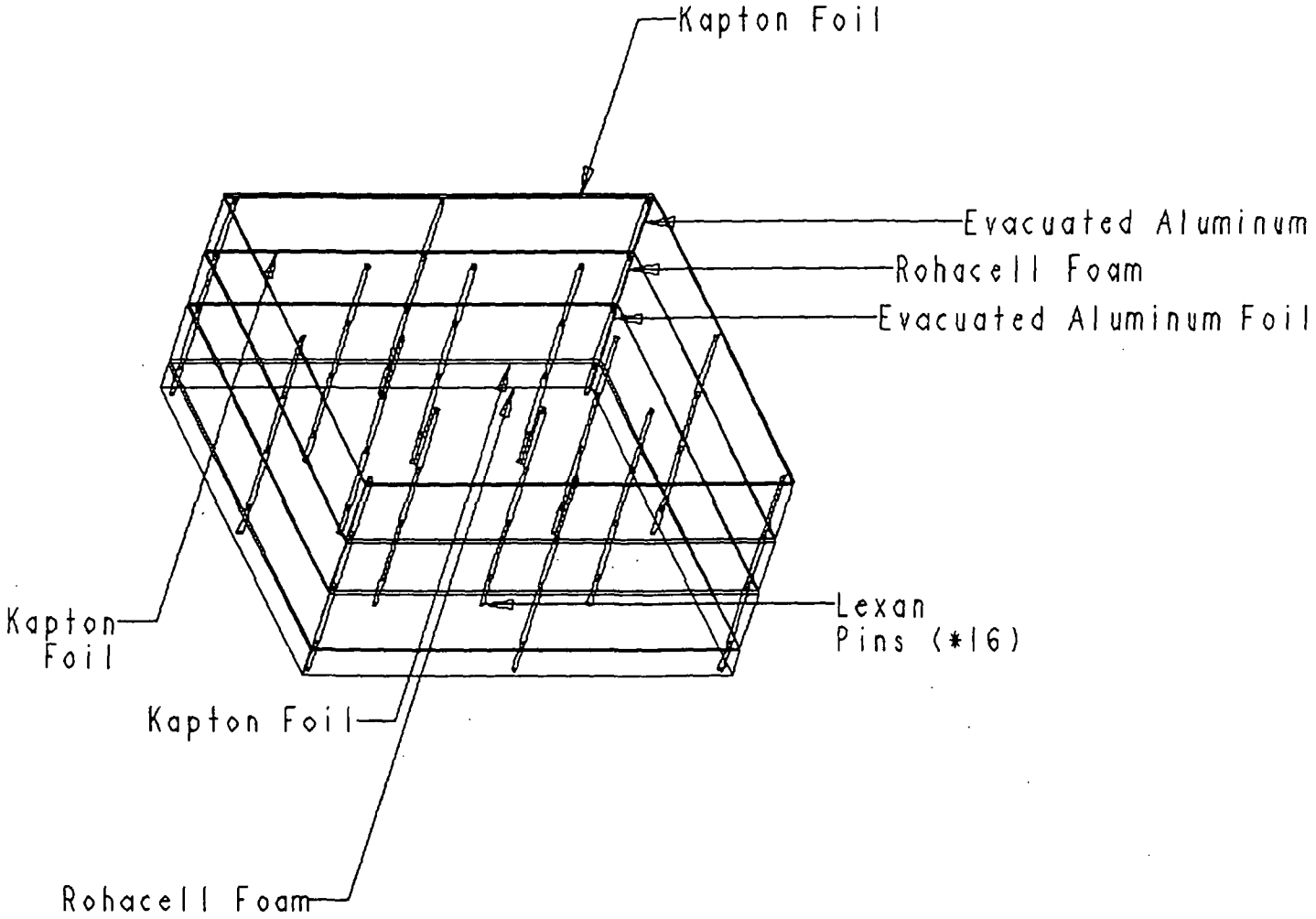

Fig. 7.2 Insulation Tile

layer of evacuated aluminum foil to prevent condensation and ice formation on the tanks.

A thin insulation material is not sufficient to impede the heat flux into the cryogen for the maneuvering fuel tanks. Additional insulation material covering the entire surface area is also needed, especially in the case of the LH_2 tank. As stated previously, materials with low density and favorable thermal properties are desired. However, it is also necessary to have materials that do not become brittle from exposure to cold temperatures or have a short lifetime. The three materials chosen are kapton, aluminum foil specially manufactured for use in cryogenic insulation, and also a foam material called Rohacell.[57] Each of these materials possess features which are compatible with requirements of weight and heat flux reduction. Table 7.2 indicates the material along with its thermal conductivity and density.

Material	Conductivity (W/mK)	Density (kg/m^3)
Kapton[7]	0.12	1420
Aluminum foil	0.00016	40
Rohacell foam[10]	0.0173	49.66

Table 7.2 Material Properties

A layered configuration of kapton, aluminum foil, kapton, foam, kapton, aluminum foil, kapton, and foam is designed to be manufactured in tile form. This configuration not only provides an excellent heat flux impedance, but also allows for ease in manufacture. By having materials with the lowest thermal conductivities closest to the cryogen, any heat which had not been adequately dissipated in these layers will later encounter materials that can provide an additional exponential decrease in the heat flux. Fig. 7.2 shows one tile which will be attached by 16 lexan pins.

The decision to use these materials stems from three primary factors. First, they are fairly light-weight. Second, they have desirable thermal characteristics. Finally, they have been used before in cryogenic applications, thereby satisfying the requirement of a reliable system. They will be manufactured in tile form so that they may be replaced easily if they become damaged. Another material under consideration was dacron which had been used for insulation on a space transportation vehicle.[53] This material needed to be thicker then the Rohacell foam and would consequently be more massive, so it was not used. Other forms of attachment were also considered. Instead of lexan pins, an adhesive system was researched. The adhesive, #12 PSA[58], was one found that could withstand the lowest temperatures but was still inadequate to handle the cryogenic temperatures of 50° K (-369.4° F) and 100° K (-279.4° F) for the LH_2 and LO_2 tanks respectively.

Cost and Lifetime Analysis. Since one of the primary goals of this vehicle is reusability, the endurance of the material used for the insulation system is also considered. Kapton can withstand temperatures between 4° K (-452.2° F) and 672° K (750.2° F). The temperature range experienced by the insulation system is about 50° K (-369.4° F) to 300° K (80.6° F), which is well within the envelope of extremes, therefore making the material very durable since it is not being pushed to its limits. Rohacell foam is capable of withstanding 250 thermal-mechanical cycles, which are far more extreme than that experienced in this configuration. Information concerning durability of aluminum foil will be examined in the future.

The only cost estimate available is for kapton. The raw cost of kapton is $134/kg ($60.91/lb) with an aggregate cost of $672/kg ($305.45/lb).[54] Note the aggregate cost refers to the total cost including manufacturing and labor. In the future, cost analysis of Rohacell and foil will be acquired.

7.3 Thermal Protection System

The main goal in determining the thermal protection system (TPS) for ascent and reentry is finding materials that supply adequate protection, are reusable, cost-effective, and technologically proven, while adding as little weight to the vehicle as possible. In order to design a system that will provide adequate protection while simultaneously keeping the overall weight of the vehicle low, peak heating rates and temperatures need to be determined. Due to time limitations during this phase of the design, rigorous calculations of the overall heating profile were omitted. Instead, temperature isotherms of the Space Shuttle Orbiter are used as a guide and are rescaled to fit the SSTO vehicle.

Materials. Using the Shuttle heating profiles, five main regions of thermal heating were determined. Table 7.3 indicates the isothermal regions, peak temperatures, and percentages of total surface area covered. Region 5 has such minimal heating that no special thermal protection is necessary.

Region	Maximum Temperature (°K)	Percentage Total Surface Area
1	2000	2.43
2	1755	25
3	1366	13.73
4	811	5.42
5	<811	53.42

Table 7.3 Isothermal Heating Regions

In deciding the exact materials that will be implemented into the final design, there are many factors to consider. Besides giving adequate protection, materials have to be technologically-proven, easily manufactured, and easy to implement into the design. With these constraints in mind, a combination of four different thermal protection systems will be used on the exterior of the vehicle.[55]

For the highest temperature region, a material known as reinforced carbon-carbon (RCC) is used as protection. This material is currently used on the Space Shuttle Orbiter and is proven to be an adequate insulator for extreme reentry environments. The trade off is that this material has a very high density, so its use is limited to areas of peak heating. The material chosen for the second highest temperature regions is an advanced carbon-carbon (ACC) standoff system. This system includes layers of coated carbon-carbon, saffil alumina, Q fiber, astro quartz, columbium, and nomex felt. The third region is encased in a superalloy bimetallic "sandwich" which incorporates layers of inconel, cerachrome, Q fiber, titanium, and nomex felt. The final material for the TPS is a titanium multiwall structure which is composed purely of titanium with a nomex felt liner. The main feature of this system is the manner in which the titanium is arranged. The multiwall feature consists of 4 layers of titanium separated by a corrugated type of titanium spacer that is in a repeated D-shape. Refer to Appendix E for the diagrams for the insulation system. Table 7.4 indicates the materials, their thicknesses, and their manufactured sizes.

Material	Thickness (m)	Size (m x m)
RCC	0.0254	0.3 x 0.3
ACC	0.0630	0.91 x 0.91
Superalloy	0.0470	0.3 x 0.3
Multiwall	0.0193	0.305 x 0.305

Table 7.4 TPS Dimensions

All of these materials, with exception of the RCC and ACC, will be attached using a bayonet clipping attachment system. This type of attachment involves a bayonet shaped greater then the surface of the sun; however, the gas temperatures behind the shock experience exponential

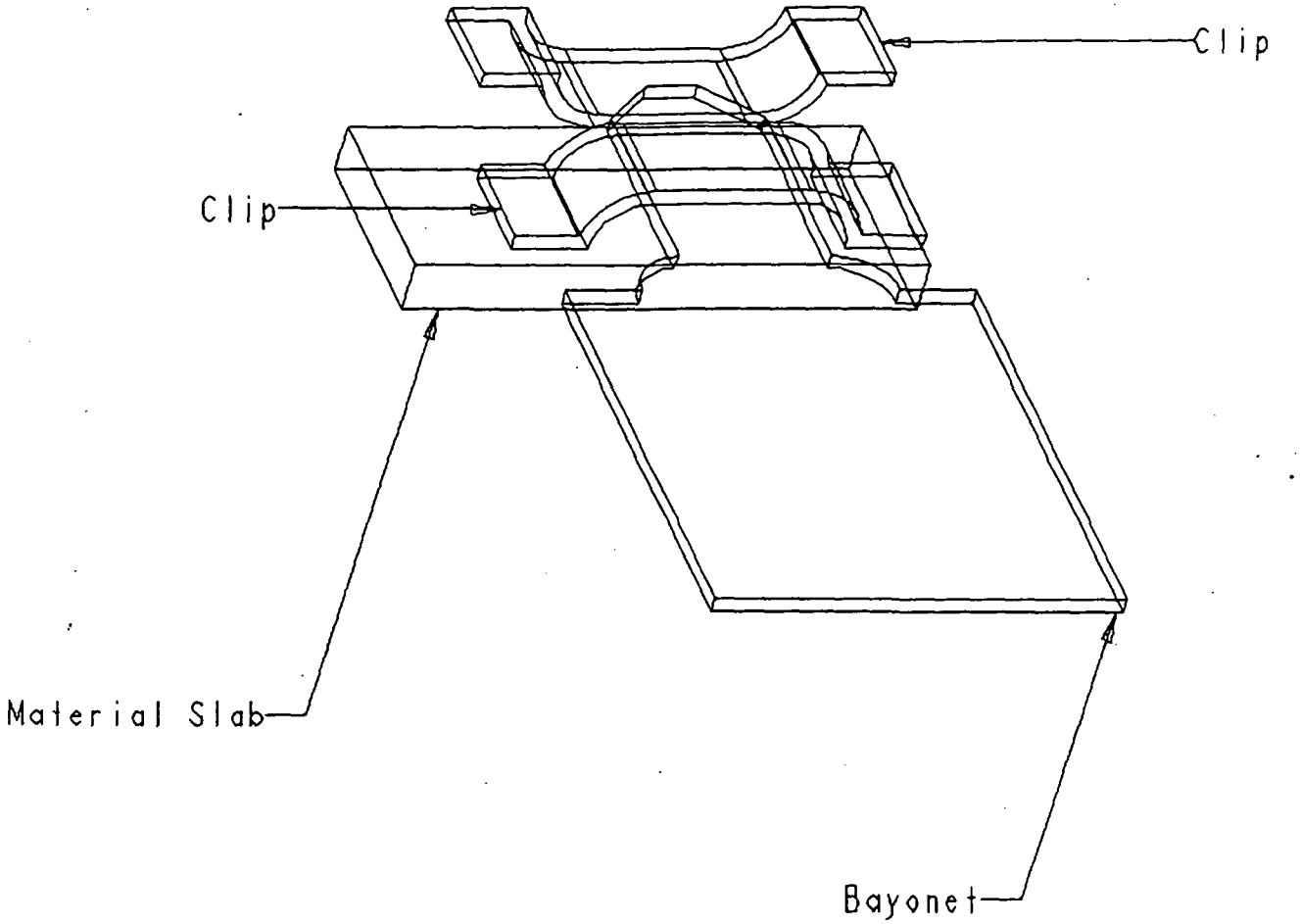

Fig. 7.3 Bayonet

decrease. By the time the hot gases reach the nose cone, the pin fastened to the underside of the TPS which is inserted into a clip that is mounted on the skin of the vehicle. Fig. 7.3 illustrates this attachment system. This design is easily attached to the external skin, and also allows for minimal complications in the event that a tile needs to be replaced. This attachment has a standard spacing between each of the tiles to allow for thermal expansion that is experienced during extreme heating. These gaps will then be lined with a quartz felt material to prevent hot gasses from directly impinging the skin of the vehicle. The felt is currently used on the Shuttle and is capable of withstanding compression due to tile expansion. It returns to its original shape when thermal expansion is no longer present. The RCC and ACC will both be attached to the skin using columbium pins.

In the future, the thermal protection system can be optimized by using computational fluid dynamics (CFD). An analysis of this nature would involve the solution to Equation 7.12. The operator indicates the gradient of the

$$\nabla^2 T = q_{source} \qquad (7.12)$$

three-dimensional temperature governed by the external geometry coordinate system, and q_{source} refers to the source heating caused by the shock wave around the vehicle. Once again, this is a nonhomogeneous partial differential equation which needs to be evaluated on small elements of the ship continuously over the entire surface area. An analysis of this nature is beyond the present scope but in the future can be used to decrease both the weight and cost of the TPS.

Limiting Dimensions. The nose cone and leading edges of the vehicle need special thermal consideration since they are the most affected by heating. Each part is governed by specific heating equations relative to the geometry and location on the ship. In order to obtain minimum dimensions, an unsteady form of these equations is implemented in the form of a FORTRAN program[51] which calculates the maximum temperature experienced by the configuration.

At reentry velocities, a detached bow shock forms in front of the nose cone. At the shock, the temperatures are primary form of heat transfer is conduction. Radiation, both

to and from the wall, is also present but is neglected in an effort to simplify the calculations. To legitimize this assumption, research shows that velocities below 8500 m/s (27,888.5 ft/s) do not have large contributions from radiation.[49]

A boundary layer is formed in the region between the bow shock and nose cone. Boundary layer thickness is dependent on the velocity of the craft and the atmospheric density, with a maximum equaling the distance from the nose to the shock. The boundary layer acts as a thermal blanket to absorb some of the heat transferred to the craft. Since the ability of the boundary layer to absorb heat is dependent on its thickness, the heat that reaches the craft varies with altitude and velocity. However, given that the maximum thickness is limited to the distance to the bow shock, the thermal advantage is subsequently restricted.

From a thermal point of view, the most important dimension on the craft is that of the nose cone radius. In order to determine an adequate protection system, a peak heating must be determined. This peak heating occurs at the stagnation point of the nose. An unsteady analysis was performed in order to compensate for the decrease in velocity which is directly proportional to the heat flux. The FORTRAN program[51] (see Appendix F for documentation of the program) used the inputs of thermal conductivities, velocities, and altitudes as functions of time (Equations 7.13 and 7.14) to determine heating according to Equation 7.15. This program then output the temperatures of the nose cone relative to position along the descent trajectory. t is time,

$$v(t) = \frac{1}{\tan 6^\circ}(-96.656 + 0.375t) \quad \text{m/s} \qquad (7.13)$$

$$h(t) = 9.8638 \times 10^4 - 96.656t + 0.1875t^2 \quad \text{m} \qquad (7.14)$$

$$q_{w_{cone}} = CV_\infty^3 \left(\frac{\rho_\infty}{r_{cone}}\right)^{0.5} \quad \text{W/m}^2 \qquad (7.15)$$

$v(t)$ is velocity as a function of time, C is a constant, V_∞ is the velocity of the vehicle, ρ_∞ is the density in the freestream, r_{cone} is the radius of the nose cone.

After several iterations, the minimum nose cone radius was found to be 0.4 m (1.3124 ft). This value is based on the thermal conductivity of reinforced carbon-carbon (RCC). However, the design of the craft might require a larger radius for structural or system modulation purposes, which would actually reduce the peak temperature. The present design has a nose cone radius of 1.7 m (5.5777 ft) which is substantially larger than the minimum. In the future, an optimized nose cone should be incorporated to decrease the overall size and therefore weight of the vehicle.

The conductive heating experienced by the nose cone also applies to the leading edges. The amount of heat transferred depends on the placement, geometry (e.g. swept angle, surface area), and boundary layer thickness. Because of the thicker shock layer in front of the leading edges, a thicker boundary layer will absorb more heat. Equations 7.16-7.18 are used to determine heating rates for the leading edges. Λ_{eff} is the sweep of the wings, and $q_{w_{LE}}$ is the heat flux at the leading edge. Heat flux at the leading edge is comprised of an equation for heat flux to a cylinder, $q_{w_{cyl}}$, and heat flux to a flat plate, $q_{w_{FP}}$. P_e is the pressure at the edge of the boundary layer, u_e is the velocity at the edge of the boundary layer, x is the distance along the plate, and h_{aw} is the enthalpy at the wall.

$$q_{w_{LE}} = \left(q_{w_{cyl}}^2 + q_{w_{FP}}^2 \sin^2 \Lambda_{eff}\right)^{0.5} \quad \text{W/m}^2 \qquad (7.16)$$

$$q_{w_{cyl}} = 1.29(10)^{-4}\left(\frac{\rho_\infty}{r_{cyl}}\right)^{0.5}\left(1 - 0.18\sin^2 \Lambda_{eff}\right)V_\infty^3 \qquad (7.17)$$

$$q_{w_{FP}} = \frac{0.0104}{\text{Pr}_w}\left(\frac{p_e u_e}{x}\right)^{0.5} h_{aw}^{0.85} \quad \text{W/m}^2 \qquad (7.18)$$

Detailed calculations for the radius of the leading edge are beyond the scope of this phase of the design but will be carried out in the near future using techniques similar to that used for the nose cone. It might also be noted that the wings must be located within the bow shock. If the wings are outside, they will become impinged by the shock and will burn off immediately. At this early design stage, the actual location of the shock was not determined but in the future requires immediate attention.

Cost and Lifetime Analysis. The materials selected for the TPS must withstand repeated thermo-mechanical cycles. The layout of the TPS is directly related to the temperature gradient of the ship. Each material is used on regions which experience maximum temperatures that are well within their respective design limits. The raw costs of these materials range from $66/kg ($30/lb) for titanium to $2202/kg ($1001/lb) for RCC.[59] It should be noted that the raw cost is approximately 20% of the total cost of the system. Research has been done showing that RCC and ACC systems are capable of withstanding 5000 thermal cycles without any signs of wear.[8]

7.4 Radiation Shielding

Human Tolerances. The first step in selecting a suitable radiation shield for the SSTO vehicle is to determine safe radiation limits. The main criteria are limits set for LEO by the National Council on Radiation Protection.[64] These guidelines give limits for vital organ,

ocular lenses, and skin in terms of Blood Forming Organ (BFO) doses. A BFO dose is the radiation that is experienced at a five centimeter depth in the tissue. Table 7.5 shows these radiation limits.

It is important to note that there are two main types of radiation that occur during a space mission. The first is normal galactic cosmic rays. These rays are always present in space, but for design specifications of a flight time limited to seven days, these rays do not affect the welfare of the crew.

The purpose of radiation shielding is to protect against the increased radiation that is experienced during an intense solar flare. During a solar flare, the crew in LEO may be exposed to radiation as high as 400 rems in a matter of minutes. This is well above the safety limit for one-time exposure to intense radiation, and would most certainly be fatal. This extreme amount may be reduced to a 20 rem exposure with adequate radiation shielding.

Materials. The next step in determining the necessary radiation shielding involves researching materials. The reports show results of radiation protection for lead, gold, aluminum, lithium hydride, carbon dioxide, and water.[60] Of these materials, the best radiation protection is provided by water, followed by lithium hydride, and aluminum. Aluminum was chosen because of its long life, relatively low cost, and ease of application.

	Vital Organ (rems)	Ocular Lens (rems)	Skin (rems)
Career limit	100-400 *	400	600
Annual limit	50	200	300
30 day limit	25	100	150

* depending on gender and age

Table 7.5 Radiation Limits

Laboratory tests found that coverage of 24 g/cm^2 (0.3406 lbm/in^2) of aluminum is required to adequately protect a crew against the strongest recorded solar flare. Solar flares are currently predictable 24 hours in advance with studies being conducted by the National Oceanic and Atmospheric Administration (NOAA) for predictions as far as a week ahead. Because the bottom of the ship will be facing the sun, only one side of the command module will be covered with the aluminum. Since radiation is unidirectional the crew will be protected against the fatal exposure of the flare. The minimum shield thickness is 8.89 cm (3.5 in.), and the mass related with this configuration is 997 kg (2193.4 lb).

In the future, more weight saving and effective systems could be used. One such option is the layering of heavy and light materials, and another is the use of magnetic shielding. Currently, NASA is investigating these choices to check on their feasibility and determine the component materials for the alternating layers. Also, if solar flares are predictable 7 days in advance, it may be possible to schedule flights around the flares so the need for protection would be obsolete.

Cost and Lifetime Evaluation. The lifetime of aluminum is indefinite and is therefore a very good candidate for the radiation protection. The raw cost of aluminum is $6.61/kg ($3/lb) with an aggregate cost of $33.05/kg ($15/lb).

7.5 Conclusion

Thermal analysis is an extremely important part in the design of the SSTO vehicle. The main areas of concern are fuel tanks, the thermal protection system, and radiation protection. To protect the fuel against high rates of mass boiloff, a layered configuration of kapton, aluminum foil, and Rohacell foam is used. The layers create a more effective barrier against heat flux than a single material, thereby reducing weight. The TPS is designed to cover sixty-five percent of the vehicle and consists of ACC, RCC, superalloy bimetallic sandwich, and titanium, which protects the SSTO vehicle against the aerodynamic heating present on reentry. Finally, the aluminum radiation shielding was calculated to weigh 997 kg (2193.4 lb) and is 8.89 cm (3.5 in.) thick. This shielding only covers the side of the command module oriented towards the sun. This protection will bring radiation to survivable levels. Research and calculations show that the systems described above will protect this vehicle through all stages of flight.

8.0 ORBITAL MECHANICS

8.1 Introduction

Orbital mechanical calculations include finding which orbits are possible for the SSTO vehicle to achieve, how much fuel it will take for orbital maneuvering, the optimum launch locations, in-space stability and control requirements, and requirements for rendezvous with a space station and/or other vehicles. Orbital mechanics also entails looking into various abort scenarios and their requirements.

8.2 Orbits

General Orbits. An orbit around a body is not a circle. Actually, the orbit is an ellipse with the body at one of the ellipse's foci. A circular orbit is just a special case where the two foci lie on top of each other.

In order for the reader to understand orbital terminology, brief definitions for the various orbital elements are

presented here. See Fig. 8.1 for a visual representation of the orbital elements.

Generally, the body which is being orbited around is considered to be located at the point O, one of the two foci of an ellipse; the other foci is vacant. The center of the ellipse is the point C. The radius r is the distance of the object from the point O at any time. It is important to remember that, for an orbit around the Earth, the radius is the distance to the center of the Earth, not the altitude of the orbiting object. Thus, the radius of the orbit is the altitude plus the radius of the Earth (6378.1 km, or 3443.9 n.mi.). Due to convention, however, orbits are referred to by the

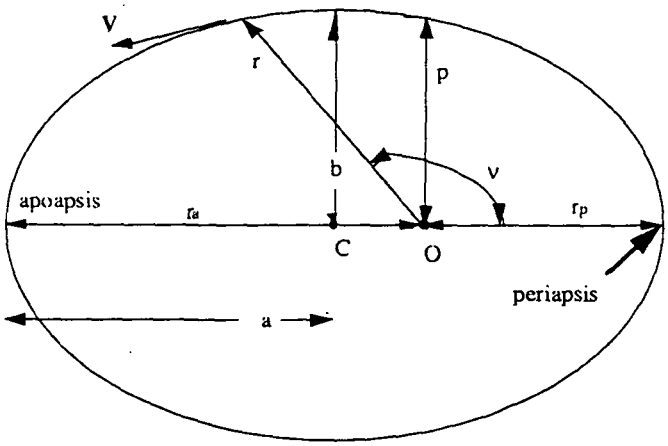

Figure 8.1 Orbital Elements

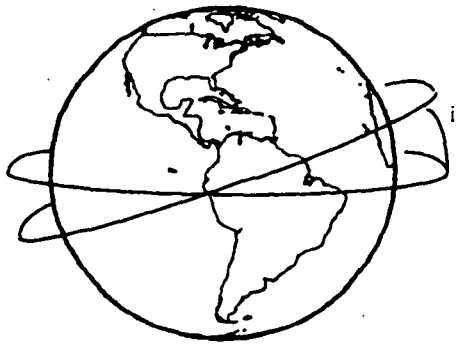

Figure 8.2 Orbital Inclination

height of their altitude; this convention will be followed throughout the remainder of the orbital mechanics section.

The velocity vector, V, is always tangent to the ellipse at any given instant, and the speed, v, is the magnitude of V.

The periapsis is the point on an orbit closest to the body, while the apoapsis is the point on an orbit farthest from the body. Any variables associated with these two points are usually denoted by a subscript p or a, respectively. For instance, the radius of periapsis is denoted by r_p.

The variable v represents the angle between the radius of periapsis and the current radius of the orbiting object. The variable p is called the semi-latus rectum and is the height of the ellipse when $v = 90°$.

The distance from the center of the ellipse to the apoapsis or periapsis is denoted by the variable a while the height of the ellipse is denoted by b. Note that the radius of periapsis plus the radius of apoapsis is equal to $2a$, and also note that a is a variable; do not confuse it with the subscript a, which is used to relate a variable to the apoapsis.

The other critical orbital element is the inclination angle, i. This element defines the angle made between the object's orbit and the plane of the Earth's Equator (see Fig. 8.2).

When calculating the orbit of an object, the orbital elements can be combined in order to calculate four necessary values: the specific energy, specific angular momentum, the eccentricity, and the period of the orbit. The specific energy is given by

$$\varepsilon = \frac{v^2}{2} - \frac{\mu}{r} = \frac{-\mu}{2a}, \qquad (8.1)$$

where μ is the gravitational constant of the object being orbited around. For the Earth, $\mu = 3.986 \times 10^5$ km^3/s^2 (1.406×10^{16} ft^3/s^2). The angular momentum is given by

$$h = rv\sin\phi = rv\cos\beta, \qquad (8.2)$$

where ϕ and β are defined in Fig. 8.3.

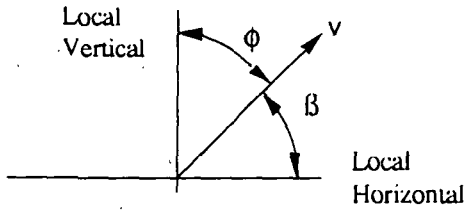

Figure 8.3 Definition of ϕ and β

The angular momentum and energy are constant as long as drag is assumed to be negligible.

The eccentricity of an orbit (e) is a measure of how "elliptic" the orbit is. An eccentricity of one means that the orbit is circular. The eccentricity of an elliptical orbit is given by

$$e = \frac{r_a - r_p}{r_a + r_p} = \sqrt{1 + \frac{2\varepsilon h^2}{\mu^2}}. \qquad (8.3)$$

The final value which needs to be calculated for an orbit is its period. For an ellipse, the period is given by

$$T = \frac{2\pi a^{3/2}}{\sqrt{\mu}}. \qquad (8.4)$$

Circular Orbits. As stated above, the circular orbit is a special case of an elliptical orbit. For a circular orbit, the radius and velocity are constant, and the velocity is given by

$$V_{cs} = \sqrt{\frac{\mu}{r_{cs}}}, \qquad (8.5)$$

where the subscript *cs* denotes a circular orbit.

To calculate the period of a circular orbit, just set $a = r_{cs}$ in the equation for the period of an ellipse.

The velocities and periods of the circular orbits at the inner and outer operating ranges of the SSTO vehicle (250 km (135 n.mi.) and 833 km (450 n.mi.), respectively) were calculated and are detailed below.

Circular Orbit at a 250 km (135 n.mi.) Altitude. For a circular orbit at an altitude of 250 km (135 n.mi.), the velocity necessary is 7.755 km/s (4.192 n.mi./s) and the orbital period is 89.50 minutes.

Circular Orbit at an 833 km (450 n.mi.) Altitude. For a circular orbit at an altitude of 833 km (450 n.mi.), the velocity necessary is 7.435 km/s (4.019 n.mi./s) and the orbital period is 101.6 minutes.

Transfer (Elliptical) Orbits. An elliptical orbit is used to transfer between two circular orbits which lie in the same plane; in order to transfer between these two orbits using the smallest ΔV, and hence the smallest amount of fuel, the periapsis and apoapsis of the transfer orbit are set so that they are at the same altitudes as the two target orbits (see Fig. 8.4).

The worst-case scenario for the SSTO is a transfer between the 250 km (135 n.mi.) circular orbit and the 833 km (450 n.mi.) circular orbit. The calculations and the results for this orbit are summarized below.

The worst-case scenario for reentry is a deorbit burn which will take the SSTO from a circular orbit of 833 km (450 n.mi.) to 80 km (43 n.mi.). A summary of the results for this transfer is also included.

Elliptical Orbit Between 250 km (135 n.mi.) and 833 km (450 n.mi.) Altitudes. The worst-case transfer orbit necessary would be an elliptical orbit with the periapsis at 250 km (135 n.mi.) and the apoapsis at 833 km (450 n.mi.); for this orbit, V_p = 7.916 km/s (4.279 n.mi./s) and V_a = 7.279 km/s (3.935 n.mi./s). The period for this orbit is 95.44 minutes.

Reentry Transfer Orbit. The reentry transfer orbit in a worst-case scenario is an elliptical orbit with the apoapsis at an altitude of 833 km (450 n.mi.) and the periapsis at 80 km (43.0 n.mi.). At the apoapsis, the velocity is 7.229 km/s (3.908 n.mi./s), while at the periapsis the velocity is 8.069 km/s (4.362 n.mi./s). The reentry time is one half the period of the ellipse. The period is 93.69 minutes, so the reentry time (to an altitude of 80 km (43.0 n.mi.)) is 46.85 minutes.

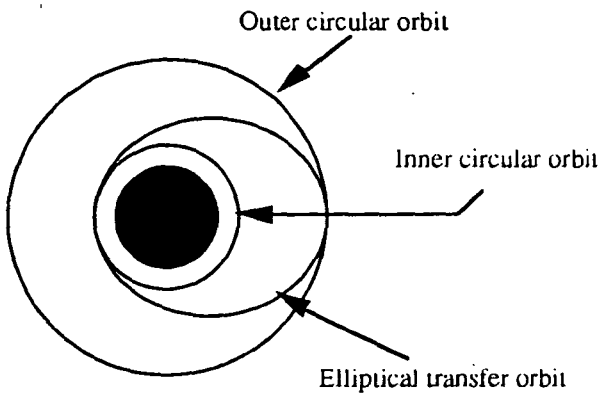

Figure 8.4 Transfer Orbit Between Two Circular Orbits

8.3 Orbital Maneuvers

Generally, maneuvering between two orbits is purely propulsive; that is, maneuvering relies solely on a specific impulse applied to the vehicle in order to change its velocity (or energy). When applying an impulse to the vehicle, the impulse can either lie in the same plane as the vehicle's orbit (coplanar orbit) or an out-of-plane impulse can be applied in order to change the orbital inclination.

Coplanar Orbital Maneuvers. When a coplanar impulse is applied to an orbiting vehicle, it has the effect of changing the shape of the vehicle's orbit. In order to change from an elliptical orbit to a circular orbit, the impulse is applied either at the periapsis or the apoapsis of the elliptical orbit, along vehicle's flight path. This is because at the periapsis or apoapsis of an elliptical orbit, the flight path angle equals 90°, and for a circular orbit the flight path angle always equals 90°. The magnitude of the impulse needed to change the orbit is equal to the final velocity desired at that point minus the initial velocity at that point ($\Delta V = V_f - V_i$).

Out-of-plane Orbital Maneuvers. Out-of-plane impulses applied to the vehicle have the effect of changing the orbital inclination angle *i*. However, large changes in *i* become very expensive in terms of the impulse needed to accomplish the plane change. The impulse (ΔV) and the

change in the inclination angle of the orbit (Δi) are related by

$$\Delta V = 2V_o \sin\left(\frac{\Delta i}{2}\right), \qquad (8.6)$$

where V_o is the velocity of the vehicle before the impulse is applied.

For a plane change of 60°, $\Delta V = V_o$,, which means that the out-of-plane impulse needed is equal to the velocity of the vehicle, somewhere in the neighborhood of 7.6 km/s (4.108 n.mi./s)![67] In order for the vehicle to be able to perform plane changes, some method other than purely propulsive maneuvering, such as an aero-assist plane change, is necessary.

Aero-Assisted Plane Changes. Aero-assisted plane changes are a relatively new concept and are still largely theoretical. In essence, the vehicle does a deorbit burn in order to reenter the atmosphere. Once the vehicle is within the confines of the atmosphere, the aerodynamic properties of the lifting body are used to turn the vehicle. After the turn is complete, the vehicle boosts itself up into orbit again. While this maneuver is still very expensive in terms of fuel consumption, the fuel needed for an aero-assist maneuver can be as low as 60% of that needed for a purely propulsive plane change. There are three basic types of aero-assist maneuvers which were examined: aeroglide, aerocruise, and aerobang.

Aeroglide. Essentially, this maneuver has the vehicle reentering the atmosphere with the engines off. There are some fuel savings when compared to a propulsive plane change, but the craft must enter deep into the atmosphere in order to accomplish the plane change. During an aeroglide maneuver, there is also a problem with skin heating on the order of that experienced during reentry.[69]

Aerocruise. For this maneuver, the thrust of the vehicle is kept equal to its drag. This allows for control of how deep the vehicle reenters the atmosphere and how much heating occurs. The depth of penetration into the atmosphere and the amount of heating are subject to the change in the angle of inclination, Δi, and the amount of time spent performing the maneuver. The fuel savings for this maneuver are difficult to quantify because they depend directly on how the maneuver is performed.[68]

Aerobang. For this maneuver, the thrust applied to the vehicle is equal to the maximum amount of thrust available. This allows control of the depth of reentry while allowing the maneuver to be completed in a short amount of time. This translates into overall fuel savings because the plane change maneuver is concentrated around the line of nodes (the line where the two planes intersect). This aero-assist maneuver concept is very new, and no estimates for the amount of fuel savings are available at this time.[70]

8.4 Ascent Trajectory

Orbital mechanics is responsible for calculating the final portion of the ascent trajectory, the portion which is outside of the Earth's atmosphere. Since the major concern for the SSTO vehicle design has been the overall weight, the trajectory calculation has focused on keeping the fuel consumption low rather than minimizing the time of ascent.

During its ascent through the atmosphere, the SSTO vehicle climbs with the underside towards the ground in order to make use of the lift provided by the vehicle. When the SSTO vehicle leaves the atmosphere, it needs to perform a roll in order to point the underside away from the Earth. This will allow the thermal protection system to protect the crew from solar heating.

The program OPGUIDE was used to optimize the ascent trajectory; at the peak of the ascent trajectory (an altitude of 150 km (81 n.mi.)), the main engines are burned so as to insert the SSTO into an elliptical orbit with the apoapsis at 250 km (135 n.mi.). When the SSTO reaches 250 km (135 n.mi.), its velocity will be 7.725 km/s (4.176 n.mi./s).

8.5 Summary of Basic Mission and Its Required ΔV's

Summary of Basic Mission. The SSTO has been designed around what is considered to be a worst-case scenario. This scenario is the one which will result in the highest fuel consumption and has been outlined below.

The SSTO will deploy its initial payload at an altitude of 250 km (135 n.mi.). Carrying the payload to a higher altitude before deployment would result in greater overall fuel consumption. After the payload has been deployed, the SSTO will transfer to another orbit in order to retrieve a satellite or other payload for return to Earth. The transfer orbit will take the SSTO from its 250 km (135 n.mi.) orbit out to 833 km (450 n.mi.), where it will insert into a circular orbit.

After inserting into the outer circular orbit, the SSTO will retrieve a satellite (estimated as having a weight of 9000 kg (19,800 lbm)) and then perform a deorbit burn in order to return to Earth. The deorbit burn will put the SSTO into an elliptical transfer orbit to take it to an altitude of 80 km (43 n.mi.).

When the SSTO reaches 80 km (43 n.mi.) it will be traveling at a speed of 8.069 km/s (4.357 n.mi./s); in order to avoid skipping off the Earth's atmosphere, it must be traveling at 7.90 km/s (4.266 n.mi./s) or slower. This means that the SSTO will have to perform a propulsive braking ΔV of at least 0.169 km/s (0.0913 n.mi./s).

Due to the large amounts of fuel required to accomplish plane changes, the worst-case scenario described above assumes that the SSTO will not change its orbital inclination. Missions requiring less fuel than the worst-case scenario may be able to use the excess fuel for small plane changes (1°-2°).

Summary of Required ΔV's. The ΔV's required for orbit transfers in the mission outlined above have been calculated and are listed in Table 8.1.

Maneuver	ΔV Required
Circularize at 250 km	30 m/s
Transfer to 833 km	161 m/s
Circularize at 833 km	157 m/s
Deorbit burn	207 m/s
Propulsive Braking	169 m/s
Orbital Corrections	50 m/s
Total	774 m/s

Table 8.1 Orbital ΔV Requirements

8.6 Effect of Launch Location on Launch Velocity Due to the Earth's Rotation

There are some savings on the ΔV's necessary to achieve orbit due to the rotation of the Earth. The Earth is rotating at a rate of 360°/24 hours, or $\omega = 7.272 \times 10^{-5}$ rad/s. The rotational velocity at any point on Earth is equal to the angular speed multiplied by the radius of rotation. The radius of rotation is the distance of the point on the Earth's surface from the Earth's rotational axis. This has been calculated for a spherical Earth model, and the radius of rotation (r_r) is given by

$$r_r = R_e \cos\theta, \tag{8.7}$$

where R_e is the equatorial radius of the Earth and θ is the latitude of the launch site (see Fig. 8.5).[2]

At the Equator, the rotational velocity is equal to 0.464 km/s (0.251 n.mi./sec); at a latitude of ±20° from the Equator, the rotational velocity is 94% of the velocity at the Equator; at ±30°, the velocity is 86.6% of the possible velocity gained at the Equator. After the latitude passes ±30°, the velocity drops off rapidly and the savings from the Earth's rotation are negligible. At this time, three possible launch locations for the SSTO have been chosen: Kennedy Space Center, FL, White Sands, NM, and northeastern Australia. The velocities gained at each of these locations are listed in Table 8.2.

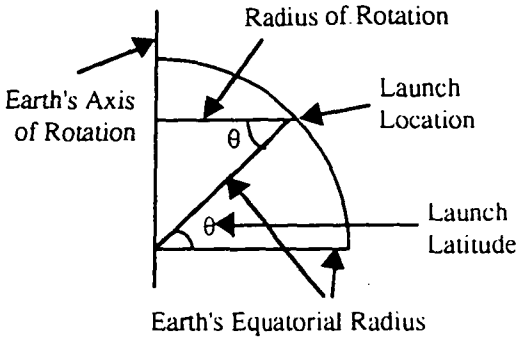

Figure 8.5 Effect of Launch Latitude on Radius of Rotation

Launch Site Location	Velocity Gained From Earth's Rotation
Cape Kennedy	0.410 km/s
White Sands	0.380 km/s
Australia	0.429 km/s

Table 8.2 Velocity Gained at Launch Site Due to Earth's Rotation

8.7 Abort Scenarios

During the ascent of the vehicle, if anything unexpected occurs which may jeopardize the mission, the vehicle, or the crew, it is desirable to have several options for aborting the flight. These options include Return to Launch Site (RTLS), Abort Once Around (AOA), Abort to Orbit (ATO), and Abort to Alternate Site (ATAS). Two of these abort scenarios have already been covered sufficiently in Section 2.0 and will not be reiterated here. However, the other two scenarios depend directly on orbital characteristics and are of particular interest at this time: AOA and ATO.

Abort Once Around. AOA is used in cases where the orbiting vehicle has enough momentum and altitude to make it all the way around the Earth but not enough to reach the desired orbit. Fig. 8.6 shows the time-in-orbit limits for an unpropelled vehicle due to atmospheric drag limitations. This figure shows that the minimum altitude for one orbit, which takes about 1.5 hours, is about 120 km (65 n.mi.).

Abort to Orbit. ATO is used in a situation where the SSTO vehicle has enough energy to maintain a sustained orbit for 50 hours. The minimum altitude for this orbit is about 185 km (100 n.mi.) (see Fig. 8.6).

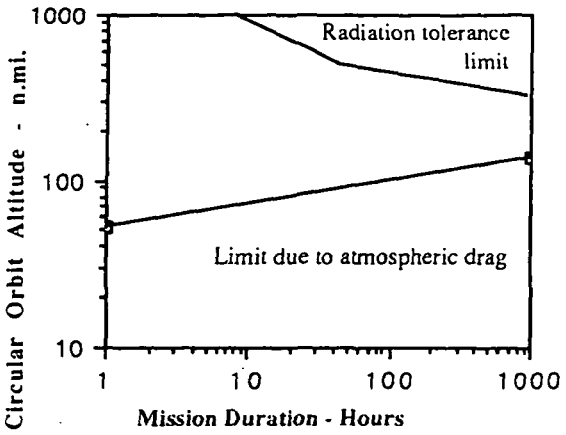

Figure 8.6 Limits on Mission Duration Due to Drag [2]

8.8 In-Space Stability and Control

In outer space, it is not possible to use aerodynamic properties to provide control for the vehicle. Reaction Control System (RCS) jets provide control for pitch, roll, and yaw maneuvers, as well as translational control during short-distance maneuvers such as rendezvous.

RCS Jets. In order to maintain stability and control in outer space, an array of 48 RCS jets is needed. Four jets are needed to roll around each axis in each direction. These jets are fired so as to produce a coupling moment which will rotate the SSTO vehicle without allowing it to translate. There are three axes (x, y, and z) and two directions of rotation for each axes (positive and negative), which leads to a total of 24 necessary RCS jets. With 48, the SSTO vehicle has a doubly redundant system.

Each of the RCS jets is throttleable; that is, the thrust from the jet can be controlled. The throttling factor, T, can be varied from 0.1 to 1 and is multiplied by the maximum thrust to give the amount of thrust being produced by the jet. The maximum thrust of each RCS jet is 71,000 N (15,962 lb.).

The rate of rotation around an axis is found by the equation

$$\Sigma F_i d_i = I_{aa}\alpha, \tag{8.8}$$

where F_i is the force produced by a jet (71,000 N/jet * T_i, where T_i is the throttle factor for the jet), d_i is the perpendicular distance of the jet from the axis being rotated around, and the subscript i denotes the fact that there are 4 jets firing at one time to produce a moment, each with its own distance and throttle factor. I_{aa} is the moment of inertia about the axis a, and α is the rate of angular acceleration about axis a. The angular velocity ω and the angular position θ can then be found by solving the equation for α and integrating. I_{aa} was left as a variable because it changes depending on the in-flight conditions: how much fuel is left, whether or not the SSTO is carrying a payload, etc. The results of the integration for pitch, roll, and yaw maneuvers are summarized below.

Pitch. The RCS jets provide a pitching moment about the y-axis of the vehicle, where the origin lies at the center of mass. The pitch rate (ω_y) provided by the jets is given by

$$\omega_y = \frac{71000t}{I_{yy}} \sum_{i=1}^{4} d_i T_i \text{ rad/s}, \tag{8.9}$$

where t is the time the jets are fired. The angle the craft has pitched after firing the jets for a time t is given by

$$\theta_y = \frac{35500t^2}{I_{yy}} \sum_{i=1}^{4} d_i T_i \text{ rad}. \tag{8.10}$$

Roll. The RCS jets provide a rolling moment about the x-axis of the vehicle. The roll rate (ω_x) provided by the jets is given by

$$\omega_y = \frac{71000t}{I_{xx}} \sum_{i=1}^{4} d_i T_i \text{ rad/s}, \tag{8.11}$$

and the angle the craft has rolled after firing the jets for a time t is given by

$$\theta_x = \frac{35500t^2}{I_{xx}} \sum_{i=1}^{4} d_i T_i \text{ rad}. \tag{8.12}$$

Yaw. The RCS jets provide a yawing moment about the z-axis of the vehicle. The yaw rate (ω_z) provided by the jets is given by

$$\omega_y = \frac{71000t}{I_{zz}} \sum_{i=1}^{4} d_i T_i \text{ rad/s}, \tag{8.13}$$

and the angle the craft has yawed after firing the jets for a time t is given by

$$\theta_z = \frac{35500t^2}{I_{zz}} \sum_{i=1}^{4} d_i T_i T t^2 \text{ rad}. \tag{8.14}$$

8.9 Rendezvous

There are several situations in which the SSTO vehicle may be required to rendezvous with another orbiting object, such as when the vehicle is trying to recover a satellite or intercept a space station. During a rendezvous, the SSTO vehicle should be maneuvered using automatic controls with a manual backup. The Global Positioning System (GPS) will be accurate enough to get the SSTO vehicle within 50 m (164 ft) of the target object. Inside this 50 m (164 ft)

radius, the flight controls would be transferred to other tracking systems. However, no computer algorithm could possibly account for all of the possible situations which may arise; allowing for manual control as a backup would permit a more flexible response to unforeseen circumstances.

Orbits Used For Rendezvous. Since the speed of an object in orbit is inversely proportional to the square root of its radius, objects with lower altitudes move faster. Thus, if it is desired to catch up with an object in orbit, the SSTO vehicle must be inserted into a lower orbit and later transferred up to the same orbit as the target vehicle. Conversely, if the SSTO vehicle needs to slow down to wait for the target vehicle, it must translate up to a higher orbit and then come back down later.

8.10 Cost Evaluation

Empty Weight	Total Orbital Fuel	Times S.F. of 1.02	Percent of Empty Weight	Total Orbital Fuel Cost
55000 kg	11315 kg	11541 kg	20.98 %	$8,540
56000 kg	11504 kg	11734 kg	20.95 %	$8,683
57000 kg	11693 kg	11927 kg	20.92 %	$8,826
58000 kg	11882 kg	12120 kg	20.90 %	$8,969
59000 kg	12071 kg	12313 kg	20.87 %	$9,111
60000 kg	12260 kg	12505 kg	20.84 %	$9,254
61000 kg	12449 kg	12698 kg	20.82 %	$9,397
62000 kg	12639 kg	12891 kg	20.79 %	$9,540
63000 kg	12828 kg	13084 kg	20.77 %	$9,682
64000 kg	13017 kg	13277 kg	20.75 %	$9,825
65000 kg	13206 kg	13470 kg	20.72 %	$9,968
66000 kg	13395 kg	13663 kg	20.70 %	$10,111
67000 kg	13584 kg	13856 kg	20.68 %	$10,253
68000 kg	13773 kg	14049 kg	20.66 %	$10,396
69000 kg	13962 kg	14242 kg	20.64 %	$10,539
70000 kg	14152 kg	14435 kg	20.62 %	$10,682
71000 kg	14341 kg	14628 kg	20.60 %	$10,824
72000 kg	14530 kg	14820 kg	20.58 %	$10,967
73000 kg	14719 kg	15013 kg	20.57 %	$11,110
74000 kg	14908 kg	15206 kg	20.55 %	$11,253
75000 kg	15097 kg	15399 kg	20.53 %	$11,395
76000 kg	15286 kg	15592 kg	20.52 %	$11,538
77000 kg	15475 kg	15785 kg	20.50 %	$11,681
78000 kg	15665 kg	15978 kg	20.48 %	$11,824
79000 kg	15854 kg	16171 kg	20.47 %	$11,966
80000 kg	16043 kg	16364 kg	20.45 %	$12,109

Table 8.3 Required Orbital Fuel and Its Costs

The only costs associated with orbital mechanics are those related to fuel used during maneuvering. Each ΔV required by the SSTO vehicle will result in a certain amount of fuel consumption. The method for calculating the fuel required and the cost of this required fuel have been summarized below.

Fuel Necessary for ΔV Changes. To accomplish a ΔV change, a certain amount of fuel is required. Thus, as fuel is burned, the total mass of the SSTO vehicle is changed. The relationship between the mass before the burn and the mass after the burn is given by

$$\frac{M_i}{M_f} = \exp\left(\frac{\Delta V}{g_o I_{sp}} \right), \qquad (8.15)$$

where M_i is the mass of the SSTO vehicle before the burn, M_f is the mass of the SSTO vehicle after the burn, g_o is the gravitational constant at sea level (9.81 m/s^2, or 32.2 ft/s^2), and I_{sp} is the specific impulse of the SSTO vehicle's engines (444 s for the OMS engines). The amount of fuel burned is then given by M_i minus M_f.[66]

The amount of fuel necessary for orbital maneuvers is dependent directly on the SSTO's empty weight, which has been defined as the weight of the vehicle without the payload or any fuel. The amount of orbital fuel needed as a function of the empty weight has been summarized in Table 8.3.

Cost of Fuel Used for Orbital Maneuvers. The SSTO's OMS engines require an 85.7% LO_2/14.3% LH_2 mix of fuel. The LO_2 costs $0.113 per kilogram ($0.051 per pound), and the LH_2 costs $4.50 per kilogram ($2.045 per pound). Therefore, the fuel mixture has a cost of $0.74 per kilogram ($0.034 per pound) of mixture. The cost of this mixture as a function of the empty weight is also included in Table 8.3.

8.11 Conclusion

The SSTO design has the capability to operate in the range of altitudes up to 833 km (450 n.mi.). The SSTO has been allotted an amount equal to about 21% of its empty weight for orbital fuel, which leaves it without the capability of performing large orbital plane changes. However, the use of non-propulsive means for making plane changes, such as aero-assisted maneuvers, may make plane changes feasible in the future. The ascent trajectory was calculated and optimized using the program OPGUIDE, and the reentry orbit was calculated down to an altitude of 80 km (43 n.mi.). The ascent trajectory from ground level to the outer limits of the atmosphere, as well as the reentry trajectory from 80 km (43 n.mi.) to the ground, are discussed in Section 9.0.

9.0 ASCENT/REENTRY AERODYNAMICS

9.1 Introduction

Vehicle performance analysis was completed in the areas of stability and control, vehicle down-range and cross-range capabilities during reentry, and aerodynamics.

The implementation of a lifting body was decided upon to create the lift required to achieve a safe reentry into the earth's atmosphere and horizontal landing. A previously tested lifting body, the HL-20 was used to provide baseline lifting body geometry. Performance characteristics were defined by a lifting body aerodynamic model called the Generic Hypersonic Aerodynamic Model Example (GHAME). GHAME provided the best reference for the conceptual design input because the model uses both analytical and empirical data of generic lifting body designs. The values provided by GHAME were used to accomplish other design and analysis tasks. The values presented for aerodynamic coefficients in this document are attainable performance goals. Future design input will be focused on achieving the values presented here. Aerodynamic performance goals were also derived from current Space Shuttle specifications because it became apparent that the SSTO vehicle has a size and weight that is of roughly the same magnitude as that of the Space Shuttle. The ascent and reentry profiles of the Space Shuttle were also used as the baseline design. From the ascent and reentry trajectories, in addition to aerodynamic coefficient design goals, stability, control, and vehicle range capabilities were estimated.

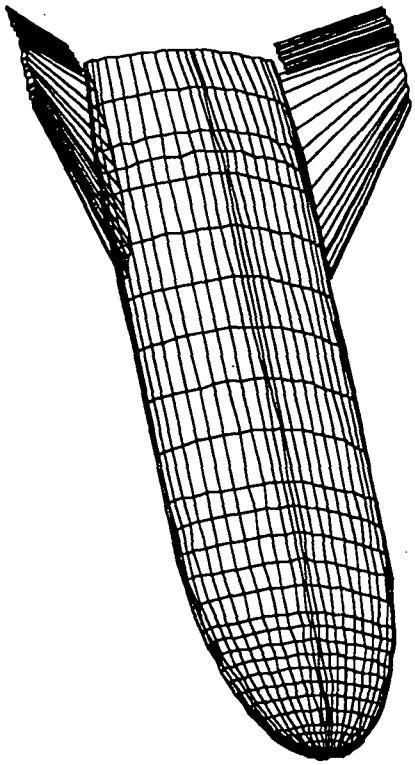

Figure 9.1 Optimized Geometry

9.2 Aerodynamics

After researching the shapes of past lifting bodies, the HL-20 lifting body vehicle design became the geometric model for this design. The HL-20 was selected based on the availability of previously published data and the fact that its lifting body design produced L/D values that fell within

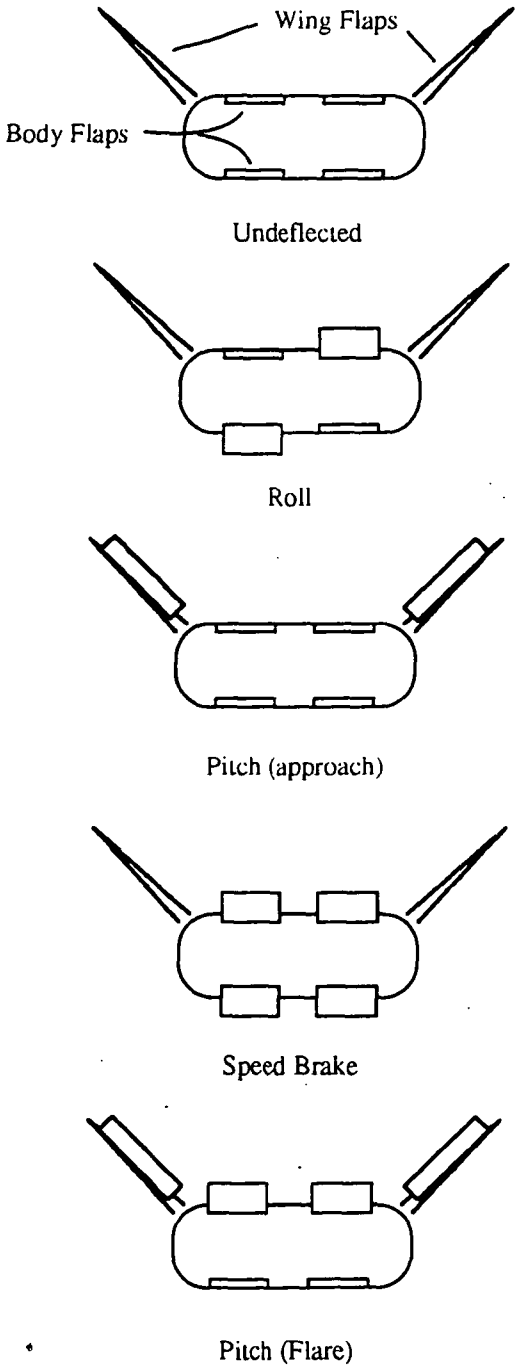

Figure 9.2 Control Surface Configurations

initial design goals for the SSTO vehicle. With this geometry, the programs, FUSEX and SHAB (the supersonic/hypersonic arbitrary body program), were used to optimize the vehicle geometry to provide the most efficient fit of all vehicle components (fuel tanks, payload bay, etc.) while maintaining the lifting body geometry of the HL-20. The resulting geometry is illustrated in Fig. 9.1.

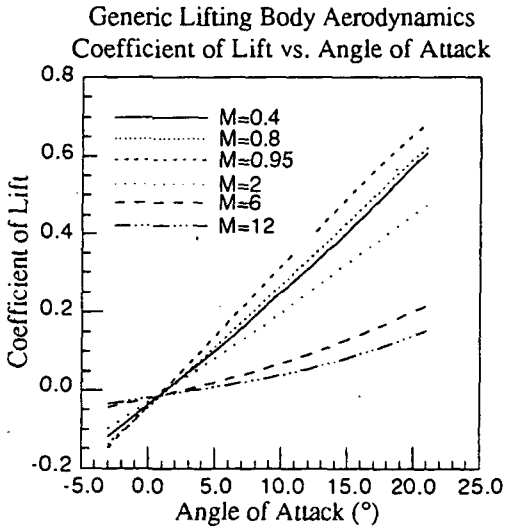

Fig. 9.3 Generic Lifting Body c_l vs. α

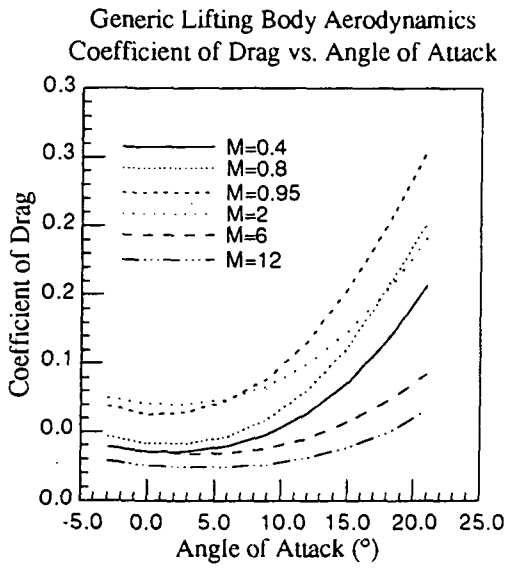

Fig. 9.4 Generic Lifting Body c_d vs. α

Control surfaces and body flaps were implemented to provide vehicle control in all axes of rotation. The HL-20 utilizes similar control methods, which simplified the process of sizing these surfaces because they only needed to be scaled up for this application. The control surfaces are attached to very low aspect-ratio wings near the aft end of the fuselage. They have a very high sweep angle and a high dihedral (30°). Due to this fact, the control surfaces provide negligible lift to the vehicle and are useful only for vehicle control. The body flaps and wing control surfaces can be actuated either in sync or differentially to provide pitch, yaw, and roll control as indicated in Fig. 9.2.

The aerodynamic coefficients in Figures 9.3-9.6 are generic coefficients produced from the GHAME consisting of four models for lifting body vehicles, two aerodynamic and two aero-thermodynamic. The empirical wind tunnel data from these models is linearized and averaged. This set of data outlines the aerodynamic performance goals of this SSTO vehicle because it is produced from empirical data, which includes anomalies not found in analytical models.

The data for the generalized lifting body is presented in Figures 9.3-9.6. The values generated by the generalized lifting body vehicle model are very similar to the HL-20 design specifications. However, L/D profiles as shown Fig. 9.6 contain values that are slightly higher than would be normally seen for lifting bodies. This is caused by the implementation of supersonic vehicle models in the GHAME. On average, lifting bodies would have L/D's of 3.5, but can have L/D's as high as 4.5 using body flaps and ailerons.

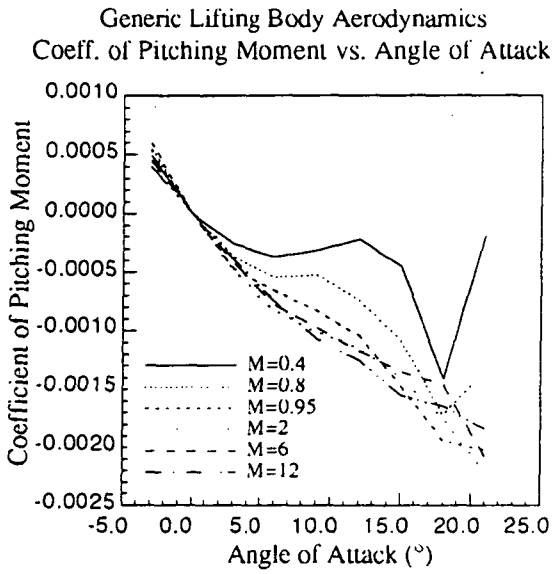

Fig. 9.5 Generic Lifting Body c_m vs. α

Trim effects for the generalized vehicle model are presented in Figures 9.7 and 9.8. The trim values correspond to body flap orientations designed to produce maximum or minimum L/D. Trim effects above transonic speeds have little effect on the L/D of the vehicle. At subsonic speeds, the body flaps and ailerons can be used

effectively to control the vehicle and produce a maximum L/D of 5.5.

From the L/D data in Fig. 9.6, landing speed and attitude profiles for ascent and reentry were compiled. The vehicle will make its final landing approach at an angle of attack of 10° and a speed of 102.9 m/s.

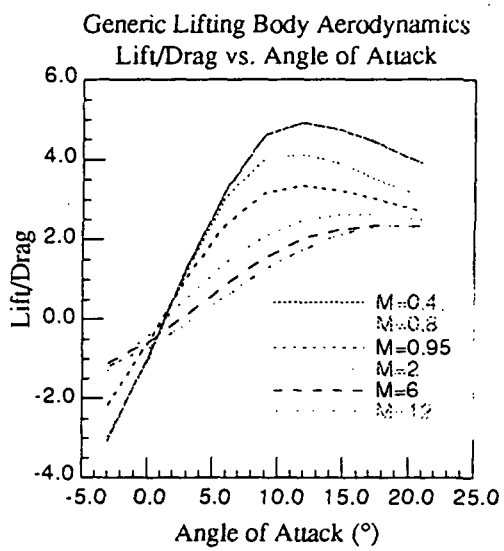

Fig. 9.6 Generic Lifting Body L/D vs. α

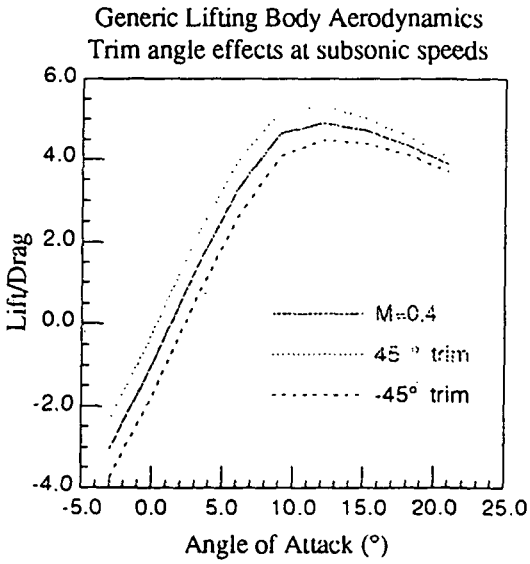

Fig. 9.7 Generic Lifting Body Subsonic Trim Effects

With the generic model for aerodynamics, vehicle geometries were design to match it. Using SHAB, hypersonic aerodynamic data was computed and compared with the GHAME model. The optimized vehicle design, as illustrated in Fig. 9.1, compared well with the GHAME, shown in Fig. 9.9-9.11. Notable differences in the two models is that the optimized vehicle has higher L/D profiles at small angles of attack and lower L/D for larger angles of attack. To further optimize the vehicle, subsonic and supersonic wind tunnel tests will be conducted in the future.

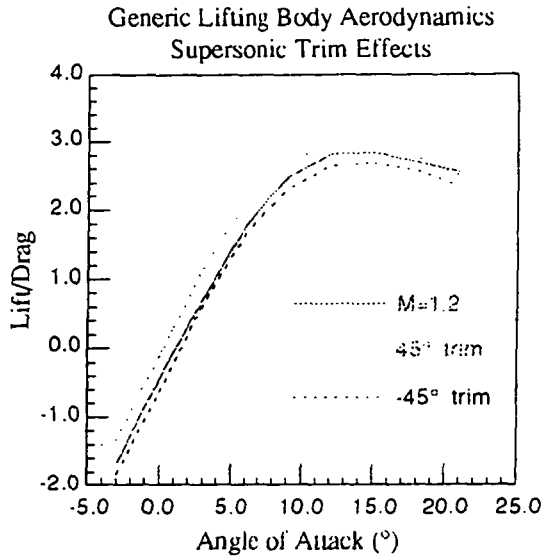

Fig. 9.8 Generic Lifting Body Supersonic Trim Effects

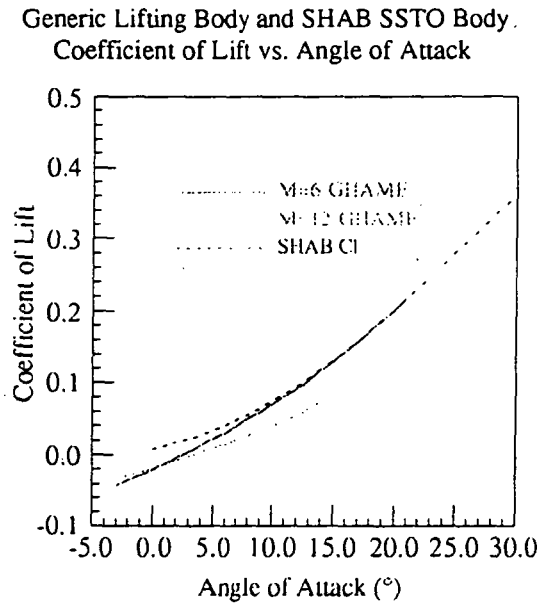

Figure 9.9 Optimized Vehicle c_l

For ascent, attitude profiles were not studied because all maneuvers are due to rocket-engine gimbaling and not aerodynamic maneuvers. For reentry, the aerodynamics of the vehicle becomes crucial for cross-range, down-range, and landing maneuvers. The aerodynamics above 90 km (55.89 mi.) were considered negligible because at these altitudes the

flow regime is in a transition state between continuum and free-molecular flow. At hypersonic speeds, it is crucial for

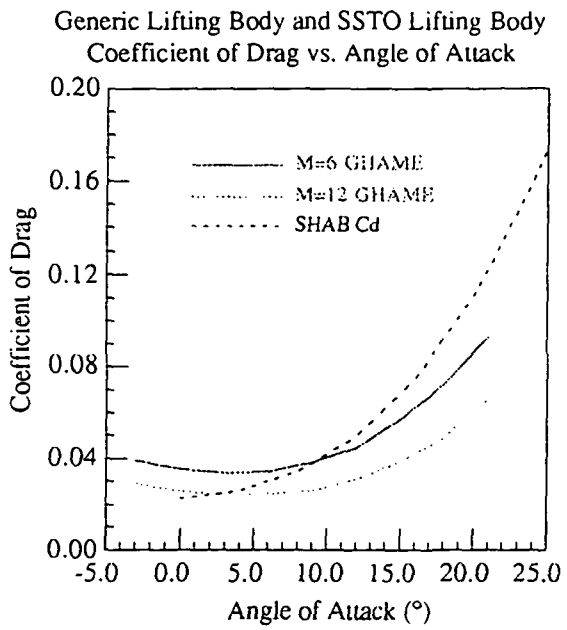

Figure 9.10 Optimized Vehicle c_d

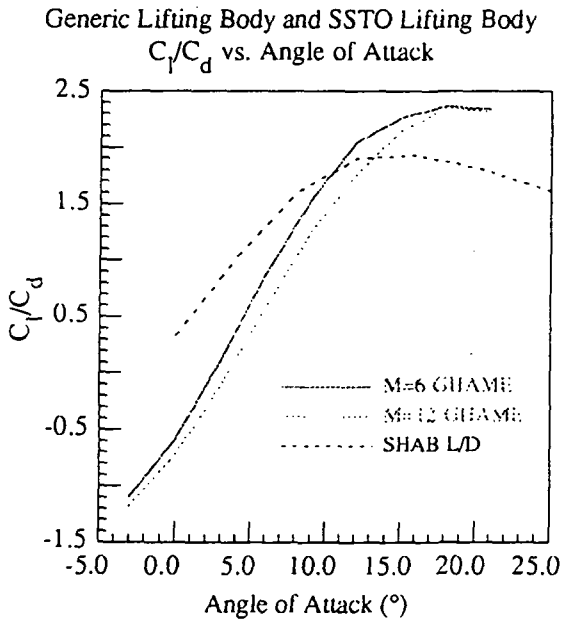

Figure 9.11 Optimized Vehicle L/D

the vehicle to fly at an L/D greater than 1.3 to stay within the 3g load limit. Therefore, the vehicle will fly at an angle of attack greater than 10° to decelerate from hypersonic to supersonic speeds. At supersonic speeds, the attitude of the vehicle will depend on the landing site.

9.3 Ascent and Reentry Trajectories

A spreadsheet program was created to calculate complete ascent and reentry flight trajectory data. Data from this spreadsheet includes flight path, aerodynamic forces, vehicle mass, thrust level (during ascent), ascent and reentry profiles, and down-range and cross-range capability estimates. The equations used in the spreadsheet are based on the equations of motion. The reentry glide path is shown on Fig. 9.11. The glide path is only accurate from an altitude of 90 km (55.89 mi.) to an altitude of 20 km (12.42 mi.). The rest of the flight path will be determined by landing site and weather conditions. Fig. 9.12 shows velocity and altitude changes versus time.

The ascent flight path is shown in Fig. 9.13. The throttling level of the engine is superimposed on the plot. The flight angle can be determined by utilizing Fig. 9.13 and the range that would be required to reach the desired landing site.

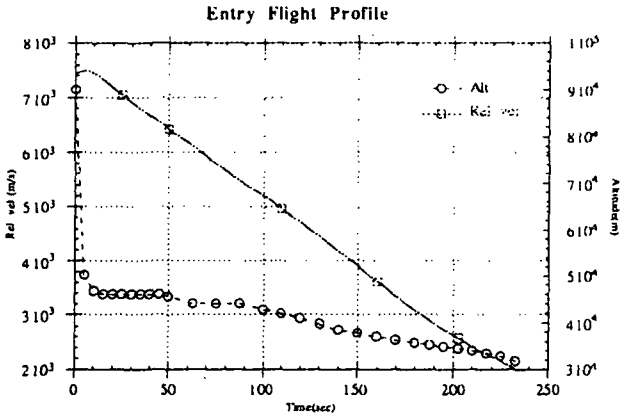

Fig. 9.12 Reentry Flight Profile

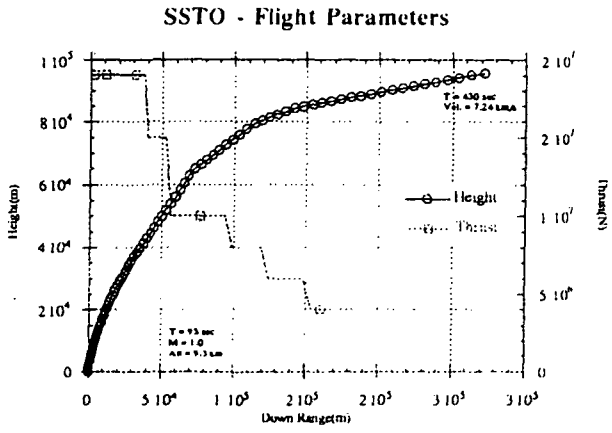

Fig. 9.13 Ascent Profile

Down-range and Cross-range. The maximum down-range and cross-range envelope is shown in Figure 9.14. Assumptions made in the range calculations are that the maximum vehicle acceleration must not exceed 3g, it must be able to provide an L/D of 1.3 at hypersonic speeds, and it must have a minimum L/D of 3.5 at landing.

9.4 Stability and Control

The three major segments of stability and control analysis are subsonic, supersonic, and hypersonic velocities. The equations of motion are the same for all velocities, but lift and drag coefficients differ. For this reason, the stability and control analysis was done for all three flow conditions with the HL-20 as a reference. In addition, preliminary longitudinal stability analysis at hypersonic speeds were performed using SHAB.

Twelve basic differential equations of motion for a six-degree-of-freedom analysis were found and utilized for the procedure. Equations 9.1-9.6 were used to calculate the values found in Figures 9.15-9.20, with nomenclature as follows: m^c is pitching moment, χ is heading, Y is side force, μ is bank angle, and β is side slip angle.

$$I_{yy}\dot{q} = m^c - I_{xz}p^2 + I_{zz}pr - I_{xx}rp + I_{xz}r^2 \qquad (9.1)$$

$$\dot{V} = m^{-1}(-D\cos\beta + Y\sin\beta + T\cos\beta\cos\alpha) - g\sin\gamma \qquad (9.2)$$

$$\dot{\gamma} = \frac{1}{mV}\left[\begin{matrix}-D\sin\beta\sin\mu - Y\sin\mu\cos\beta \\ +L\cos\mu + T\begin{pmatrix}\cos\mu\sin\alpha \\ +\sin\mu\sin\beta\cos\alpha\end{pmatrix}\end{matrix}\right] - \frac{g}{V}\cos\gamma \qquad (9.3)$$

$$\dot{\alpha} = q - \tan\beta(p\cos\alpha + r\sin\alpha) - \frac{1}{mV}\cos\beta(L + T\sin\alpha) + \frac{g\cos\gamma\cos\mu}{V\cos\beta} \qquad (9.4)$$

$$\dot{x} = V\cos\gamma\cos\chi \qquad (9.5)$$

$$\dot{h} = V\sin\gamma \qquad (9.6)$$

Vehicle moments of inertia, pitch, roll and yaw moments, mass, lift, and drag coefficients, and thrust levels during ascent contributed to the stability and control characteristics.

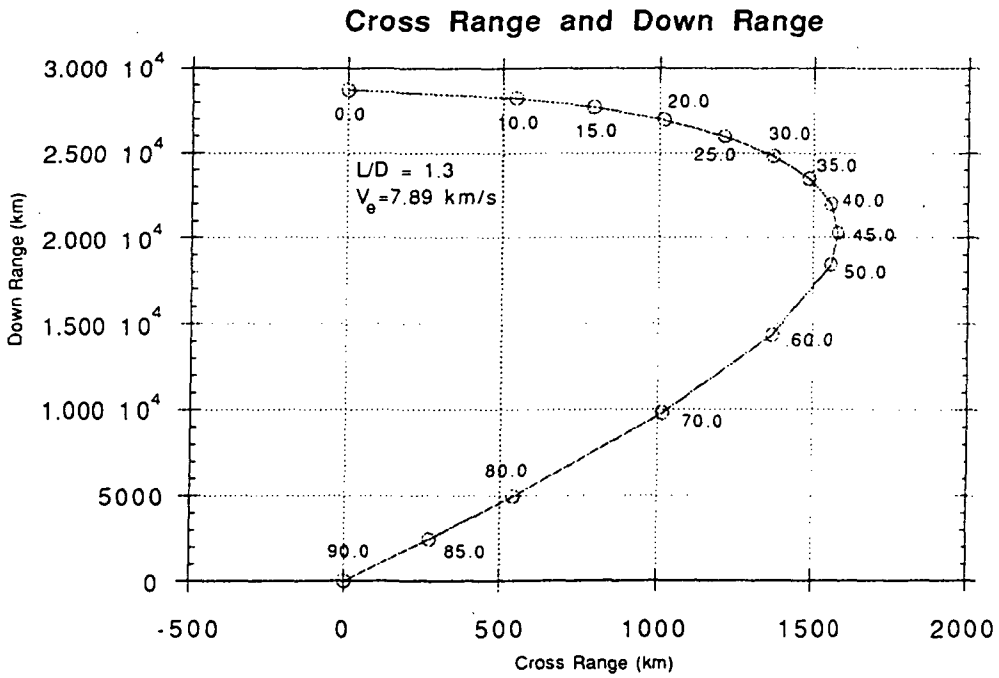

Fig. 9.14 Cross Range and Down Range Capability

For hypersonic flow, Newtonian theory was used to approximate aerodynamic forces. Equations 9.7 and 9.8 were used in this hypersonic analysis.

$$C_p = 2\sin^2\theta \tag{9.7}$$

$$L/D = \cot\alpha \quad \text{(flat plate)} \tag{9.8}$$

Published HL-20 stability and control data was also very useful for this analysis. The body of the HL-20, although much smaller, has a geometry similar to the SSTO vehicle. This allowed for HL-20 stability and control data to be used to approximate the characteristics of the vehicle. Graphs of lateral stability derivatives at all three velocity stages were derived from this data and are presented in Figures 9.15-9.20. In Figures 9.15 9.17, and 9.19, the dashed line represents hypersonic flow and the solid line represents subsonic flow. In Figures 9.16, 9.18, and 9.20, the dashed line corresponds to a Mach number equal to 1.5 and the solid line corresponds to a Mach number equal to 3.

The assumptions that were made in the stability and control analysis were for ascent: angle-of-attack is constant and zero, flight path angle is effectively constant through certain time intervals, and bank angle, side slip angle, roll, and yaw are negligible. During reentry, entry velocity was approximated as Mach 29, mass was a constant, and c_l and c_d were considered constant for each segment of the analysis (subsonic, supersonic, and hypersonic).

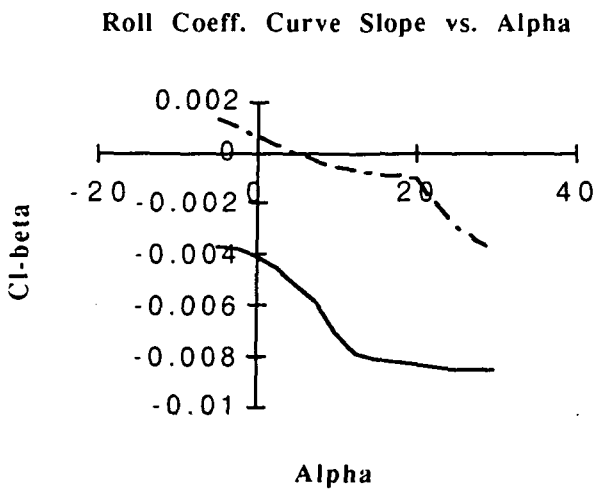

Fig. 9.15 Roll Coefficient Curve Slope vs. α, Subsonic

It must be stressed that the said stability and control analysis is not for the SSTO, but is based upon the HL-20 and what the optimized SSTO's stability and control characteristics should look like. In all lifting body aircraft, which include the Space Shuttle Orbiter and delta-winged aircraft, stability is an important issue because these aircraft are inherently unstable. Preliminary longitudinal stability analysis demonstrates these inherent instabilities in the SSTO, see Fig. 9.21, the LB CG = 31 line. These stability issues can be addressed by using control surfaces and reaction control system jets. In fact, this is an ongoing study in the Space Shuttle. It performs stability and control tests for every mission during re-entry using both its control surfaces and reaction control jets. So, this is the way that the SSTO can address its stability and control issues.

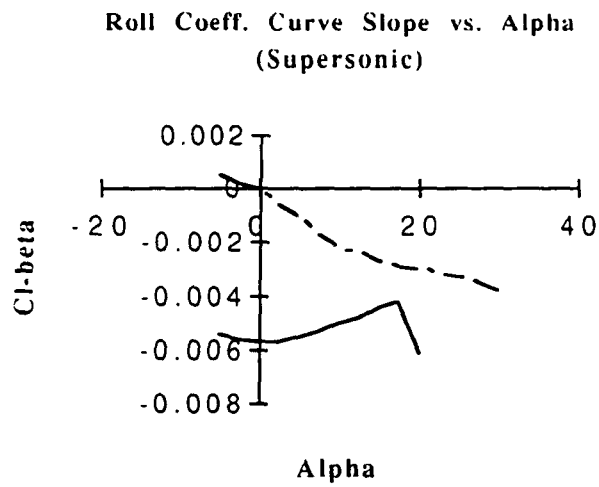

Fig. 9.16 Roll Coefficient Curve Slope vs. α, Supersonic

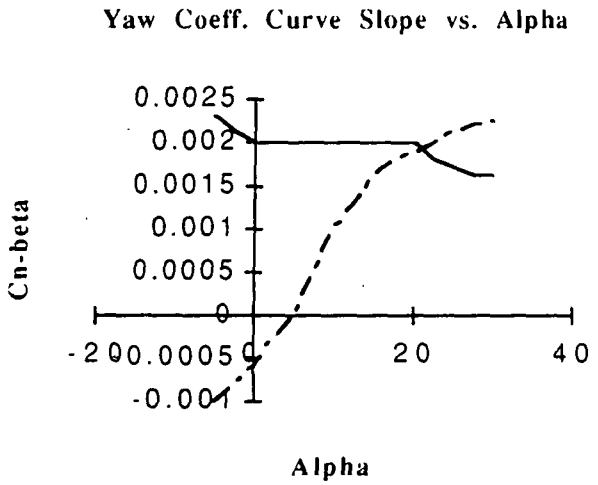

Fig. 9.17 Yaw Coefficient Curve Slope vs. α, Subsonic

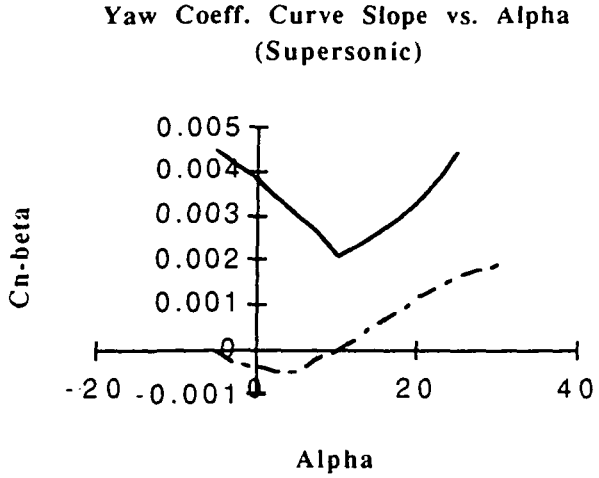

Fig. 9.18 Yaw Coefficient Curve Slope vs. α, Supersonic

Longitudinal stability analysis for the SSTO was performed at hypersonic speeds using SHAB. The predominant factor in its stability is the center of gravity (CG) or center of pressure which, for this analysis, are assumed at the same location. The effect of the fins is minimal whether the fins are large, small, or horizontal. Using the correct CG at 31 m aft of the nose, as given by the Layout team, the SSTO is not stable. However, if the CG was moved forward, the SSTO will become increasingly

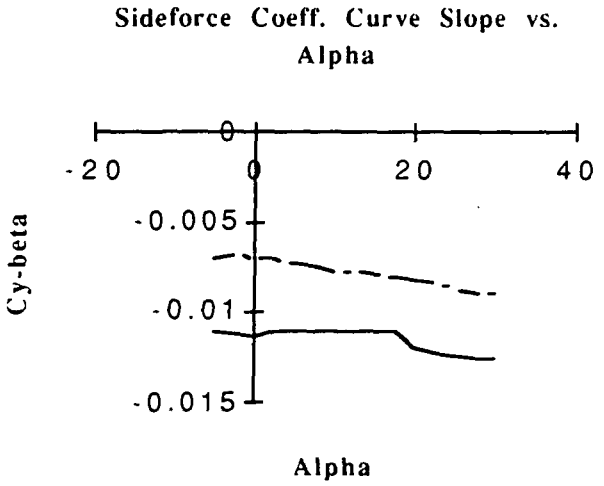

Fig. 9.19 Sideforce Coefficient Curve Slope vs. α, Subsonic

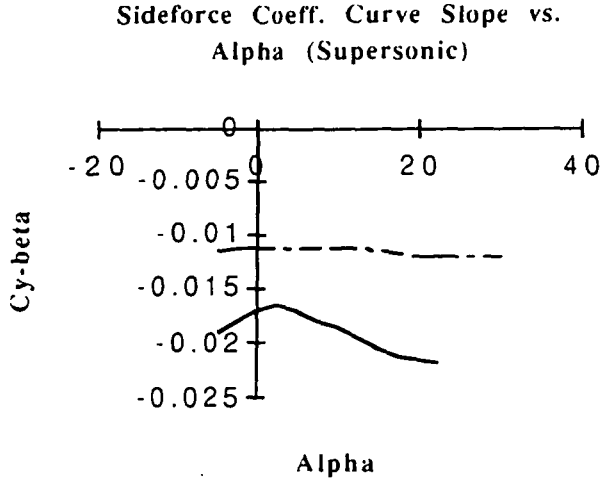

Fig. 9.20 Sideforce Coefficient Curve Slope vs. α, Supersonic

stable, see Fig 9.21-9.22, (LB means lifting body only and Wing 1 includes the body and the fins at 45° inclination.) Since the vehicle has a CG on the body where it is stable, the use of control surfaces and reaction control jets can stabilize the vehicle.

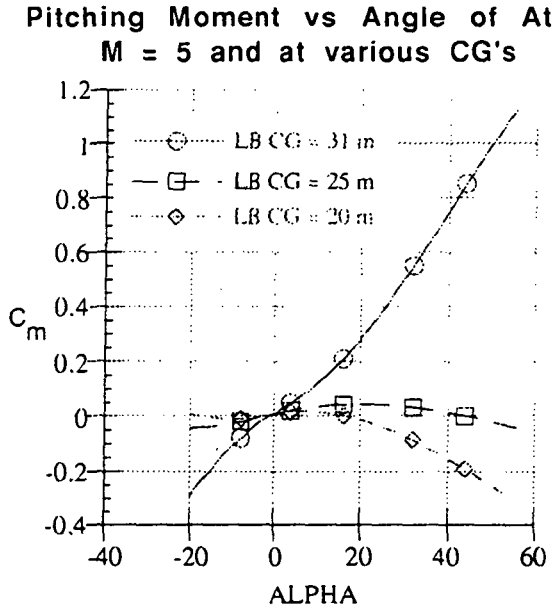

Figure 9.21 Pitching Moment vs. α Lifting Body Only

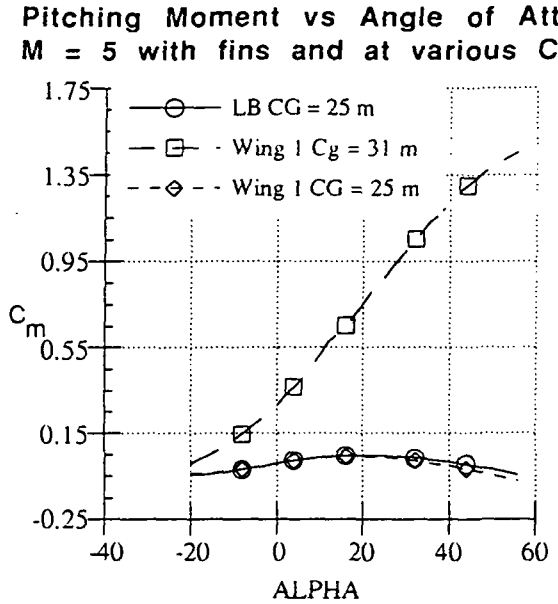

Figure 9.22 Pitching Moment vs. α
Vehicle with fins.

Under these designed performance capabilities, the vehicle will be stable through all velocities, bank angles, flight path angles, side forces, and thrust ranges that will be utilized during a mission. SHAB predicts that a 30 degree body flap deflection and a 30 degree wing flap deflection will provide stable flight.

9.5 Conclusion

The aerodynamic analysis that has been presented contains only preliminary estimates. The main goal was to create a vehicle that would eventually have the specified capabilities without further major design changes. This means that the aerodynamic specifications, specifically L/D estimates, are only guidelines and final vehicle goals. As the design process continues, there will be changes suggested to the vehicle geometry designed to improve its aerodynamic performance and reach the performance goals that have been set. The current stability and control estimates are subject to change as the design process continues, but the values presented here should not change by a large amount unless major design changes are implemented. Further, as the amendments to the design become less and less drastic and advanced analysis software becomes available to the team, a complete aerodynamic analysis of the vehicle can be completed to change current estimates into accurate computed values that can be verified experimentally.

10.0 INTERNAL AND CREW SYSTEMS

10.1 Introduction

The SSTO vehicle posed a unique problem in terms of crew systems, avionics, and power. An emphasis in the design considerations was placed on economics, reusability, and fast turnaround ground operations with a minimum ground support facility. To meet these design criteria, the requirements of each system and sub-system were examined. Options were explored and weighed against each other, and a final decision was reached. Decisions were based on some the following criteria: the reliability and availability of technology, mass considerations, and cost.

10.2 Environmental Control and Life Support System

Introduction. The Environmental Control and Life Support System (ECLSS) provides the habitable environment for the crew. The system supplies water of potable quality, stores metabolic wastes, and supports Extravehicular Activities (EVA's). The ECLSS is also responsible for air cooling of the avionics, thermally conditioned storage of food, and for detection and suppression of fires.

The ECLSS is responsible for providing nitrogen, oxygen, and water to the crew. It maintains the command module and habitation module atmosphere with regard to the temperature, humidity, pressure, and composition. The hardware needed to accomplish this task is located primarily by the modules themselves, with each module having a separate but not isolated Atmospheric Control System (ACS).

Temperature and Humidity Control Subsystem. The Temperature and Humidity Control (THC) subsystem provides avionics cooling, ventilation, air particulate control, and module air temperature and humidity control.

Avionics Cooling. Some electronic components generate large amounts of heat during operation. This heat has a negative effect and is countered using various cooling methods.

Cold Plate (CP) Cooling. A liquid coolant, usually water, is circulated between a thermally conductive plate and a heat exchanger. The avionics equipment is mounted to the plate and uses it as a heat sink. This method is effective for removing large amounts of heat slowly but is heavy.

Forced Air (FA) Cooling. Thermally conditioned air is circulated through a cooling rack to which the avionics

are mounted. The heat is removed by convection, and the warmed air is recirculated back to a heat exchanger. FA cooling is good for quick removal of heat and is light, but consistent temperature control over the entire rack is difficult to maintain.

The avionics units have many different heat generation profiles. To accommodate them all, both CP and FA cooling will be used where appropriate.

Ventilation System. Good air circulation is vital in eliminating the buildup of carbon dioxide (CO_2) pockets. Abnormal concentrations of CO_2 cause headaches, nausea, and in extreme concentrations death.

Command module ventilation is accomplished by an Electric Fan and Backup Fan Unit (EFBU). A similar setup is used for the habitation module, but it is capable of maintaining the atmosphere of both modules if the command EFBU fails. In the case of habitation EFBU failure or primary power failure, the command compartment can be sealed off and minimal life support maintained for 24 hours using less than 1 kilowatt of energy per hour. See Figure 10.1 for typical EFBU placement (the EFBU is designated by "Fans" in the diagram).

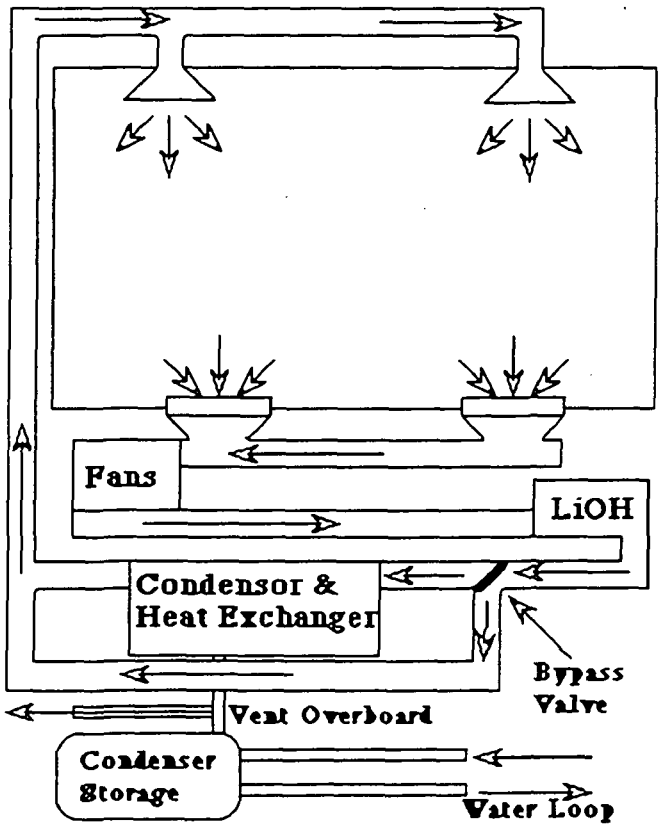

Figure 10.1 Air Loop

Johnson Space Center set the maximum Air Face Velocity (AFV) as 0.215 m/s (0.667 ft/s). This is to eliminate breezes which can be distracting after prolonged exposure. A minimum AFV of 0.076 m/s (0.25 ft/s) is needed to control CO_2 pocket buildup. A computer model of the air flow at this minimum velocity is necessary to ensure that no "dead" air zones exist.

Air Particle Control. Small airborne particle removal is accomplished by utilization of an activated charcoal filter placed after the EFBU's. The charcoal also removes odors which could otherwise become distracting.

Module Air Temperature and Humidity Control. The THC uses a condenser/heat exchanger, slurper, avionics waste heat, and a bypass valve to accomplish its purpose.

Air enters the THC portion of the air loop in Figure 10.1 (the THC portion is designated by "Condenser and Heat Exchanger"). The oxygen-nitrogen mixture passes the bypass valve. A sensor determines the temperature of the air at this point. If it's cool enough (below 28.9° C, 84° F)[1], the bypass valve opens and allows the air to flow around the heat exchanger. If the air is too cool (below 18.33° C, 65° F)[78], heat from the avionics can be used to heat the air. A slurper built into the condenser removes any excess humidity (5%-95%)[79] from the air at this point. The water removed by the condenser is either stored in a stainless tank or vented overboard if the tank is full.

Atmosphere Control and Supply. The purposes of the ACS are to maintain oxygen and nitrogen pressure, to vent and relieve modules, and to store and distribute cryogenic oxygen and nitrogen.

Atmosphere Composition. The ACS system maintains a breathable atmosphere at 21.7% oxygen (O_2) and 78.3% nitrogen (N_2), except during pre-EVA where the pressure is reduced to 0.738 bar (10.7 psi) and the O_2 percentage is increased slightly. The O_2 is maintained at 21.7% to reduce the risk of fire, and larger percentages of O_2 are physiologically damaging. An atmosphere monitor located in the THC air loop relays composition to the O_2 and N_2 Internal Distribution system.

Oxygen and Nitrogen Pressure Control. As shown in Figure 10.2, N_2 and O_2 pressure controls accept input from a Cabin Pressure Sensor. Atmosphere composition is controlled by the pressure regulation of the two gases.

Vent and Relief. The Positive Relief System and the Negative Relief System maintain the pressure at 1.014 bar (14.7 psi) during normal operations. The Emergency Pressure Relief System (EPRS) is used to depressurize the cabin/command module. See Figure 10.2.

Oxygen and Nitrogen Storage & Distribution. Liquid oxygen and nitrogen exit their storage tanks and are piped to the gas conditioning assembly. The cryogenic liquids are converted to gases and sent to the Internal Distribution system. Pressure control valves reduce the pressure of the gases so they can be released into the atmosphere.

Atmosphere Revitalization. CO_2 is removed by use of two parallel Lithium Hydroxide (LiOH) canisters. Only one operates at a time, and flow is diverted to second canister as the first is exchanged for a fresh can.

Monitoring of trace contaminates is accomplished by a Carbon Monoxide sensor. A maximum concentration level of 28.6 ppm is allowed.[81]

Fire Detection and Suppression. Fire is detected using crew senses and a Ionization smoke detector. Suppression is accomplished by use of chemical fire extinguishers in habitated areas, and halon in non-habitated areas. In extreme emergency, cabin depressurization is possible using the EPRS.

Waste Management System. Urine is collected along with cabin air using a suction device. The mixture is separated by fans and the air is returned to the cabin after deodorization. The urine is stored for ground disposal. Fecal matter is captured in a plastic bag, dehydrated by exposure to space, and stored for ground disposal. Both of these functions are combined in a commode unit.

Water Management System (WMS). Water for THC and potable applications will be stored in four stainless steal tanks fitted with metal bellows pressurized by N_2 to maintain the tanks at a constant pressure. Potable water produced by the fuel cells will be stored and excess vented overboard. See Table 10.1 for daily usage amounts.

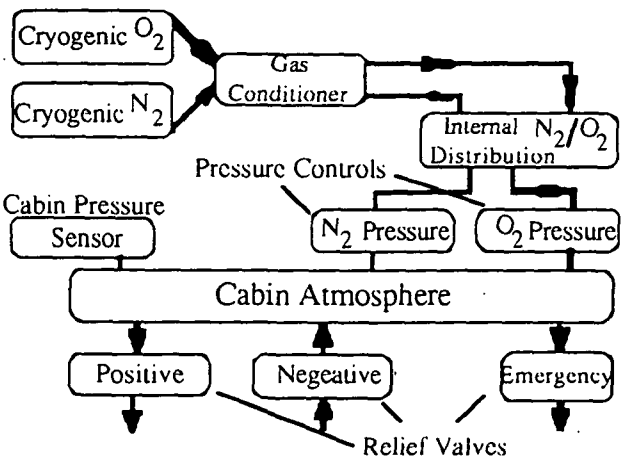

Figure 10.2 ECLSS/ACS Functional Diagram[80]

Emergency Life Support. In case of ECLSS failures, the command module will be sealed and placed on minimal life support. The command module EFBU has a 24 hour battery backup and enough O_2 and N_2 to support a 2 crew members at minimal levels for 24 hours. See Table 10.2 for minimal amounts.

	Min.	Nom.	Max.	Units
Food Prep	0.726	0.889	1.233	kg/day/person
Drinking Usage	0.272	1.700	3.590	kg/day/person
Food	0.227	0.617	0.617	kg/day/person

Table 10.1 Solid/Liquid Usage Amounts[82]

	Min.	Nom.	Max.	Units
Oxygen	0.635	0.798	0.944	kg/day/person
Nitrogen	2.291	2.89	3.406	kg/day/person
Leakage	0.227	0.227	0.227	kg/element/day

Table 10.2 Gas Usage Amounts[83]

Table 10.3 displays the consumable amounts that will be taken on a mission.

Gases	54.88	kg/mission
Water	57.88	kg/mission
Solids	7.40	kg/mission

Table 10.3 Mission Consumable Totals[84]

10.3 Electrical Power System

Overview. The Electrical Power System (EPS) generates and distributes power to the vehicle for the life support system, the communications and navigation systems, the engine monitoring and control systems, and the flight control system. The EPS also generates power for the cargo bay. During normal operations it is estimated that the command and habitation modules will require 3-5 kW (2212-3686 ftlb/s) of power, 1.5 kW (1106 ftlb/s) for the ECLSS and 1.5-3.5 kW (1106-2580 ftlb/s) for avionics. The cargo bay will require 2-4 kW (1475-2949 ftlb/s) of power. The EPS will be capable of producing three-phase 400 Hz 115 V AC, one-phase 400 Hz 28 V AC, and 28 V DC power.

Primary Power Generation. The power required, the mission duration, and the power generation system's mass are the three driving factors considered when selecting a power source. There are five commonly utilized power sources: batteries, Fuel Cell Powerplants (FCP's), solar arrays, nuclear reactors, and Radioisotope Thermal Generators (RTG's).

Batteries were not selected. Batteries are good for short duration use, generally on the order of hours. They were considered to be too heavy to use as a primary power source.

Solar arrays were not selected. Solar arrays can only be used in orbit, thereby limiting their usefulness.

Nuclear reactors were not selected. Nuclear reactors pose environmental concerns for fuel disposal, crew training, and radiation exposure.

Radioisotope thermal generators were not selected. RTG's are better suited for long duration use but produce radiation that is detrimental to electronic equipment. This forces RTG's to be mounted on booms some distance from the vehicle and/or the addition of significant radiation shielding at a significant mass penalty.

Fuel cell powerplants were selected as the primary EPS. FCP's produce power from the conversion of chemical energy to electrical energy. An oxidizer and a fuel are fed in to the cell, which is roughly similar to a battery in internal arrangement (see Figure 10.3). Electricity is generated from the oxidation reaction within the cell but without high temperatures and other complications associated with combustion. Hydrogen and oxygen are the most common reactants used in current operational FCP's. A useful result of using the FCP's is the production of water which may be used by the ECLSS.

The Rockwell International FCP, Types MMMXX and MMMXXI, were selected due to their proven track record on the Space Shuttle. Three FCP's will be used on the SSTO vehicle, each with a voltage output of 27.5-32.5 V DC. Each FCP is capable of producing 2.0-7.0 kW (1475-5161 ftlb/s) at steady-state and up to 12.0 kW (8847 ftlb/s) for fifteen minutes. The mass of each FCP (excluding coolant) is 115.7 kg (255 lbm). The coolant is Fluorinert (FC-40) and has a total mass of 35.3 kg (77.8 lbm). The oxidizer will be 1417 kg (3124 lbm) of LO_2 stored in four 0.032 m^3 (11.24 ft^3) tanks. The fuel will be 167 kg (368 lbm) of LH_2 stored in four 0.606 m^3 (21.4 ft^3) tanks.[85] Table 10.4 provides a summary of the Electrical Power System mass.

Backup Power Generation System. The same power generation sources considered for the Primary Power Generation System were re-examined for application as a backup power generation system. Batteries were selected as a backup power generation system. Lithium batteries provide very high energy densities, on the order of 650 W-hr/kg for a primary or non-rechargeable battery.[86] The batteries will provide the vehicle with 39 kW-hr in emergency situations, such as a three FCP failure. The batteries will provide approximately 24 hours of power for the emergency ECLSS and avionics essential for reentry and landing.

Component	kg	lbm
FCP (3)	347.1	765
coolant (total)	35.3	77.8
LO_2	1417	3124
LH_2	167	368
Battery	60	132.3
Total	2026.4	4467.1

Table 10.4 EPS Mass

Electrical Power Distribution System. The Electrical Power Distribution System (EPDS) is designed to be fail-operational/fail-safe and is therefore capable of delivering sufficient power for safe operation after sustaining two failures. Three redundant main DC busses, each connected to its own FCP, provide power to distribution busses. Solid state inverters convert 28 V DC power to 115 V AC, 400 Hz, three-phase power. A multipoint ground standard for the DC distribution system will be utilized. Single point grounding would have been preferred but would have resulted in a mass penalty in excess of 2000 kg (4400 lb).

DC control busses originate from each main DC bus. Since the main DC busses are cross tied, failure of two main DC busses does not interrupt power to any control bus. Typically, the control busses provide power to redundant loads such as guidance, navigation, and control systems, insuring that a single bus failure will not compromise more than one of a multiply redundant system. DC control busses also provide power for auxiliary power unit (APU) controllers, valves, and heaters; RCS and OMS valves and heaters; air data probes and actuators; hydraulic controls; and landing gear.

Each main DC bus provides power for an inverter. The inverters are connected in a phase-locked array to produce 115 V AC, 400 Hz, three-phase power. Each of the three redundant three-phase AC buses is isolated, is capable of supplying nominal power of 2.25 kW (1659 ftlb/s), and is grounded to structure in a single point. No provisions are made to cross tie AC buses to accommodate inverter failures. Power reliability for critical loads is obtained by redundant systems operating on separate busses. The AC busses provide power for various avionics equipment and three-phase motors. It is estimated that over 200 three-phase motors will be required to drive valves, deployment/retract mechanisms, latches, actuators, motorized positioning devices, etc.[87]

Figure 10.4 shows a schematic of the Electrical Power Distribution System.

The mass of the EPDS which consists primarily of various gauge copper wiring, Specification MIL-W-5086, is estimated to be 1361.7 kg (3000 lbm).[88]

10.4 Avionics

Overview. Avionics is a term used to represent the electrical and electronic devices and systems used in aviation, missilery, and astronautics. Included in this definition are the communication and tracking system, display and monitoring system, and guidance navigation and control system. The estimated mass of the avionics system is 3000 kg (6614 lbm).

The SSTO vehicle will incorporate a state-of-the-art avionics suite. Despite the fact that much of the technology has been discovered over a decade ago, the avionics will represent one of the most advanced and integrated systems operational in the aerospace industry. A comprehensive fail-operational/fail-safe concept will be applied to the avionics system and be achieved through complex redundancy management techniques. The SSTO vehicle will help pioneer the use of fly-by-light technology which is the use of fiber optics in place of conventional metallic wiring to reduce weight.

The SSTO vehicle will feature a four computer central processing complex which will provide software services to all vehicle subsystems that require them. Each General Purpose Computer (GPC) will be connected to a network of digital data busses which will distribute input/output commands and data to/from bus terminal units located throughout the vehicle. Dedicated Line Replaceable Units (LRU's) will interface as necessary with bus terminal units. During flight critical phases such as ascent and reentry, the system will be configured in four redundant, independent strings. During less critical mission phases, such as on-orbit, each GPC can run appropriate software to perform a wide variety of mission and payload support functions.

Communication and Tracking System. In order to meet the mission requirement of continual ground contact, an extensive Communication and Tracking (C&T) system is required. Despite a complex C&T system, there will be a communication blackout due to gas ionization during reentry. The C&T system is responsible for providing atmospheric flight links and orbital communications links during all other phases of flight. Uplinks and downlinks are supported by various stations in the following frequency bands: S-band, 2-4 GHz; C-band, 4-6 GHz; Ku-Band, 12-14 GHz.[89]

During the atmospheric flight regime the SSTO vehicle will maintain three flight links: C-band, Phase Modulated (PM) S-band, and Ultra High Frequency (UHF). The radar altimeter, which provides height above local terrain from 1.5 km (5000 ft) to touchdown, is C-band. A post-blackout navigation aid is L-band tacan (tactical air navigation) data. Tacan provides slant range and bearing to a selected ground station. Conventional transponders which provide Air Traffic Control with data such as altitude, heading, and speed are also L-band. Tracking and 2-way communication of voice and data is accomplished by way of S-band (PM) links directly to the ground or through NASA's Tracking and Data Relay Satellite (TDRS) system. Finally, UHF is used as a voice link with ground control and Air Traffic Control.

During the orbital flight regime, the SSTO vehicle will maintain four communication links: Ku-band, S-band Frequency Modulation (FM), S-band (PM), and UHF. The Ku-band system will determine range and angle to detached satellites for rendezvous missions and provide a 2-way voice and data communication link through the TDRS network. Again, as in the atmospheric flight regime, tracking and 2-way communication of voice and data is accomplished by way of S-band (PM) links directly to the ground or through the TDRS network. Wide-band data transmission directly to the ground is achieved with a S-band (FM) link. A 2-way UHF voice interface with the audio system is available, giving crew members performing EVA the capability of communication with the ground.

The Radio Frequency links maintained by the system are shown in Table 10.5.

Display/Monitoring Systems. The SSTO vehicle's avionics systems is capable of performing much of the monitoring previously only capable by ground support. With the improvements made in Built In Test (BITE) technology in the past decade, LRU's are capable of monitoring themselves and sending fault information to three Centralized Maintenance Computers (CMC). The CMC is itself an LRU and not one or a part of the general purpose computers. The CMC records fault information and displays one of the multifunctional displays in the command module. Ground personnel are able to access the information in the CMC via one of three control/display units in the command module. Fault histories contained in the CMC aid ground personnel in system and LRU troubleshooting after every mission. The CMC's also record engine fault and performance data to be used for future performance optimization.

Flight Regime	Links Available	Purpose
Atmospheric	C-band	Radar Altimeter
	S-band (PM)	Tracking, 2-way voice/data
	UHF	Voice
Orbital	Ku-band	2-way voice/data via TDRS
	S-band (FM)	data transmission
	S-band (PM)	Tracking, 2-way voice/data
	UHF	EVA

Table 10.5 Communication and Tracking System

The display and instrumentation in the command module will be similar to the appearance of a "glass cockpit"

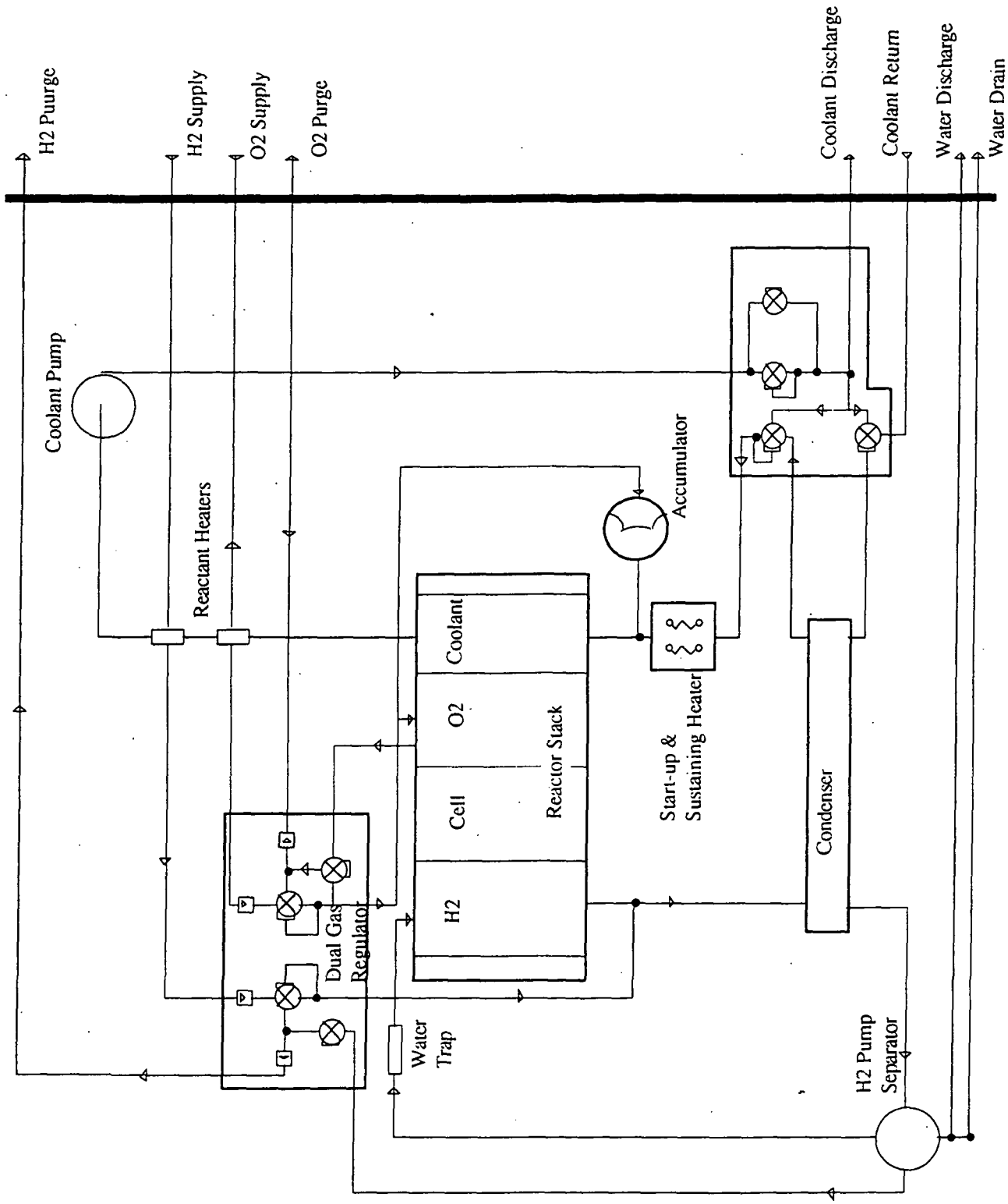

Figure 10.3 Fuel Cell Powerplant Schematic

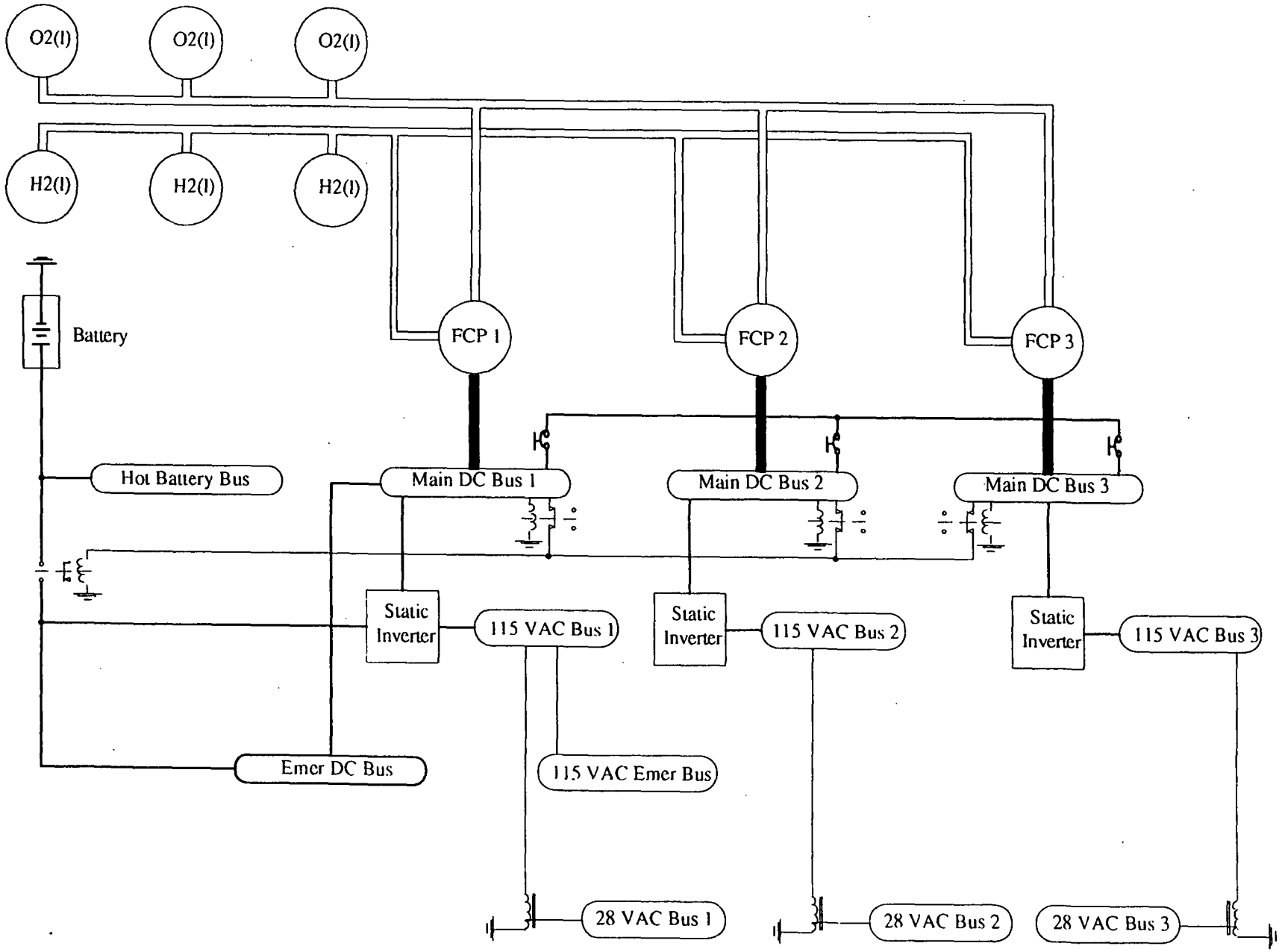

Figure 10.4 Electrical Power Distribution System

aircraft. The term "glass cockpit" refers to the multiple Cathode Ray Tubes (CRT's) used in many modern aircraft. The SSTO vehicle will utilize Liquid Crystal Displays (LCD's) instead of CRT's to reduce the weight of the display system. The LCD's will serve as multifunctional displays (MFD's), which means they are not dedicated to displaying information on only one system. On any given MFD, a crew member will have the ability to display: video; engine monitoring and performance data; a primary flight display which integrates attitude, heading, indicated airspeed, and vertical speed; a navigation display; and other miscellaneous displays. The video is from a network of fiber optic cameras. Cameras will be located in the command module, habitation module, cargo bay, avionics bays, and engine areas. Cameras will also be located on the exterior of the vehicle for landing views and vehicle damage monitoring.

Guidance Navigation & Control System. The Guidance Navigation and Control (GN&C) system is responsible for taking sensor input and processing that information such that control effectors keep the vehicle on the correct flight profile. Table 10.6 shows a summary of the system at each flight phase.[90]

Two Differential Global Position System/Global Navigation Satellite Systems (DGPS/GNSS) used in conjunction with three ring laser gyro Inertial Navigation Units (INU's) comprise the primary navigation sensor system. A GPS determines position by triangulating the position of the receiver with the positions of a least four GPS satellites. Velocity information is obtained from Doppler shifts in the carrier frequency of each of the satellites. Differential GPS determines vehicle attitude information by using multiple sensors to determine the position of different "points" on the vehicle and translates the differences to pitch, roll, and yaw. To be used for navigation in addition to positioning, a system must be able to isolate a failed satellite. A minimum of six GPS/GNSS satellites are required to be in direct line of site at all times to detect a failed satellite. Thanks to the high orbital altitude, the SSTO vehicle will have no problem meeting this requirement.

Data from the DGPS/GNSS's are input to the INU's. The INU then outputs three signals, an autonomous DGPS/GNSS, an autonomous INU, and a hybrid DGPS/GNSS-INU, to the GPC's for comparison. The GPC's compare the autonomous DGPS/GNSS and autonomous INU signals with each other to see if the hybrid signal is acceptable. If the hybrid signal is acceptable, it is compared with signals from the 3-axis rate gyro assemblies and 2-axis accelerometers. If the hybrid signal is not acceptable, the autonomous INU signal is compared with signals from the 3-axis rate gyro assemblies and 2-axis accelerometers. After a complex comparison algorithm, the INU's are updated (depending on mission phase) using the best data available.

The attitude and position information obtained from the sensors is then used to keep the vehicle on its planned flight path. This is achieved in different methods for different mission phases. On each engine (OMS and main) there is an Engine Interface Unit (EIU). The EIU controls engine throttling and gimbaling based on instructions received from the GPC's. Similarly, for aerodynamic control, an aero-servoamplifier receives instructions from the GPC's and actuates aerodynamic control surfaces.

Mission Phase	GN&C Function	Sensor	Control Effector
Ascent	Thrust Vector Control (TVC); RCS/OMS control; abort management	INU's (3); 3-axis rate gyros (4); 2-axis body mounted accelerometers (4)	Main engine actuators, reaction control thrusters, OMS actuators, aerosurface actuators
Orbit	Attitude/translation control; INU alignment; rendezvous	DGPS/GNSS (2); INU's; rate gyros; accelerometers	OMS actuators, reaction control thrusters
Reentry	Blended RCS/acrodynamic control; angle of attack/bank angle modulation; g-loading; INU alignment	DGPS/GNSS; INU's; rate gyros; accelerometers; air data transducer assemblies (4)	OMS actuators, reaction control thrusters, acrosurface actuators
Terminal Area Energy Management (TAEM)	-	DGPS/GNSS; INU's; rate gyros; accelerometers; air data transducer assemblies (4)	aerosurface actuators
Approach and Landing	-	DGPS/GNSS; INU's; rate gyros; accelerometers; air data transducer assemblies (4)	aerosurface actuators, nosewheel steering actuators, wheel brakes

Table 10.6 GN&C System

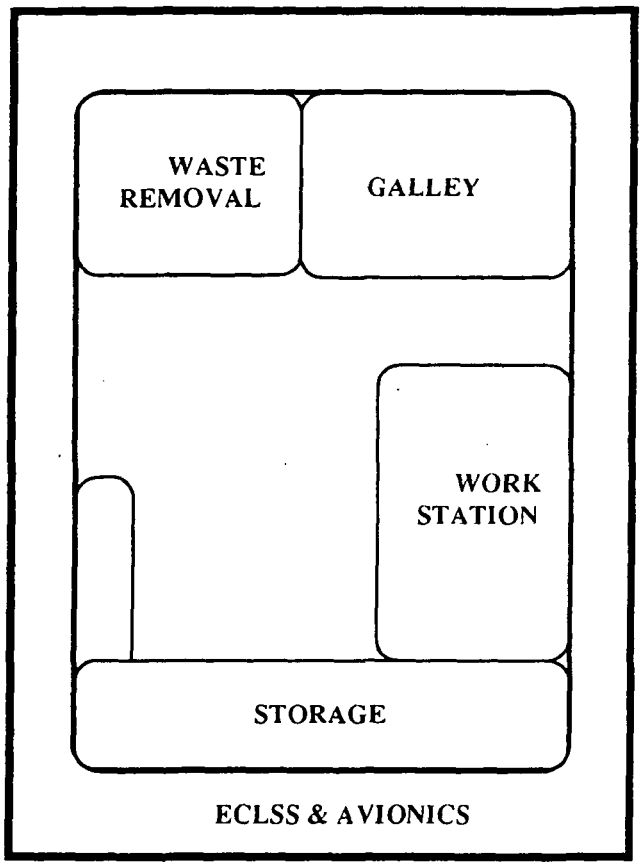

Figure 10.7 Habitation Module Top View

Due to potential hazards of using hydrazine, an alternative fuel or hydraulic power system is desired. The only alternative available at this time is the use of an AC motor pump to provide hydraulic pressure. It is anticipated that multiple AC motor pumps could supply sufficient hydraulic pressure, but power consumption figures for the pumps are not available. Without the pump power requirements, it was impossible to determine whether the pumps would overtax the EPS. As more information becomes available, it may become possible to eliminate the APU's and the hydrazine.

10.7 Cost and Lifetime Evaluation

The avionics, power, and crew systems each contain multiple sub-systems and hundreds of components. After examining existing costs for components each of the three main sub-systems, an estimate of $15,000/kg ($6818/lb) was made. With a launch mass of approximately 7000 kg (15400 lbm) in avionics, crew, and power systems, the cost is approximately $120 million.

The industry standard for measurement of reliability and lifetime is Mean Time Between Failure (MTBF) and number of cycles (a cycle being a take-off and landing). An average target MTBF of between 20,000 and 40,000 operational-hours would give an average lifetime of approximately 80-160 cycles.

10.8 Conclusion

The crew systems, avionics, and power system detailed uses a combination of proven equipment and new technology. With this blend of resources, the vehicle will perform with a high level of reliability at a reasonable cost. This design provides a baseline SSTO vehicle configuration that meets and exceeds all specified requirements while being adaptable, expandable, and upgradeable.

11.0 CONCLUSION

11.1 Final Conceptual Summary

Objectives. The objectives of the design are to be reliable, timely, reusable, man-rated, cost-effective, and single-stage. The design is based entirely on existing and proven technology. The design is also focused on keeping the vehicle simple. With these design bases, reliability cannot be questioned. With a maximum turnaround time of three days and a mission duration of three days, the SSTO vehicle will readily be available for transport of a payload to orbit. The vehicle loses none of its propulsive systems during launch so it is considered entirely reusable. The vehicle is fail-safe two seconds after launch. In the event of an engine-out during launch, the vehicle has many options for an abort scenario. Therefore, the spacecraft is essentially man-rated. The design is cost-effective compared to any previous commercial space venture and a profit margin will exist. The fact that the SSTO vehicle can transport multiple payloads to orbit in one mission also improves its cost-effectiveness. Finally, the vehicle is single-stage. One propulsion system launches the craft to orbit.

11.2 Future Considerations

Before the vehicle can be fully proven in meeting the design objectives, several considerations must be taken into account. Many of the cost estimates were very rough due to

fluctuations in the design and time constraints. When the project is concluded, the cost estimates should be very accurate. The next phase of the design process will place more emphasis on analysis of the design than on market research. Thermodynamic and aerodynamic properties will be analyzed using computational fluid dynamics. It will aid to streamline the body's shape and locate any thermal problem areas. Aerodynamic models of the SSTO vehicle will be built and tested in a wind tunnel after sufficient finite element analysis. Weight reduction is necessary in the future. It is not unrealistic to have a goal of using only four engines to achieve orbit. Space optimization is very important as well.

Part B:

Model Reports

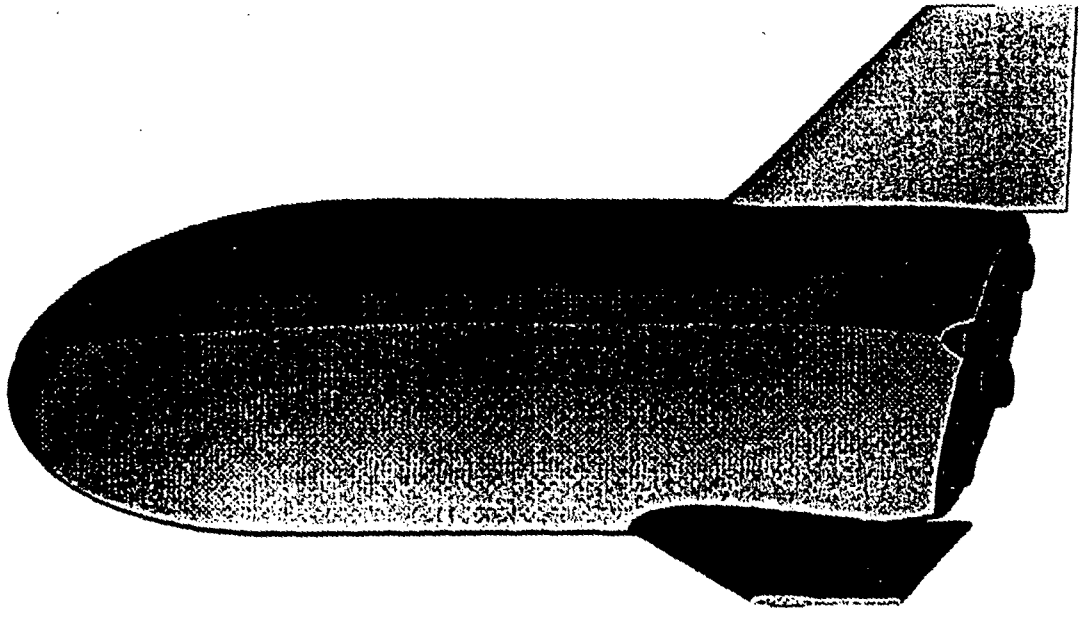

1.0 INTRODUCTION

1.1 Introduction

In any project, the first step is a conceptual design. This step has now be completed by the University of Minnesota Spacecraft Design Team. The team, in conjunction with a USRA/NASA program, has completed a conceptual design for a single stage to orbit vehicle. With any design experience, proper closure must be achieved. In order to achieve this goal, and further the design project, eight models have been developed and tested. These models will serve as a validity tool for the team's conceptual design, as well as provide proper design closure for team members.

1.2 Conceptual Design

The design of a SSTO vehicle offered many challenges. Along with these challenges came even more solutions. The current design configuration is a vertical launch/horizontal landing vehicle. The mass of the SSTO vehicle on takeoff is 680,400 kg (1,500,000 lb). The empty mass with orbital fuel is 83,000 kg (183,000 lb). When landing, the vehicle's mass equals 68,000 kg (150,000 lb) with a payload, and 58,900 kg (130,000 lb) without a payload. These landing masses are assuming the vehicle is either carrying a maximum payload of 9,100 kg (20,000 lb) and all orbital fuel is expended, or no payload with orbital fuel expended. The vehicle can carry a payload of 9,100 kg (20,000 lb) to an altitude of 833 km (450 n.mi.). The vehicle incorporates three RD-701 engines for the main propulsion system. The RD-701s provide enough thrust for engine-out capability just 0.9 seconds after lift-off. Once on orbit, the OMS (two RL10s) and RCS systems takeover.

The structural frame components of the vehicle are mainly carbon-carbon composites. The vehicle skin is composed of carbon epoxy, and the fuel tanks are also carbon-carbon. Although these materials are expensive, the mass savings is the justification for their high cost. The thermal protection system (TPS) also uses carbon-carbon composites in certain areas. Inconel and titanium are also used in the TPS system were temperatures permit.

1.3 Models and Tests

There are primarily eight areas of the conceptual design that are being tested and/or modeled by the team. The eight projects can be broken down into three types, operational models, flight models, and component models. These models are briefly mentioned here, and are the main focus for the rest of this report.

There are two operational models of the SSTO vehicle. The first is a complete detailed ground operations model. This model describes the steps necessary for a complete cycle of launching, landing, and turnaround of the vehicle. The second model is a interactive simulation involving the final stages of rendezvous between the SSTO vehicle and an orbiting satellite.

The two flight models will cover both subsonic and hypersonic flight regimes. The subsonic model will mainly focus on landing conditions of the SSTO vehicle. It will incorporate the entire vehicle conceptual design including all adjustable control surfaces. This model will also serve as a display model. The hypersonic model will look closely at reentry conditions and the controllability of the vehicle at hypersonic velocities. Again the hypersonic modle will include adjustable body flaps and wing flaps.

The last three models involve distinct features of the conceptual design. Two of the models center on computer analysis predictions. The first model involves modeling a simple engine mount on the computer, analyzing the mount, and then constructing a physical model. This physical model will then be tested under the same conditions as placed on the computer model. The second involves the cryogenic fuel tank insulation system. A physical model will be constructed and compared to the theoretical computer model. In both tests, the feasibility of testing actual vehicle components is beyond the team's ability. To compensate, these two models will examine the accuracy of the computer tools used in developing the conceptual design. The third model in this component group involves the propulsion system. The SSTO vehicle was designed with extendible skits to increase performance. This model will examine the performance to two nozzles that differ in the same area ratios as in the actual conceptual design.

2.0 SUBSONIC WIND TUNNEL MODEL

2.1 Introduction

In this past quarter large steps have been taken to complete and test a subsonic wind tunnel model of the SSTO vehicle. To date most of the model has been constructed and testing is being scheduled for the month of July. The initial steps included determination of dynamic instability and redesign of the control surfaces in order to create a staticly stable craft in the subsonic regieme. Pro Engineer, MATLAB, and MasterCAM have been used extensively this quarter.

2.2 Model Design and Construction

Computer modeling. Milling of the subsonic wind tunnel model of the SSTO requires that the model be broken into surfaces that the milling machine can work with. The Pro-Engineer model of the SSTO is broken into four main pieces. These pieces consist of:

- The front nose piece of the SSTO Vehicle
- The bottom rear piece of the SSTO Vehicle
- The top rear piece of the SSTO Vehicle

The nose piece includes both top and bottom surfaces. The length of this piece is 0.63 m (10.37 in) long. The bottom rear piece is an L-shaped piece which also includes both surfaces. The piece is constructed this way in order to have a place to mount the sting. The length of this piece is 0.337 m (13.25 in) long with the L section 0.102 m (4 in) long. The top rear piece fits into the L shaped section of the bottom rear piece. These figures are shown in figure 2.1.

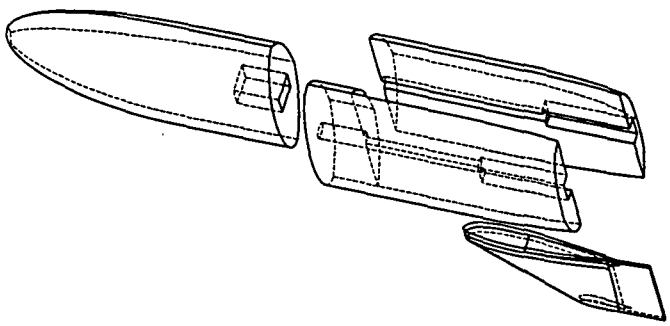

Figure 2.1 Model Layout

Several steps were used to cut the original Pro Engineer model into the millable pieces.To obtain the front nose piece the display of the model is first rotated to provide a side view. The second step in the process is to cut the fuselage in half with a cutting plane at the desired location and the rear half of the fuselage is removed. The front nose piece of the SSTO remains and is saved as its own file.

The bottom surface is obtained in much the same manner as the top surface. Starting with the complete Pro Engineer model in a side view, the model is cut in half with a cutting plane, and the front half of the fuselage is removed. This leaves the rear half of the fuselage. The top rear section of the model has to be removed. This is accomplished by drawing two cutting planes so that when the top section is removed an L-shaped section remains of the dimensions listed above.

The top rear section is created in a very similar way to the bottom rear section except the bottom section is removed and the top section remains.

Since the two vertical stabilizers are similar, only one of the stabilizers must be created. This is done by creating a spilne shape of a NACA 23-012 airfoil and fitting it to the dimensions of the horizontal stabilizers. The stabilizer section is cut 1.59 mm (.0625 in) above and below the chord line. This cut provides the top and bottom surfaces of the horizonatal stabilizer, which will be attached to a 3.175 mm (0.125 in) aluminum plate for attachment to the model.

The results of this dissection process leave five seperate entities in five seperate Pro Engineer files. Each of these surfaces will be milled into pieces which can be assembled into the subsonic wind tunnel model. The modeling process can be accomplished asfter a scaling of the full sized SSTO is accomplished.

Scaling. The size of the model is based on the dimensions of the wind tunnel and the force limits of the sting. The model size is determined from four criteria.

- The model, in any instance, cannot block more than 7% of the wind tunnel's cross sectional area.

- The aerodynamic forces created by the model will not excede the set force limits of the sting. Exceding these force maximums will damage the sting.

- The model, in any instance, cannot interfere with the boundary layer of the wind tunnel.

- When mounted for testing, the model will fit within the size constraints of the test section of the wind tunnel.

The maximum blockage the SSTO model will induce during testing is when it is placed at an angle of attack of 7 degrees. This is the maximum angle of attack to be used during testing. The actual SSTO design is 51 m (167.32 ft) long by 20 m (65.62 ft) wide. A 7% blockage of the wind tunnel being used for testing is 0.093 m^2 (1 ft^2). Using this information the maximum length and width the model can be is 1.05 m 3.44 ft) by 0.42 m (1.38 ft) respectively. This corresponds to approximately a 1/49 scale model.

The maximum forces that the sting can withstand can not be exceeded. These forces sre shown in table X1.

		Direction		
Lift	Drag	Roll	Pitch	Yaw
222 N	222 N	2.8 Nm	8.5 Nm	8.5 Nm

Table 2.1 Maximum sting forces

The maximum speed for testing in the wind tunnel will be 22.86 m/s (75 ft/s.) Using a program written in MATLAB the roll, pitch, and yaw moments can be calculated.(see appendix for sample program) At 22.86 m/s (75 ft/s.), with elevon deflection of 30 degrees and body flap deflection of 10 degrees, the model produces just under the allowable pitch moment. Roll is not of concern since we will not be testing under conditions which would cause a roll moment.

The model cannot interfere with the boundary layer of the wind tunnel. At 1/49 scale and 7 degrees angle of attack the nose of the SSTO model is approximately 0.22 m (0.72 ft) from the center of the wind tunnel. The distance from the center of the wind tunnel to the top is 0.48 m (1.58 ft). Under these maximum test conditions, the model is well out of the boundary layer region of the test section.

Finally, the size of the model is limited by the size of the wind tunnel's test section. The distance from the sting to the forward edge of the test section is 0.61 m (2 ft). Calculations show that this allows for a model no larger that 1/100 scale. The relative sizing with the wind tunnel at this scale is shown in figure X.2.

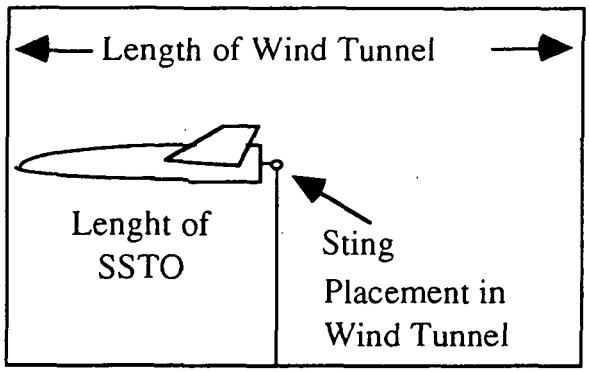

Figure 2.2 Wind Tunnel Setup

Modeling processes. Once the scaling of the model is determined, the construction process for the model can begin. The milling of the surfaces from Pro Engineer will be performed by a Computerized Numerical Control milling machine, or a CNC milling machine. The path of the model's surfaces will be set up with a Computer Aided Manufacturing (CAM) program, MasterCAM.

The first step in the modeling process involves downloading the Pro Engineer files discussed earlier in this section: the SSTO vehicle's nose piece, bottom rear, top rear and stabilizer sections. Each surface is brought into MasterCAM, and the scaling factor is applied to the surface. The surface is now viewed by the computer as the size of the model desired.

With MasterCAM, the instructions for the CNC mill are programmed. The instructions are called the toolpaths and consist of a series of three dimensional coordinates. Each of the coordinates corresponds with a point on the model's surface. The CNC follows the toolpath through the coordinates, directing a cutting tool to shape the model's surface from a piece of wood.

The pieces of wood are prepared with any milled areas needed for clearance or assembly. These areas are cut out prior to milling with the CNC as it is easier to cut a square block of wood rather than a piece with curved surfaces. For the subsonic model, this will include a milled channel through the rear of the model--both top and bottom rear pieces--for the sting to enter the model, a clearance hole in the nose piece for the sting attatchment nut, and two 3.18 mm (0.125 in) slots in the bottom for the horizontal stabilizer attatchment.. Also, two reecessions are milled out of the bottom piece to allow for the body flap plugs to be inserted.

All sections will be milled out of wood. For the nose piece, bottom rear, and top rear sections Perfect Plank is used. Perfect Plank is a pine laminate consisting of many 25.4 mm x 50.8 mm x 76.2 mm (1 in x 2 in x 3 in) pieces. This wood is ideal since it has no deefects such as knots. The horizontal stabilizers use a single piece of pine since they are much smaller than the otheer pieces of the model.

Control surfaces are implemented into the model to determine the effects of their current size and placement. The horizontal stabilizers are costructed of a top and bottom surface of the airoil with a 3.18 mm (0.125 in) piece of aluminum sandwiched in between to act as a stiffener, elevon, and attatchment piece to the main body. The wooden airfoil sections are epoxied onto the aluminum. The aluminum pieces are the exact dimensions of the center of the airfoil a top view of the piece is in figure X3.

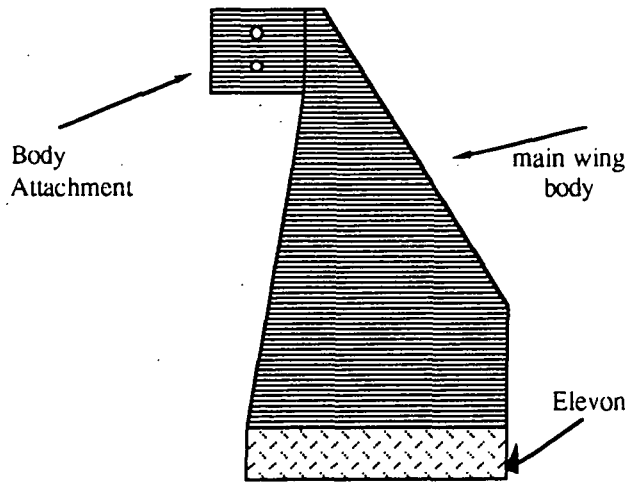

Figure 2.3 Aluminum center for stabilizers

The body flaps are milled from wood. Each body flap will have a certain deflection angle and be able to be added to and removed from the SSTO model's main body. By switching the body flaps, the model can be tested with different control surface orientations and angles. The body flaps are attached to the fuselage with a set screw. This will allow for quick and easy adjustment of the body flap angles.

The final model will allow for the placement of the sting on the center of gravity of the SSTO model. The model will also allow for the adjustment of the control surfaces for investigations into their effects.

Mounting the SSTO model on the Sting. The sting measure the forces and moments of the model in the wind tunnel. The forces and moments are measured at the tip of the sting. Since the forces and moments recorded by the sting need to be measured at the center of gravity of the vehicle, the sting must either be placed at the center of gravity or transformation calculations are used to translate the forces and moments to the desired location. By placing the sting at the center of gravity greater accuracy is achieved because it is not necessary to use equations to translate to forces and moments. Placement of the sting at the center of gravity also eliminates any moments due to the weight of the model thus increasing the envelope in which we can test at.

To position the sting at the center of gravity, the sting is placed inside the model. A mounting plate is placed 50.8 mm (2 in) forward of the center of gravity on the L-shaped section of the bottom rear piece. This is done to place the reference point of the sting, where the actual measurements occur, at the center of gravity of the model. The refernece point is ,located 50.8 mm (2 in) aft of the attacment point of the sting. A clearance channel is milled into the rear of the vehicle in both the top rear and bottom rear sections. The sting enters through the rear of the vehicle and is attatched onto the mounting plate. To allow the sting to be bolted to the mounting plate a clearence hole is bored in the nosepiece. In order to attatch the sting, the nose piece and top rear sections must be removed to allow the sting to be secured to the mounting plate.

2.3 Test Conditions and Expected Results

Test conditions. The purpose of testing the model in the wind tunnel is to determine the forces on the vehicle in the subsonic regime. Since the SSTO vehicle is unstable the exact location of the aerodynamic center is also sought.

Lift, drag, and the pitch moment are the most important parameters to be tested. These will be tested with the vehicle at several angles of attack. The maximum angle of attack that the vehicle is dynamically controllable in the subsonic regime is 7 degrees. A range of angles will be tested between 0 and 7 degrees. The testing will also determine the effectiveness of the controll surfaces. The elevons of the horizontal stabilizers will be at 0 and 30 degrees for testing. The body flaps will only deflected on the bottom of the SSTO vehicle and will be tested at 0 and 10 degrees. This is not the maximum deflection, however to test at a higher angle the sting could be damaged at 22.86 m/s (75 ft/s.) the test matrix is presented in table 2.

2.4 Conclusion

In summary we believe that the MATLAB information is accurate and should allow testing of this model in the subsonic wind tunnel without major problems and without damage to the wind tunnel or the sting.

The model is still under construction and should be completed by the end of June 1994. The testing should be completed by the end of July 1994. It is hoped that by that time we will have some data from PMARC_12 to compare the wind tunnel data to.

Alpha degrees	elevon at 0°	elevon at 30°	Body flap at 0°	Body flap at 10°
0	X		X	
2	X		X	
4	X		X	
6	X		X	
0		X	X	
2		X	X	
4		X	X	
6		X	X	
0	X			X
2	X			X
4	X			X
6	X			X
0		X		X
2		X		X
4		X		X
6		X		X

Table 2.2 Test Matrix

3.0 DYNAMIC CONTROLLER FOR THE SSTO VEHICLE SUBSONIC REGIME

3.1 Executive Summary

The SSTO vehicle is not a dynamically stable vehicle without dynamic controllers to control pitch about the center of gravity. Dynamic pitch controllers are utilized by the elevons to input a pitch rate command while minimizing steady state error, rise time and settling time. A MATLAB program was designed to simulate the aerodynamic characteristics of the SSTO vehicle in the subsonic regime. The model was linearized in state-space form, and feedback control with a pitch rate to elevon deflection servo was used to simulate various inputs. Velocities, altitudes, angles of attack, and flight path angles were defined for different flight regions, and the response of pitch rate is created and graphed against the input signal for robustness of the signal. The proposed controller design is defined:

$$K(s) = \frac{.005 * s^2 + 2.5 * s + 2}{0.05 * s^2 + 0.85 * s + 1,}$$

with a gain of 0.49 to Kq, where Kq utilizes pitch as it's feedback signal. The controller can be constructed with an electronic circuit using operational amplifiers for the elevon signal.

3.2 Introduction

Dynamic controllers are not new to aircraft and aerospace application. The X-29 fighter with its forward swept wings require dynamic controllers to insure stability and control. Missiles auto pilots are also used to handle the pitch control in flight. The more complicated the controller the heavier the weight; however, more complicated controllers are needed for the more unstable craft. The SSTO vehicle, despite it's unstable nature, is controllable using only one feedback signal, pitch rate.

Initial approximations of the stability of the SSTO was conducted to confirm the SSTO's dynamic instability, but confirming the craft is statically stable. The sum of moments about the center of gravity was used to determine static stability. The static stability occurs when the graph of Cm, coefficient of moment, versus angle of attack, α, crosses the zero axis of Cm. For different elevon deflections of +/- 30 degrees, stable angles of attack ranges from -7 to 7 degrees. However, the slope of Cm versus alpha is greater than 0, which signifies dynamic instability. Therefore, this proves the need for a dynamic controller.

Three equations governed the SSTO vehicle's pitch motion.

$$dq/dt = M / Iyy$$
$$dV/dt = - g * \sin \gamma - D/m$$
$$d\gamma/dt = - g / V * \cos \gamma + L / (m*V)$$

The variables are defined: q is the pitch rate, M is the sum of the moment of the vehicle about the center of gravity, Iyy is the moment of inertia, V is velocity, g is gravity, γ is flight path angle, D is the sum of drag forces, m is mass of the SSTO vehicle, and L is the sum of the lift forces on the SSTO vehicle.

Other assumptions for the SSTO vehicle performance include many presumptions about the characteristics of lifting bodies. The fuselage of the vehicle was assumed to be a low aspect ratio symmetrical wing with a lift slope of 2.0 / radian. The horizontal stabilizers were assumed to be small cambered wings. The elevons on the rear of the horizontal stabilizers were flat plate extensions. The center of lift on the fuselage was positioned as at 5.0 m forward of the center of gravity, which is 50% of the length of the fuselage. All other distances are consistent with the geometry of the SSTO vehicle. Since, the landing sequence is deadstick, no thrust force is added to the equation. The lift and drag calculations are the sum of all the forces of each individual piece of the vehicle. The moment equation utilizes simple moment arms around the center of gravity to the drag and lift forces.

The size of the SSTO vehicle's fuselage is 51m by 18m wide. The wings are 5m long at the tip and 15m at the base, with a 30 degree dihedral angle. The length of the wing is 10m. The mass of the SSTO is for the lightest configuration with no payload retrieval. Since, the elevons have a larger influence on the pitch control of the SSTO vehicle, the body flaps of the SSTO are eliminated in the pitch model.

MATLAB utilizes a μ-tools folder for analyzing systems and their responses. The experimental model must be put into state-space form. The state-space system of ydot = A x + B u, and z=C x + D u, where x are the states, u are the inputs, and A, B, C, and D are the system matrices. The three governing equations are linearized and calculated at δ trim of the elevon. The system matrix can be analyzed with root locus, bode, and nyquist diagrams to assist in control design. The open loop system characteristics are analyzed to better design the closed system with feedback of pitch rate output. The controller is simulated through MATLAB and the feedback control is used with a STARP function. The closed loop root locus, bode and nyquist diagrams are created to show the characteristics of the response of the system. A time response with an input signal can be produced to show how the system responds to various pitch rate commands. These graphs show the rise time, settling time, and overshoot performances of the controller. The entire block diagram is shown in Figure 3.1.

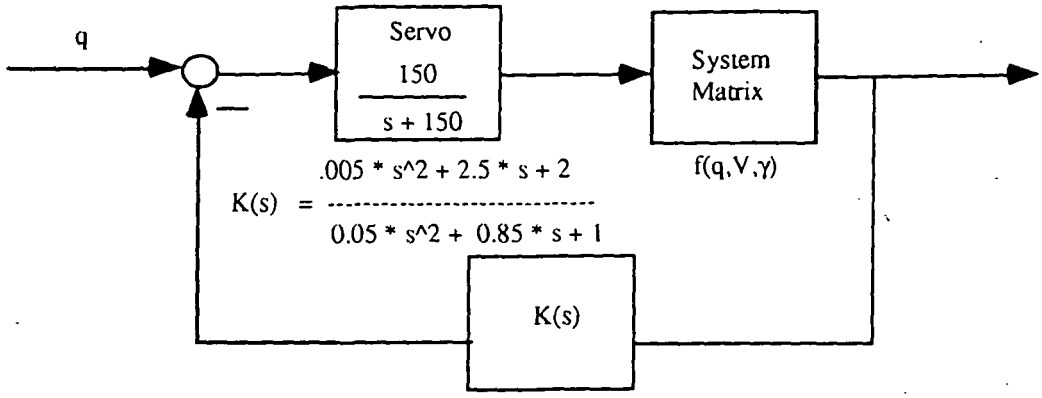

Figure 3.1 Controller Block Diagram

The two main pitch commands used in dead stick landings are the pushover and the flare. These commands are assumed to last 2-4 seconds at a maximum pitch rate for the SSTO of 10 degrees / second. These commands are investigated at altitudes ranging from 15,000m (50,000 feet) to sea level. The velocities range from 400 to 100 m/s. The angles of attack range from 0 to 7 degrees, and the flight path angles range from 0 to 30 degrees.

3.3 Results

The pitch rate controller had to serve two purposes. It had to stabilize the vehicle in basic maneuvers, a flare and a push over. Also it had to have characteristics of a fast response time, minimal steady state error, no oscillations, and similar performance at different altitudes, velocities, and angles of attack. The pitch rate controller described below meets all of the these criteria. The main response tested is a 3 second 5 degrees/second pitch rate input. The first second has no response, the next 3 seconds has a 5 degree/second input, and the last 4 seconds returns to a zero pitch rate input. This represents a flare condition; meanwhile, a push over will have the same response yet only reversed. Since the SSTO vehicle does not need to do high response maneuvers, like a fighter, the SSTO does not need to have a radical pitch input of +/- large pitch rates in a short amount of time.

The open loop characteristics of the system has one unstable root. This root was calculated at 6.9 on the real axis of the root locus. This root had to be drawn towards the imaginary axis to induce a stable response. In addition, the bandwidth of the closed loop system is on the magnitude of 10^{-1} Hz. A higher bandwidth is required to create a better response at low freqency

while keeping high frequency noise at a low magnitude. A lag-lead compensator achieves these characteristics with a relatively simple design.

The pitch rate controller is mathematically modeled at a function of the frequency domain, s:

$$K(s) = \frac{.005 * s^2 + 2.5 * s + 2}{0.05 * s^2 + 0.85 * s + 1}$$

a lag-lead compensator with a gain of 0.49. The equivalent electrical circuit has ratios of resistance times capacitance of R_1C_1 and R_2C_2 of 0.00435 and 0.00370, respectively. The circuit, shown in Figure 3.2,

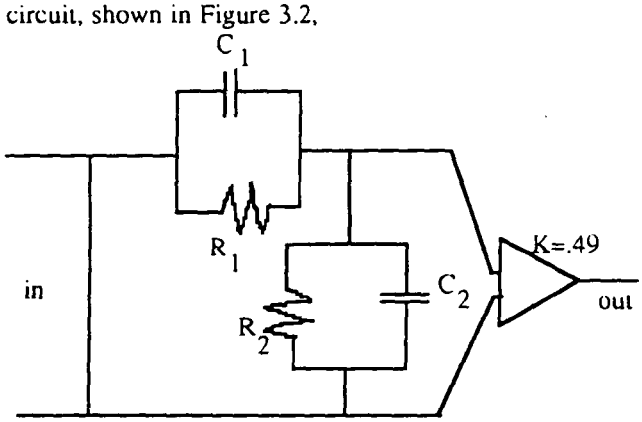

Figure 3.2 Electronic Equivalent Circuit

has an amplifier of an equivalence of 0.49. Since the SSTO vehicle is using fly-by-wire, an electrical circuit simulating the controller would be the standard for installation barring technological advance in controller theory and modeling.

The controller gives the closed loop system the following characteristics in the optimum controller flight envelope. The bandwidth of the system is 300 Hz. The rise time of the controller of an average of 0.2 seconds. Settling time ranges from 1 to 2 seconds. Overshoot is minimized on most situations, except for low speeds at low angles of attack. Oscillations are kept to a single damped period in most cases. Steady state error is less than 1% in optimum controller conditions. All of these characteristics change as a function of the altitude, velocity, and angle of attack.

An optimum flight envelope for the controller is displayed *in table 3.1. The envelope shows the best flight conditions* for the controller. Although flight patterns can be altered from this envelope, the performance of the controller can improve in some areas while at the same time decrease performance in other areas. A velocity performance graph is shown in Figure 3.3.

The changes on controller characteristics are greatly affected by angle of attack and velocity, while altitude improves on the effect on the controller. If speed is higher than the optimum flight envelope it brings about a faster rise time. However, overshoot and oscillation are induced causing slight instability. Lower speed eliminates overshoot and increases damping on the system. On the other hand, a slower response time and steady state error increases as the velocity decreases from the optimum point at the specified altitude. As the angle of attack decreases the controller performance loses all around performance. At high speeds, higher angles of attack induces oscillations at the beginning of the input response. These comparisons can be viewed in the Graphs 1-5 in the Appendix G.

Altitude (m)	Angles of attack	Velocity (m/s)	Flight path angle
15,000	5	600	10
14,000	5	600	10
13,000	7	550	10
12,000	7	500	10
11,000	7	500	10
10,000	5	450	7.5
9,000	5	425	7.5
8,000	5	400	7.5
7,000	5	350	7.5
6,000	5	300	7.5
5,000	5	250	5
4,000	5	225	5
3,000	5	200	5
2,000	5	175	5
1,000	5	150	5
0	7	120	5

Table 3.1 Optimum Flight Envelope for the Controller

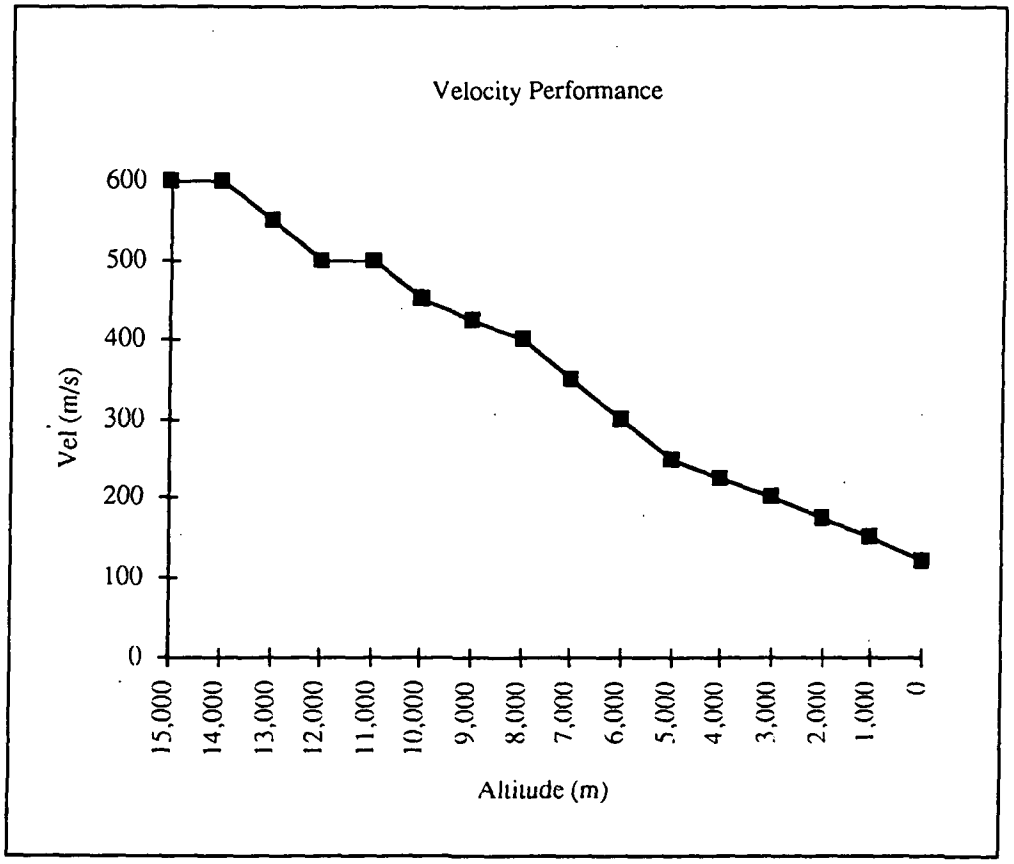

Figure3.3 Optimum Velocity Performance for Altitude.

3.4 Conclusion

This controller is a versatile for the entire subsonic regime. Although this controller would not be installed on a fighter, for a low performance landing of the SSTO vehicle, this lead-lag controller does what it was set out to do. The controller has a fast response time with little oscillation. Oscillation and slow rise time in the response would cause pilot to overcompensate. A damped response would appear as the SSTO vehicle is sluggish in response. Although, not desirable, simulation time for the pilots would train the pilots to expert certain responses to certain inputs. Also, an auto pilot response can be easily programmed and maintained with a damped response like this one.

Future work to be done on the dynamic control of the SSTO vehicle include testing and roll control. Wind tunnel testing will enhance the assumptions made for this mathematical model. The accurate data of actual lift and drag and placement of the aerodynamic center of the craft will give a slight change in the characteristics of the open loop system. Thus adjustments of the controller design can be made so implementation on the controller can occur.

Other future considerations in research would be to involve roll control in the pitch response controller. With the absence of a rudder, horizontal stability will be very difficult to induce. The roll controller can use differential changes in the elevons and body flaps to maintain dynamic stability. The process for creating a controller such as this can be performed in a similar way to the process described here.

In conclusion, for the SSTO vehicle to land like an aircraft, a pitch controller is necessary to maintain dynamic stability. The controller is easily modeled and can be installed into a fly-by-wire avionics system. The response of the controller is very good with a distinct flight performance envelope. However, this performance envelope is not restrictive. Different speeds, angles of attack and altitude will increase performance in some areas and decrease performance in others. However, the controller is proven to allow a pilot or computer to land the SSTO vehicle in the subsonic regime.

The 5 graphs included in Appendix G show the time response comparisons of the pitch rate controller. For all plots, the pitch rate input is a 3 second pitch rate input of 5 degrees per second. The solid rectangular line is the input signal and the other lines are the response of the SSTO vehicle. The graphs are in radians per second; therefore, a 5 degree/second pitch input is equal to .087 radians per second.

Graph 1 - Comparison of optimum altitude performance of 15,000 m to 11,000m.

Graph 2 - Comparison of optimum altitude performance of 10,000 m to 5,000 m.

Graph 3 - Comparison of optimum altitude performance of 5,000m to sea level.

Graph 4 - Comparison of optimum performance at altitude of 5,000 m for velocities of 300 to 200 meters per second at an angle of attack of 5 degrees.

Graph 5 - Comparison of optimum performance at altitude of 5,000 m at a velocity of 250 m/s and angles of attack from 3 to 7 degrees.

HYPERSONIC MODEL

4.1 Introduction

One of the key elements in finalizing the design of an aerospace vehicle is the experimental verification. This engineering dogma was practiced by the Hypersonic Aerodynamics Team by performing wind tunnel testing on a scaled SSTO model.

Prior to this test our aerodynamic data originated from NASA's Supersonic/Hypersonic Arbitrary Body (SHAB) program, a panel method software for preliminary analysis of high speed aerospace vehicle designs. SHAB provided us with load coefficients for specific wing/body configurations and flow conditions. The data produced by SHAB was used to estimate aerodynamic loads on the SSTO model which served to define and determine test parameters for the trisonic wind tunnel at Marshall Space Flight Center (MSFC).

The supersonic/hypersonic wind tunnel test at MSFC is intended to study control and stability, and aerodynamic performance of the SSTO lifting body design. The test was performed in the trisonic wind tunnel at MSFC for eight different wing/body configurations at three Mach numbers (2.74, 3.78, 4.96) for a -2 to 40 degrees AOA sweep.

In these section, the trisonic wind tunnel at MSFC is described to familiarize the reader with the equipment used for testing; the model design process, based on test and facility driven factors, is reviewed; pre-test analysis is discussed; and test results are compared to SHAB data.

4.2 Trisonic Wind Tunnel at MSFC

The tunnel is an intermittent trisonic blowdown wind tunnel operated from pressure storage to vacuum or atmospheric exhaust. The test section measures 14 x 14 inches in two of the interchangeable sections. The transonic

section provides for Mach numbers of 0.20 through 2.50 and the supersonic/hypersonic section provides for Mach 2.74, 3.48, and 4.98. In the supersonic/hypersonic range, speeds are varied by tilting fixed contour nozzle blocks contained in the test section. Downstream of the test section is a hydraulically controlled sector that provides for AOA's of ±10 degrees with various offsets extending the pitch limits to 90 degrees (see figure 4.1).

Static stability models are normally mounted on a sting and balance furnished by NASA. MSFC trisonic wind tunnel personnel selected an appropriate sting-balance based on various criteria. The ranges of forces and moments at starting and running conditions is a key factor; therefore, it is common protocol to request a pre-test report containing specific information on expected aerodynamic loads on the model. Other factors involved in the selection process are: space limitation of the model balance cavity, proper tunnel placement, and correct balance-model placement.

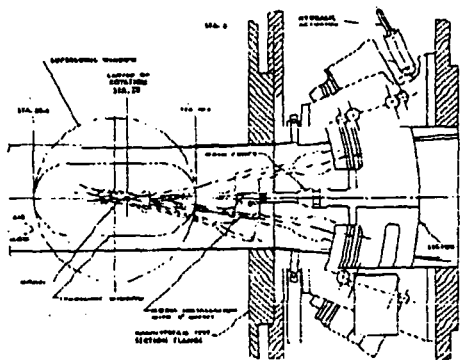

Figure 4.1 Supersonic Test Section

The maximum model size is largely dependent on model geometry, Mach number, and Reynolds number. It is considered a "rule of thumb" that model sizing launch vehicle configurations can be tested with reliable results if the model base diameter is three inches or less, the length is fourteen inches or less, and the model blockage is five percent of the total test section area or less.

All model force and moment data are measured by internal strain gage balances and recorded by a solid state digital data acquisition system. The digital data is later transferred to a VAX machine for analysis. Various methods of flow visualization are available for the trisonic wind tunnel. Direct shadow, or shadowgraph method, Schlieren stills, and Schlieren video are used frequently. The SSTO model tests were taped using Schlieren video.

4.3 Model Design

The fuselage for the model was downloaded from FUSEX to Pro-Engineer. Wings and body flaps were created afterwards. These were then integrated into the fuselage to check for correct placement and size. The cross-section used for the wings was a NACA 23012 type airfoil, which was recommended to us by NASA because of its aerodynamic performance in the hypersonic regime due to the flatness of the airfoil lower section and its excellent lift capabilities.

The 6302 T6 aluminum model was originally scaled to 1/335 so its projected area at a 45 degree AOA would create a five percent blockage in the 14 x 14 inches supersonic test section. The scale factor was later increased to accommodate the sting mount recommended by MSFC.

SHAB was then used to determine the required wing and body flap configurations for stable flight in the hypersonic region. This data obtained from SHAB in the form of force and moment coefficients was later utilized to calculate aerodynamics loads expected while testing as well as performing stress analysis on various sections of the vehicle model.

A test proposal was sent to MSFC detailing the size of the model and its basic configuration. The load estimates obtained from SHAB were included for the scaled model as to provide the trisonic wind tunnel personnel with enough information to recommend a sting-balance.

After MSFC replied to our proposal the model had to be scaled up to 1/256 due to the unavailability of the appropriate sting-balance; therefore, a 0.5 inches diameter sting-balance was recommended. The new scale factor increased the test section blockage at 45 degrees AOA to ten percent, still the model remained under wind tunnel test article sizing limits of fourteen inches total length and three inches base diameter (see model dimensions in Table 4.1). It is possible, but not certain that the high blockage area of the SSTO model at high angles of attack could choke the air flow in the tunnel thus making data collection virtually impossible. At the time of this writing the model was still undergoing wind tunnel testing for the high AOA conditions at MSFC.

total model length	7.82 inches
wing span	5.54 inches
base width	3.06 inches
model height	1.58 inches
blockage area @ 45°	20.1 inches^2

Table 4.1 Model Dimensions

The first consideration while designing the method for attaching the model to the sting was the proper placement of the sting-balance. The sting-balance center needs to be located as close as possible to the C_p location of the test article. The calculated distance from the sting-balance center to the C_p location is approximately 0.1 inches. The diameter of the bored sting hole was determined by the dimension of the sting.

The next step was to design a mechanism to hold the sting in place as well as the wings and body flaps. The model is composed of five assembly parts: fuselage, two wings, and two body flaps. A transversal cut through the center of the fuselage in the horizontal plane from the base of the model to one inch forward of the bored hole end proximal to the nose area was used. In conjunction, a threaded pin on the top surface and a push-pin from the bottom surface of the fuselage were used to engage the sting-balance adapter pin holes. Four #8 stainless steel screws, two forward of the pins and two aft of the pins were used to clamp down the sting-balance adapter. This mechanism allowed for the model to hold the sting by using pins and frictional force due to clamping to secure the adapter in place.

The fuselage CAD file was then cut apart into three different sections: the bottom half, and the top half which was split along the transversal vertical plane into two symmetrical pieces. These cuts were performed on the CAD file to ease the machining process; the body was indeed machined as one solid piece. This information was then transferred to a program called MasterCam, which controlled the machining equipment.

The wings design was also transferred to MasterCam after splitting it into two halves. After machining, the wings were bent at the root into a 30 degree dihedral angle to the base. Then, the flat plate elevons were bent to the desired deflections.

Two sets of wings and three sets of body flaps were machined with different deflections to determine the best configuration for safe reentry of the SSTO. The wings were machined with 20 and 30 degrees elevon deflections, while the body flaps were machined at 0, 20, and 30 degrees. The wings were secured to the model by using four #8 stainless steel screws to secure the wing's flat base inserted in the model through slots machined on the aft part of the fuselage. The body flaps were machined as set blocks with a flat top surface and a slanted bottom surface to the desired deflection angle. These were held in place by the aft two screw used for the wings setting them inside square slots machined on the bottom surface of the model. A three-view drawing of the final model design can be found in Appendix A.

4.4 Pre-Test Analysis

Aerodynamic loads on the model and the stresses on the wing root were calculated as part of a pre-test report requested by MSFC. Model aerodynamic loads were estimated to verify that all forces and moments encountered by the model during testing would be well below the sting limits by at least a safety factor of four.

Axial and normal loads were calculated using the following formulas:

$$L_A = C_A \cdot q \cdot A_{ref},$$
$$L_N = C_N \cdot q \cdot A_{ref}.$$

The maximum loading in our test sequence occurs at Mach 2.74 where the dynamic pressure (q) is at its highest, 6.38 lb/in^2. The reference area used for calculations was estimated at 23.93 in^2.

SHAB output showed that a wing-body configuration consisting of wing flaps deflected at 20 degrees and body flaps deflected at 30 degrees, and an AOA of 44 degrees provided maximum loading conditions. Table 4.2 contains the maximum axial and normal loads estimates for the SSTO model.

Axial Force	Normal Force
C_A = 0.11529	C_N = 0.97694
L_A = 17.6 lbs	L_N = 149 lbs

Table 4.2 Aerodynamic Loads

Maximum pitch moments were calculated using the formula,

$$M_P = C_M \cdot q \cdot A_{ref} \cdot L_{ref}.$$

The same flow conditions and reference area were used for this calculation. The reference length was estimated at 2.31 inches. The wing-body configuration used previously for calculating the axial and normal loads provides maximum pitch moment conditions. Table 4.3 contains the maximum positive and negative pitch moment estimates for the SSTO model.

Maximum Pos. Pitch Moment @ 21° AOA	Maximum Neg. Pitch Moment @ 44° AOA
C_M = 0.02810	C_M = -0.01852
M_P = 9.91 lb-in	M_P = -6.53 lb-in

Table 4.3 Pitch Moments

It is inherent in an intermittent supersonic wind tunnel that, during the starting or stopping sequence, a high energy force is applied to the model due to the shock wave moving through the test section. This force is much greater than the normal running aerodynamic loads. The "Normal Shock" theory is considered to provide the most acceptable approach to determine these loads. This theory assumes that a normal shock exists at the leading edge or nose of the model and is extended in one direction only. A plot of normal shock theory starting coefficient as a function of Mach number is presented in Figure 4.1. The normal shock theory starting coefficient is defined as,

$$C_S = \frac{F_S}{P_{stag} \cdot A_{proj}}.$$

On the basis of experiments conducted by the MSFC Experimental Aerophysics Branch, it is recommended that two-thirds the normal shock starting load be used for all bodies of revolution with small fins or vanes.

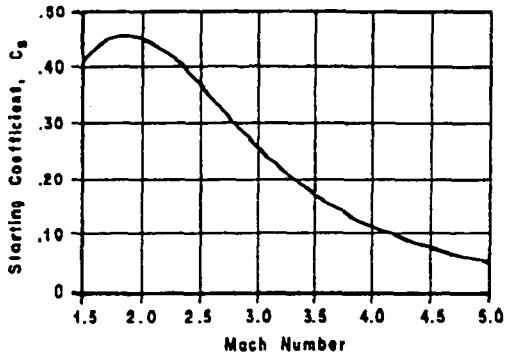

Figure 4.2 Starting Load Coefficient vs. Mach Number

The stagnation pressure used for the calculation of starting loads was 45.0 lb/in. Starting loads were calculated for two AOA; 36 and 44 degrees. The starting load at 44 degrees AOA is specified for reference as the maximum possible load. Starting loads are only be encountered at the beginning of an AOA sweep, thus the maximum starting load that could be encountered during testing of the SSTO model would be for the configuration stated previously for running-loads at 36 degrees AOA. Starting loads for both AOA's are included in Table 1.4.

Maximum Starting Load @ 36° AOA	Maximum Starting Load @ 44° AOA
A_{proj} = 16.7 in^2	A_{proj} = 20.1 in^2
F_S = 225 lbs	F_S = 225 lbs

Table 4.4 Starting Loads

Stress analysis was performed on the wings to verify that starting loads were below ultimate strength by a minimum safety factor of four. Stress analysis was not performed on the fuselage, sting attachment section, nor body flaps because all members were in compression and no real concerns were expressed by the MSFC trisonic wind tunnel personnel.

Newtonian theory for hypersonic flow was used to estimate aerodynamic loads. This theory predicted a detached shock wave on the wings. Therefore a simple wing-elevon configuration was used in the analysis. Lift and drag coefficients,

$$C_L = 2 \cdot sin^2(\alpha) \cdot cos(\alpha),$$
$$C_D = 2 \cdot sin^3(\alpha),$$

were calculated for a thin-plate wing at 45 degrees AOA and an elevon at a deflection angle of 30 degrees to derive lift and drag forces,

$$L = C_L \cdot q \cdot S,$$
$$D = C_D \cdot q \cdot S,$$

on the wings and elevons at a dynamic pressure of 6.38 lb/in^2 (Mach 2.76) using a wing reference area of 4.04 in^2, an elevon reference area of 0.67 in^2. Lift and drag coefficients for both wing and elevon are included in Table 1.5, as well as the total resultant force on the wing and elevon combined.

Wing	Elevon	Wing-Elevon
L = 18.02 lbs	L = 2.05 lbs	R = 32.6 lbs
D = 18.02 lbs	D = 7.67 lbs	

Table 4.5 Aerodynamic Loads on Wing-Elevon

The shear and normal stresses on the root of the wing were approximated by,

$$\tau = \frac{R}{W_{base}},$$
$$\sigma = \frac{M_{root} \cdot W_{base}}{I},$$

where the moment at the root was calculated using beam static equilibrium formulas. Table 1.6 contains the results of this analysis.

Shear Stress	Normal Stress
260.8 psi	6.26e3 psi

Table 4.6 Wing Root Stresses

The stress values were found to be well below the ultimate strength of 6302 T6 aluminum. As a result, the SSTO hypersonic test model was approved by MSFC for testing.

4.5 Test Procedures

The supersonic/hypersonic wind tunnel test goals are to study control and stability, and aerodynamic performance of the SSTO lifting body design. Based on this statement the group designed a test matrix to investigate both the maximum L/D and stability flight regimes at three distinct Mach numbers; 2.74, 3.48, 4.96.

According to SHAB output data, maximum L/D conditions occur around 15 degrees AOA for the Mach numbers above, and stability is obtained at approximately 25 degrees AOA for the 20 degree elevon deflection, 30 degree body flap deflection configuration. Therefore tests were conducted for an AOA sweep of negative two to positive forty degrees, as to cover as much of the flight regime as possible to account for any offset errors SHAB may have produced.

This AOA sweep required a change of sting during testing due to the limited ±10 degrees range of the sector. The two stings used were; an eight degrees offset sting, and a 30 degrees offset sting. The first sting would cover the negative two to eighteen range and the second sting would cover the twenty to forty range. Sting changes required that, the model be taken out of the tunnel, the new sting be calibrated, and the model be set up again.

The maximum run time is about forty seconds for supersonic flow with vacuum exhausting. Force tests require approximately eight seconds per AOA, thus limiting each test run to six force measurements. Mach numbers are changed between runs by automatically tilting and translating a set of fixed contour blocks inside the test section by hydraulic means.

Eight configurations were tested at MSFC. A no-wings / zero-degrees-body-flaps-deflection, a twenty-degrees-elevons-deflection / zero-degrees-body-flaps-deflection, and a twenty-degrees-elevons-deflection / zero-degrees-body-flaps-deflection were tested as baselines to derive the contribution to lift and drag due to the wings and body flaps, as well as, to provide Professor Candler[4] with test data on the fuselage of the SSTO to compare results against a hypersonic CFD code he developed.

Elevon Deflection	Body Flap Deflection
-no wings	0 degrees
20 degrees	0 degrees
30 degrees	0 degrees
20 degrees	20 degrees
30 degrees	20 degrees
20 degrees	30 degrees
30 degrees	30 degrees
20 degrees/30 degrees	0 degrees

Table 4.7 Wing-Elevon/Body-Flap Configurations

Four wing-elevon/body-flap configurations were also tested as defined in Table 1.7. The last configuration was intended to study lateral stability of the SSTO by offsetting elevon deflection between the two wings by ten degrees.

The total number of successful runs needed to complete the test is ninety-six.

Before the model is mounted on the sting, a dimensional check and measurement of the moment transfer distance are made. The balance is dead-weight loaded and checked through the tunnel data system, and proper load sensitivities are set up before running. After the model is mounted and secured on the sting adapter, base pressure lines are placed aft of the body and connected to the pressure data acquisition system. The sting and pressure lines are then wrapped in adhesive tape; the tunnel is closed; and the test sequence begins.

4.6 Test Results

At the time of this writing, wind tunnel tests were still being performed on the SSTO model; therefore, this report only compares the lower AOA wind tunnel data against SHAB output. That is, the analysis is limited to correlating data around the maximum L/D region. A complete analysis of the model should be available as soon as more wind tunnel data is available from MSFC.

Wind tunnel results and SHAB output show that there is no large difference in L/D results over the Mach numbers tested; therefore, these two sets of data were only compared at the highest Mach number, 4.96 (see Appendix C).

SHAB output matches wind tunnel data accurately for the no-wings/0-body-flap-deflection configuration. For other configurations, SHAB is not as accurate, creating an offset between the two L/D curves (see Appendix C). This discrepancy may be explained by the inaccuracy of the SHAB program to model the attachment area between the wings and the fuselage.

According to SHAB data, a maximum L/D of 1.695 is obtained at fifteen degrees AOA with elevons and body flaps deflected at twenty degrees. According to wind tunnel data, a maximum L/D of 1.846 is obtained at twelve degrees AOA with the same configuration. These results confirm that the SSTO vehicle will attain maximum L/D conditions around the ten to fifteen degrees AOA range.

4.7 Conclusion

The results of this test show that SHAB data is fairly accurate, and may be used as a design tool for supersonic/hypersonic body design. Based on these premise, it is safe to conclude that stability may be reached around twenty-nine degrees AOA for the twenty degrees elevon deflection/thirty degrees body flap deflection; therefore, the SSTO is stable and controllable in the hypersonic region. Since, all the data was not available, no further conclusions are not warranted.

5.0 STRUCTURE

5.1 Introduction

The objective of this project was to determine how well theoretical models predict strain and failure. A simple frame was chosen because of availability and ease to manufacture. I-DEAS (finite element analysis software) and the Force Stiffness Buckling Method (physical non-destructive test) were used to get the theoretical results. The I-DEAS model produced reasonable results, but differed from the experimental results by up to 36%. The Force Stiffness Buckling Method predicted failure much more accurately, with an error of only about 5.5%. I-DEAS is still a very useful design tool in the early stages of the SSTO design process, but physical testing is irreplaceable.

5.2 Test Model

It was necessary to design a frame that could be compared to an I-DEAS model with good accuracy, built

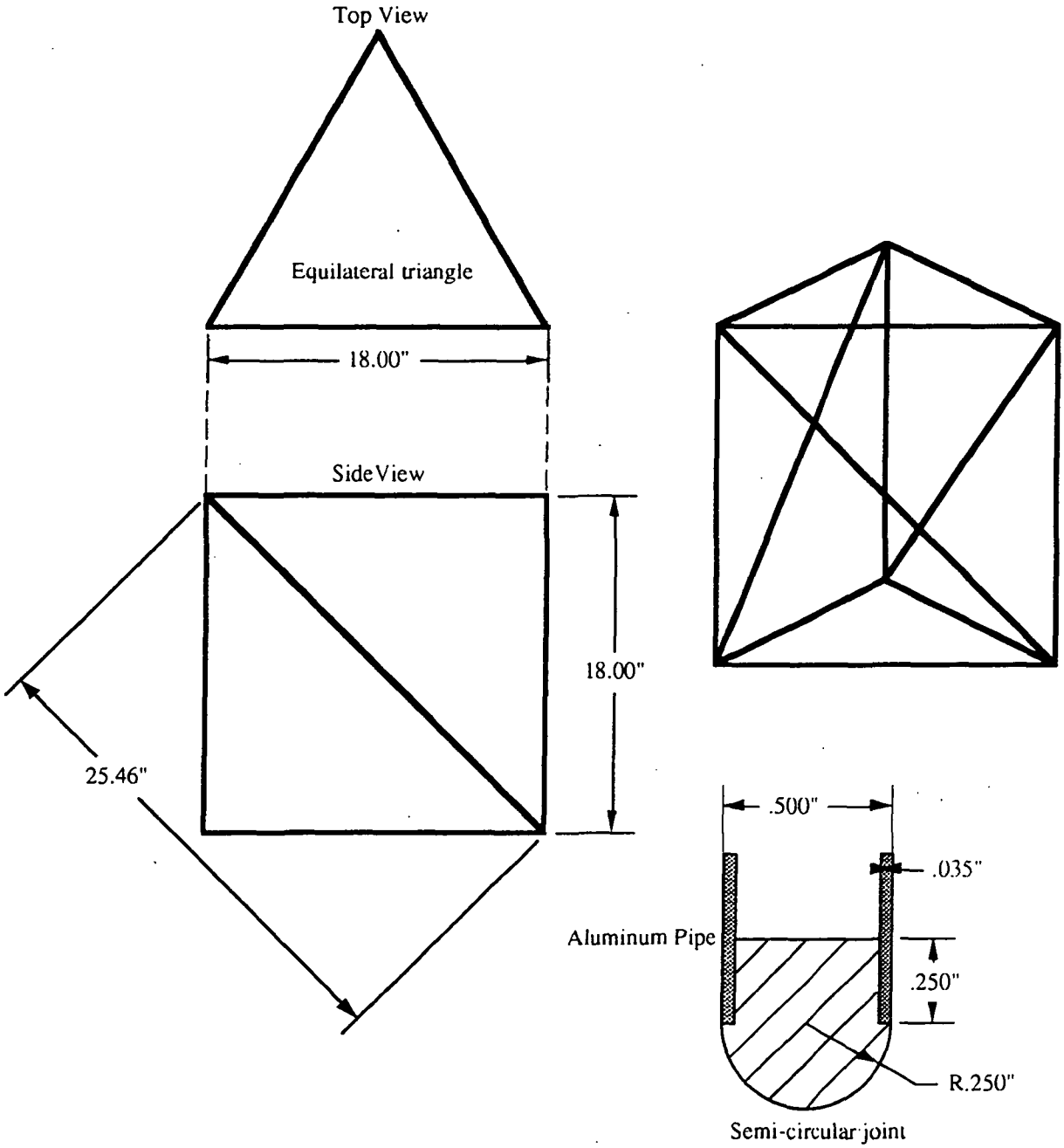

Figure 5.1 Structural Model

easily, and tested with the available equipment. These restrictions determined the size of the model, approximately 18"x18"x18", and its complexity, see Figure 5.1. Also, they determined which material could be used, aluminum 6061. The pipe cross sections, see Table 5.1, were chosen based on an I-DEAS mass optimization of the test model and material availability. In order to apply axial loads with no moments, hemispherical joints were inserted into the ends of vertical pipes. The I-DEAS model of the optimized structure could carry up to 15,200 N (3424 lbs) with maximum and minimum element forces of 293 N (65.9 lbs) and 101 N (22.7 lbs) respectively.

5.4 Test Fixture

The test fixture consisted of three main components a steel table, a steel plate and a pump and actuator, see Figure 5.2. The pump and actuator were attached to the table and steel plate with chains. This allowed the actuator to apply a compressive load on the test model. For the non-axial test, the model was angled with 1" aluminum blocks, see Figure 5.3. A crane attached to the steel plate and a large plywood shield were used as safety devices.

	Outer Diameter	Thickness	Length	Number
Top and Bottom	0.5"	0.035"	18"	6
Vertical	0.5"	0.035"	18"	3
Diagonal	0.3125"	0.035"	25.46"	3

Table 5.1 Structure Model Materials

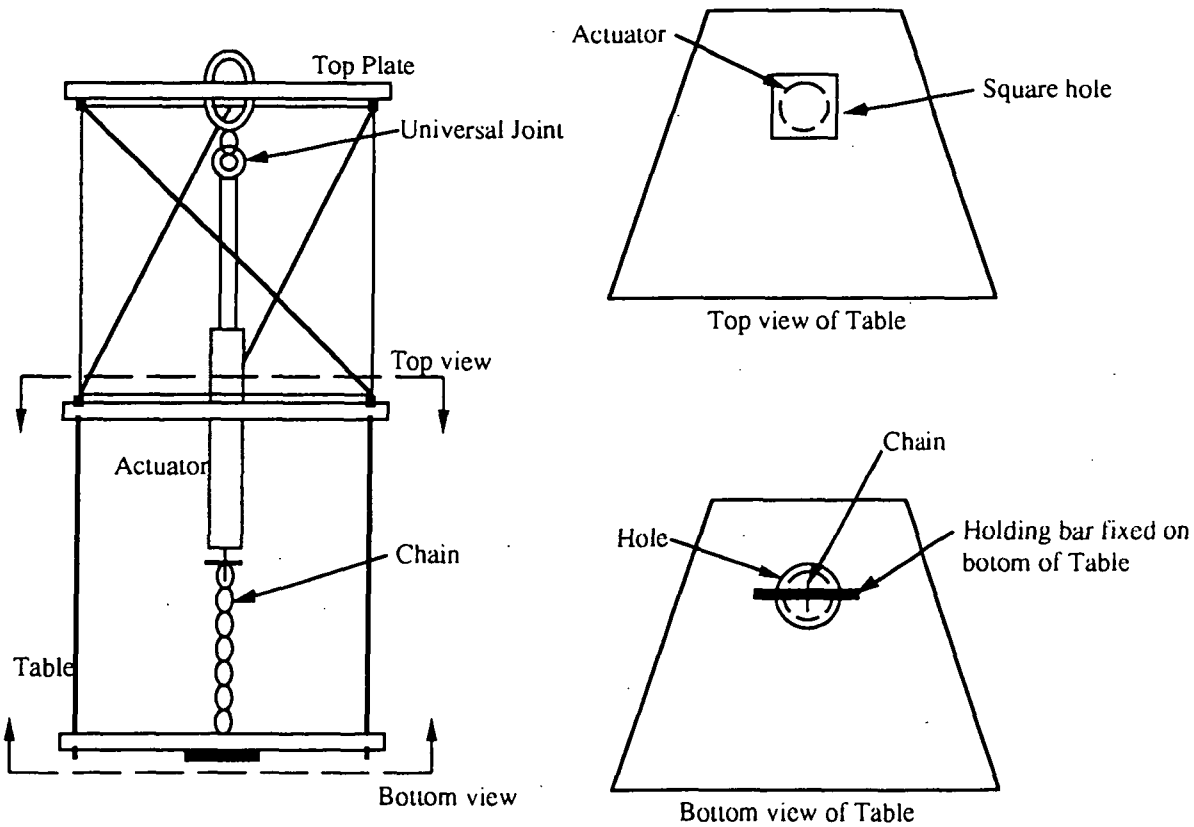

Figure 5.2 Structural Setup

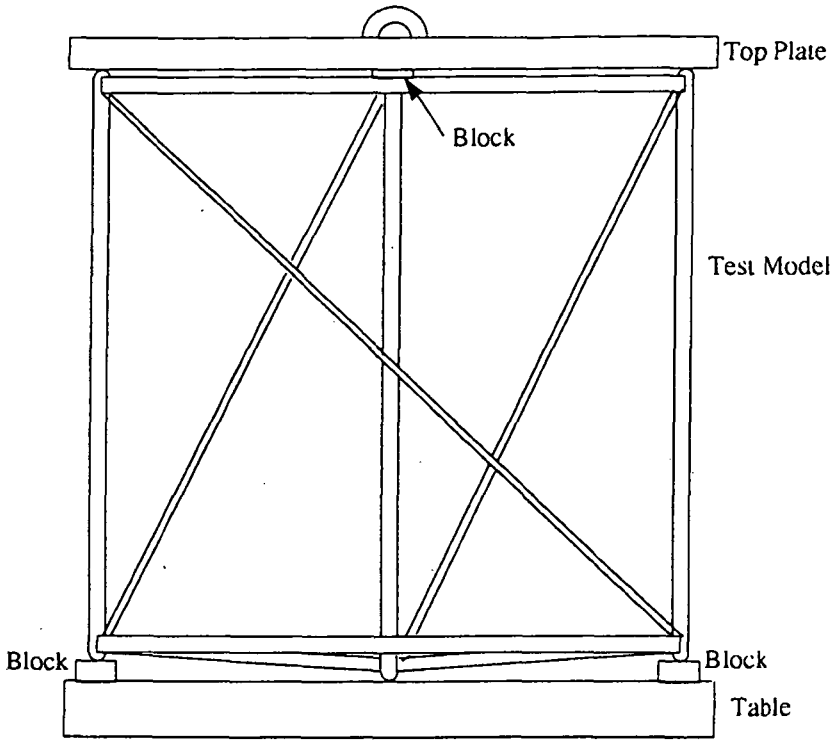

Figure 5.3 Structual Model and Setup

5.3 Test Procedure

Three procedures, an axial loading test, a non-axial loading test, and a failure test, were performed. The model was tested axially by applying a compressive load in 250 lb intervals from 250 to 1500 lbs. Then, the model was tested with an angled load in 250 lb intervals from 250 to 1000 lbs. Strain data was collected from ten strain gages applied to the test model, six on the three vertical pipes and four on two of the diagonal pipes. All of the strain gages were applied in pairs, back to back, to allow for measurement of the bending strain. The test data was compared with the I-DEAS analysis, and also with the Force Stiffness Buckling Method. Note that the critical strain used in the Force Stiffness Buckling Method was determined from the test data after failure. After the data and analysis were compared the model was brought to failure to verify the analytical buckling loads.

5.5 Results

Beam 1 on the test model buckled at 2200 lbs, during an axial test.

Figures 5.4 and 5.5 show the bending strain Force Stiffness Buckling Method. To use this method the load divided by the bending strain is plotted versus load. From the plots the buckling load is simply the x intercept. This method predicted that the buckling load of beam 1 is 3760 lbs, and 2080 lbs for beam 2. The large difference in the predicted failure loads occurs because the strain gages in beam 1 and beam 2 are measuring the strain in two different planes. That is, because the strain gages on beam 2 are in the buckling plane they yield a better estimate.

Figure 5.6 shows another variation of the Force Stiffness Buckling method. In this method the load divided by the total strain is plotted versus load. The buckling load is determined by the intersection of the experimental data and the inverse of the critical strain. This method is usually more accurate than the bending strain method. However for this test it was less effective, because too few data were taken during the test.

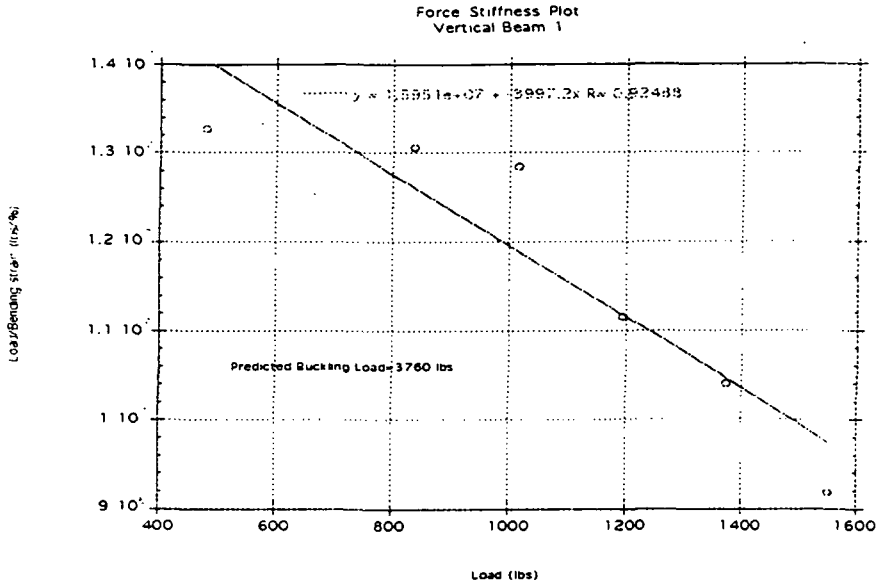

Figure 5.4 Force Stiffness Buckling Method

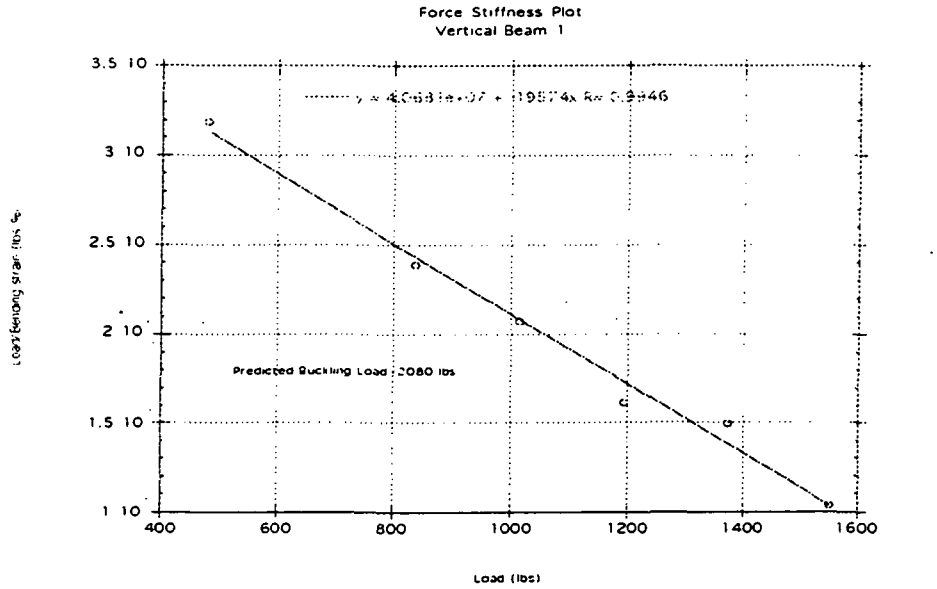

Figure 5.5 Force Stiffness Buckling Method

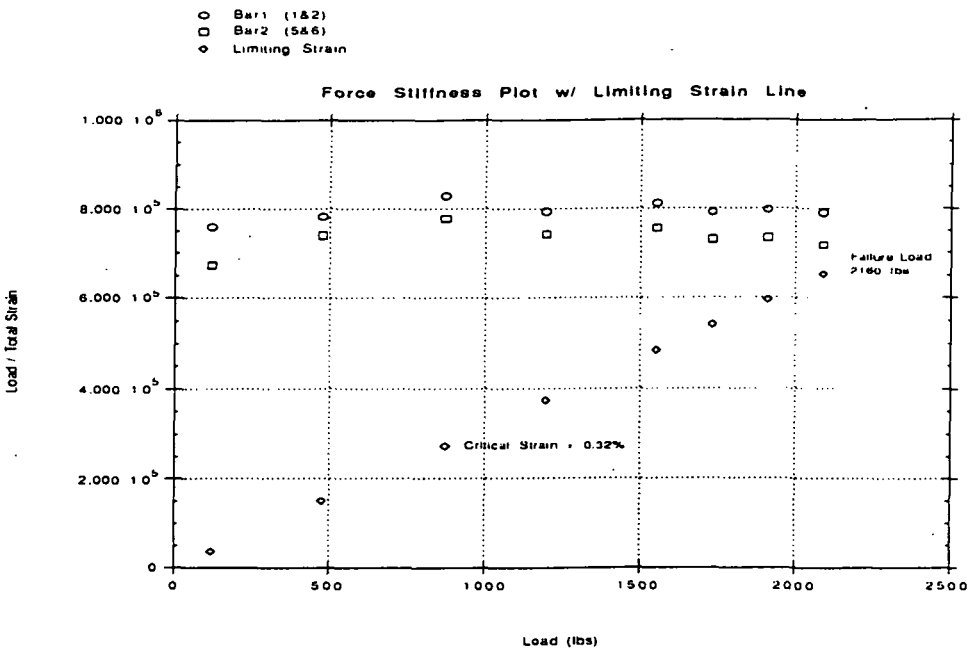

Figure 5.6 Force Stiffness Buckling Method

5.6 Conclusion

I-DEAS gives a rough estimate of failure which is adequate for conceptual design work. However, physical testing is necessary later in the design process to get *sufficiently accurate results. This is shown by the* difference in buckling load errors, 36% from I-DEAS and 5.5% from the Force Stiffness Buckling Method.

		Strain Gages									
Load (psi)	Load (lbs)	1	2	3	4	5	6	7	8	9	10
0	120	-94	-78	-1	7	-104	-104	3	-4	-86	-99
100	478	-301	-265	10	5	-333	-348	12	-4	-308	-326
150	657	-394	-348	16	7	-436	-438	19	2	-407	-429
200	836	-519	-455	24	10	-568	-603	26	0	-535	-562
250	1015	-617	-538	31	13	-671	-720	32	2	-638	-668
300	1194	-760	-653	40	18	-819	-893	42	8	-793	-828
350	1373	-860	-728	49	21	-918	-1010	49	12	-896	-936
400	1552	-981	-812	57	25	-1013	-1163	58	17	-1026	-1053
0	120	-72	-75	-3	0	-83	-103	5	-7	-72	-79

Table 5.2 Non-axial test data.

		Strain Gages									
Load(psi)	Load (lbs)	1	2	3	4	5	6	7	8	9	10
0	120	-70	-100	13	22	-91	-105	16	14	-116	-79
110	513.8	-307	-328	63	77	-360	-386	28	16	-347	-298
150	657	-390	-407	76	94	-449	-479	30	19	-429	-366
200	836	-520	-525	97	126	-592	-634	36	23	-564	-483
250	1015	-625	-618	114	149	-708	-765	40	26	-672	-575
300	1194	-738	-713	135	178	-826	-900	47	30	-788	-670

Table 5.3 Axial test data.

		Strain Gages									
Load (psi)	Load (lbs)	1	2	3	4	5	6	7	8	9	10
	120	-83	-75	8	2	-84	-94	3	1	-73	-82
100	478	-324	-287	14	5	-310	-336	8	-7	-294	-306
210	871.8	-565	-486	23	-8	-535	-585	13	-11	-516	-531
300	1194	-822	-683	33	-9	-763	-845	18	-15	-738	-757
400	1552	-1070	-844	44	-12	-963	-1092	26	-19	-944	-975
450	1731	-1266	-922	54	-13	-1076	-1293	35	-20	-1083	-1127
500	1910	-1537	-860	68	-19	-1078	-1523	42	-21	-1205	-1215
550	2089	-2286	-358	142	-119	309	-3216	33	-21	-1628	-1047
570	2160.6	Failure!!!									

Table 5.4 Failure test data.

		Load / Bending Strain			Load / Total Strain (Avg. of strains)		
Load (psi)	Load (lbs)	Bar1 (1&2)	Bar2 (5&6)	Bar3 (9&10)	Bar1 (1&2)	Bar2 (5&6)	Bar3 (9&10)
	120	1.500E+07	1.200E+07	1.333E+07	7.595E+05	6.742E+05	7.742E+05
100	478	1.292E+07	1.838E+07	3.983E+07	7.823E+05	7.399E+05	7.967E+05
210	871.8	1.104E+07	1.744E+07	5.812E+07	8.295E+05	7.784E+05	8.327E+05
300	1194	8.590E+06	1.456E+07	6.284E+07	7.934E+05	7.425E+05	7.987E+05
400	1552	6.867E+06	1.203E+07	5.006E+07	8.109E+05	7.552E+05	8.088E+05
450	1731	5.032E+06	7.977E+06	3.934E+07	7.911E+05	7.307E+05	7.833E+05
500	1910	2.821E+06	4.292E+06	1.910E+08	7.968E+05	7.343E+05	7.893E+05
550	2089	1.084E+06	5.926E+05	3.596E+06	7.901E+05	7.186E+05	7.809E+05

Table 5.5 Force Stiffness data table.

ANIMATION / AIR LOCK

6.1 Introduction

In order to utilize the interior volume of the ship more effectively, a radical airlock design was proposed. The tubular "L" shape saved space, but it needed to be determined if it limited maneuverability severely.

Testing an astronaut's ability to move through the airlock was a two step process. The animation of the testing maneuvers was the first step. The airlock and an average sized adult human in a space suit were created in Pro/ENGINEER. Pro was used to verify that the diver did in fact fit inside the airlock. Then, Advanced Visualizer was employed to create an animation of the maneuvers. This animation could serve an instructional role by visually explaining to the diver the maneuvers to be performed for the physical model.

The second step of this testing process was the building of a life-sized airlock. This full-sized mockup was submerged in a pool to simulate weightlessness. A diver performed the maneuvers demonstrated in the animation. The maneuvers were an exit from the command module to open space and a turn around maneuver inside the airlock.

6.2 Airlock Animation

To understand the complications associated with an astronaut moving through the SSTO airlock system, it was necessary to create a simulation of various astronaut maneuvers using the Advanced Visualizer animation tool. By viewing this animation, we verified that an SSTO crew member with full life-support gear will be able to safely navigate the airlock in several situations.

Pro/ENGINEER Assembly and Visualization. To create a reasonable animation, it was first necessary to create several new objects in Pro/Engineer. These objects included a detailed crew module, an L-shaped set of airlock tubing, airlock doors, and a simulated astronaut. The astronaut was created with movable limbs, to simulate natural human motion. By assembling these parts together in Pro/Engineer, it was possible to see that an astronaut of average size could safely fit inside the 3.5 foot diameter tubing with plenty of clearance(see Appendix K).

The point of creating this model was to prove that an astronaut would be able to maneuver through the airlock, therefore, details such as controls for opening and closing the airlock doors were omitted from the Pro/Engineer drawings. These details were not ignored, but due to time constraints could not be included in this version of the model.

Although the Pro/Engineer drawings provided us with a good idea of how the airlock parts would fit together and that an astronaut would fit inside, it was necessary to transfer the parts to Advanced Visualizer to simulate astronaut motion through the airlock.

Advanced Visualizer. When transferring the parts to Advanced Visualizer, it was decided that the two upper arms, two forearms, two thighs, and two lower legs would each make up one part. That is, the left and right parts of the body would not move separately from each other. This "joining" limited the amount of natural human motion we could create, but it allowed us to bring one object into the scene rather than two, expanding our allowable animation length.

It was decided that the animation would include two scenes, allowing us to create the animation and have time left over for editing. The first scene would show a crew member exiting from the crew module, maneuvering into the airlock, and exiting the ship through the top airlock door. The second scene would show a second crew member maneuvering from the crew module into the airlock, turning around, and re-entering the crew module. These two scenes were then joined in the middle so that the second crew member would enter the airlock while the first crew member was still inside, proving that two crew members could fit inside the airlock at the same time, in case of emergency.

It was not difficult to create near natural human motion using the simulated astronaut, and the maneuvers through the airlock were completed successfully. The airlock model also fit very well inside the bulkheads of the ship, with little wasted space. Therefore, we can conclude that an airlock of 3.5 feet in diameter would be safely navigable for an average-sized astronaut, and that such an airlock could easily be placed within the existing SSTO shell.

6.3 Physical Mockup

Developing Airlock and Mockup Design. The rough idea for what size the airlock should be came from the dimensions of the SSTO and the approximate size of an astronaut in a space suit. From examining the dimensions of an average adult male and adding bulk to represent the space suit, a dimension of approximately 1.1 m (3.5 feet) in diameter was chosen for the airlock. This size allows easy transit through the airlock. The "L" shape of the airlock permits the astronauts to either enter the cargo bay or leave the ship for open space. This "L" shape also facilitates the construction of the mockup. To ease transport to the testing site, the mockup was broken into three sections (two straight sections four feet long, and a jointed section with one four foot long extension piece). For simplicity and ensuring the diver's safety, the doors for the mockup were omitted.

Concept Verification. To verify that the design would be compatible with the astronauts before is was built, the airlock was simulated using Pro/ENGINEER. First, a solid model of an astronaut wearing an extra-vehicular activity suit (EVA) was made using Pro. The astronaut was then "assembled" in various positions with the solid model of the airlock. This allowed the fit between the astronaut and the chip to be verified (See Appendix K).

Mockup Construction. The materials used to build the mockup were chosen for their strength and low cost. The frame cross sections, used to keep the walls circular, were made of 1" x 2" x 8' pine lumber. Each eight foot piece of lumber was cut into two frame parts (a horizontal piece 3.75' long and a vertical piece 4.5' long.) Two horizontal and two vertical pieces were used to make the square frame section. The extra length of the vertical members gave the frame a set of "feet" to stand on. Two screws in each corner were used to hold the members together.

The frame sections were held together with cross members made from 2" x 2" x 8' pine lumber. These were cut into 48" lengths to match the length of the wall material. Ninety degree steel angle brackets were used to secure the cross members to the frame sections and supply a degree of rigidity to the structure. Screws were used to fasten the brackets and cross members.

A 50' roll of 48" wide vinyl coated wire fencing material was purchased to make the walls of the airlock mockup. This was chosen to allow us to see inside the mockup while being sturdy and inexpensive. Since the airlock was to have a 3.5' diameter, the material was cut to approximately 12' lengths and rolled into the proper size cylinder, using a frame section as a guide. Self locking nylon cable ties were used to secure the rolls of fencing into cylinders and attach them to the frame.

6.4 Conclusions

This projects was performed to determine that the proposed airlock configuration is maneuverable. From a systems layout perspective, the animation and the full-sized mockup demonstrate that the "L" shape airlock is feasible. The 3.5 foot diameter of the airlock is adequate for an astronaut to maneuver in. The two step process for testing this mockup was essential. The animation maps out the maneuvers to be performed and demonstrates that no major geometric conflicts arise. The actual physical mockup shows that the size and general shape of the airlock is maneuverable. In conclusion, the proposed airlock design (i.e. the tubular "L" shape configuration) is feasible. It saves space and money without compromising the astronaut's ability to complete their mission.

7.0 OPERATIONS MODEL

7.1 Introduction

The operations model for the SSTO is designed to give a realistic and factual picture of the facilities, procedures, and personnel needed to operate the SSTO. The operation of the SSTO is built around the singular goal of making inexpensive, timely and reliable access to space a reality. This motivating force drove the maintenance, launch, and landing portions of the operations model to their final form. Safety, being a prime concern, is considered in every aspect of operation.

7.2 Maintenance

The maintenance model was designed with safety, operational effectiveness, and economic effectiveness as the overriding criteria.

Objective. The purpose of this model is to establish an initial maintenance program for the SSTO vehicle. The program was developed with the goal of a three day maintenance turn time.

Maintenance Program Content. The maintenance program is divided into three phases: post-flight vehicle safing, scheduled maintenance, and pre-flight servicing. Each phase is independent and accomplishment times cannot overlap. Maintenance operations for the SSTO have been designed to facilitate easy integration by commercial operations.

Method of Development. The maintenance program was developed by examining established procedures and determining their applicability to the SSTO vehicle. Each phase of the maintenance program implements knowledge gained by NASA through the Space Shuttle program and by commercial airlines though mandatory maintenance programs. Both sources must be integrated due to the fact that NASA has the operational experience with space vehicles whereas commercial airlines have developed efficient, cost-effective maintenance programs.

The tasks involved in post-flight vehicle safing were developed based on current space program documents, primarily Space Transportation System Facilities and Operations. Shuttle procedures were examined and similar procedures were adapted to make them applicable to operations of the SSTO.

Tasks contained in the scheduled maintenance portion of the program were developed mainly through consultation of personnel in various fields. In-house vehicle specialists who were consulted include crew systems engineers, propulsion engineers, structures engineers, and thermal analysis engineers. Additionally, Bruce Ferche, currently an Avionics Project Engineer for Northwest Airlines and formerly a Maintenance Engineer for the Space Shuttle, was also contacted. Mr. Ferche was able to provide insight as to what procedures needed to be accomplished and explained the similarities and differences between government and commercial operations. Expertise from Shelley Hilden's and Jared Kirsling's co-op experiences at NASA and Northwest Airlines were also used. Commercial airline maintenance procedures were used wherever possible in order to minimize downtime and provide compatibility with existing commercial airlines' maintenance programs.

The pre-flight servicing tasks were again modeled after the current shuttle program document. The procedures were again adapted to the systems of the SSTO. This section was also modeled after commercial airline post-"check" procedures.

Time/Manpower Estimates. The driving force in developing this maintenance program was the requirement of a three day turn time. Past experience with new technology vehicles such as the Boeing 747-400 and Airbus Industrie A320 have demonstrated that time estimates for initial maintenance programs are usually greatly underestimated. For example, Northwest Airlines recently completed the first "D-Check" of a B747-400. The D-Check was anticipated to take approximately 22 days and actually took 34 days.

The estimates contained in the turnaround servicing portion of the operations model reflect a mature program. Initially, inspections may need to be accomplished after every flight. This is a result of using new technologies that do not have proven operational performance records. As the program grows, reliability databases will be developed for all components. Based on the information obtained from these databases, intervals for inspections and scheduled removals can be developed. By managing the inspections and scheduled maintenance in a segmented check, it will be possible to eliminate unnecessary inspections and maintenance.

7.3 Payload Integration Procedures

Purpose. The primary purpose of the SSTO is to insert and retrieve payloads from a Low Earth Orbit (LEO) for commercial uses. Payload integration is concerned with removal and installation of payload modules. This is done in such a way to provide quick and effective integration with minimum labor and time required. Two separate modules are used with the SSTO. The first has a 4.57 m (15 foot) diameter and is 9.14 m (30 foot) long. The second module is 4.57 m (15 foot) in diameter and 4.57 m (15 foot) long.

Pre-Flight Planning. Elements of pre-flight planning include shipping of the payload module to the customer, the type of payload, and the type of mission.

The payload is loaded and sealed in the payload module by the customer. To facilitate this, the payload module is shipped to the customer prior to launch. A representative of the commercial operator will be present during loading of the payload to certify it and insure proper installation. The customer certification is necessary to reduce the liability of the SSTO operator should any difficulties arise with the deployment as a result of improper module loading.

Biological payloads must be handled with a different set of guidelines. Biological experiments or other payloads which cannot be loaded into a module days before flight will be integrated immediately prior to flight.

Mission type must be considered for optimization of flights. It is ideal to launch and retrieve a payloads in the same mission. This was a stated design goal given by Northwest Airlines. Similarly, this is a priority in the DC-Y program. For this reason, payloads should compliment each other. This means that size and weight of the payloads must be considered. This is due to the limited adaptability of the module in space.

Installation Operations. The payload module for non-biological payloads should arrive at least one day prior to the scheduled launch date. This should allow sufficient time to integrate the payload. The arrival of biological payload will be scheduled in conjunction with the customer.

After arrival, the payload will be stored as necessary. Integration is determined by maintenance. An estimate of 1.5 hours and 3 personnel are needed to complete integration.

Removal Operations. Removal is similar to the installation procedures. Biological payloads, when applicable, will be removed at a similar time to the crew. The non-biological payload will be removed in the hangar. A representative of the customer will be present to supervise remove from the vehicle. The payload will then be shipped to the customer. Any necessary maintenance will then be performed. Excluding maintenance, removal is estimated to take 1.5 hours and 3 personnel.

7.4 Launch

The launch procedures were designed to provide the quickest and most economical launch system for the SSTO. However, safety was a prime motivating factor in the launch model. Safety along with commercial considerations drove the research and development of the launch model

Operation Control Units. The operation control units for the launching of the SSTO were modeled after the System Operation Control Units of Northwest Airlines. This was done to make the launch procedure of the SSTO as compatible with a commercial airline as possible. However, some significant modifications were made.

An Operations group was added to the operational control units currently used by the airlines. This is due to the unique operating conditions of the SSTO. The operations group will act much like the control tower at a commercial airport. However, they will not be government employees and will also have the responsibility of preparing the vehicle on the launch pad for launch. The Operations group will act as both launch and landing control. This is modeled after both NASA mission control and commercial carriers.

Pre-Launch Planning. The pre-launch planning is designed with a commercial carrier in mind. It is designed to be an addition to an already existing support and command structure. Northwest Airlines was again the major influence in this area. However, the planning operations are easily adaptable to any commercial carrier.

The most significant difference in pre-launch planning for the SSTO and pre-flight planning for an air craft is the added coordination needed with different federal agencies. Since the craft is launch like a ballistic missile, U.S. space command should be notified of each launch. This is to avoid any possible confusion concerning an ICBM (Intercontinental Ballistic Missile) launch. In addition, more FAA/ATC coordination is needed to gain the airspace needed to launch the SSTO. Finally, the U.S. is a signatory member of the United Nation Convention on registration of space vehicles.

As such, any company launching a payload into orbit must notify the UN of this.

An added difference between the SSTO and commercial air craft's pre-flight planning the need for the SSTO to fully plan all abort scenarios. The craft must have the ability to land at a different space port in the event of an emergency. This means that the other spaceports must be prepared and be able to communicate with the SSTO and dispatch.

Pre-Launch Procedures. The pre-launch procedures, like the pre-launch planning, are modeled after the commercial airline industry. The craft must be certified safe by the maintenance chief and approved by dispatch. These are the safety procedures used by current commercial carriers.

Launch Operations. Launch operations were developed with a quick and reliable launch in mind. A combination of airline and space shuttle experience makes the launch operations as timely and cost effective as possible. The space shuttle was the driving force behind most of the safety and the fueling procedures. The airlines on the other hand drove the ground handling and the command and control side of the operations. By combining both private industry and government experience, the launch operations were streamlined and refined to make them both practical and economical.

Ascent. The main concern during the ascent portion of the launch operations is related to abort scenarios. The SSTO must have reliable communication with the ground in the event of an emergency, and it must be clearly known who has operational control of the vehicle. Both dispatch and Operations control will be able to communicate with the SSTO during ascent; however, Operations control will have operational control until the craft is in orbit. This is done because operations control will have the personal and expertise to make decisions regarding any abort scenario.

7.5 Landing

Landing operations for the SSTO were designed with safety and efficiency as a priority.

Control groups. The control groups consist of dispatch, operations control, and Air Traffic Control (ATC). Dispatch is provided by the commercial operator and can be easily incorporated into the system that they are currently running. Operations control operates like a control tower on a commercial airstrip. Dispatch and operations control information was supplied by Northwest Airlines. ATC is only concerned with the SSTO when it is flying in commercial airspace, which is from 0 to 60,000 feet. ATC will be contacted whenever the SSTO will be entering this area. The information on the requirements from ATC was taken from talking directly to the FAA.

Aborting to a secondary landing site. Aborting to a secondary landing site will only be done when it is not possible to abort to a spaceport. The problem of getting the SSTO back to a spaceport is a difficult one. Through discussions with propulsion engineers, the plan for returning the SSTO to a spaceport from a secondary landing site was formulated. The propulsion engineers foresaw no difficulties in using the engines for the return flight to a primary spaceport. The altitude of 80,000 feet for the flight was chosen because it is above the operational limits of all commercial aircraft.

Aborting to a spaceport. Aborting to a spaceport will be similar to a nominal landing. The fire and emergency crews will prepared for any emergency that may arise.

Vehicles needed after SSTO roll out. The vehicles that are being used for the landing procedures are modeled after current NASA procedures. These procedures were taken from a NASA document on facilities and operations[2]. The contamination vehicle will have two people in Self Contained Atmospheric Protective Ensemble (SCAPE) suits. One person will drive and the other will take readings. They will stay in the SCAPE suits in case contamination occurs after vehicle safing. This will allow the vehicle to remain at the site all the time. The fan vehicle will have to displace a minimum of 5660 cubic meters of air. This information was again taken from a report on NASA facilities and operations.[2]

The crew egress system consists of a ladder truck that will come up and allow the crew to leave the vehicle. There is a pressurized compartment at the top of the ladder so that any potentially harmful contaminants will not enter the SSTO. In case of contamination, crew egress system personnel will be wearing SCAPE suits. There will be a crew transport vehicle at the edge of the safety perimeter.

The tug/tow vehicle is used to tow the SSTO to the maintenance bay hanger. The commercial operator that operates the SSTO will be able to use a commercially available tug/tow vehicle. This is because the SSTO is lighter at landing than widebody commercial airliners.

FAA regulations. After consulting the FAA about their regulations and examining the FAR's, it was discovered that the SSTO does not fall under any FAA regulations. This puts the operator of the SSTO in a unique position for writing the regulations governing the SSTO. The exception to this is for the noise restrictions imposed on the SSTO. The noise restrictions are laid out in FAR parts 91.817 and 91.821, and deal with civil aircraft noise. Specifically, these regulations deal with sonic booms and civil supersonic airplane noise limits. The noise restrictions need to be addressed because it was discovered that the shock wave noise that is heard on the ground is dependent on the shape of the body of the aircraft[4]. If it can be shown that the shock wave

makes a very minimum amount of noise, the FAA may be persuaded to allow supersonic flight over the United States.

Landing Schedule. Research from the ascent reentry group and a NASA document on facilities and operations[2] allowed a good estimation of the time it would take to go from a deorbit burn to the vehicle entering the maintenance bay hangar. Ascent reentry engineers recommended a time of 40 to 45 minutes for the vehicle to go from deorbit burn to roll out.

Next, a standoff radius must be established. This is the minimum distance at which all vehicles must be kept until the areas safety has been established. The radius of 700 feet was taken directly from a NASA document[2]. It was decided to maintain a 700 to 1000 foot radius from the vehicle.

7.6 Conclusion

The operations model for the SSTO provides a realistic plan for the operation of a commercially viable space vehicle. This was accomplished by incorporating NASA experience with space operations and commercial air carriers experience. Safety, economic viability, and reliability were the prime motivating factors in development of the operations model.

8.0 Supersonic Rocket Nozzle Evaluation Group (SRNEG) Final Model Report

8.1 Introduction

The SSTO is designed with extendible nozzle skirts to increase the performance of the vehicle. Though it means a weight penalty, and added mechanical complexity, the ISP of the engines should increase significantly warranting these penalties. The utility of these skirts, as well as knowledge of the flight envelope/flight performance was also desired.

Soon after beginning, it was decided that scale models of the real nozzles used should be tested. This was instead of generic nozzles for qualitative testing. However, research eventually proved this virtually impossible. The geometry of the nozzles is uniquely determined by the gas used, and the temperature of the gas (i.e.. γ, the ratio of specific heats). Neither of these could be duplicated. These γ effects, and the extreme pressures required forced expectations to be lower. The experiment will use a 3 and a 30 area ratio nozzle. These were selected to give a more manageable difference in the thrusts of the engines.

8.2 Proposal

Theory. According to compressible flow theory, a nozzle with a single fixed exit area will only perform optimally at one pressure ratio (Ref. 1 and 4). If the reactants of an engine are fixed, then it follows that there is only one pressure, and hence altitude, that a nozzle will perform best at. If the pressure is too high at the exit, it will be underexpanded. If the pressure is to low at the exit it will be overexpanded. In the best underexpanded case, there is still internal energy in the flow that has not been converted to kinetic energy. In the worst case, standing shocks develop in the nozzle which convert the kinetic energy back into internal energy. The overexpanded case experiences pressure drag that can be on the order of the engine thrust. A nozzle that was pressure adaptive would be the ideal configuration, but this is not currently feasible. The next choice then is to use multiple nozzles with different area ratios. The different area ratios are made possible by having extendible skirts. Our design uses two different area ratios to increase the performance while keeping the mechanical complexity of many nozzle skirts down.

Experiment. To demonstrate the advantage of the extendible skirts and to obtain "flight" data, a model needed to be built. The defining characteristic of the model was that it would yield the maximum information possible about the engine performance at different altitudes (pressure ratios). From this basic statement, it was decided that a test bed should be created with the lowest friction (or other nuisance forces) possible. From this test bed, different configurations would be investigated, with the two main variables being the area ratio and the pressure ratio. The problem of actuating the nozzle extension is not a concern yet. If these experiments were to give positive results, the mechanics of the extension would be the next avenue of investigation.

8.3 Work To Date

Trade Analysis. Once our objectives were defined, the best way to accomplish them needed to be found. The force measurement was the most important factor to be weighed. Many different configurations were considered. A previous experiment to measure the thrust produced by a single nozzle used a wheeled sled that deflected a spring with a known elasticity. The same sled configuration pushing on a post fitted with a strain gauge was also considered. These allowed the force to be measured while keeping the friction to a minimum, but did not address the problem of forces related to a high pressure line needed to power the model. Thoughts were given to placing the line so as to reduce the effects, but this proved to be difficult, and there would always be some element of guessing associated with the force imparted by the line. The logical conclusion was to disconnect the line from the model. The use of a dual diaphragm was suggested to pressurize the entire area around the model, but finding diaphragms strong enough would have been difficult. The configuration settled on was that of

an "air bearing" (Fig. 1) suggested by the shop foreman of the University of Minnesota's Physics Machine Shop.

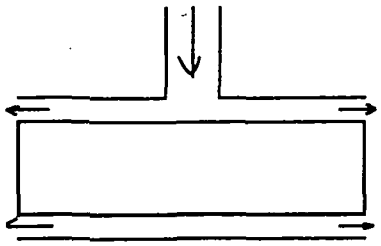

igure 8.1 Air Bearing

The concept is that air flowing in through the line pressurizes the area around the bearing which is not connected to the sheath. Since they are not connected, air will escape between them. If the gap between them is kept small enough, the losses will be small, and a virtually frictionless environment is created.

This seemed like a very good concept, so it was analyzed. Unfortunately, the theory went against intuition and seemed to say that it would not work. It was later realized that an unstated assumption in the analysis was that the mass flow through an angular wedge was constant. This is not the case. The proof that it will work can be seen by imagining the limiting case where the bearing has displaced all the way to one side and is about to touch the wall. There will be virtually no mass flow here, so the velocity will be close to zero, and the pressure close to static. On the opposite side, there will be mass flow, and hence the velocity will be non zero. This decreases the pressure below static thereby drawing the bearing back to the center. This was shown to be the case when a working system, very much like the one proposed, was witnessed in action. There was no noticeable friction, and it was definitely floating in the sheath.

Once the method of measuring the force produced was decided on, the nozzle sections needed to be dealt with. The cross section of the nozzles is a somewhat complicated collection of conic sections that would be a challenge to machine. The bearing, with its high tolerances, would also be a challenge. To machine them together for each different area ratio would be a waste of resources. Therefore, it was decided that a single bearing would be created, and multiple separate nozzles.

8.4 Generations of Designs

The bearing is the most critical piece of this design, therefore, it will be concentrated on here.

First Generation. Figure 8.2 shows the first design of the bearing to be completed. The overall length was about 10cm. The removable nozzles were to be fitted into the right side.

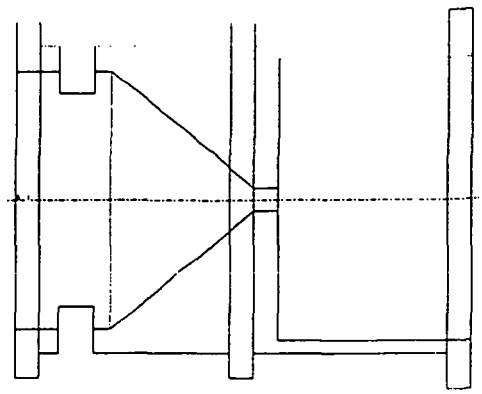

Figure 8.2 First Design

Second Generation. This design (Fig. 8.3) arose because it was found that the nozzles were too large to fit into the bearing. It also made the machining less complicated. This is due to the use of pre honed smooth bushings that this smoothed out design would float inside of.

Final generation. Figure 8.4 displays the final design (Figure 8.5 shows dimensions). They feature a flange on the left which the nozzle and convergent section connect to. This flange, as well as a snap ring put into the right groove are used to restrain the model. Holes are drilled into the center groove to allow the air to enter.

Figure 8.6 shows an assembled drawing of all of the parts. It depicts the thirty area ratio nozzle, the bushings, and the bearing. The bearing also has a plug in the left hand side which was omitted by the shop in favor of boring the hole from the right and not going all the way through.

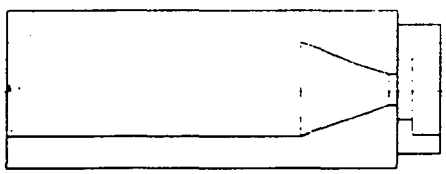

Figure 8.3 Scond Design

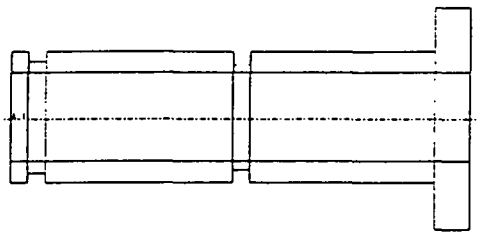

Figure 8.4 Final Design

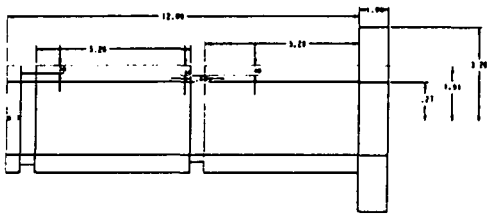

Figure 8.5 Final Design with dimensions

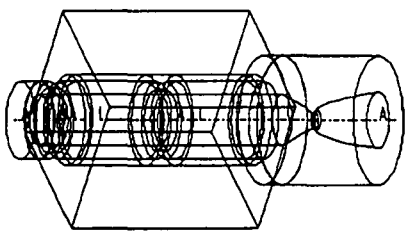

Figure 8.6 Assembled drawing

Machining. Our designs were machined by the AEM shop. The major difference between the final design and the one manufactured is that the bushings are not present. This modification came from shop. After talking to them we decided to try the air bearing without the bushings and just having the sheath reamed to 1/1000in inner diameter greater than the outer diameter of the bearing. This came from the concern that the bushings may come loose during operations.

Figures 8.7 and 8.8 show the 30 and 3 area ratio nozzles as machined by the shop.

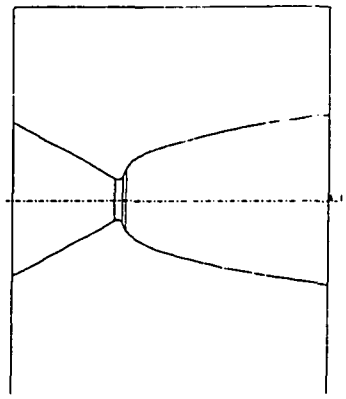

Figure 8.7 30 Area ratio nozzle

Preliminary Testing. The designs were tested by venting the 3 area ratio nozzle to atmosphere. Through demonstrations at IT week, we were convinced that the assembly was safe, and that the air bearing was working.

(Fig 8.8). With this nozzle we will be able to test the air

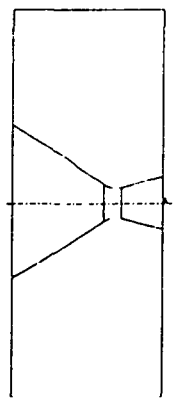

Figure 8.8 3 Area ratio nozzle

8.5 Fluidyne Testing

In order to achieve the necessary pressure ratios to test the nozzles, the Fluidyne Test Group, a subdivision of ASE, was contacted. We were able to use their vacuum sphere to lower the exit pressure of the nozzles. The major tests that were conducted at Fluidyne are:

Direct Thrust Measurements. This was accomplished by having the front of the bearing push on an

C2

aluminum bar fitted with strain gauges. The output of the strain gauges was recorded by a computer. It was then later transformed into thrust.

The main principle in designing the load cell for the air bearing was equation 1. A safety factor of 2.25 was added to the thickness of the beam to insure that the beam would remain in the linear region.

$$\text{Equ 1} \qquad \sigma = \frac{My}{I}$$

With a thickness of .75" and a height of .5" we had a beam that would be able to measure between 0 to 120 lbs with a 3% accuracy. Figure 9 shows the complete test assembly.

Pressure Ratio Measurements. This was done by measuring static pressure in the chamber. The pressure the nozzle exited to was also recorded. From these two pieces of data we are able to obtain the pressure ratio and then be able to find theoretical thrust measurements.

Thermocouple measurements. A thermocouple was installed to measure the temperature in the chamber. There was some concern with the changing temperature affecting the speed of sound greatly enough to skew the data.

Shadowgraph System. This system allowed us to take still photos of the exiting flow of the nozzle. This allowed us to see the form of the flow. It also allows us to determine the MACH number of the exiting flow.

8.6 Fluidyne setup

Channel 8. Fluidyne gave us permission to run our tests on Channel 8 at their facility in Plymouth, MN. The assembled parts were mounted on a one foot square piece of quarter inch plate steel along with the strain apparatus. These were then attached to a frame made at Fluidyne with three screws.

The pressure was measured by a "psi machine." It was internally calibrated and had up to 150 ports to measure pressure. One was dedicated to measuring the chamber pressure, and ten in the channel were averaged to give the exit pressure. These measurements, along with the thermocouple data and the strain data were recorded by on sight computers.

Three tanks of Nitrogen were used for three different tests. At the beginning of each test, channel 8 was scaled, and evacuated by connecting it to a vacuum sphere. The pressure in the sphere stayed at around 700Pa. This means that the pressure ratio dropped as the tanks emptied.

The first run used the 30 area ratio nozzle and was run only for a few seconds to test the integrity of the model. The second run was basically the same. The 3 area ratio nozzle was used, and an attempt at filming it was made.

The third run used the 3 area ratio nozzle again. Shadowgraphs were taken at the first two of the fifteen data points. The final run was with the 30 area ratio nozzle. Shadowgraphs were taken on the first two data points again. Seventeen points were taken.

Pressure ratios ranged from 6800 to 230 over the entirety of the tests. The temperature dropped as low as -27C.

Results The Graph 8.1 shows the major result of this project. The most useful result gained from this project was the fact that the over a large range of pressure ratios the thrust of the 30 AR nozzle is significantly greater than the thrust of the 3 AR nozzle. The greatest increase in the thrust can be seen at about 2200 pressure ratio. The initial rise in the percent increase comes from the fact that the 30 AR is on the front side of the efficiency curve while the 3 AR is on the back side of its efficiency curve. The point when the thrust of the 30 AR equals the 3 AR is when you would want to deploy the second nozzle skirt to maintain the greatest efficiency.

The drop in percent thrust after 2200 pressure ratio probably comes from the fact that the 3 AR and the 30 AR nozzle are so over driven in pressure ratio that the difference in thrust levels off . Currently this is our only thought as to why the percent increase decreases.

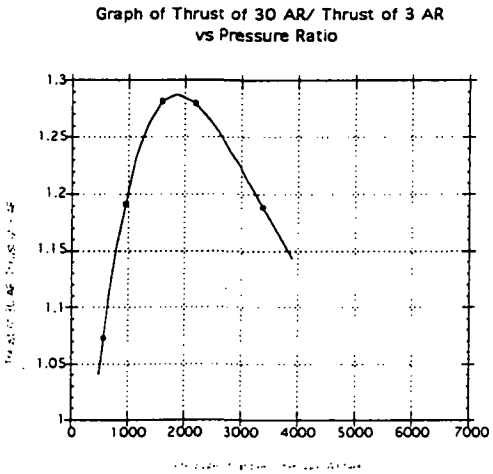

Graph 8.1 Major Nozzle Results

Conclusion

We believe that the experiment showed the validity of using the extendible skirt. The difference in area ratios of the SSTO vehicle are not as great as the test models so the increase in thrust will not be as great but there should be an advantage to using the multiple nozzles.

This experiment validates our theory and does show that further testing when the actual engine is built should be

done. We think that future testing should involve the real engine as to find the best area ratios for the nozzles to achieve the best performance over the flight regime.

In conclusion the goals of this experiment were accomplished. The further testing required of this project with the actual engine can proceed in an intelligent direction to gain more practical data for the SSTO project. The multiple nozzles should be worthwhile to study to assist in making the SSTO vehicle a more efficient vehicle, even though it requires more weight and complexity to accomplish.

9.0 EFFECT OF CONTACT RESISTANCE IN LAYERED INSULATION CONFIGURATION

9.1 Introduction

One area of concern to the thermal analysis discipline during the design of the SSTO vehicle was the insulation system for the cryogenic fuel tanks. While undergoing the design process it became evident that one of the key features in nearly all tank insulation systems was insulation consisting of many layers of thin materials. The reasoning behind this layering scheme appeared to be the additional thermal resistance gained by the addition of contact resistance between the many interfaces of materials. With this in mind, it was the goal of the thermal group to design and test an experiment to test the effects that different layering configurations has on the contact resistance and therefore on the total insulation capability of the system. Testing was done on an insulation system 0.953 cm thick, with over 40 layers of material. The results show that with the addition of one interface between two materials of rough and irregular surface texture, an increase of approximately 17 % in the total thermal resistance is obtained.

9.2 Experimental Procedure

In order to begin the testing, materials had to be chosen and a method needed to be created. The materials used for the insulation layers were kapton, mylar, felt, and Styrofoam. All of these materials consist of many layers. Kapton consisted of 20 layers totaling 0.3175 cm thick. Mylar was the same. Two layers of felt totaled 0.3175 cm thick and two layers of Styrofoam totaling 0.635 cm were used. These materials facilitated the necessary qualities similar or the same as the insulation materials to be used on the SSTO vehicle. Two experimental configurations were created and named 1-D and 2-D experiments. The 1-D experiment refers to a linear heat flux and the 2-D refers to radial heat flux.

One dimensional configuration. In the 1-D experiment, an aluminum pan 33 cm by 22.9 cm is placed on top of the insulation layers to be tested and filled with ice water. Heat flux travels through the layers of Styrofoam, kapton, felt, and mylar. An aluminum base plate is placed beneath the test layers to maintain a constant temperature heat sink which is facilitated by forcing air underneath the plate with an electric fan. The entire structure is supported by two, 14 cm tall by 5 cm wide, blocks of Styrofoam. The layering scheme for the 1-D experiment is depicted in Fig.9.1.

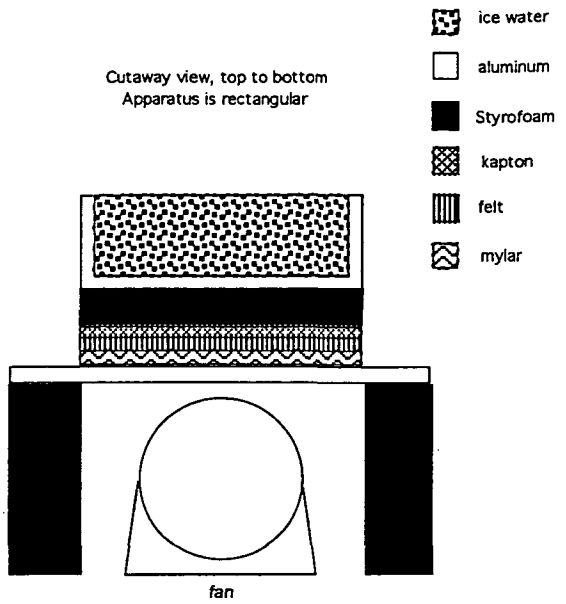

Fig.9.1: Schematic of rectangular ice filled pan experiment in the base configuration

T type (copper and constantine) thermocouples measure the voltage difference across the layering scheme. Thermocouples were placed between the aluminum pan and Styrofoam, between the Styrofoam and the insulation layers, between the insulation layers and the aluminum base plate, and in the free flowing air below the aluminum base plate. Fig. 9.2 gives a schematic of how each experiment was set up.

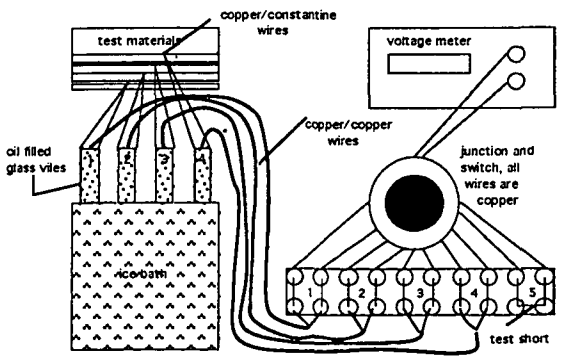

Fig.9.2: Schematic of thermocouple connections

The voltage difference measured refers to a temperature unique to the T type thermocouple. An ice bath reference junction was used for all thermocouples. The thermocouple reference junctions were placed in separate oil filled glass vials before being placed in the ice bath to avoid any contact between the thermocouples and to allow them to be surrounded completely by a

consistent temperature of 0° C. The thermocouples were all connected to a switchable junction and then one connection to a voltage meter. Accuracy of this system was good to 0.15 ° C.

Two other experiments were also completed involving the same materials which were layered differently. The second test configuration was layered mylar (10 layers), felt (1 layer), mylar (10 layers), kapton (10 layers), felt (1 layer), kapton (10 layers), and Styrofoam (from bottom up). The third test configuration was layered mylar/kapton (6 alternating layers), felt (1 layer), mylar/kapton (28 alternating layers), felt (1 layer), mylar/kapton (6 alternating layers), and Styrofoam (from bottom up). These experiments were conducted to record any change in thermal resistance due to altering the layering scheme.

A 1-D experiment was also necessary to test the conductivity of the Styrofoam being used. In order to do this, a 5.1 cm thick piece of acrylic (Plexiglas) of known thermal properties, including thermal resistance, was needed. The only layers were the acrylic on top of the Styrofoam, and the rest of the experiment was done the same as the others. The thermocouples were placed between each of the layers and at the free flowing air temperature below the aluminum base plate.

Each of the experiments were timed and conducted until they reached steady state, where the temperature at each thermocouple was constant. Voltage readings were taken at regular time intervals in order to record the transient temperatures the experimental systems experience before steady state is achieved.

Two dimensional configuration. A cryogenic experiment was also desired to test the materials in a similar environment to that which the actual materials will experience. For the 2-D experiment, an aluminum cylinder and liquid nitrogen were used. Fig. 9.3 depicts the set up. The insulation materials used were the same as the materials used in the one dimensional set up. Thermocouples were placed in the same manner and were set up the same as the one dimensional experiment. The aluminum base plate was not used in this experiment. Instead, a steel flexible foil was used. Each of the materials were wrapped tightly and sealed at one end using a spray adhesive. The adhesive was applied in a manner that would not effect the results of the experiment. The steel foil was wrapped on the outside of the layering scheme and acted as the heat sink, with an electric fan blowing on it as well to maintain the largest temperature difference possible. The apparatus sat on a Styrofoam block and was also capped with a vented Styrofoam cover.

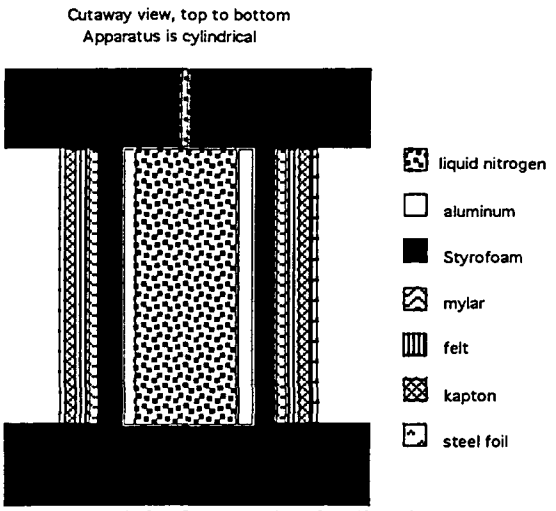

Fig. 9.3: Schematic of cylindrical test configuration with liquid nitrogen

Liquid nitrogen was poured into the aluminum cylinder and was maintained full for the duration of the experiment. The experiment was conducted until steady state was reached. The liquid nitrogen kept a constant temperature of -195° C. A 205° C temperature difference was noted on the outside layer for a final temperature of 10.0° C.

9.3 Data Reduction

The first step in analyzing the test experiment was to determine if in fact it was possible to measure one-dimensional heat flow with the designed experiment. To do this, the experiment was modeled using I-DEAS finite element modeler (This was only done for the rectangular shaped pan set-up and not for the cylindrical experiment. This was due to the radial symmetric properties of the cylinder forcing radial heat flow). This computer program was used to analyze the steady state heat flux throughout the entire physical structure. A two-dimensional and a three-dimensional model that was completely to scale was entered into I-DEAS. All of the materials used in the experiment were also represented in the I-DEAS model with the proper thermal conductivity of each. Fig. 9.4 shows a three-dimensional representation of the model used for finite element analysis.

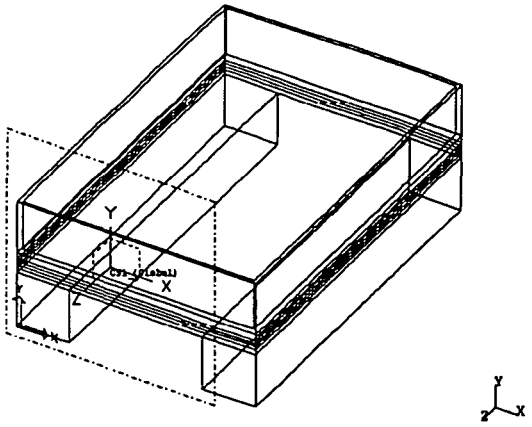

Fig.4: Three-dimensional view of model used for finite element analysis

The physical representation was divided up into elements with nodes separated by approximately 1 cm in actual distance. Fig. 4.5 shows the two-dimensional computer representation complete with mesh.

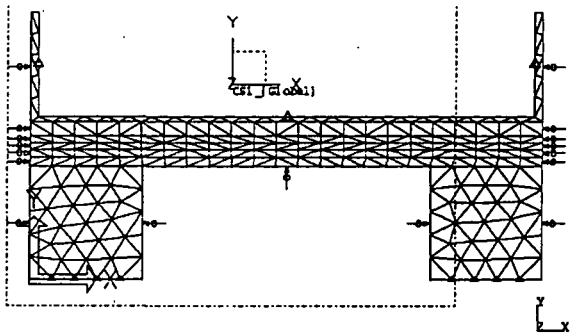

Fig.4.5: Two-dimensional test model complete with element mesh and boundary conditions

In order to obtain a solution, it was necessary to make some assumptions about the boundary conditions of the model. These included an interior pan temperature of 0° C, a temperature on the bottom of the Styrofoam support blocks of 20° C, and a constant convection coefficient of 15 W/mK. These boundary conditions are noted in Fig.4.5 by triangles located on the surface where constant temperature boundaries are observed and by arrows pointing towards the surfaces where convection boundaries are located.

Experimentally, the only data reduction that was necessary was the conversion of the voltage readouts to the corresponding temperature was acquired with the thermocouples used. This chart was used to plot a graph of temperature vs. voltage. For the rectangular pan experiments, since such a small range of temperatures were measured, the voltage temperature relationship of the thermocouples was exactly linear. However, for the cylinder experiment which measured temperatures ranging from -195° C to 25° C, it was necessary to plot a wide range of values for the conversion from voltage to temperature and then derive a curve fit to the points. This graph is shown in Fig.4.6.

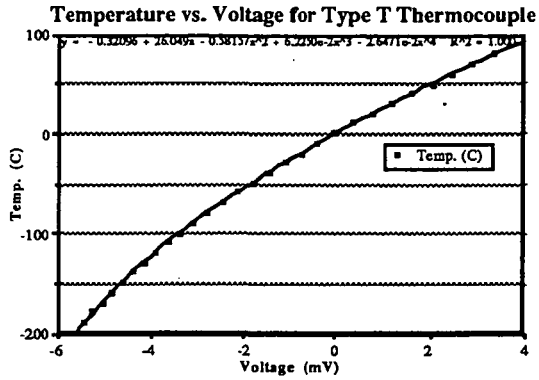

Fig.4.6: Graph of temperature vs. voltage output for T-type thermocouple

The resulting equation was then used to accurately determine the temperatures throughout the experiment.

All of the experiments that were conducted were based on basically the same theoretical background. A configuration was set up in which there was a region of cold constant temperature, a reference material of known thermal conductivity, a test material (or configuration of multiple layers), and an external ambient condition.

Since the experiment was designed such that temperatures are measured at key locations in the configuration without direct influence of outside conditions, it is possible to calculate the thermal resistance that is produced by the test materials. It is assumed that through the test material the only relevant parameters are the conduction through the material and, in the case of the multiple layered insulation, resistance due to the contact between the materials. The conduction in the system can be analyzed as a circuit where the thermal conductivities and areas combine according to the specific geometry and create a resistance. The temperature gradient across the test section provides the voltage drop, and the current is analogous to the heat in or out of the system (in this case heat would be flowing in). Fig. 4.7 represents a

schematic of the circuit used to find the heat transfer through the rectangular pan test model which consists of a plane wall through the test section. Equations 7.1 and 7.2

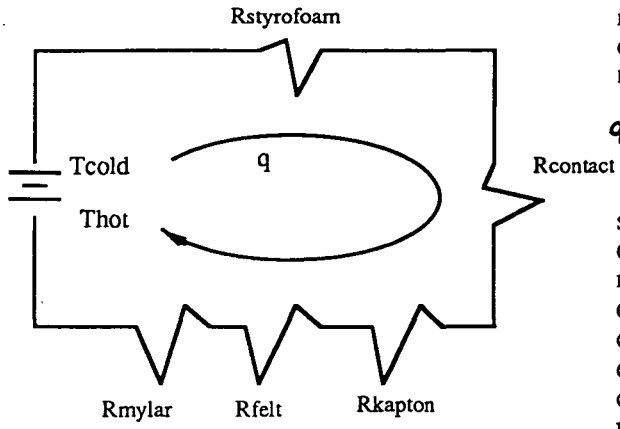

Fig. 7.7 Thermal Circuit

represent the resistances of the geometries present in both test set-ups. Equation 7.1 represents the resistance for a plane wall

$$R_{t,cond,planewall} = \frac{L}{k} \qquad (7.1)$$

$$R_{t,cond,cylinder} = \frac{\ln\left(\frac{r_2}{r_1}\right)}{2\pi Lk} \qquad (7.2)$$

and Equation 7.2 represents that for a cylinder. In the equations, k represents the thermal conductivity through the material, r_1 represents the inner radius of the insulation, r_2 is the outer radius, and L refers to the thickness of the material over which the resistance is being measured.

To obtain the heat flux, q, through the configuration, the temperature was evaluated before and after a reference material of known thermal conductivity and thickness (and therefore known thermal resistance). Equation 7.3 describes this in mathematical terms for the general steady state case

$$q = \frac{(T_2 - T_1)}{R_{total}} \qquad (7.3)$$

where T_1 and T_2 are the temperatures before and after the material examined respectively, and R_{total} is the thermal resistance of the material between the two temperatures measured.

Since all tests were allowed to reach a steady state condition the heat flux is assumed to be constant through the test section. With this in mind it is then possible to evaluate the thermal resistance provided by the test material by evaluating the temperature on both sides of the test material and then applying Equation 7.3.

7.4 Results and Discussion

The modeling of the experiment in I-DEAS shows that there is indeed a large area of one-dimensional heat flow in the center region of the rectangular pan. The I-DEAS output shows that over nearly the entire bottom of the pan, the constant temperature regions are parallel with the edge of the pan. The only regions that have curvature to constant temperature zones are small portions near the edge of the pan and inside the support blocks of Styrofoam. Since heat flux travels perpendicular to constant temperature zones, this confirms that it is possible to measure one dimensional heat flux with this configuration. Furthermore, since the region of one-dimensional heat flux is very large, the possibility of collecting bad data due to errors in direct alignment of the thermocouples is minimized.

The first test completed was the experiment to determine the conductivity of the Styrofoam to be used as a reference material in all of the insulation layer tests. For this experiment, the reference material of Plexiglas had a thermal conductivity of 0.152 +/- 0.0017 W/mK. This value along with the final temperatures of 1.7° C at the pan edge, 16.2° C between the Plexiglas and the Styrofoam, and 20.8° C at the Styrofoam edge, resulted in a conductivity for Styrofoam of 0.0589 +/- 0.00587 W/mK. The uncertainty in this calculation is within 9.97 % of the calculated value. One point to note is that the conductivity obtained for Styrofoam was for two layers each with a thickness of 0.3175 cm. This was done for the reason that an identical two layer system was used for all test configurations as a reference material.

Fig. 7.9 shows a graph of the temperature variation through the experimental set-up for the base configuration vs. time.

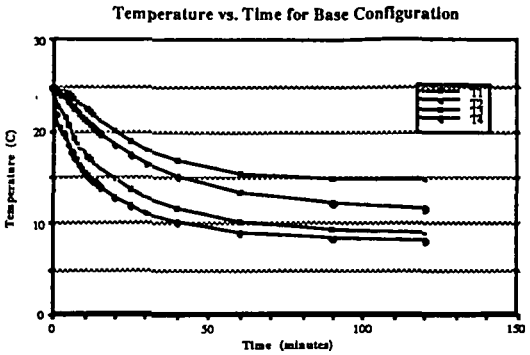

Fig.9.9: Graph of temperature variation vs. time for base configuration

The data given represents the temperature from the outside of the insulation layers (top line of graph) through to the temperature between the insulation layers and the Styrofoam reference material (bottom line of graph). Using the temperature data given, along with a temperature of the pan of 0.0 +/- 0.15° C, the thermal resistance of the insulation layers was obtained. The thermal resistances of the three rectangular pan experiments along with the results of the cylindrical configuration is shown in Fig. 9.10.

Fig. 9.10: Chart of Thermal resistances for all test configurations

Test	Resistance (m^2K/W)	Error (+/-)	Error (%)
base	.0872	.00298	3.41
2	.0728	.002	2.75
3	.0716	.00162	2.27
cylindrical	.1785	.01782	9.98
theoretical plane wall	.0871	.000669	.768
theoretical cylinder	.264	.0244	9.26

Here it is important to note that although the cylindrical configuration has a much higher resistance than the other tests, this value is relatively in accordance with the theoretical value. Theory predicts that the cylindrical test should have a resistance that is nearly 3 times larger than that for a plane wall. In the tests that were done the cylindrical configuration resulted in a 2.5 times increase in the resistance of the insulation layers. It is also important to note that the theoretical calculations are done using experimental conductivities that include the contact resistance present when the same material is layered to create a thickness of 0.3175 cm.

The results obtained from the experimental tests which are displayed in Fig.9.10, yield some rather interesting observations. The first observation is that the thermal resistance of the insulation materials actually declined when the configuration was altered from the base state. This fact tends to make us believe that there is something inherent in the base configuration which significantly adds to the thermal resistance. Since the resistances of configurations 2 and 3 are nearly the same, it seams that the contact resistance between two hard, smooth surfaces (such as the mylar and kapton) does not vary greatly. This seems to be true whether the junction is between two of the same materials or two dissimilar materials. The one point that is present in the base configuration but not in the other two is the junction between felt to felt. It appears that the contact resistance that is gained by the junction between two materials that are irregular in texture is very significant to the overall thermal resistance.

Another interesting point obtained in this experiment was that when experimentally derived thermal conductivities were used in the theoretical calculations, the plane wall results correlated rather well. On the other hand the cylindrical calculations differ by over 32 %. This may be a result of drastically differing thermal conductivities of the materials at cryogenic temperatures. However, this discrepancy does tend to make one think that further testing of insulation materials in various configurations is necessary to get a complete picture of the actual workings of the system.

9.5 Conclusion

Overall, the results obtained in the experimentation on contact resistance were very good. It was determined that contact resistance changes very little when creating junctions where at least one of the materials is a smooth surface. On the other hand, the results show that when a junction was created between two materials that are rough and irregular in texture, the resistance of the entire system was increased by approximately 17 %.

In the future it would be interesting to look into the effect of additional rough interface junctions on the thermal resistance of insulation systems. If an increase in resistance for each junction is comparable of that obtained for the one junction

tested, a significant aid in the design of thermal insulation systems may be obtained.

References

1. *Temperature Measurement Handbook*, Omega Engineering, Inc., Stamford, Connecticut

2. Frank P. Incropera, David P De Witt: *Introduction to Heat Transfer*, John Wiley and Sons, Inc: New York, 1985

3. Berg, Steve: University of Minnesota Dept. of Aerospace Engineering and Mechanics

4. Professor C. J. Scott: University of Minnesota Dept. of Mechanical Engineering

5. Professor E. Sparrow: University of Minnesota Dept. of Mechanical Engineering

6. Mike Richards: Graduate Student, University of Minnesota Dept. of Mechanical Engineering

APPENDIX A

Vehicle Specification Sheet

Purpose: To provide a reliable, timely, reusable, man-rated, and cost-effective single-stage-to-orbit transportation vehicle.

Mass Table

Component	Mass (kg)
Crew Systems/Avionics	7,000
Fuel Tanks	10,200
Fuel Tank Insulation	500
Orbital Maneuvering Fuel	15,000
Payload	9,100
Radiation Shielding	1,000
RD-701 Engines (3)	13,700
RL-10 OMS Engines (2) and RCS Jets (48)	2,000
Thermal Protection System	10,500
Structures:	
Frame	9,000
Landing System	3,500
Skin	2,000
Propellants:	
Liquid Hydrogen	55,400
Liquid Oxygen	496,700
RP-1	45,300
Empty Mass with Orbital Fuel	83,000
Takeoff Mass	680,400
Landing Mass (with payload)	68,000
Landing Mass (with no payload)	58,900

Fuel Tank Volumes

Fuel Tank(s)	Volumes (m^3)
Liquid Hydrogen (2)	427 each
Liquid Oxygen (1)	470
RP-1 (2)	30 each

Material Table

Component	Material(s)
External Heat Shielding	Carbon-Carbon, Inconel, Titanium
Frame	Carbon-Carbon Composite
Fuel Tanks	Carbon Epoxy, Kevlar
Inner Skin	Carbon Epoxy
Landing Gear	AerMet 100, Titanium Alloys
Radiation Shielding	Aluminum
Tank Insulation	Aluminum, Kapton, Rohacell

Engines

RD-701

Exit Diameter of Chamber	2.265 m
Fuel	RP-1, LH_2
I_{sp}-vacuum:	
Stage 1 (LO_2, LH_2, RP-1)	415 s
Stage 2 (LO_2, LH_2)	460 s
Length of Chamber	5.001 m
Mass	4444 kg
Nozzle Ratio Area	60/170
Number	6
Oxidizer	LO_2
Throttle	40-100%
Thrust-vacuum:	
Stage 1 (LO_2, LH_2, RP-1)	$4x10^6$ N
Stage 2 (LO_2, LH_2)	$1.59x10^6$ N

RL-10

Exit Diameter of Chamber	0.8 m
Fuel	LH_2
I_{sp}-vacuum	444 s
Length of Chamber	2 m
Mass	145 kg
Nozzle Ratio Area	61
Number	2
Oxidizer	LO_2
Throttle-vacuum	30-100%
Thrust	71,000 N

RCS

Exit Diameter of Chamber	0.2 m
Fuel	gaseous H_2
I_{sp}-vacuum	400 s
Length of Chamber	1 m
Mass	51 kg
Nozzle Ratio Area	61
Number	48
Oxidizer	gaseous O_2
Throttle	10-100%
Thrust-vacuum	4500 N

Static Properties

Flight Scenario	x-axis location (m)	y-axis location (m)	z-axis location (m)
With ascension fuel, orbital fuel, and payload	11.42	0.0	-0.10
With orbit fuel and payload and without ascension fuel	14.29	0.0	-0.55
With payload and without ascension or orbital fuel	16.72	0.0	-0.62
Without ascension fuel, orbital fuel, or payload	14.97	0.0	-0.72

Center of Mass Locations

Flight Scenario	I_{xx} (kgm^2)	I_{yy} (kgm^2)	I_{zz} (kgm^2)
With ascension fuel, orbital fuel, and payload	2.74×10^7	6.28×10^7	6.81×10^7
With orbit fuel and payload and without ascension fuel	3.41×10^6	2.70×10^7	2.95×10^7
With payload and without ascension or orbital fuel	1.81×10^6	2.34×10^7	2.43×10^7
Without ascension fuel, orbital fuel, or payload	1.76×10^6	2.28×10^7	2.37×10^7

Moment of Inertia Values

Cryogenic Boil-Off Rates

Hydrogen Tank	3.7143 kg/day (each)
Oxygen Tank	8.0557 kg/day

Ascent/Reentry Times

Vertical Launch to 463 km Orbit	44 min.
Reentry to Earth with Horizontal Landing	78.5 min.

Crew/Internal Systems

Crew Size	2
Navigation Systems:	Global Positioning System Global Navigation Satellite Systems
Supplied Internal Power	
Crew Modules	3-5 kW
Payload Bay	2-4 kW

Communication Systems

Flight Regime	Links Available	Purpose
Atmospheric	C-band	Radar Altimeter
	L-band	Tacan
	S-band (PM)	Tracking, 2-way Voice/Data
	UHF	Voice
Orbital	Ku-band	2-way Voice/Data via TDRS
	S-band (FM)	Data Transmission
	S-band (PM)	Tracking, 2-way Voice/Data
	UHF	EVA

On-Board Consumables

Water	57.88 kg/mission
Solid Food	7.40 kg/mission
Gases	54.88 kg/mission

ORIGINAL PAGE IS
OF POOR QUALITY

APPENDIX B

B

Total	Requirement	Category
72	Recycling Air/Water System	
88	Multi-Functional Avionics	
52	Internal Navigation	
116	GPS Capable	
84	Ground Station Tracking	
90	On-board workstations	
0		
285	Safety Factors in Design	Ascent / Reentry
38	Sound Reducing Design	Ascent / Reentry
81	Analytical Analysis	Ascent / Reentry
88	Physical Analysis	Ascent / Reentry
0	Drag Parachute for Landing	Ascent / Reentry
0		
80	Low Orbit	Orbital Mechanics
78	Low Accelerations	Orbital Mechanics
83	Low Impulses (Delta V's)	Orbital Mechanics
9	Multiple Orbits/Missions	Orbital Mechanics
231	Pre-Packaged Metal Tiles	Thermal Analysis
215	Carbon-Carbon Standoff Tiles	Thermal Analysis
71	Inside Insulation for LOX & LH2	Thermal Analysis
188	Outside Insulation for LOX & LH2	Thermal Analysis
270	Separate Cryogenic Tanks	Thermal Analysis
76	Integrated Tank System	Thermal Analysis
164	Ship Insulation	Thermal Analysis
128	Insulation Suits for People	Thermal Analysis
222	No wing configuration	System's Layout / Weight Distribution
164	Winged Configuration	System's Layout / Weight Distribution
235	Modular Cargo Bays	System's Layout / Weight Distribution
84	Modular Engine Components	System's Layout / Weight Distribution
86	Modular Avionics Components	System's Layout / Weight Distribution
84	Quick Access to Parts	System's Layout / Weight Distribution
4	Center of Gravity Stability	System's Layout / Weight Distribution
185	Fail-Safe Landing System	System's Layout / Weight Distribution
31	20,000lb Cargo Max	System's Layout / Weight Distribution
115	Standardized Docking System	System's Layout / Weight Distribution
150	Cargo Arm	System's Layout / Weight Distribution
0		
188	Lightweight Durable Material	Structures / Weights
42	Semi-Monocoque	Structures / Weights
177	Proven Materials	Structures / Weights
16	Lifting Body	Structures / Weights
159	Top Loading	Structures / Weights
240	Side Loading Canister	Structures / Weights
221	Side Loading Pre-Shape	Structures / Weights
212	Module Size/Weight Limit	Structures / Weights
230	Multiple Module Size	Structures / Weights
102	Acceleration Damping	Structures / Weights
118	Standardized Manufacturing	Structures / Weights
144	New Inspection Techniques	Structures / Weights
63	Easy Manufacture/Multi-Vendor	Structures / Weights

ORIGINAL PAGE IS
OF POOR QUALITY

B

APPENDIX C

Fig.1. NASP Derivation.

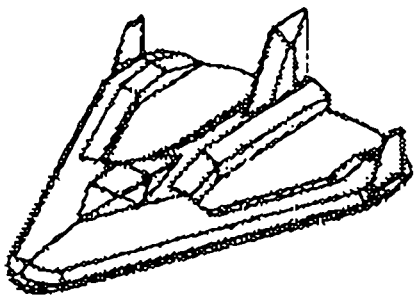

Fig.2. Skunk-works Derivation.

Fig.3. Modified Skunk-works.

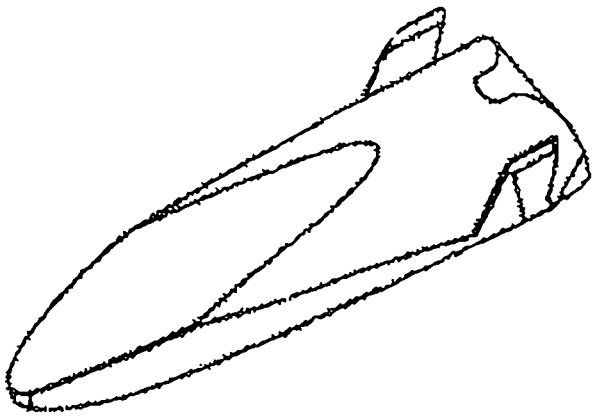

Fig.4. Lifting Body Design

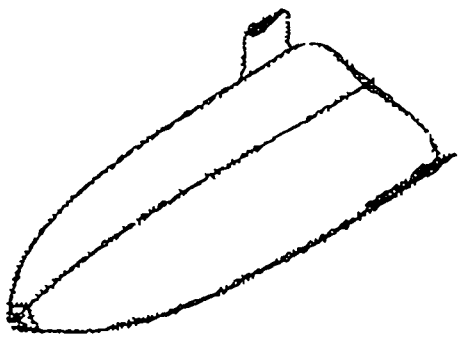

Fig.5. Smoothed Lifting Body Design.

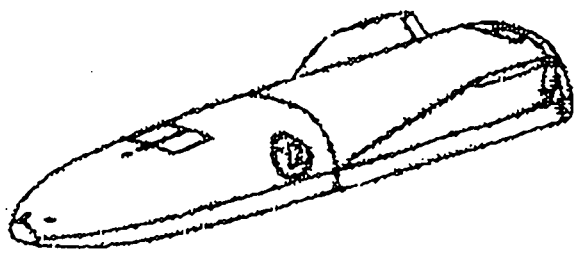

Fig.6. The Final Design.

APPENDIX D Spaceport Facilities

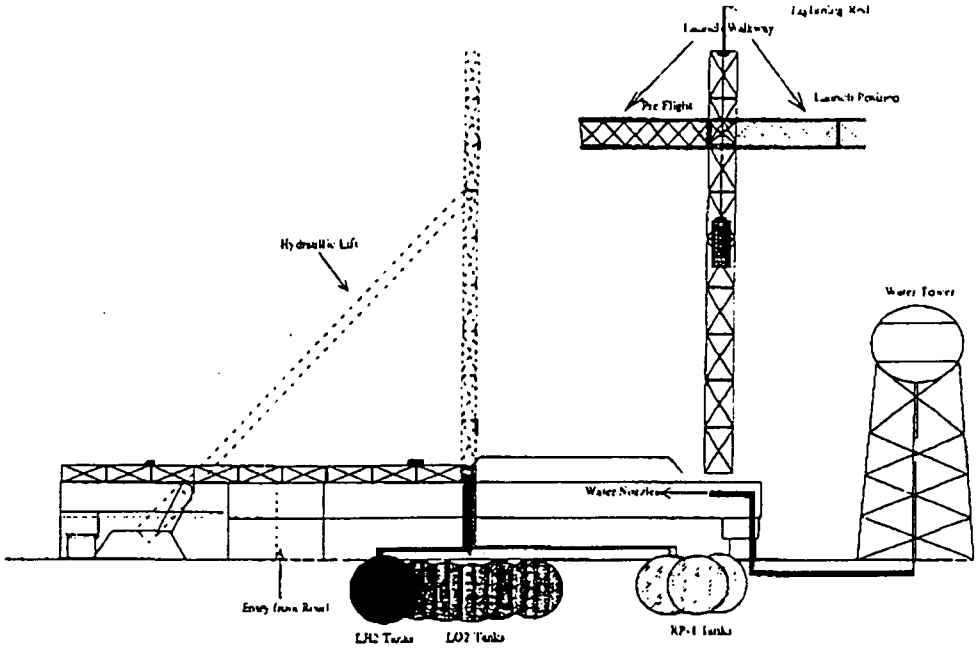

Space Port
Landing Pad (Side View)

Figure 1 Launch Pad Side View

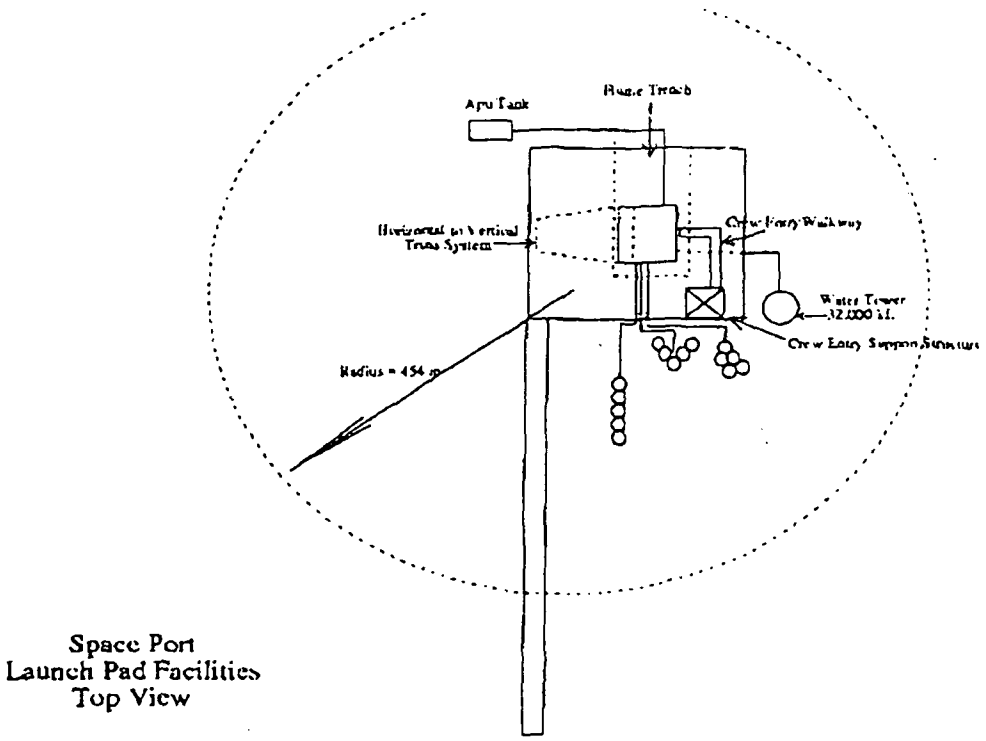

Figure 2 Launch Pad Top View

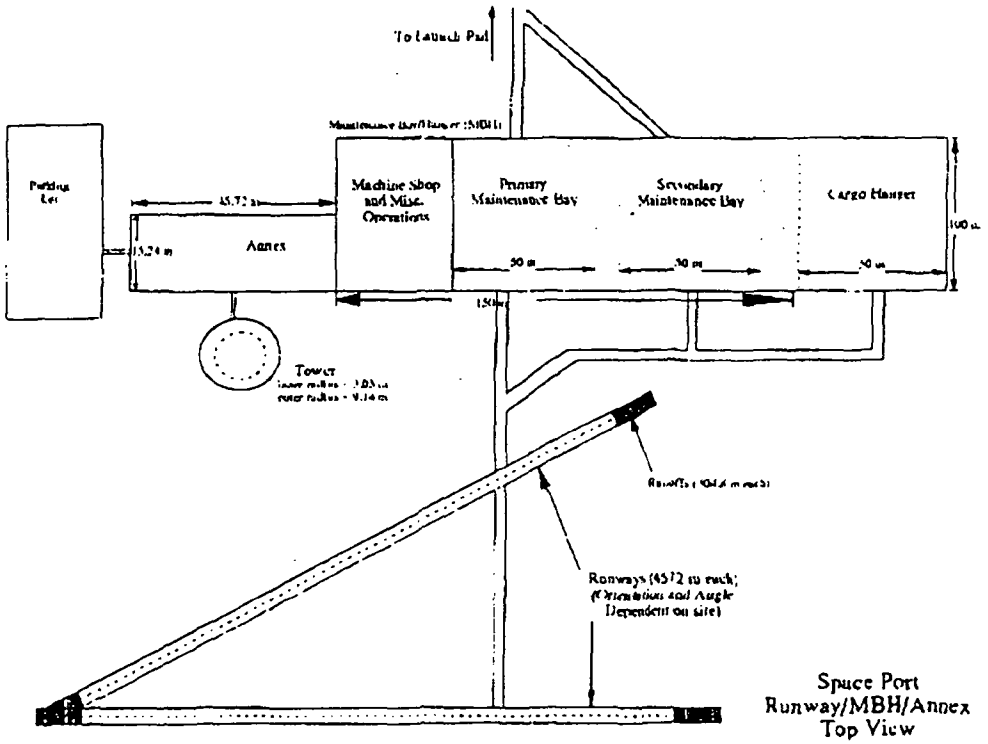

Figure 3 Runway/MBH/Annex Top View

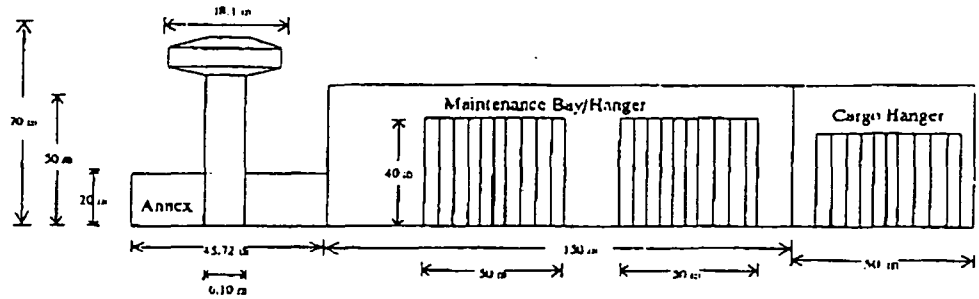

Space Port
Maintenance Bay/Hanger
(Front View)

Figure 4 MBH Front View

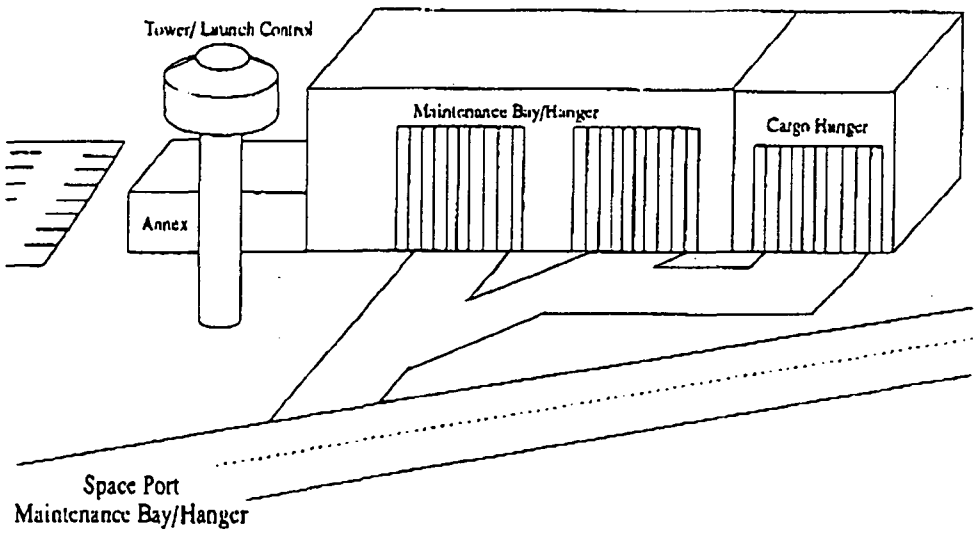

Figure 5 Maintenance Bay/Hanger

APPENDIX F Nose Cone Radius Program

```
      program main
      implicit real*4 (a-h,o-z)
      dimension x(201),t(201,2),rkq(201),cq(201),
     c          tw(5001),tb(5001),tim(5001),alt(5001)
c
      write(6,*) 'itmax,fo,il,emiss'
      read(5,*) itmax,fo,il,emiss
c
c     itmax : number of time iterations
c     fo    : non-dimensional fourier number to determine time step < 0.5
c     il    : number of grid points
c
      stebol=5.6697e-08
c
      alt(1)=  98.638
      rinf0=3.170e-06
      tinf0=180.65
c
      cc=1.83e-04
      rn=0.4          ! nose radius
c
      ilm1=il-1
      twall=300.0
      dxgas=0.2542e-04
c
      rl=0.0254       ! material thickness
      dx=rl/float(ilm1)
      rhoq=1656.3     ! material density
      time=0.0
c
      do 10 i=1,il
      x(i)=dx*float(i-1)
      t(i,1)=twall
10    continue
c
      tw(1)=twall
      tb(1)=twall
      tim(1)=0.0
c
      twpeak=0.0
c
      do 500 j=2,itmax
      dt=1.0e+10
      do 103 i=1,il
      xx = t(i,1)
      rkq(i)=487.60*xx**(-1*0.38152)
      cq(i) = (211.43 + 2.2810*xx - 1.4487e-3*xx*xx
           + 3.6019e-7*xx*xx*xx)/1000.0
      alph=rkq(i)/cq(i)/rhoq
      dt=min(dt,fo*dx*dx/alph)
103   continue
      time=time+3.8e+06*dt
      tim(j)=time
      alt(j)=  9.8638e+4 - 96.656*time + 0.1875*time*time
```

```
     .       -1.4648e-4*time*time*time + 3.2286e-8*time*time*time*time
      alt(j)=alt(j)/1000.0
c     uinf = function of time.
      uinf = 10*(-1*96.656 + 0.375*time)
      rhoinf=1.2250*exp(-alt(j)/7.28)
      tinf=  260.0
      if (alt(j).gt.30.0) tinf=  226.51+2.5375*alt(j)
      if (alt(j).ge.48.0.and.alt(j).le.50.0) tinf=270.65
      if (alt(j).gt.50.0) tinf=270.65-1.488*(alt(j)-50.0)
      if (tinf.lt.180.65) tinf=180.65
      rminf=uinf/sqrt(1.4*287.05*tinf)
      rkgas=1004.0/0.72*1.458e-06*sqrt(t(1,1)**3)/(110.3+t(1,1))
      tgas=cc*sqrt(rhoinf)*uinf**3/sqrt(rn)*
     c    (1.0-t(1,1)/tinf/(1.0+0.2*rminf*rminf))*dxgas/rkgas+t(1,1)
c
      t(1,2)=t(1,1)+dt/(rhoq*cq(1))*
     c      (0.5*(rkq(1)+rkq(2))*(t(2,1)-t(1,1))/dx
     c                    -rkgas*(t(1,1)-tgas)/dxgas)
     c              /(0.5*(dx+dxgas))
     c -dt/(rhoq*cq(1))*4.0*emiss*stebol*t(1,1)**3*(t(1,1)-t(2,1))/dx
      if (mod(j,10).eq.0) write(6,*) time,alt(j),' twall= ',t(1,2)
      tw(j)=t(1,2)
      twpeak=amax1(tw(j),twpeak)
      do 101 i=2,ilm1
      t(i,2)=t(i,1)+dt/(rhoq*cq(i)*dx*dx)
     c      *(0.5*(rkq(i)+rkq(i+1))*(t(i+1,1)-t(i,1))
     c      -0.5*(rkq(i)+rkq(i-1))*(t(i,1)-t(i-1,1)))
101   continue
      t(il,2)=t(il,1)+dt/(rhoq*cq(il)*dx*dx)
     c      *(0.5*(rkq(ilm1)+rkq(il))*(t(ilm1,1)-t(il,1)))
      tb(j)=t(il,2)
      do 102 i=1,il
      t(i,1)=t(i,2)
102   continue
500   continue
c
      write(6,*) ' peak wall temperature: ',twpeak
c
      do 501 i=1,itmax
      write(8,901) tim(i),char(9),tw(i),char(9),tb(i)
501   continue
901   format(e14.6,a1,e14.6,a1,e14.6)
c
      stop
      end
```

APPENDIX G Dynamic Controller Graphs

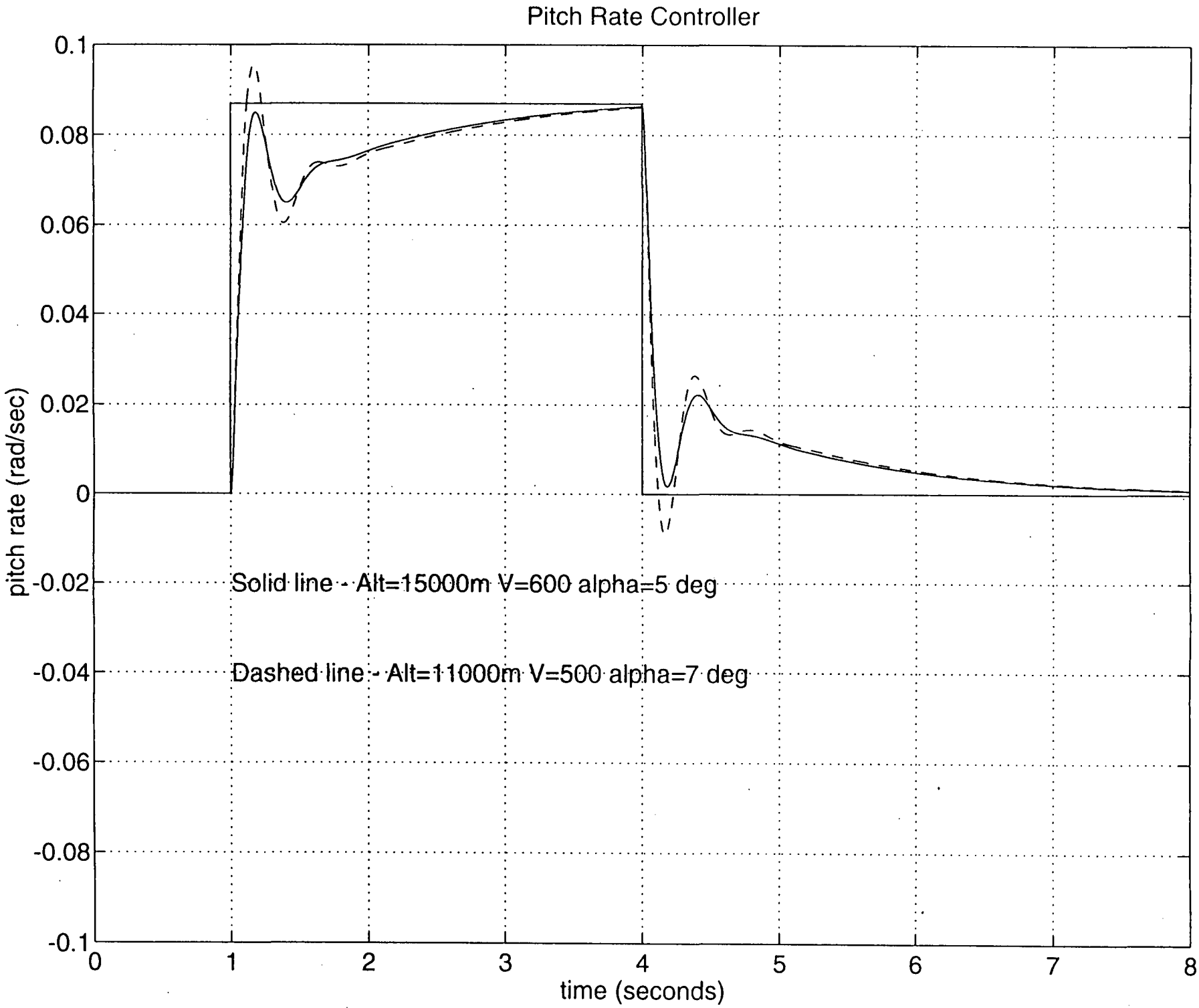
Pitch Rate Controller
0.1
0.08
0.06
0.04
0.02
0
-0.02
-0.04
-0.06
-0.08
-0.1
pitch rate (rad/sec)
0
1
2
3
4
5
6
7
8
time (seconds)
Solid line - Alt=15000m V=600 alpha=5 deg
Dashed line - Alt=11000m V=500 alpha=7 deg

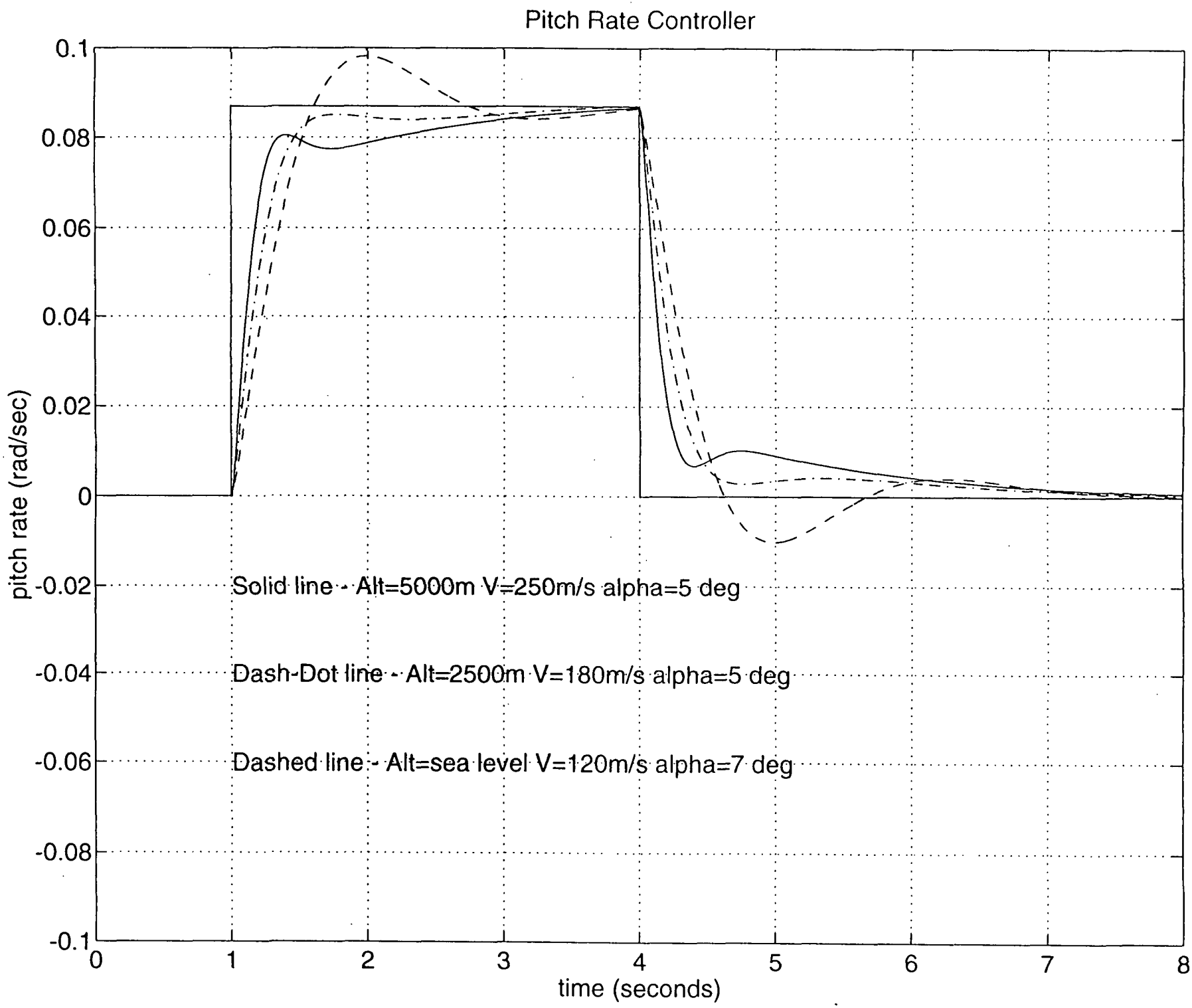
Pitch Rate Controller
0.1
0.08
0.06
0.04
0.02
0
-0.02
-0.04
-0.06
-0.08
-0.1
pitch rate (rad/sec)
0
1
2
3
4
5
6
7
8
time (seconds)
Solid line - Alt=5000m V=250m/s alpha=5 deg
Dash-Dot line - Alt=2500m V=180m/s alpha=5 deg
Dashed line - Alt=sea level V=120m/s alpha=7 deg

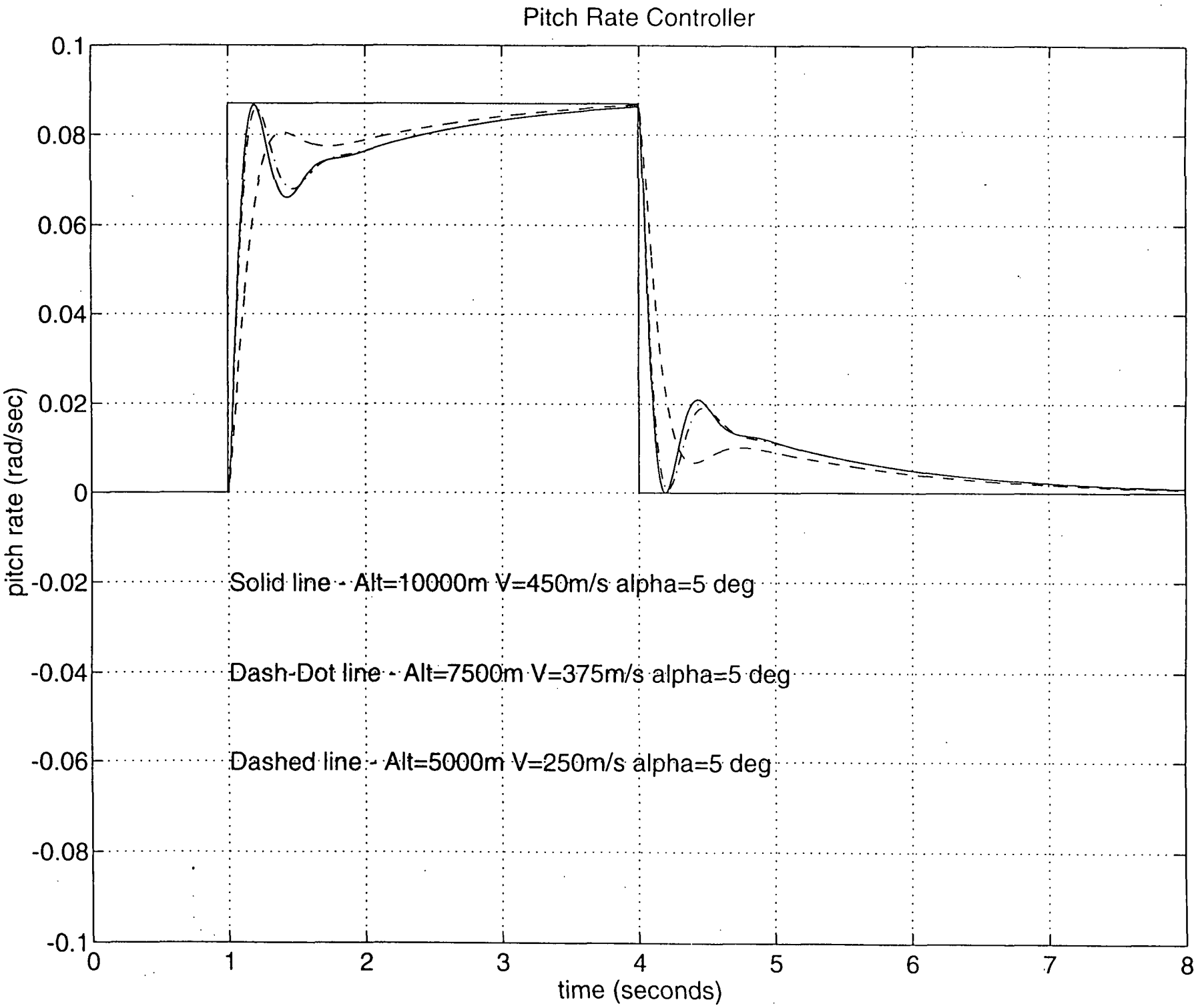
Pitch Rate Controller
0.1
0.08
0.06
0.04
0.02
0
-0.02
-0.04
-0.06
-0.08
-0.1
pitch rate (rad/sec)
0
1
2
3
4
5
6
7
8
time (seconds)
Solid line - Alt=10000m V=450m/s alpha=5 deg
Dash-Dot line - Alt=7500m V=375m/s alpha=5 deg
Dashed line - Alt=5000m V=250m/s alpha=5 deg

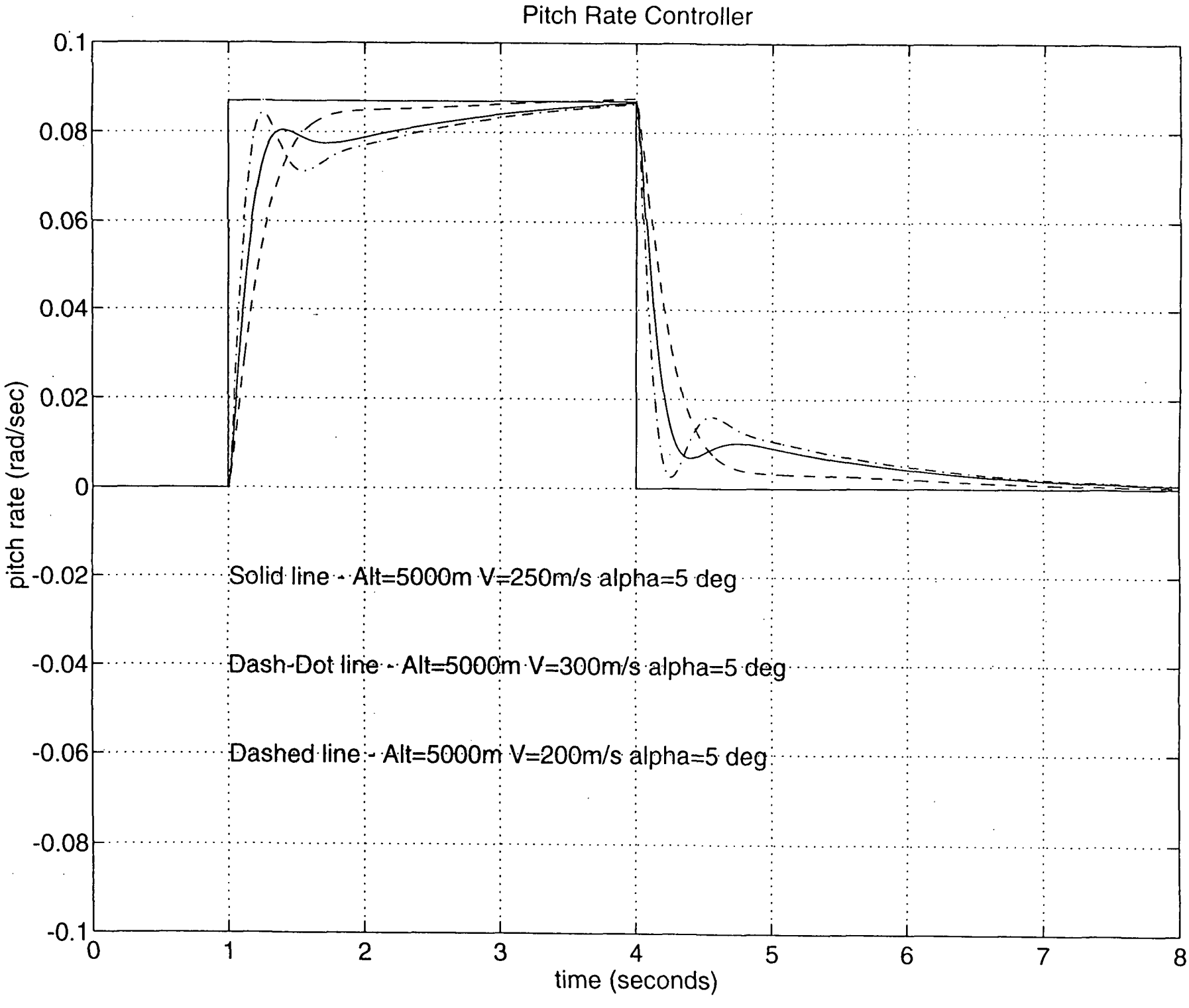
Pitch Rate Controller
0.1
0.08
0.06
0.04
0.02
0
-0.02
-0.04
-0.06
-0.08
-0.1
pitch rate (rad/sec)
0
1
2
3
4
5
6
7
8
time (seconds)
Solid line - Alt=5000m V=250m/s alpha=5 deg
Dash-Dot line - Alt=5000m V=300m/s alpha=5 deg
Dashed line - Alt=5000m V=200m/s alpha=5 deg

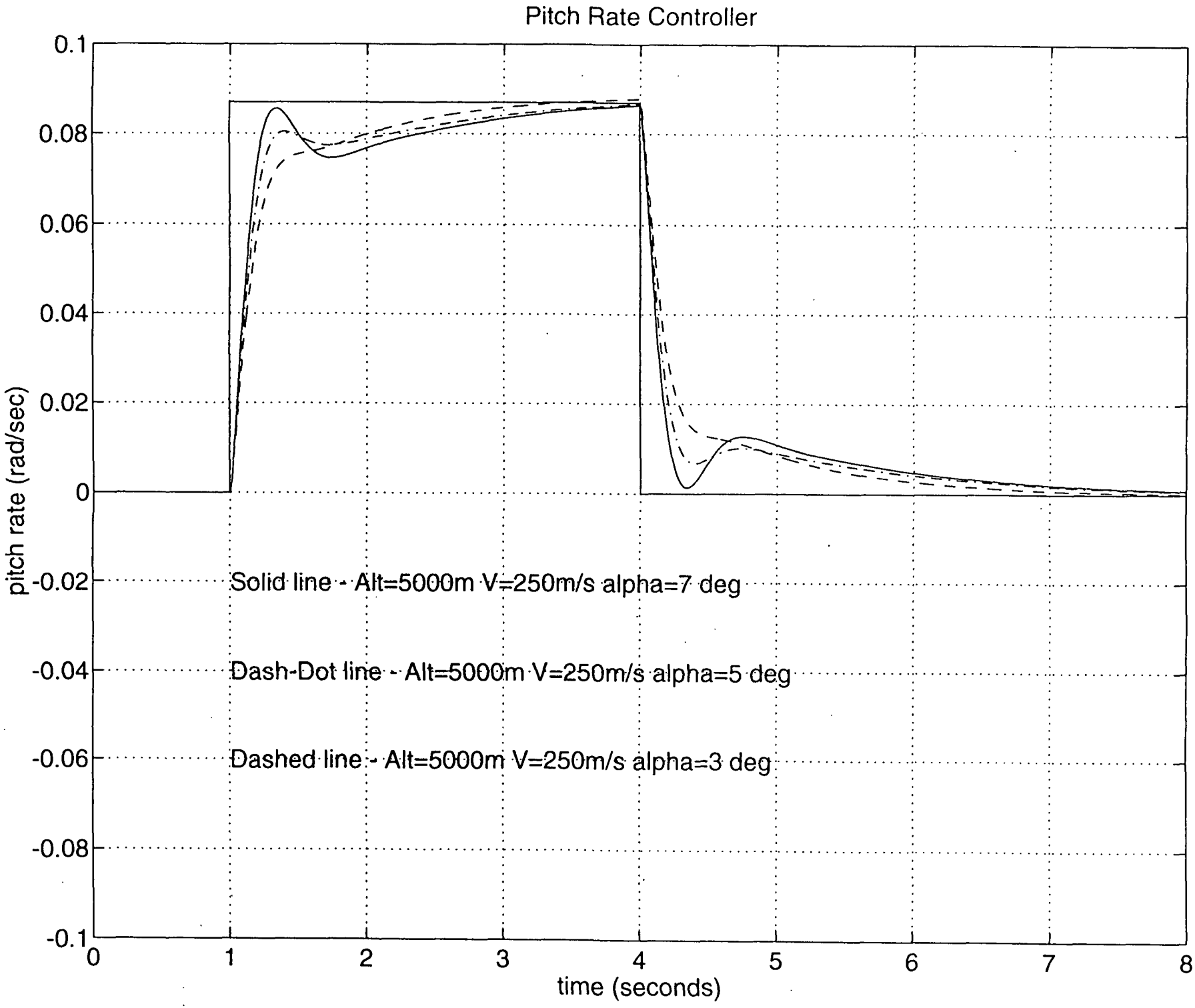
Pitch Rate Controller
0.1
0.08
0.06
0.04
0.02
0
-0.02
-0.04
-0.06
-0.08
-0.1
pitch rate (rad/sec)
0
1
2
3
4
5
6
7
8
time (seconds)
Solid line - Alt=5000m V=250m/s alpha=7 deg
Dash-Dot line - Alt=5000m V=250m/s alpha=5 deg
Dashed line - Alt=5000m V=250m/s alpha=3 deg

APPENDIX H Hypersonic Model

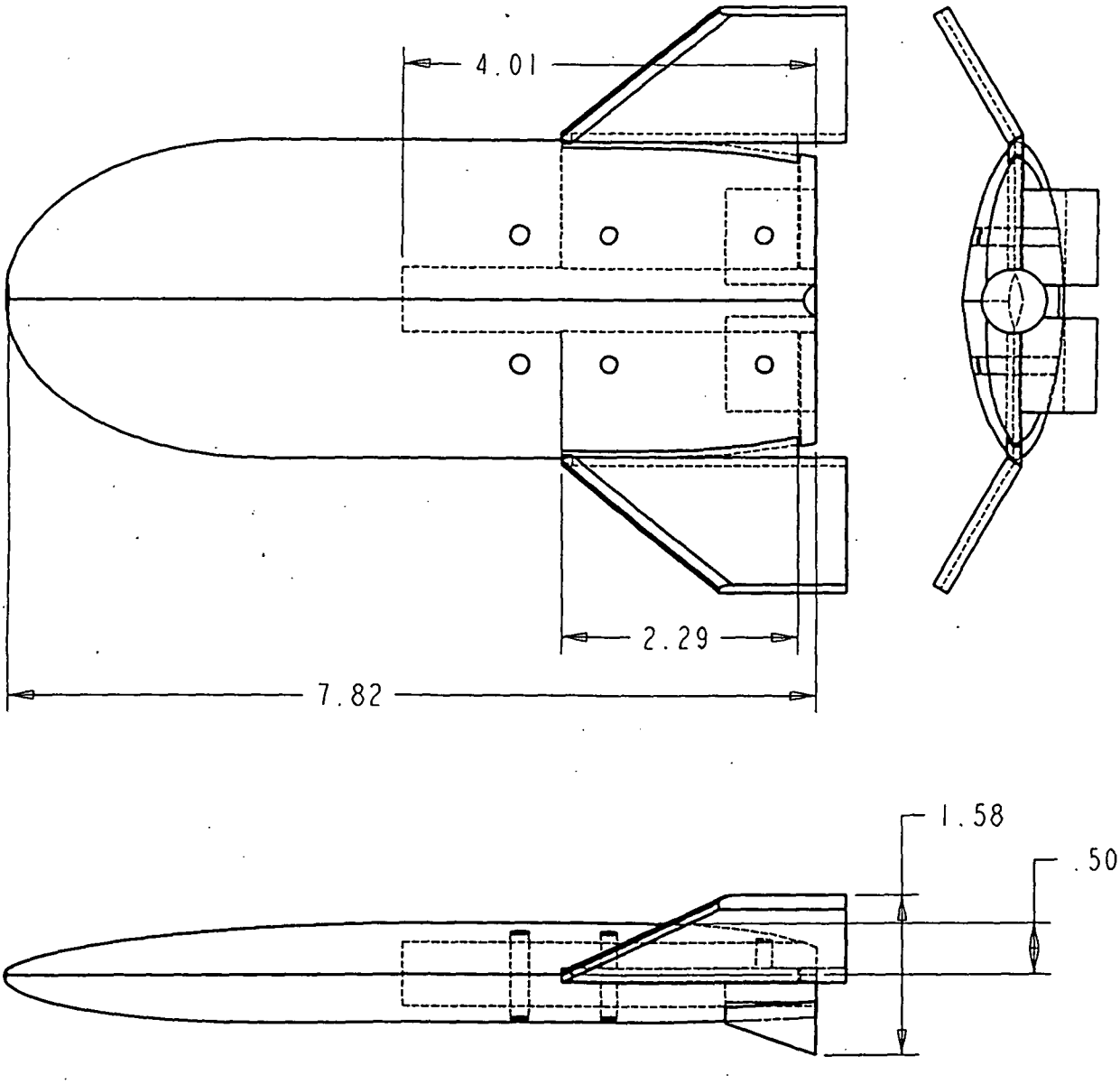

APPENDIX I Hypersonic Model Test Schedule

TWT 740					Mach Number		
Configuration	α	β	δ_{BF}	δ_{EL}	2.74	3.48	4.96
Body only	A1	0	0	-			
Body with wings			0	20			
			20	20			
			30	20			
			30	30			
			20	30			
▼	▼	▼	0	30			
Body only	A2	0	0	-			
Body with wings			0	20			
			20	20			
			30	20			
			30	30			
			20	30			
	▼	▼	0	30			
	8	B	0	20/30			
▼	"	"	0	20			
Body only	A3	0	0	-			
Body with wings			0	20			
			20	20			
			30	20			
			30	30			
			20	30			
▼	▼	▼	0	30			
Body only	A4	0	0	-			
Body with wings			0	20			
			20	20			
			30	20			
			30	30			
			20	30			
	▼	▼	0	30			
	30	B	0	20/30			
▼	"	"	0	20			

A1 = -2 to +8 degrees

A2 = +8 to +18 degrees

A3 = +20 to +30 degrees

A4 = +30 to +40 degrees

B = -6 to +6 degrees

APPENDIX J Hypersonic Wind Tunnel Results

Hypersonic Wind Tunnel Data

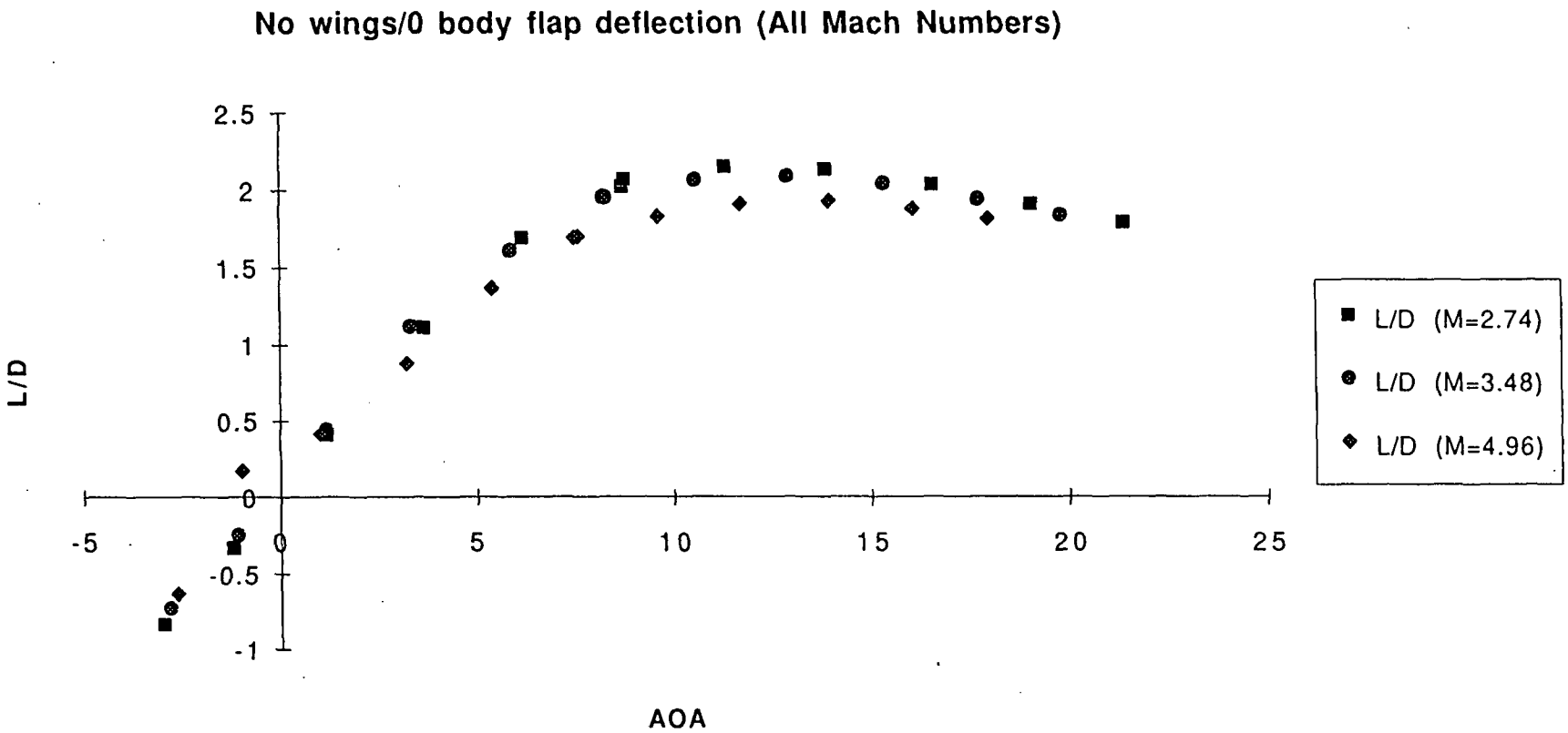

Hypersonic Wind Tunnel Data

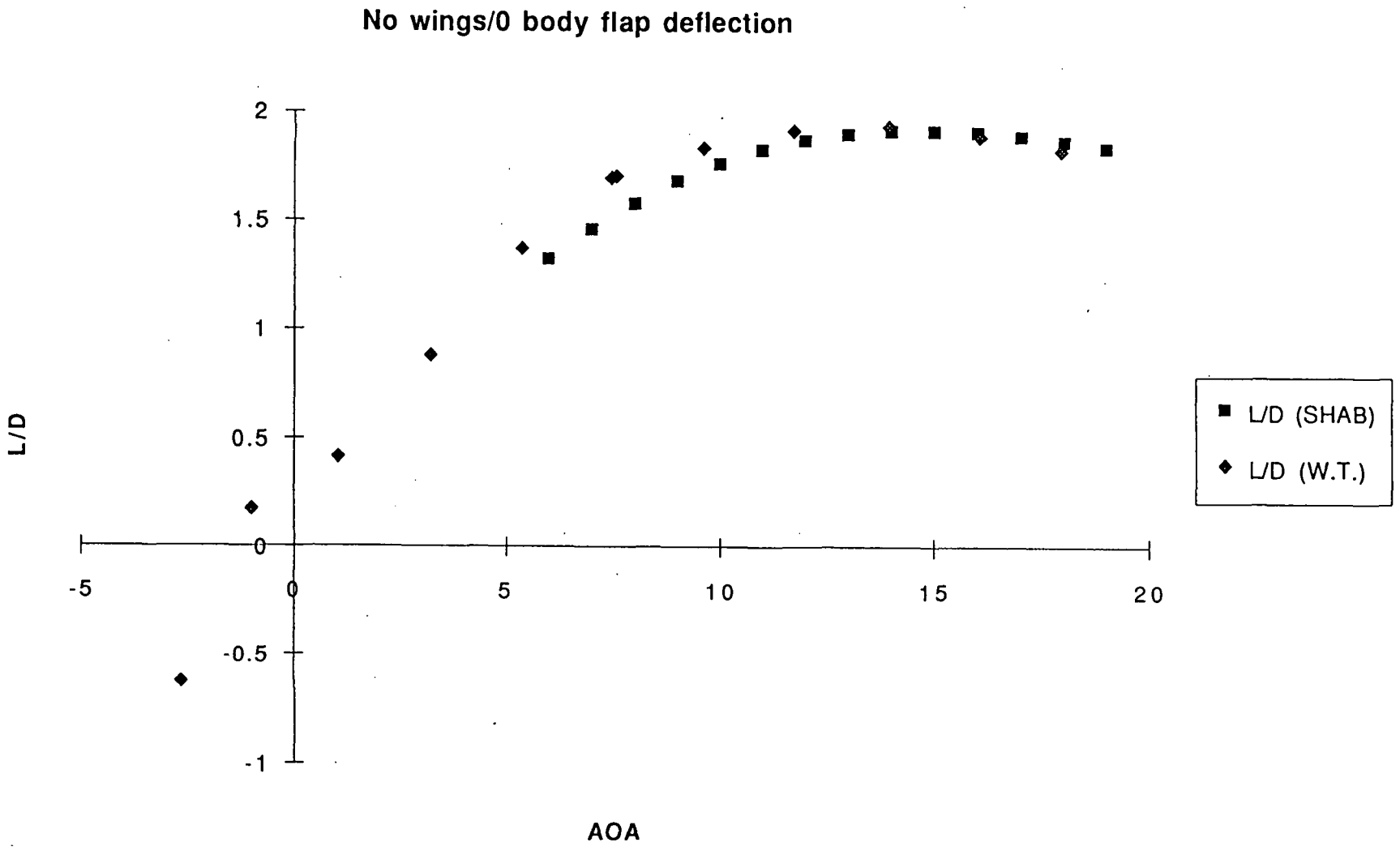

Mach 4.96

Hypersonic Wind Tunnel Data

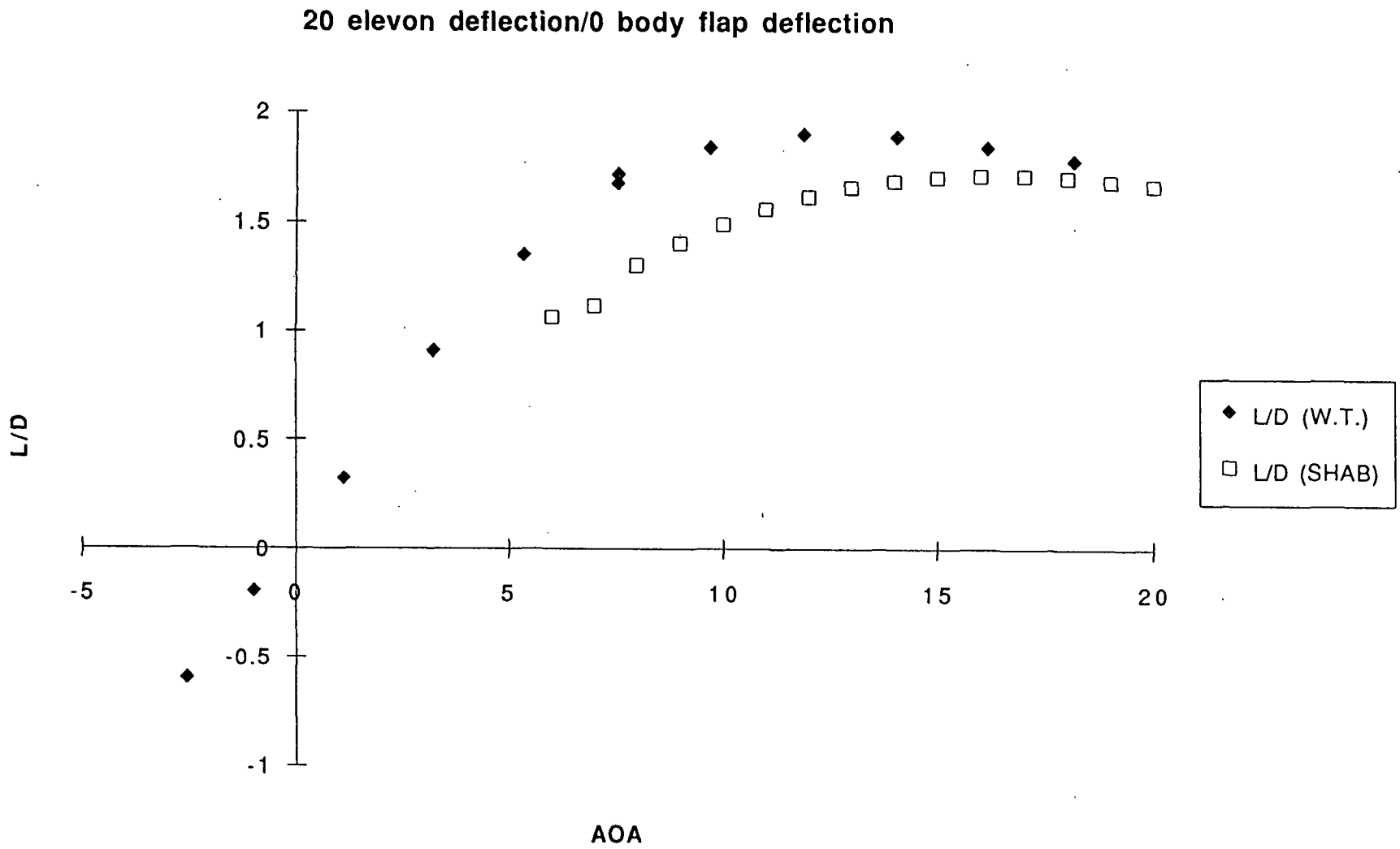

Mach 4.96

Hypersonic Wind Tunnel Data

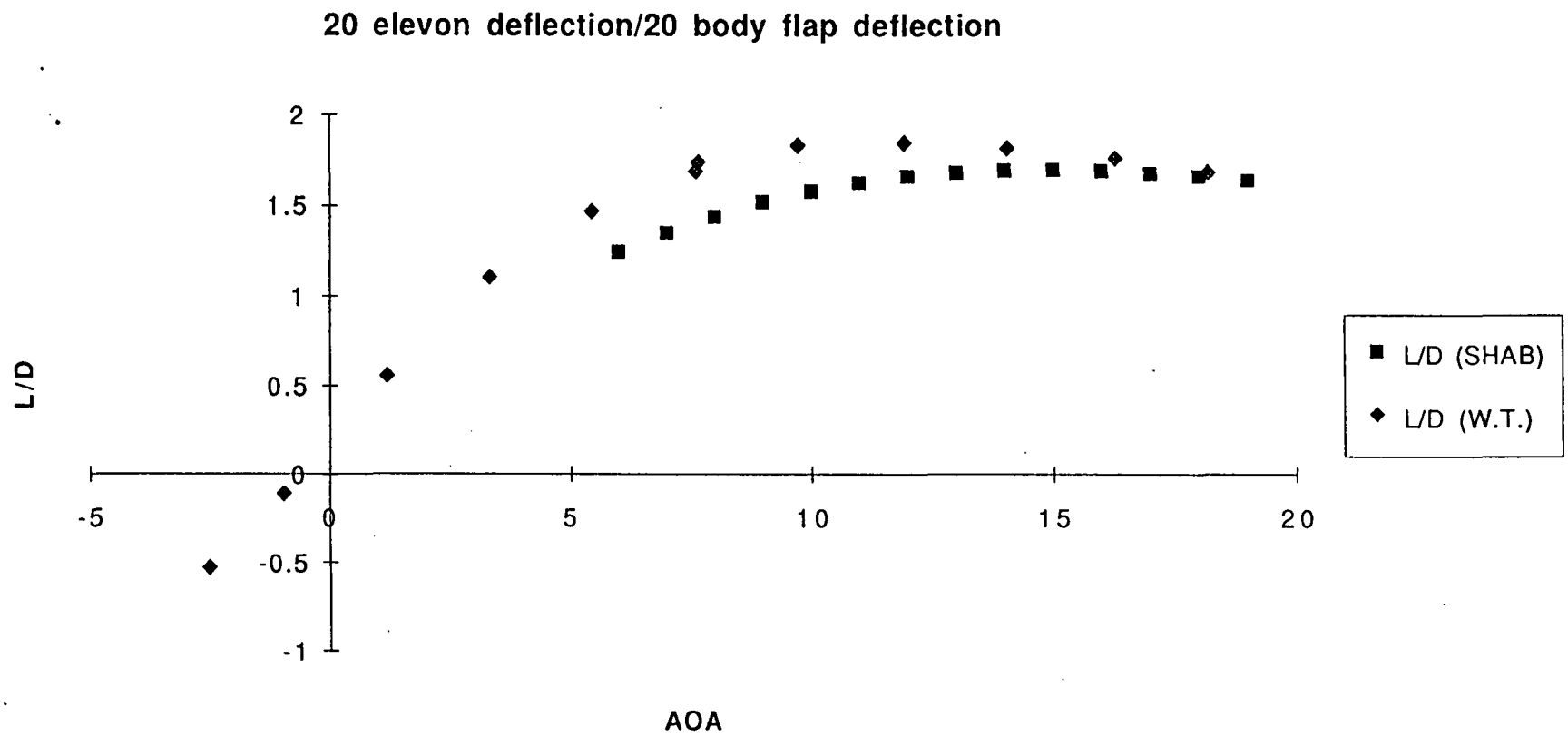

Mach 4.96

Hypersonic Wind Tunnel Data

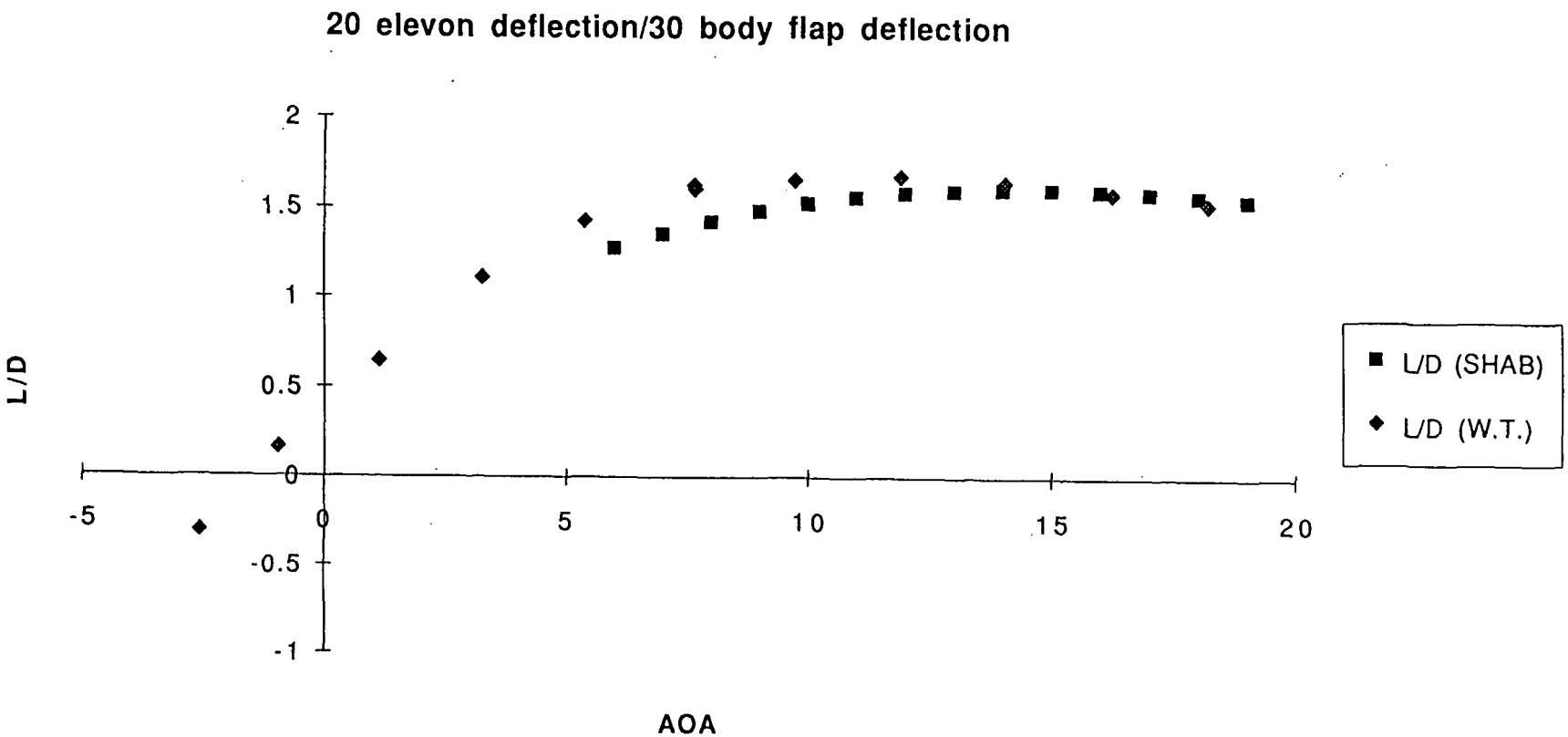

Mach 4.96

APPENDIX K Animation / Airlock Drawings

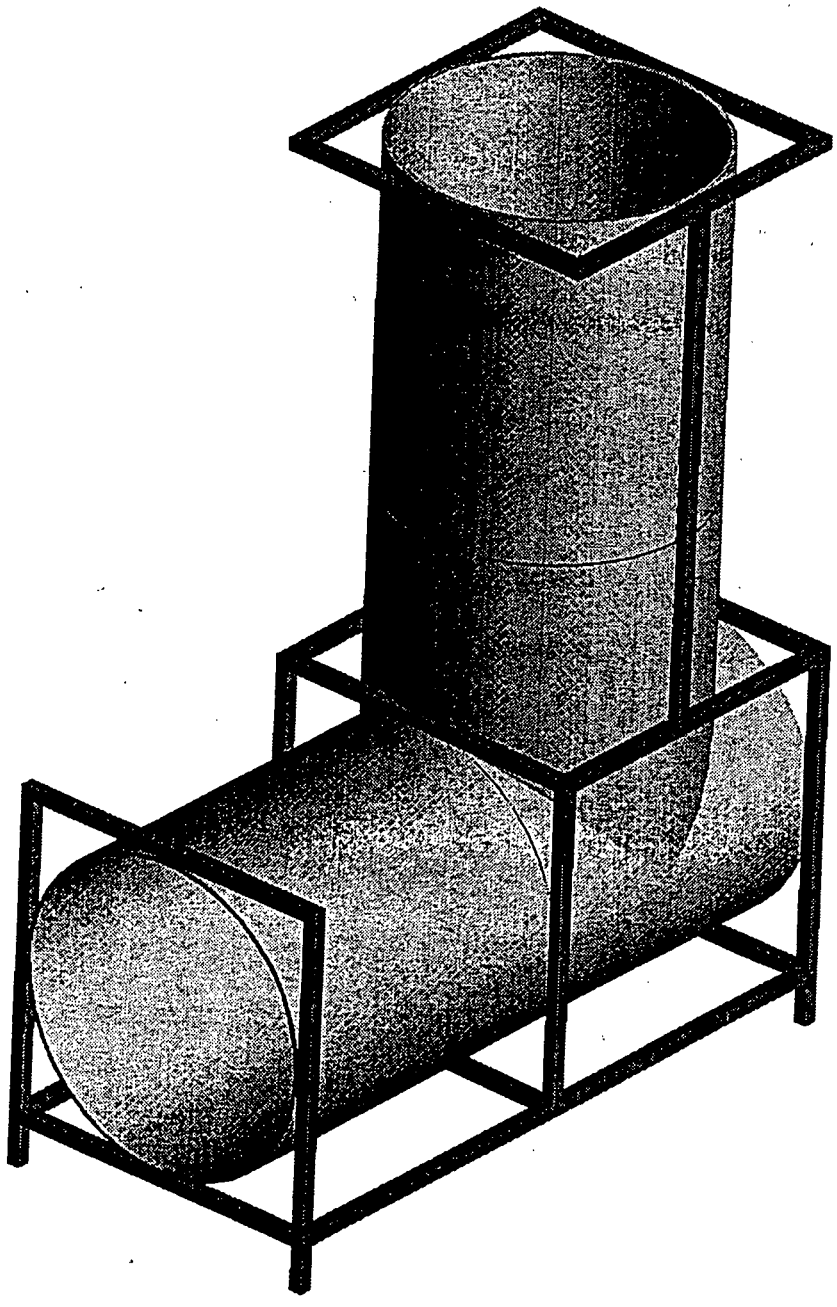

Front / Top View of Airlock Mockup.

Front View

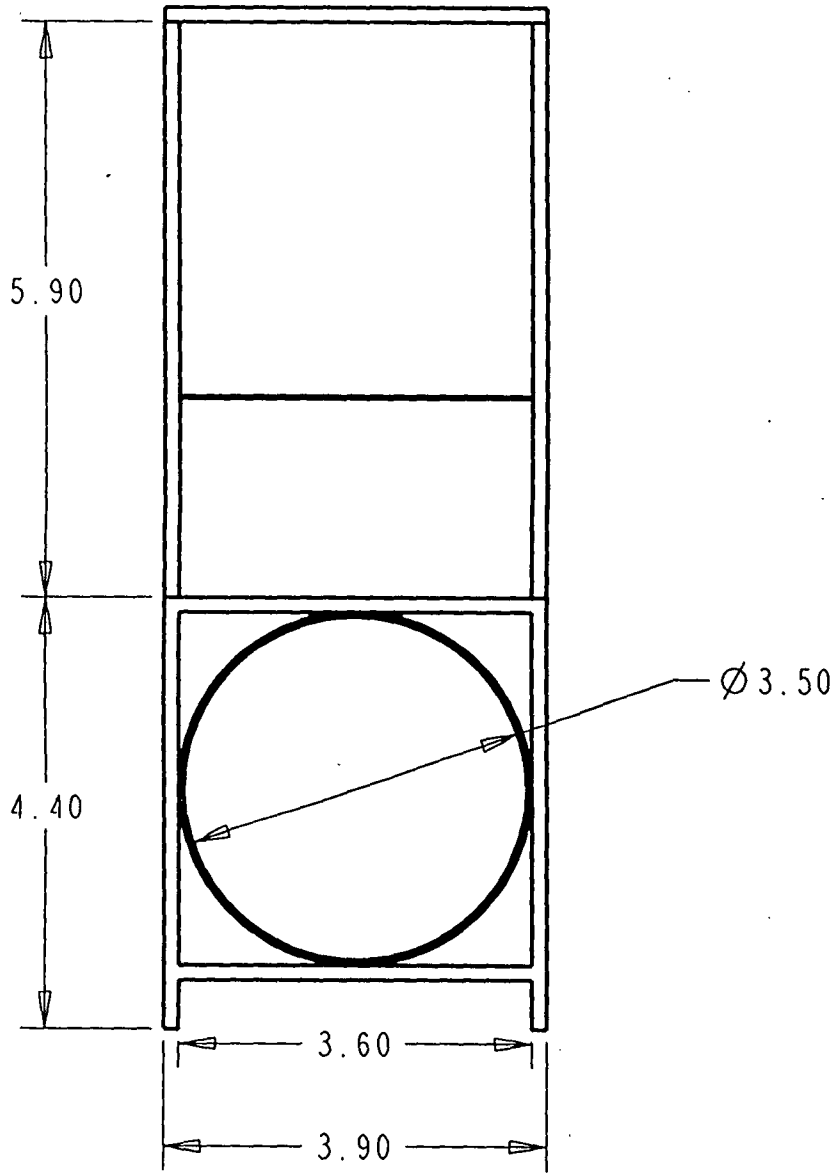

Top View

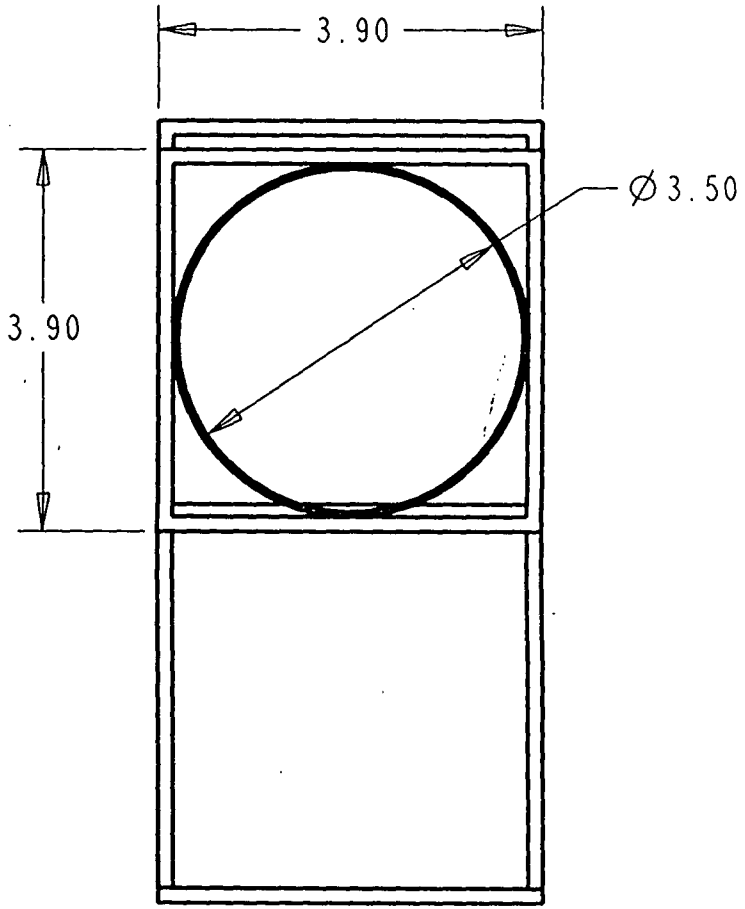

All dimensions in feet.
Frame made of 2"x2" lumber.
Walls made of thin wire fencing.

Side View of Airlock Mockup.

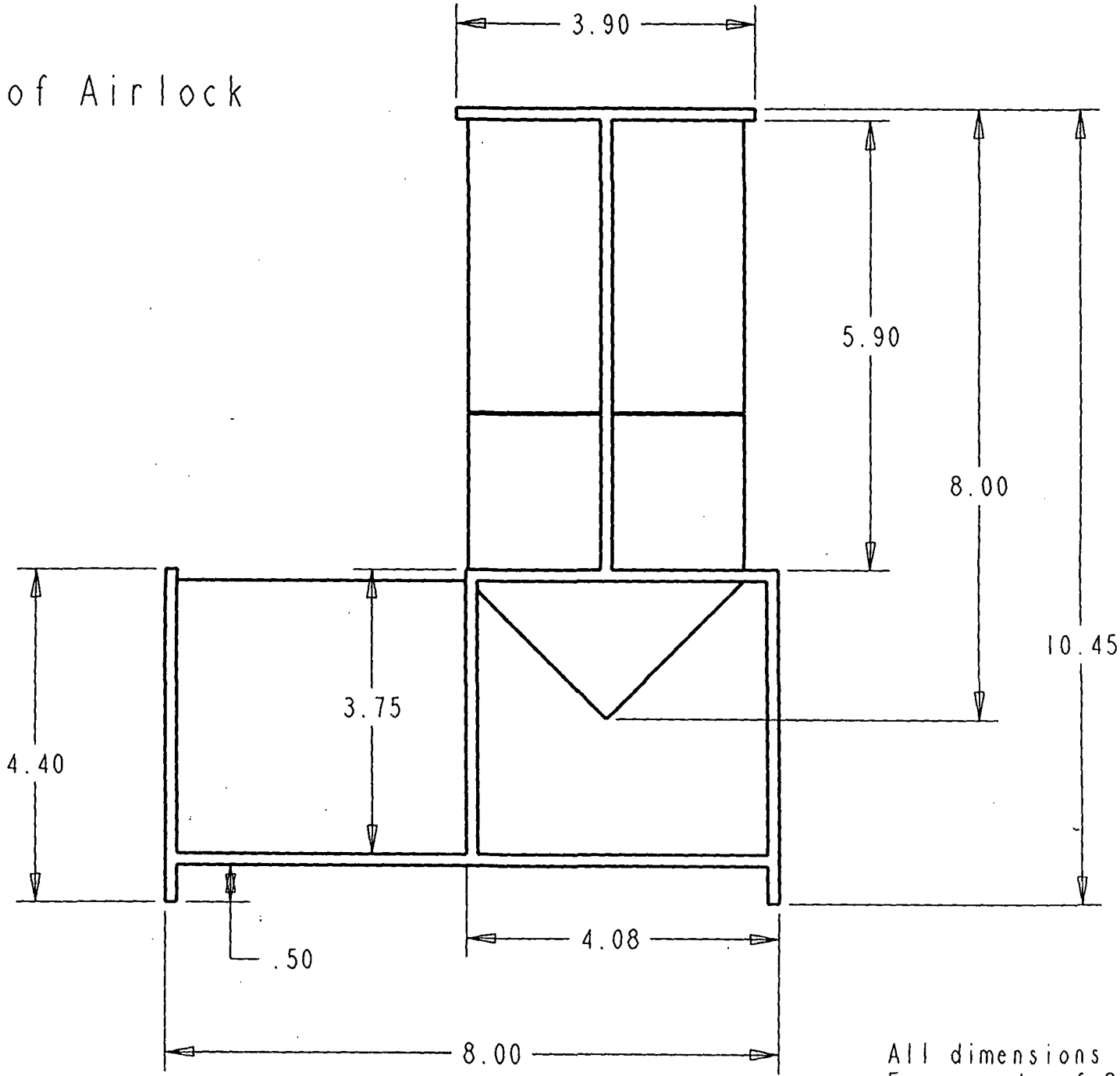

All dimensions in feet.
Frame made of 2x2 lumber.

REFERENCES

1. Rhodes, Russ, "Space Launch Vehicle Operations Efficiency," Rockwell International, March 23, 1992, pp. 6.
2. *Ibid*, pp. 23.
3. Final Report, "Access to Space: Option 3 Team," NASA, July 1993.
4. Payton, Gary, "Single State to Orbit: Counting down," *Aerospace America*, April 1991, pp. 36-39.
5. *Air Force*, December 1993, pp. 14.
6. David A. Fulghum, "Skunk Works Design May Cut Launch Costs," *Aviation Week & Space Technology*, Aug. 16, 1993, pp.76-77.
7. Ibid.
8. Ibid.
9. Beer, Ferdinand P., and Johnston Jr., E. Russel, *Vector Mechanics for Engineers*, 5th ed., McGraw-Hill, New York, 1988, pp. 204-221, 396-425.
10. Ibid.
11. Ibid.
12. Ibid.
13. Huzel, D. K., "Modern Engineering for Design of Liquid-Propellant Rocket Engines," *Progress in Astronautics and Aeronautics, AIAA*, Vol. 147, 1992.
14. Ibid.
15. Edelman, Duane Northwest Airlines, Bloomington, MN.
16. Beddingfield, S.T., Deputy Director, Shuttle Projects Management, "Space Transportation System Facilities and Operations Kennedy Space Center, FL," pp.5-6.
17. Beddingfield, S.T., Deputy Director, Shuttle Projects Management, "Space Transportation System Facilities and Operations Kennedy Space Center, FL," pp. 5-3 - 5-4.
18. Beddingfield, S.T., Deputy Director, Shuttle Projects Management, "Space Transportation System Facilities and Operations Kennedy Space Center, FL," pp. 6-14.
19. Beddingfield, S.T., Deputy Director, Shuttle Projects Management, "Space Transportation System Facilities and Operations Kennedy Space Center, FL," pp. 5-16, 5-17.
20. Beddingfield, S.T., Deputy Director, Shuttle Projects Management, "Space Transportation System Facilities and Operations Kennedy Space Center, FL," pp. 5-23, 5-24.
21. Stanley, S.O., Talay, T.A., Lepsch R.A., Morris, W.P., and Wurster, K.E., "Conceptual Design of a Fully Reusable Man-Launched System," *Journal of Spacecraft and Rockets*, Vol. 29, #4, July-Aug. 1992, pp. 529-537.
22. Beddingfield, S.T., Deputy Director, Shuttle Projects Management, "Space Transportation System Facilities and Operations Kennedy Space Center, FL," pp. 5-23.
23. Beddingfield, S.T., Deputy Director, Shuttle Projects Management, "Space Transportation System Facilities and Operations Kennedy Space Center, FL," pp. 7-18, 7-19.
24. Beddingfield, S.T., Deputy Director, Shuttle Projects Management, "Space Transportation System Facilities and Operations Kennedy Space Center, FL," pp. 7-22.
25. Beddingfield, S.T., Deputy Director, Shuttle Projects Management, "Space Transportation System Facilities and Operations Kennedy Space Center, FL," pp. 7-10.
26. Beddingfield, S.T., Deputy Director, Shuttle Projects Management, "Space Transportation System Facilities and Operations Kennedy Space Center, FL," pp. 7-18.
27. Pratt and Whitney, Walter Library, Microfiche file NAS 1.26:183676.
28. Norlen, T.L., GME Consulting Engineers, Duluth, MN.
29. O'Konski, Douglas C., Shaw Industries, Atlanta, GA.
30. I-DEAS (Integrated Design Engineering Analysis Software), Structural Dynamics Research Corp.
31. "AerMet 100 Alloy Data," Carpenter Technology Corp., Carpenter Steel Division.
32. Lee, Stewart, *Handbook of Composite Reinforceminis*, Volume 1, VCH Publishers Inc., New York, 1993.
33. Hueter, Uwe, "Structures and Thermal Design Margins/Guidelines," NASA, Marshall Space Flight Center, September, 1985.
34. Taylor, John W.R., *Jane's All The World's Aircraft*, 18th Edition, Jane's Information Group Limited, Surrey, U.K., 1989.
35. Boyer, R.R., *Beta Titanium Alloys in the Eighties*, Metallurgical Society of AIME, PA, 1984.
36. Colins, E.W., *Physical Metallurgy of Titanium Alloys*, American Society for Metals, OH, 1984.
37. Savage, G., *Carbon-Carbon Composites*, 1st ed., Chapman and Hall Inc., New York, 1993.
38. Joels, Kerry, *Space Shuttles Operators Manual*, Valantine Books, New York, 1982.
39. Tsai, Steven W., *Composites Design* , 3rd ed., Think Composites, Dayton, 1985.

40. Philips, Leslie N., *Design With Advanced Composite Materials*, Design Council, London, 1989.
41. "Magnesium Die Casting," International Magnesium Association, McLean, 1991.
42. Ashley, Steven, "Boeing 777 Gets A Boost From Titanium," *Mechanical Engineering*, July, 1993.
43. Davis, Pamela A., Martinson, Veloria J., Yager, Thomas J., and Stubbs, Sandy M., "26 X 6.6 Radial-Belted Aircraft Tire Performance," SAE, Warrendale, PA, 1991.
44. Novotny, Paul M., and McCaffrey, Thomas J., "An Advanced Alloy for Landing Gear and Aircraft Structural Applications- AerMet 100 Alloy," SAE, Warrendale, PA, 1992.
45. Maroney, G.E., and Sledz, C.T., "Selection Hydraulic Component Materials," *Aerospace Engineering*, October, 1993.
46. Massy, Antoine, "Aircraft Tires: Bias or Radial?", *Aerospace Engineering*, July, 1991.
47. Garrison, W.M. Jr., "Ultrahigh-Strength Steels for Aerospace Applications," *JOM*, May, 1990.
48. Anderson, J.D. Jr., *Aeronautical and Aerospace Engineering*, McGraw-Hill, 1989.
49. Anderson, J.D. Jr., *Fundamentals of Aerodynamics*, McGraw-Hill, 1991.
50. Candler, G., Professor of Aerospace Engineering and Mechanics, University of Minnesota, Minneapolis, MN.
51. Candler, G., FORTRAN programming code, NASA Ames Research Center, Moffett Field, CA, 1986.
52. Chiu, S. Amanda, "Thermal Analysis of Reusable Surface Insulations," *AIAA paper* No. 92-0582, Jan. 6-9 1992.
53. "Cryogenic boiloff in Low Earth Orbit A Parametric Study Utilizing Multilayer Insulation," Task No. 313-002, Feb. 1990.
54. Farrelly, Don, Dupont Corp.
55. Hayes, D., "An assessment of Alternate Thermal Protection Systems for the Space Shuttle Orbiter," Contract No. 1-16302, NASA, 1982.
56. Incropera, F.P., DeWitt, D.P., *Introduction to Heat Transfer*, John Wiley & Sons, 1990.
57. McAuliffe, P.S., Taylor, A.H., Sparks, L.L., and Dubé, W.P., "Reusable Cryogenic Foam Insulation for Advanced Aerospace Vehicles," *AIAA paper* No. 91-0542, Jan. 1991.
58. Minco Products, Inc., "Thermofoil Heaters," Minneapolis, MN, Bulletin HS-201, Aug. 1991.
59. Moore, Arlene A., NASA Langley Research Center, Hampton, VA.
60. Nealy, John E., and Simonsen, Lisa C., "Radiation Protection for Human Missions to the Moon and Mars," NASA.
61 Olds, Prof. J.R., North Carolina State University, Raleigh, NC.
62. Tauber, Michael E., "Boundary Layer and Convective Heat Transfer Phenomena," Stanford University, Paloalto, CA.
63. Tuelcerl, S., "Cryogenic Boiloff Analysis in Low Earth Orbit for the Space Transportation Vehicle," Task No 313-022, Sept. 1990.
64. Webb, G.L., "Thermal Fatigue of a Radiative Heat Shield Panel For a Hypersonic Transport," NASA Langley Research Center, Hampton, VA, 1985.
65. Wurster, Kay E., NASA Langley Research Center, Hampton, VA.
66. Anderson, J.D., *Introduction to Flight*, 3rd ed., McGraw-Hill, New York, 1989, pp. 513-514.
67. Bate, R.R., Mueller, D.D., and White, J.E., *Fundamentals of Astrodynamics*, Dover Publications, New York, 1971, pp. 14-34, 36, 58-67, 152-153, 162-170, 181-188, 429-430.
68 Chang, H. and French, R.A., "Dynamic Performance of an Aero-Assisted Spacecraft," *Spaceflight Mechanics*, 1992, pp. 415-434.
69. Ma, D., Vinh, N.X., and Wu, C., "Analytic Theory of Optimal Plane Change by Low Aerodynamic Forces," *Spaceflight Mechanics*, 1993, pp. 1139-1154.
70. Ross, I.M., "Aerobang: A New Synergetic Plane-Change Maneuver," *Astrodynamics*, 1991, pp. 1789-1808.
71. Anderson, John D., *Hypersonic and High Temperature Gas Dynamics*, 2nd ed.
72. Ware, G., and Cruz, C., "Aerodynamic Characteristics of the HL-20," *Journal of Spacecraft and Rockets*, Vol. 30, Sept.-Oct. 1993, pp. 529-542.
73. Enns, Prof. D., University of Minnesota, Minneapolis, MN.
74. *The Space Shuttle New Reference*.
75. FUSEX Computer Software, NASA.
76. Bowers, Albion, "Generic Hypersonic Aerodynamic Model Example (GHAME)", NASA Dryden Research Facility, November 16, 1993.
77. French, James R., and Michael D. Griffin, *Space Vehicle Design*, American Institute of Aeronautics and Astronautics, Inc., Washington, D.C., 1991.
78. *Shuttle Operational Data Book*, JSC 08934, Section 4.6.1.3.1, pp. 4.6.1-15.
79. Ibid., pp. 4.6.1-12.
80. *Environmental Control and Life Support System Architectural Control Document*, SSP 30262 Revision D, July, 1991, pp. 3-34.
81. Ibid., pp. 3-8.
82. Ibid., pp. 3-49.

83. *Designing for Human Presence in Space*, NASA/MSFC/ED62, pp. 200.
84. Based on a 3 day, 2 crew mission with 3 days Emergency supplies, no EVA's, and using maximum consumption rates. Totals include only supplies that will be consumed directly by the crew.
85. Anderson, J. J., "Fuel Cell Powerplant Specification", Rockwell International, MC464-0115, December 14, 1984.
86. Griffin, Michael D., and French, James R., *Space Vehicle Design*, Third Printing, American Institute of Aeronautics and Astronautics, Inc., Washington DC, 1991.
87. Hanaway, John F., and Moorehead, Robert W., *Space Shuttle Avionics System*, National Aeronautics and Space Administration, Washington, DC, 1989.
88. Program Development Preliminary Design Office, *Shuttle-C Avionics In-House Study*, National Aeronautics and Space Administration, Marshal Space Flight Center, AL, 1988.
89. Griffin, Michael D., and French, James R., *Space Vehicle Design*, Third Printing, American Institute of Aeronautics and Astronautics, Inc., Washington DC, 1991.
90. Hanaway, John F., and Moorehead, Robert W., *Space Shuttle Avionics System*, National Aeronautics and Space Administration, Washington, DC, 1989.

INITIAL CONTRIBUTORS

System Integration

Dawn Hastreiter
Mark Peterson
Tracey Thompson

Staff

Shad Jesertiz

Mission Analysis

Dan Bahauddin
Shelley Hilden
Alex Walan

Systems Layout

David Giese
John Haurykiewicz
Kim McLaughlin
Jim Pipkin
Brian Wirth

Propulsion

Katsushi Fukasawa
Weston Heuer
Nathan Larson

Launch/Recovery/Turnaround Operations

Craig Bibeau
Gene Carlson
Phillip O'Konski

Structures

David Burger
Mike Guck
Randall Hoerth
Will Keller
Makota Ohta

Thermal Analysis

Al Born
Allan Hovda
Chris Lohff
Jim Ong

Orbital Mechanics

Scott Doudrick
Joel Luker
Debbie Turner

Ascent/Reentry Aerodynamics

Heath Bowden
Chad Rowe
Shonn Schnitzer
Tuan Trong
Teming Tse

Internal and Crew Systems

Jarad Kirsling
Bob School

Advisors

David Sager
Andrew Vano

FINAL CONTRIBUTORS

System Integration

Mark Peterson

Animation / Air Lock

John Haurykiewicz
Kim McLaughlin
Jim Pipkin

Nozzle Evaluation

Weston Heuer
Scott Doudrick

Subsonic Modle

Brian Wirth
Phillip O'Konski
Craig Bibeau

Structures

Will Keller
Makoto Ohta

Thermal Analysis

Al Born
Allan Hovda

Orbital Mechanics

Kevin Bach

Hypersonic Modle

Heath Bowden
Rafael Ortiz
Gene Carlson

Advisors

David Sager
Andrew Vano